Experimental and numerical analysis on the hydration of C_3S/C_3A systems

Shiju JOSEPH

Dissertation presented in partial fulfilment of the requirements for the degree of Doctor of Engineering Science (PhD): Civil Engineering

Examination committee:
Prof. Paul Sas, Chair
Prof. Özlem Cizer, supervisor
Prof. Koen Van Balen, co-supervisor
Prof. Jan Elsen (KU Leuven)
Prof. Yiannis Pontikes (KU Leuven)
Prof. Lucie Vandewalle (KU Leuven)
Prof. Geert De Schutter (Ghent Univ.)
Dr. Ruben Snellings (VITO)
Prof. Shashank Bishnoi (IIT Delhi)

May 2018

Acknowledgement

I express my deep gratitude to Prof. Özlem Cizer for her immense support and belief in me, that was vital to pursue the research of my interest. All these years, she motivated and helped me traverse the difficult moments. I would like to thank her for all the professional advices and patience, and also for the special paternity advice. I am thankful to my co-promoter, Prof. Koen van Balen for being the coolest promoter one can have. He was a consistent source of motivation, who provided a sense of perspective on the very nature of my research. I would like to sincerely thank Prof. Jørgen Skibsted for the warm reception I got to work in his research group in Aarhus University. In the three months at Aarhus University, he guided me through a whole new exciting world of NMR which was alien to me.

I would not have been doing a PhD today in this field if it had not been for Prof. Shashank Bishnoi. Being the best teacher I ever had, he gave me a new and an interesting view in the field of construction materials. He was also the supervisor for my Master's thesis at IIT Delhi and inspired me to pursue research in this field and continues to do so till this day. I would like to thank Dr. Ruben Snellings for helping me tackle some of the difficult problems associated with Rietveld analysis and for all the interesting discussions. I am grateful to my assessors, Prof. Lucie Vandewalle, Prof. Jan Elsen and Prof. Yiannis Pontikes who continuously contributed over the years to betterment of this thesis. I want to thank Prof. Geert De Schutter for his valuable comments during my preliminary defense.

I would like to thank my colleagues Ahmed, Anna, Aziliz, Celine, Charlotte, Hussain, Kristoff, Leidy, Maura, Naveen, Nathalie, Nishant, Rutger, Salman, Siva, Tasos, Youen for their wonderful company and continuous support during these years. Special thanks to the technicians Stephan, Gerda, Jimmy, Bernd for making my work easier. I really appreciate the wonderful company of my colleagues at Aarhus University Julian, Malene, Rene and also for all the troubleshooting during the NMR measurements. I would like to thank Kristine and Rita for doing all the administrative work and for their joyful presence. I would also like to thank my thesis students Eveline, Frederik, Haizea, Jesse, Kwok, Laura, I learned a lot with them. I want to acknowledge KU Leuven for the Doctoral scholarship and FWO for travel grant for long stay abroad.

I am deeply indebted to my parents for the sacrifices they have made for giving me a wonderful childhood, their immense moral support during difficult times in my life and for being proud of the person I am today. I would also like to thank my brother for all the love and support and sparing me alive after all the wrestling sessions we had. I also thank all my friends for adding wonderful colours to my life. And I am obliged to thank my wife for my desire to stay alive and for my passion to help the world by contributing the least to noise pollution. Nevertheless, I would like to thank for all the wonderful (at times irritating) discussions about my research. Last, but not the least, I would also like to thank the almighty, the source of infinite wisdom and knowledge, who helped me through all the difficult times: Google.

Shiju Joseph

Abstract

The early age hydration of ordinary Portland cement (OPC) is mainly driven by tricalcium silicate (C_3S) and tricalcium aluminate (C_3A) phases. A fundamental understanding of the hydration mechanism of these phases is necessary to develop numerical models which could efficiently predict the temperature rise in mass concrete or microstructural development of cement based materials. Furthermore, a scientific understanding of how sodium sulphate (Na_2SO_4) influences the hydration of these two Portland clinker phases is required to develop novel hybrid binder systems, where supplementary cementitious materials (SCM) are activated with Na_2SO_4 to reduce the clinker content significantly. This could potentially improve the sustainability of cement and concrete industry.

The primary objective of this thesis is to identify the reaction mechanisms that control the hydration of C_3S and C_3A in pure systems, and in polyphase systems where C_3S and C_3A are present in the same grain similar to a Portland cement clinker. The effects of fineness, filler, water to cement ratio (w/c), temperature profiles on the hydration reactions were investigated in pure C_3S systems. Investigated parameters in pure C_3A systems were gypsum content, fineness, and w/c ratio. In C_3S-C_3A polyphase systems, studied parameters are gypsum content, Na_2SO_4 and fineness. Complementary analytical techniques such as isothermal calorimetry, thermal analysis (TGA), X-ray diffraction (XRD), ^{27}Al and ^{29}Si MAS NMR are performed for an in-depth quantitative study.

New mechanisms have been proposed for the hydration of pure C_3S and C_3A systems. Numerical modelling has been used to study the mathematical feasibility of the proposed mechanisms. In this thesis, a new microstructural modelling platform, CemRS (Cementitious Reaction Simulator) has been developed in C++ to model different reaction mechanisms efficiently without the need of truncation of the particles size distribution. The model uses a statistical modelling approach to model the particle size distribution, which makes it much faster than the existing modelling platforms. CemRS is effectively used to model the hydration of C_3S and C_3A reactions in pure systems.

Besides this new microstructural modelling platform, a densified volumetric growth (DVG) hypothesis is proposed for the main peak of C_3S hydration. This modified nucleation and growth-based mechanism assumes that the hydration of C_3S is controlled by the internal surface area of C-S-H which is dependent on its bulk density. Numerical modelling shows that such a model is capable to capture the effect of fineness and fillers without the need of changing the parameters for fitting.

Research findings reveal that w/c does not have any effect on the hydration kinetics of C_3S until 1 day, while there is only a marginal effect by 28 days. Although hydration kinetics is not affected by w/c ratio, C/S ratio of C-S-H is influenced by w/c ratio. When C_3S is cured at a lower temperature (20°C) and then cured at higher temperature (40°C), there is an increase in

the degree of hydration and vice versa. These effects are explained based on the DVG hypothesis.

For the hydration of pure C_3A -gypsum systems, current study has validated from the experimental results and numerical modelling that the hydration before depletion of gypsum could be explained based on a surface-controlled mechanism. Without rejecting the current mechanism (adsorption of calcium and/or sulphate ions on C_3A surface), which explains the retardation of C_3A in the presence of gypsum, it is proposed here that the retardation could be due to the surface coverage of C_3A from ettringite precipitation. After depletion of gypsum, the main hydration peak is analyzed and discussed using a dissolution-controlled mechanism. The numerical model can capture the hydration peak, including the peak broadening effects that are found with increasing gypsum content and decrease in fineness. It has been found that w/c ratio has a significant influence on the overall degree of hydration of C_3A in systems with and without gypsum. With an increase in w/c, the degree of hydration of C_3A increases, which is attributed to the increase in the free water with the increase in w/c ratio.

In C_3S-C_3A polyphase systems, hydration of C_3A significantly affects the hydration of C_3S. Although the current hypothesis of an inhibiting effect of AFm on nucleation and growth of C-S-H could explain some of the studied systems, it cannot explain the retardation caused in severely-over-sulphated systems and systems with Na_2SO_4. Hence a new mechanism is proposed for these systems. It has been proposed that the hydration of C_3S is retarded by the surface coverage of ettringite crystals on the reactive surface of C_3S. This switches the hydration of C_3S to a dissolution-controlled mechanism after 24 hours. Hydration of C_3A is strongly affected by the hydration of C_3S, which is a result of the increase in reactive front due to C_3S dissolution. With the addition of Na_2SO_4, a recrystallisation of ettringite from AFm phases was observed. Hence the risk of cracking in concrete due to the recrystallisation of ettringite should be further studied while designing hybrid binder systems with Na_2SO_4.

Samenvatting

De hydratatie van gewoon Portland-cement (OPC) op jonge leeftijd wordt voornamelijk door de hydratatie van de tricalciumsilicaat- (C_3S) en tricalciumaluminaat (C_3A) fasen bepaald. Een fundamenteel begrip van het hydratatiemechanisme van deze twee fasen is nodig om numerieke modellen te ontwikkelen die op efficiënte wijze de temperatuurstoename van beton door de ontwikkeling van de micro-structuur van cement te voorspellen. Bovendien is een wetenschappelijk inzicht van de manier waarop natriumsulfaat (Na_2SO_4) de hydratatie van deze twee Portlandklinkerfasen beïnvloedt, nodig om nieuwe hybride bindmiddelsystemen te ontwikkelen, waarbij cement vervangende materialen (SCM) worden geactiveerd met Na_2SO_4 om het klinkergehalte aanzienlijk te verminderen. Dit zal de duurzaamheid van de cement- en betonindustrie kunnen verbeteren.

Het primaire doel van dit proefschrift is om de reactiemechanismen te identificeren die de hydratatie van C_3S en C_3A in zuivere systemen regelen, en in polyfasesystemen waarbij C_3S en C_3A in dezelfde korrel aanwezig zijn, zoals dat het geval is in Portland cementklinker. Het effect van fijnheid, vulstof, water/cement-verhouding (w/c), temperatuurprofielen werd onderzocht in zuivere C_3S -systemen. De onderzochte parameters in pure C_3A -systemen zijn het effect van het gehalte aan gips, de fijnheid en de w/c-factor. In C_3S - C_3A -polyfasesystemen zijn de onderzochte parameters het gehalte aan gips, aan Na_2SO_4 en de fijnheid. Verschillende analytische technieken zoals isothermie calorimetrie, thermische analyse (TGA), X-straal diffractie (XRD), ^{27}Al en ^{29}Si MAS NMR werden uitgevoerd voor een diepgaand kwantitatief onderzoek.

Er zijn nieuwe mechanismen voorgesteld voor de hydratatie van pure C_3S - en C_3A -systemen. Numerieke modellering is gebruikt om de wiskundige haalbaarheid van de voorgestelde mechanismen te bestuderen. In dit proefschrift is een nieuw microstructureel modelleringsplatform, CemRS (Cementitious Reaction Simulator), ontwikkeld in C++ om verschillende reactiemechanismen efficiënt te modelleren zonder de noodzaak om de deeltjesverdeling af te toppen. Het model gebruikt een statistische modelleringsaanpak om de deeltjesgrootteverdeling te modelleren, waardoor het veel sneller is dan de bestaande modelplatforms. CemRS wordt effectief gebruikt om de hydratatie van C_3S - en C_3A -reacties in zuivere systemen te modelleren.

Naast dit nieuwe platform voor microstructurele modellering, wordt een hypothese voorgesteld uitgaande van de verdichting van volumetrische groei (densified volumetric growth - DVG) die de belangrijkste piek van C_3S -hydratie uitlegt. Dit gemodificeerde nucleatie- en groei-gebaseerde mechanisme gaat er van uit dat de hydratatie van C_3S wordt beheerst door het specifieke oppervlak van C-S-H dat afhankelijk is van de dichtheid. Numerieke modellering toont aan dat een dergelijk model in staat is om het effect van fijnheid en van inerte

toeslagstoffen in rekening te brengen zonder de passende parameters te hoeven veranderen (wat voor de meest bestaande modellen wel noodzakelijk is).

Onderzoeksresultaten tonen aan dat w/c-factor tot 1 dag geen effect heeft op de hydratatiesnelheid van C_3S, terwijl er slechts een marginaal effect is op 28 dagen. Hoewel de hydratatiesnelheid niet wordt beïnvloed door w/c, wordt de C/S-verhouding van C-S-H beïnvloed door w/c-factor. Wanneer C_3S uithardt bij een lagere temperatuur (20°C) en vervolgens uithardt bij hogere temperatuur (40°C), neemt de hydratatiegraad toe en omgekeerd. Deze effecten worden verklaard op basis van de DVG-hypothese.

Deze studie valideert aan de hand van experimentele resultaten en van numerieke modellering dat bij de hydratatie van zuivere C_3A -gipssystemen, de hydratatie vóór uitputting van gips kon worden verklaard op basis van een mechanisme met gecontroleerde oppervlakte. Zonder het huidige mechanisme (adsorptie van calcium- en sulfaationen op het C_3A -oppervlak) te verwerpen, hetgeen de vertraging van C_3A in de aanwezigheid van gips verklaart, wordt hier voorgesteld dat de vertraging kan worden veroorzaakt door de oppervlaktebedekking van C_3A uit ettringietprecipitatie. Na uitputting van gips, wordt de belangrijkste hydratatiepiek uitgelegd aan de hand van een oplossingsgestuurd reactiemechanisme. Het numerieke model kan de hydratatiepiek vastleggen, inclusief de piekverbredingseffecten die worden gevonden met toenemend gipsgehalte en afname in fijnheid. Er is gevonden dat w/c-factor een significante invloed heeft op de totale mate van hydratatie van C_3A in systemen met en zonder gips. Met een toename in w/c–factor neemt de mate van hydratatie van C_3A toe, wat wordt toegeschreven aan de toename in wateractiviteit met de toename van w/c-factor.

In C_3S - C_3A -polyfasesystemen beïnvloedt de hydratie van C_3A significant de hydratatie van C_3S. Hoewel de huidige hypothese van een remmend effect van AFm op nucleatie en groei van C-S-H alle bestudeerde systemen zou kunnen verklaren, behalve bij ernstig overgesulfateerde systemen en systemen met Na_2SO_4, wordt voor deze systemen een nieuw mechanisme voorgesteld. Er is voorgesteld dat in deze systemen de hydratatie van C_3S wordt vertraagd door de oppervlaktebedekking van ettringietkristallen op het reactieve oppervlak van C_3S. Hiermee schakelt de hydratatie van C_3S na 24 uur over naar een oplossingsgestuurd mechanisme. Hydratatie van C_3A wordt sterk beïnvloed door de hydratatie van C_3S. Dit is een gevolg van de toename in reactief front als gevolg van C_3S -oplossing. Met de toevoeging van Na_2SO_4 werd een herkristallisatie van ettringiet uit AFm-fasen waargenomen. Daarom moet het risico van barsten in beton als gevolg van de herkristallisatie van ettringiet verder worden bestudeerd bij het ontwerpen van hybride bindmiddelsystemen met toevoeging van Na_2SO_4.

Glossary

Cement Notations

C	CaO
S	SiO_2
A	Al_2O_3
F	Fe_2O_3
$	SO_3
N	Na_2O

Cement Phases/Hydrates

C_3S	Alite
C_2S	Belite
C_3A	Aluminate
C_4AF	Ferrite
$C\$H_2$	Gypsum
$C\$H_{0.5}$	Bassanite
C$	Anhydrite
C-S-H	Calcium Silicate Hydrate
C-A-S-H	Calcium Aluminate Silicate Hydrate
CH	Calcium Hydroxide / Portlandite
AFm	Al_2O_3-Fe_2O_3-mono
AFt	Al_2O_3-Fe_2O_3-tri
$C_4(A,F)X_2.nH_2O$	General notation for all AFm phases
h-AFm/ OH-AFm	hydroxy AFm
m-AFm	monosulphoaluminate AFm
$C_6A\$_3H_{32}$	Ettringite
$C_{12}A_7$	Mayenite
C_3AH_6	Hydrogarnet
N$	Sodium sulphate

Abbreviations

AAM	Alkali Activated Materials
BNG	Boundary Nucleation and Growth

C/S Ratio	Calcium to Silicon ratio
CemRS	Cementitious Reaction Simulator
DoH	Degree of Hydration
DTG	Differential Thermo Gravimetry
DuCOM	Durability Model for COncrete
DVG	Densified Volumetric Growth
EDS	Energy Dispersive Spectrometry
HymoStruc	Hydration, morphology and structure development
HydratiCA	Hydration by Cellular Automata
ICSD	Inorganic Crystal Structure Database
IPKM	Integrated Particle Kinetics Model
JMAK	Johnson Mehl Avrami Kolmogorov
LHD	Lamellar Double Hydroxide
MAC	Mass Attenuation Coefficient
MAS	Magic Angle Spinning
MCL	Mean Chain Length
N&G	Nucleation and Growth
NDG	Nucleation and Densified Growth
NMR	Nuclear Magnetic Resonance
OPC	Ordinary Portland Cement
O$	Over-sulphated
P$	Properly sulphated
ppm	parts per million
PONCKS	Partial or No Known Crystal Structures
PSD	Particle Size Distribution
PSZ	Partially Sintered Zirconia
QXRD	Quantitative X-Ray Diffraction
RCC	Reinforced Concrete Structures
REV	Representative Elementary Volume
RH	Relative Humidity
SANS	Small Angle Neutron Scattering
SCM	Supplementary Cementitious Materials
S/N ratio	Signal to Noise Ratio
sO$	Severely over-sulphated
STEM	Scanning Transmission Electrom Microscopy
sU$	Slightly under-sulphated
TAH	Third Aluminate Hydrate
TEM	Transmission Electron Microscopy
TGA	Thermogravimetric Analysis
U$	Under-sulphated
WC	White Cement
w/c	water to cement ratio
WDS	Wavelength Dispersive Spectrometry
XRD	X-Ray Diffraction
XRF	X-Ray Fluorescence

Contents

Page No.

Acknowledgement i
Abstract iii
Samenvatting v
Glossary vii
Contents ix
List of Figures xiii
List of Tables xix

Chapter I General Introduction 1
1.1 Ordinary Portland Cement (OPC) 1
1.2 Alternatives to OPC 1
1.3 Motivation for the current research 3
1.4 Why studies on synthetic systems 4
1.5 Scope and outline of the thesis 5
References 6

Chapter II CemRS: Fast and efficient modelling platform for the simulation of cementitious systems 9
2.1 Introduction 9
2.2 Currently available models 10
2.2.1 Jennings & Johnson model (1986) 10
2.2.2 HymoStruc (1991) 11
2.2.3 CemHyd3D (1997) 11
2.2.4 DuCom (2003) 12
2.2.5 HydratiCA (2007) 12
2.2.6 µic (2008) 13
2.3 Effect of Truncation on degree of hydration 14
2.4 CemRS modelling platform 16
2.4.1 Structure of CemRS 16
2.4.2 Modelling PSD 17
2.4.3 Modelling kinetics 18
2.4.3.1 Dissolution-based model 19
2.4.3.2 Precipitation-based model 20
2.4.4 Microstructure 20
2.4.4.1 2D microstructure 21

2.4.4.2 Generating a microstructural image 21
2.4.4.3 Periodic boundary condition 21
2.4.4.4 Densification of C-S-H 23
2.4.4.5 Impingements 24
2.5 Limitations of the platform 25
2.6 Conclusions 26
References 26

Chapter III Modeling the effect of fineness and filler in early age hydration of tricalcium silicate 29

Abstract 29
3.1 Introduction 30
3.2 DVG Hypothesis and mathematical modeling 32
3.3 DVG mechanism in CemRS modeling platform 36
3.3.1 Generating the particle size distributions 36
3.3.2 Assumptions and simplifications of the model 36
3.3.3 Layered densification 37
3.3.4 Depth of dissolution 37
3.4 Simulations in CemRS 38
3.4.1 Simulation of published experimental results 38
3.4.2 Simulation of original experimental results 40
3.4.2.1 Materials and Characterization 40
3.4.2.2 Experimental procedure 41
3.4.2.3 Results 43
3.4.2.4 Simulations 44
3.5 Discussion 48
3.5.1 C-S-H densification 48
3.5.2 Outer growth rate 48
3.5.2.1 Effect of particle size on the growth rate 49
3.5.3 Filler effect 50
3.5.4 Calibration and prediction 50
3.6 Conclusions 51
References 51

Chapter IV Effect of the densification of C-S-H on hydration kinetics of tricalcium silicate 55

Abstract 55
4.1 Introduction 56
4.1.1 Densification of C-S-H 56
4.2 Experimental Protocol 58
4.2.1 Materials 58
4.2.2 Temperature profiles 58
4.2.3 Isothermal calorimetry 59
4.2.4 Thermogravimetric analysis 59
4.2.5 Quantitative X-ray diffraction 60
4.2.6 X-ray compositional micro analysis 61
4.3 Experimental Results 61
4.3.1 Effect of water to cement ratio 61

4.3.2 Effect of temperature profile 67
4.4 Activation Energy 70
4.5 Proposed Mechanism 72
4.6 Conclusion 74
References 74

Chapter V A quantitative study of the C_3A hydration 79
5.1 Introduction 79
5.1.1 Hydration of C_3A 79
5.2.2 Kinetics of reaction 80
5.2 Experimental protocol 83
5.2.1 Materials 83
5.2.2 Sample preparation 83
5.2.3 Experimental techniques 84
5.3 Experimental results 85
5.3.1 Hydration of C_3A without gypsum 85
5.3.2 Hydration of C_3A with added gypsum 87
5.3.2.1 Effect of gypsum content 87
5.3.2.2 Effect of fineness of C_3A 88
5.3.2.3 Effect of w/c 89
5.3.2.4 Instantaneous activation energy 92
5.4 Numerical modelling 93
5.4.1 Theory & Assumptions 94
5.4.2 Numerical simulations & Validation 97
5.5 Discussion 103
5.5.1 Before depletion of gypsum 103
5.5.2 After gypsum depletion 104
5.5.2.1 Arguments for a dissolution controlled mechanism 105
5.5.2.2 Arguments against nucleation and growth based mechanism 107
5.7 Conclusions 107
References 108

Chapter VI Hydration of polyphase C_3S-C_3A model cements in the presence of Na_2SO_4 113
6.1 Introduction 113
6.1.1 C_3S hydration 114
6.1.2. C_3A hydration 115
6.1.3. Hydration of C_3S-C_3A model systems 117
6.2 Experimental protocol 118
6.2.1 Materials 118
6.2.2 Methodology 120
6.2.2.1 Isothermal calorimetry 121
6.2.2.2 Hydration stoppage 121
6.2.2.3 Thermogravimetric analysis 121
6.2.2.4 Quantitative X-ray diffraction 121
6.2.2.5 ^{29}Si MAS NMR 122
6.2.2.6 ^{27}Al MAS NMR 123

6.3 Results 123
6.3.1 Studying hydration kinetics using isothermal calorimetry 123
6.3.1.1 Effect of sulphates on the hydration kinetics 123
6.3.1.2 Effect of fineness on the hydration kinetics 126
6.3.2 Study on paste after hydration stoppage 127
6.3.2.1 ^{29}Si MAS NMR 127
6.3.2.2 ^{27}Al MAS NMR 129
6.3.2.3 TGA 129
6.3.2.4 X-ray diffraction 129
6.3.3 Comparison of the results from the different experimental techniques 130
6.3.3.1 Degree of hydration 130
6.3.3.2 Portlandite content 133
6.3.3.3 Ettringite content 135
6.4 Discussion 137
6.4.1 Hydration kinetics of C_3S 137
6.4.2 Hydration kinetics of C3A 139
6.4.3 Implications of use of Na_2SO_4 in Portland cement systems 140
6.5 Conclusions 141
References 141

Chapter VII Conclusions and Perspectives 147
7.1 Hydration of C_3S in pure systems 147
7.2 Hydration of C_3A-gypsum systems 148
7.3 Hydration of C_3S-C_3A systems 150
7.4 Future Perspectives 151

Appendix I 153
Appendix II 161
Appendix III 163

List of figures

		Page No.
	Chapter I	
Fig. 1.1	Effect of Na_2SO_4 on the strength of OPC, White cement (WC), OPC replaced with 50% fly ash (OPC 50%), WC replaced with 50% fly ash (WC 50%) at 3, 7 and 28 days.	**4**
Fig. 1.2	Structure of the PhD thesis	**6**
	Chapter II	
Fig. 2.1	Schematic of hydration in Jennings and Johnson's model; Microstructural image (Left); Adjusting for overlaps (Right)[4]	**10**
Fig. 2.2	Schematic of hydration of cement grains in HymoStruc microstructure model[5]	**11**
Fig. 2.3	Microstructure developed from CemHyd3D for a Type I OPC paste after 14 days of hydration[2]	**12**
Fig. 2.4	Microstructure simulated with HydratiCA for an idealized OPC paste after 180 min hydration[2]	**13**
Fig. 2.5	Microstructural slice from µic of C_3S at w/c of 0.5 for a degree of hydration of 0.5; Red –C_3S, blue – C-S-H, green – CH, black – pores/water	**14**
Fig. 2.6	Effect of truncation of PSD on the degree of hydration of alite using a modified BNG model. UT - PSD without truncation, T 0.2 - PSD truncated at 0.2µm, T 0.5 - PSD truncated at 0.5µm	**15**
Fig. 2.7	Effect of truncation of PSD on the number of simulated particles and numerically calculated Blaine surface area	**15**
Fig. 2.8	Effect of number of particles on the required simulation time	**16**
Fig. 2.9	Simplified structure of CemRS	**17**
Fig. 2.10	Statistical particle size distribution	**18**
Fig. 2.11	Logical overview of modelling and validating a hypothesis in CemRS	**19**
Fig. 2.12	Dissolution of C_3S and growth of C-S-H at a particular time step	**19**
Fig. 2.13	2D image slice of; non-periodic boundary (left), periodic boundary (right)	**22**
Fig. 2.14	Schematic representation of periodic boundary condition in 2D (adapted from[14])	**22**
Fig. 2.15	Scanning transmission electron microscopy images of C_3S hydration	**24**
Fig. 2.16	Discretization of layers of C-S-H	**24**
Fig. 2.17	Overlaying cubic grid on the vector microstructure (from[14])	**25**
	Chapter III	
Fig. 3.1	Flowchart of DVG Model	**32**
Fig. 3.2	Conceptual volumetric densification and growth of C-S-H around C_3S shrinking core grain (top) and filler (bottom)	**33**

Fig. 3.3	Cumulative particle size distributions of alite fractions taken from published experimental results [9] (Set #1)	**39**
Fig. 3.4	Rate of heat release of alite fractions from published experimental results [9] (Set #1)	**39**
Fig. 3.5	Microstructural slices of particle fractions before the start of reaction (Set #1)	**39**
Fig. 3.6	Comparison of rate of heat evolution and degree of hydration of different alite fractions on the simulation and published experimental results	**40**
Fig. 3.7	Left: Particle size distribution of original experimental results of three different fineness of C_3S (a30, a36, a44) and two quartz powders (Qz28 and Qz45) and slag (sg). (Set #2). Right: Particle size distribution of original experimental results of C_3S (AN) and two quartz powders (Qc and Qf) and three fly ashes (f10, f20 & fU). (Set #3)	**41**
Fig. 3.8	Isothermal calorimetry data for the original experimental results for different mix compositions given in Table 2 (Set #2)	**43**
Fig. 3.9	Isothermal calorimetry data for the original experimental results for different mix compositions given in Table 3 (Set #3)	**43**
Fig. 3.10	Portlandite content from isothermal calorimetry (line) and TGA (marker) for pastes with 100% alite, and 33% of alite replaced with fly ash and quartz	**44**
Fig. 3.11	Comparison of rate of heat evolution and degree of hydration of different mixes on the simulation and results from original experimental data (Set #2)	**45**
Fig. 3.12	Comparison of rate of heat evolution and degree of hydration of different mixes on the simulation and results from original experimental data (Set #3)	**46**
Fig. 3.13	Microstructural slices of simulation from Set #2. a) #2 M1 at time=0, b) #2 M1 at time=20hr, c) #2 M3 at time=0, d) #2 M3 at time=20h. grey – alite, white – hydration products.	**47**
Fig. 3.14	Microstructural slices of simulation from Set #2. a) #3 M4 at time=0, b) #3 M4 at time=20hr, c) #3 M5 at time=0, d) #3 M5 at time=20h. grey – alite, white – hydration products.	**47**
Fig. 3.15	Densification of C-S-H, Unfractioned C_3S (Set #1), for time 0, 8hrs and 20hrs (left to right)	**48**
	Chapter IV	
Fig. 4.1	Particle size distribution obtained from laser diffraction for the three particle fineness of C_3S used in the study	**58**
Fig. 4.2	Temperature regimes used in the study (in °C)	**59**
Fig. 4.3	Effect of w/c on cumulative heat release of 'An' at 20°C up to 28 days (top) Heat release up to 7 days for w/c 0.5 and 0.6 at 40°C (bottom)	**62**
Fig. 4.4	Comparison of the chemically bound water associated with the decomposition of C-S-H measured from thermal analysis for '*An' at* w/c ratio 0.5 and 0.66 at 20°C (1, 3, 7 and 28 days) and 40°C (1, 3, 7, 28 days)	**63**
Fig. 4.5	Comparison of the degree of hydration of 'An' calculated from isothermal calorimetry and quantitative X-ray diffraction	**64**

Fig. 4.6	Effect of w/c on C/S ratio measured using EDS (10kV) and WDS (15kV) on polished samples of *'An'* after 7 days of hydration.	**66**
Fig. 4.7	Effect of w/c (0.4, 0.5, 0.66) on the portlandite content (per 100g anhydrous) calculated from thermal analysis for 'An' at 20 °C (top) and 40 °C (bottom)	**66**
Fig. 4.8	C/S ratio calculated for 'An' by coupling the degree of hydration and portlandite content from isothermal calorimetry and TGA (top) and from QXRD and TGA (bottom).	**68**
Fig. 4.9	Isothermal calorimeter results at 20°C and 40°C for three particle fineness Ac, An and Af (w/c: 0.5). Rate of heat release up to 1 day (top) and degree of hydration calculated from the cumulative heat release up to 7 days (bottom).	**68**
Fig. 4.10	Effect of different temperature profiles (Fig. 2) on the hydration kinetics of three particle fineness (w/c: 0.5); a) An (calorimeter data and TGA data indicated by blue and black markers referring to the degree of hydration calculated using portlandite content); b) Ac (calorimeter data); c) Af (calorimeter data).	**69**
Fig. 4.11	Portlandite content (per 100 g of paste) in 'An' at all temperature profiles (Fig. 2) up to 28 days (w/c: 0.5).	**70**
Fig. 4.12	Rate of heat release vs degree of hydration at 20°C and 40°C (w/c: 0.5)	**71**
Fig. 4.13	Activation energy calculated for the three-different fineness at w/c 0.5 using Eq. 6	**72**
Fig. 4.14	Instantaneous activation energy calculated for '*Ac'*, '*An'* and '*Af'* for w/c 0.5. Dashed line indicates the calculated average activation energy	**72**
Fig. 4.15	Backscattered electron image of cement paste hydrated for 13 hours which shows Hadley grains	**73**

Chapter V

Fig. 5.1	A typical heat release curve of C_3A hydration	**81**
Fig. 5.2	Particle size distributions of gypsum and different fineness of C_3A (Ac, Af)	**83**
Fig. 5.3	^{27}Al MAS NMR spectra of anhydrous C_3A	**85**
Fig. 5.4	Degree of hydration of C_3A (Ac) without gypsum at 0.5 and 1 w/c	**85**
Fig. 5.5	Quantification of phases in hydrated C_3A without gypsum measured from ^{27}Al MAS NMR	**86**
Fig. 5.6	TG and DTG curves for C_3A (Ac) without gypsum at 1 & 7 days for w/c 0.5 & 1.	**86**
Fig. 5.7	XRD (CuKα) patterns of C_3A (Ac) without gypsum at 1 & 7 days with w/c 0.5 and 1	**87**
Fig. 5.8	Rate of heat release (left) and cumulative heat release (right) measured from isothermal calorimetry for C_3A(Af) with different amounts of gypsum	**88**
Fig. 5.9	Effect of fineness on the rate of heat release and cumulative heat release until 7 days as measured from isothermal calorimeter	**89**
Fig. 5.10	Al in total hydrates(DoH), C_3AH_6 and AFm as measured from ^{27}Al MAS NMR on Ac and Af at 7 days with w/c 1.	**89**
Fig. 5.11	Effect of w/c ratio on the rate of heat release (left) and cumulative heat release (right) of C_3A (Ac) measured from isothermal	**90**

	calorimetry for 10% gypsum (w/c 0.5 & 1) and 20% gypsum (w/c 0.36, 0.5 & 1) content.	
Fig. 5.12	Al in total hydrates (DoH), C_3AH_6 and AFm as measured from ^{27}Al MAS NMR on 10% gypsum and 20% gypsum at 7 days with w/c 0.5 & 1	**91**
Fig. 5.13	Qualitative analysis from XRD (CuKα) of AFm phases with 10% and 20% gypsum at w/c 0.5 and 1 at 7 days	**91**
Fig. 5.14	Effect of additional water injected during the calorimetry measurement after 24 hours	**92**
Fig. 5.15	Instantaneous activation energy	**95**
Fig. 5.16	Effect of dissolution rate on rate of heat release	**96**
Fig. 5.17	Effect of the parameter c_2 on the dissolution rate and on the rate of heat release	**97**
Fig. 5.18	Effect of the parameter c_3 on the dissolution rate and on the rate of heat release	**99**
Fig. 5.19	Comparison of results from model and experiments for Af at 20%, 33% and 45% gypsum; Rate of heat release (left); Cumulative heat release (right)	**100**
Fig. 5.20	Comparison of results from model and experiments for Ac at 10% and 20% gypsum	**101**
Fig. 5.21	Degree of hydration measured from isothermal calorimetry (line), ^{27}Al MAS NMR (marker)	**102**
Fig. 5.22	Comparison of variation of dissolution rate with respect to degree of hydration calculated from the simulations for Ac (blue) and Af (black) at w/c 1	**102**
Fig. 5.23	Evaporable water as measured from model and experiments (TGA and NMR) for coarse C_3A (Ac); Lines: Model, Marker: Experiments	**103**
	Chapter VI	
Fig. 6.1	Typical heat release curve and stages of C_3S hydration	**114**
Fig. 6.2	Typical heat release curve and stages of C_3A-gypsum hydration	**117**
Fig. 6.3	Particle size distributions of different polyphase C_3S-C_3A model cements used in this study	**119**
Fig. 6.4	Effect of gypsum content and Na_2SO_4 on the rate of heat release for p90 systems until 30h; Without Na_2SO_4 (left), with Na_2SO_4 (right)	**124**
Fig. 6.5	Effect of gypsum content and Na_2SO_4 on the cumulative heat release of hydration of p90 until 7 days of hydration	**125**
Fig. 6.6	Effect of gypsum content and Na_2SO_4 on p93 systems; the rate of heat release until 24h (left); cumulative heat release until 7 days (right)	**126**
Fig. 6.7	Effect of fineness of p90 on rate of heat release Effect of fineness of p90 on the cumulative heat release	**126**
Fig. 6.8	Effect of p93_C on rate of heat release Effect of p93_C on cumulative heat release	**127**
Fig. 6.9	Degree of hydration of C_3S and C_3A measured from QXRD and ^{27}Al and ^{29}Si MAS NMR	**131**
Fig. 6.10	Measured heat from isothermal calorimetry vs calculated heat from XRD and NMR	**132**
Fig. 6.11	Effect of Na_2SO_4 on degree of hydration of C_3S and C_3A at 1 and 7 days	**133**

Fig. 6.12 Portlandite content from TGA and XRD **133**
Fig. 6.13 Degree of hydration of C_3S vs portlandite content for N$ and water **134**
Fig. 6.14 Comparison of the mean chain length with and without Na_2SO_4 **134**
Fig. 6.15 Ettringite content from NMR and XRD **135**
Fig. 6.16 Percentage of aluminates present as AFt, AFm in 1 and 7 days and percentage of aluminate involved in the C_3A reaction during 1 to 7 days **136**

Appendix II

Fig. A2.1 Comparison of the heat release from [1] and from numerical model **161**

Appendix III

Fig. A3.1 Deconvolution of anhydrous p90 **163**
Fig. A3.2 Example of a deconvolution for hydrated paste **164**
Fig. A3.3 Example of a deconvolution for hydrated paste: ^{27}Al MAS NMR deconvolution of p90_4g_N$_1d **167**

List of Tables

		Page No.
	Chapter III	
Table 3.1	Coefficients of simulation	**38**
Table 3.2	Mix compositions of Set #2 (%)	**42**
Table 3.3	Mix compositions of Set #3 (%)	**42**
	Chapter V	
Table 5.1	Simulation parameters for the different mixes and the degree of hydration calculated from model and ^{27}Al MAS NMR	**98**
Table 5.2	Effect of increase in fineness, gypsum content and w/c on simulation parameters in Table 5.1. – indicates no change, ↓ indicates a decrease and ↑ indicates an increase	
	Chaper VI	
Table 6.1	Polyphase C_3S-C_3A model cements used in the study	**119**
Table 6.2	Identification of mixes used in this study	**120**
Table 6.3	Results from ^{29}Si MAS NMR and ^{27}Al MAS NMR for all the samples.	**128**
Table 6.4	Results from TGA measurements and QXRD/Rietveld analysis	**130**
	Appendix II	
Table A2.1	Coefficients used for simulation	**162**
	Appendix III	
Table A3.1	Deconvolution of ^{27}Al and ^{29}Si NMR in the hydrated systems for all mixes of Table 6.1 in Chapter 6	**165**

Chapter I

General Introduction

Development of a country mainly lies in the development of its infrastructure, which includes construction of dams, bridges, buildings etc. Most of these infrastructures are made of concrete. The popularity of concrete is due to its low cost, ease of production and use, relative robustness, versatility and being a material with most of its bulk volume made of materials available in nature in abundance with very low processing, except cement. Ordinary Portland cement (OPC) developed in the 19th century revolutionized construction industry. Portland cement clinker is made from firing of limestone (calcium source) with other sources of silica, alumina and iron oxides (e.g. clay, bauxite, etc.) in a rotary kiln at 1450ºC. Although significant research has been carried out in OPC, there are still many aspects which are unknown. The major reason for this is the complexity of the material and the reactions involved.

1.1. Ordinary Portland Cement (OPC)

A Portland cement clinker mainly consists of four major mineral phases: Alite (tricalcium silicate, C_3S), Belite (dicalcium silicate, C_2S), Aluminate (tricalcium aluminate, C_3A) and Ferrite (Tetracalcium aluminoferrite, C_4AF). Alite, which comprises around 50-70% of the total composition in a typical OPC, is the primary phase in OPC. Alite is mostly responsible for the early age properties including hardening and strength development. The major reaction products of C_3S hydration are C-S-H (calcium silicate hydrate) and CH (Portlandite, Calcium hydroxide). While C-S-H contributes to the strength development in concrete, CH is instrumental in durability of reinforced concrete structures (RCC) as it increases the pH of concrete, thereby protecting the reinforcement steel with a passivation layer. CH also enhances the reactivity of supplementary cementitious materials (SCM) through pozzolanic reaction to produce additional C-S-H. C_3A, which is mostly found in lower quantities compared to other phases (2-10%), takes part significantly in the early age heat release and is instrumental in controlling the setting time. C_3A reacts readily with water and causes flash setting. To avoid this, gypsum is added in the system to control the reaction kinetics of C_3A. While C_2S and C_4AF are instrumental to contributing in the long-term properties, their contribution to the early age properties is rather limited owing to their lower reactivity.

1.2. Alternatives to OPC

Global warming due to CO_2 emissions, high energy consumption and reducing availability of raw materials are driving forces for cement industry to use more SCM as a partial cement replacement to reduce the clinker factor (percentage of clinker in cement). Geopolymers or

alkali activated materials (AAM), facilitates 100% replacement of OPC. However, the need for using higher amounts of blast furnace slags or energy intensive sodium silicates (Na_2SiO_3) for a comparable mechanical performance with respect to OPC[1] makes it more desirable to use blended cements by partially replacing OPC with supplementary cementing materials (SCMs). Blended cements have been increasingly used for the past couple of decades and are presently used almost exclusively. The global clinker factor is estimated to be around 77-78% currently and are projected to reach around 71% by 2050[1,2]. Although European standards permit the use of 40-95% of blast furnace slag (CEM III), the use of fly ash is limited to 6-35% (CEM II) in blended cement.

SCMs are classified based on their origin as natural and artificial. However, the origin does not have an effect on its reactivity. Most of the SCMs used are by-products from other major industries, for e.g. fly ash from thermal power industry and blast furnace slags from iron industry that have estimated global annual productions of around 1 billion tons and 360 million tons respectively[3]. Other SCMs that are available in large quantities in a global scale include 1) natural resources such as limestone (primary raw material for production of cement) and clay deposits (require energy intensive processing to produce reactive calcined clays) and 2) industrial residues and by-products (biomass ash, MSWI ash, silica fume, steel and copper slag, other non-ferro slag, waste glass, bauxite residue, etc.) which need further research and technology development for their valorisation and implementation[3,4]. Concrete serves as an effective sink for these waste materials, which otherwise proves to be costly to be disposed without creating much ecological footprint. Based on chemical composition, SCMs can be broadly classified as calcites(limestone), silicates (silica fume), calcium silicates (blast furnace slag), calcium aluminosilicates (class C fly ash) and aluminosilicates (metakaoilin, natural pozzolona, calcined clay, class F fly ash). Blast furnace slag is almost fully used due to its high reactivity and efficiency. However, its availability is estimated to reduce over the decades compared to the demand of cement[3]. On the other hand, less than half of the fly ash produced globally is used in cement[5] primarily due to its lower/slower reactivity and reduced early age performances. A strategy to increase the use of fly ash, and thus reduce the clinker factor further is based on enhancing its reactivity by means of mechanical, thermal and chemical activation. For this purpose, significant initiatives have been already taken.

An efficient and a promising approach to activate fly ash in blended cement is chemical activation using sodium sulfate (Na_2SO_4). Literature results indicate that, compared to blended systems, hybrid cement systems, which are activated with sodium sulfate, have no strength reduction at later ages while there still is a significant early age strength increase[6-8]. This is unlike when activated with strong alkali hydroxides (NaOH/KOH) which accelerate early age hydration and increase the early age strength[9]. However, there is a significant reduction in later age strength and increased porosity[9,10]. Compared to systems with or without alkali hydroxides, addition of Na_2SO_4 leads to a higher degree of hydration of FA, and a higher bound water content, both indicative for an overall enhanced reaction[11-13].

1.3. Motivation for the current research

Construction activities have long history aging from the start of civilizations. It is indeed possible to erect buildings or structures which would last for centuries or even for thousands of years without a proper scientific understanding of the materials being used or understanding the mechanics as we do today. Hence it is common among laymen to ask researchers working in the field of civil engineering the need for studies in this subject. But engineering is not just erecting structures or designing a building, it must be also economical. One need to construct a structure economically with minimal wastage to call it an engineered structure. Based on the knowledge we have today, we consider many of those structures which are lasting for few thousands of years are at times overdesigned structures. A scientific and sustainable approach based on today's knowledge is needed in the current scenario to allow society to improve its infrastructure needs using precious raw materials to their full potential considering the needs for the next generations to come. One way to define sustainability is to meet the demands of today, without compromising the needs of tomorrow.

While the field of structural mechanics came a long way with a better understanding on the basic laws of physics, there is still a long way to go for the construction material field. While the design of structural elements is now based on laws of engineering mechanics, the design of materials that are used (mostly concrete) is based on experiments. While experiments can provide much of the required information about the materials, it is not always feasible to just depend upon experimental results. For e.g. to study the risk of thermal cracking in mass concrete, it is not feasible to test such large structures experimentally. Or to study the durability aspects, which is typically done at laboratories under accelerated conditions. While a typical structure is designed to last for several decades or at times centuries, it is not possible to wait for the experiments for several years or decades to start the construction. In such cases, we need to have a model which could predict the material properties. While there is a substantial development in the field of mechanics of materials and durability models, the kinetics and microstructural development still mostly relies on experimental results. An analogy could be made with human beings, if the concrete structure is a person, the kinetics and microstructure is the DNA of that person. As will be explained in the subsequent chapters, a consensus has not been reached in the literature for the mechanisms which control the hydration kinetics of different phases of OPC and are still under active debate. Hence one of the primary objectives of this research is to **improve the fundamental understanding of the kinetics and microstructural development** of major Portland cement phases such as **C_3S and C_3A**, including the **mechanisms which are controlling those reactions and the synergy between them**.

A more scientific and fundamental understanding of Portland cement hydration is also necessary for the development of novel binder systems such as hybrid cements. When industrial by-products are added to OPC or when alkalis are added to enhance the hydration of the SCMs, it is necessary to understand how these additions affect the hydration of the Portland cement phases. In blended systems, SCMs mostly react in the pozzolanic reaction with the hydration products of C_3S and C_2S hydration, portlandite (CH), to precipitate additional C-S-

H. Latent hydraulic materials such as slags are activated by CH, alkalis or sulphates, and react to form C-S-H even in the absence of Portland cement.

Fig. 1.1 shows the unpublished initial results on the effect of Na_2SO_4 (0.98M) on the strength development in blended cements. When OPC is replaced with 50% fly ash, there is a significant drop in the compressive strength in all ages as expected. However, with the addition of Na_2SO_4, a significant increase in strength is achieved both in the early days and in the later ages. The strength at 28 days with 50% replacement with fly ash activated with Na_2SO_4 is even higher than the strength of 100% OPC at 28 days, the reason of which remains not clearly explained in the literature. To tailor this binder system as a general-purpose cement, it is first essential to identify the involved reactions and kinetics. Hence, it is also an objective of this thesis to **understand how Na_2SO_4 affects the hydration of two major phases of OPC (C_3S and C_3A).**

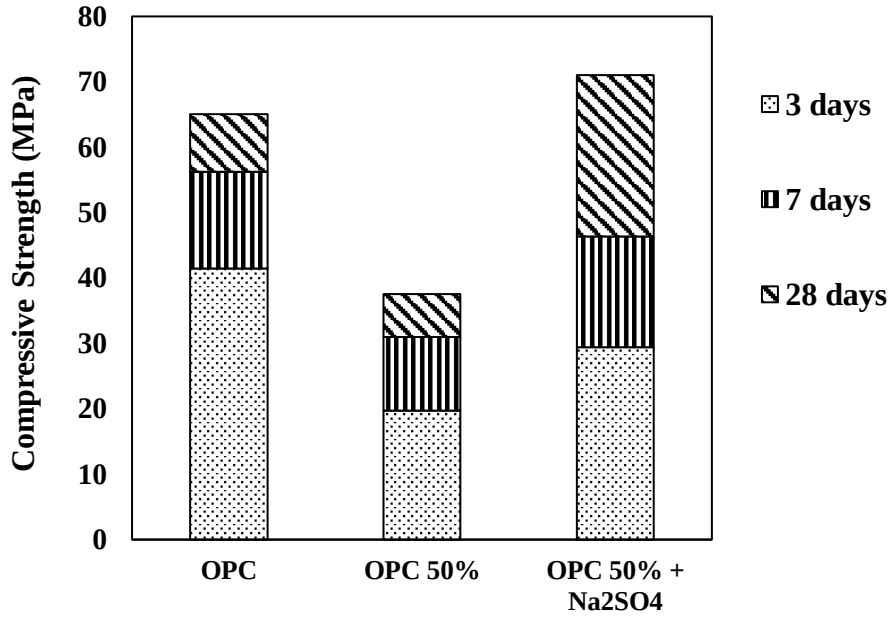

Figure 1.1: Effect of Na_2SO_4 on the strength of OPC, White cement (WC), OPC replaced with 50% fly ash (OPC 50%), WC replaced with 50% fly ash (WC 50%) at 3, 7 and 28 days.

1.4. Why studies on synthetic systems

Ordinary Portland cement or OPC is a large family of different cements. Like fingerprints, two different batches of cements can never be the same. There will always be some differences in their chemical composition or mineralogical composition or fineness of the material. Although small variations at times would not make a significant difference from an engineering point of view, it has far more bigger consequences on a scientific point of view. OPC is known to have a significant effect on the reaction rates with factors such as fineness, water to cement ratio (w/c), alkalis, gypsum content, curing conditions etc. These are cumulative effects of the coupled reactions of C_3S, C_3A, C_2S and C_4AF. Identification of the effect of each parameter on each phase is necessary to predict the behavior of a particular cement based on its chemical or

morphological composition. Another major advantage of using synthetic systems is the ease of quantification of data from the analytical techniques used. This is because, in OPC, there will be overlapping signals that will be measured from different analytical techniques, which makes it hard to accurately and precisely characterize and quantify these phases.

1.5. Scope and outline of the thesis

Apart from the General Introduction (Chapter 1) and Conclusions and Perspectives (Chapter 7), the thesis is structured in five main chapters. Fig. 1.2 shows a schematic overview of the chapters and shows how they are related to each other.

Chapter 2 introduces a new microstructural modelling platform, CemRS, that simulates the kinetics development of C_3S and C_3A hydration. CemRS ensures higher simulation speed without the need of truncation of particle size distribution and is suited to model different reaction mechanisms, where impingements of the hydration products are not assumed to influence the kinetics of reaction. The modelling platform is further used to simulate the mathematical models that are developed in Chapter 3 and Chapter 5.

Chapter 3 studies the effect of fineness and inert fillers on the hydration of C_3S. A new hypothesis based on the nucleation and growth based mechanism is proposed to explain the main hydration peak of C_3S in the presence of inert fillers. The hypothesis is further validated with numerical simulations in CemRS. The scope of the model is limited to the first 24 hours of hydration at constant temperature of 20ºC. The maximum replacement level of fillers is limited to 35%. The w/c is kept constant at 0.5 and the dilution effect due to the replacement of C_3S with fillers is not considered.

Chapter 4 further investigates the effects of different temperature regimes and w/c (0.4, 0.5 and 0.66) on the hydration and kinetics of C_3S beyond 1 day of hydration until 28 days of hydration using experimental techniques. A novel approach to measure the instantaneous activation energy is introduced. The effect of w/c on the C/S ratio of C-S-H is investigated. The experimental results are further subjected to scrutiny to study the validity of the hypothesis proposed in Chapter 3. The scope of the work is limited to triclinic C_3S with three different fineness and the temperature regimes consisted of 20ºC and 30ºC. The instantaneous activation energy is only measured at 1 and 3 days of hydration.

Chapter 5 investigates the effect of fineness of C_3A, addition of gypsum and w/c of the hydration kinetics of C_3A using experimental techniques and numerical modelling. The reaction mechanisms controlling the hydration before and after depletion of gypsum are further analyzed and new mechanisms to explain the experimental results are proposed. The degree of hydration is quantitatively measured from isothermal calorimeter and ^{27}Al MAS NMR. TGA is used to qualitatively study the hydration phases and to quantify the amounts of bound and evaporable water. XRD is used for qualitative study and not for quantitative analysis due to the lack of crystal data for the AFm phases and high preferred orientation of gypsum. The scope of the study is limited to 7 days of hydration and the effect of w/c is only investigated for the

coarse C_3A. Coarse C_3A is replaced with lower levels of gypsum contents (0%, 10% and 20%) while fine C_3A is replaced with higher levels of gypsum (20%, 33% and 45%).

Chapter 6 studies the effect of fineness, composition of C_3S & C_3A, the gypsum content and the addition of Na_2SO_4 on polyphase C_3S-C_3A systems. The mechanisms that control the reaction of C_3S and C_3A are further investigated in a polyphase system with different gypsum additions and, with and without Na_2SO_4. The effect of Na_2SO_4 is studied only on C_3S-C_3A polyphase model systems and not on pure C_3S or C_3A systems as they have been previously investigated[14-17]. The synergy between the C_3S and C_3A phases is also investigated. Two compositions of C_3S-C_3A polyphase cements (90:10 and 93:7) with two different fineness were used. The effect of varying w/c and temperature are out of the scope of this work and were kept constant at 0.5 and 20ºC respectively. The degree of hydration of C_3S and C_3A were quantitatively determined using ^{29}Si MAS NMR and ^{27}Al MAS NMR respectively along with quantitative XRD.

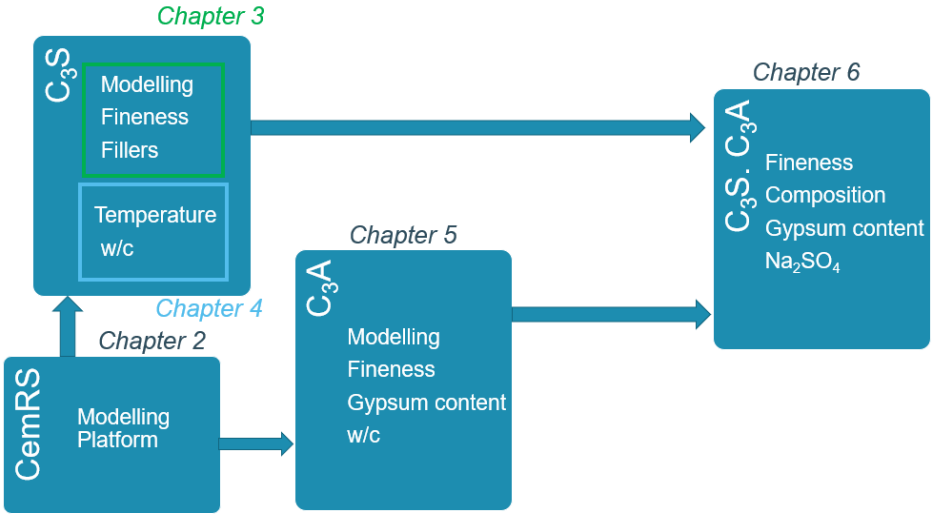

Figure 1.2: Structure of the PhD thesis

References

1. Scrivener K., John V. and E. Gartner (2016) “Eco-efficient cements: potential, economically viable solutions for a low-CO2, cement-based materials industry" *UNEP Report. United Nations Environment Programme*, Paris.
2. Schneider M., Romer M., *et al.* (2011) "Sustainable cement production - present and future" *Cem. Concr. Res.* **41**:642-650.
3. Snellings R. (2016) "Assessing, Understanding and Unlocking Supplementary Cementitious Materials" *RILEM Technical Letters* **1**:50-55.
4. Snellings R., Mertens G. and J. Elsen (2012) "Supplementary cementitious materials" *Rev. Mineral. Geochem.* **74**:211-278.
5. Scrivener K., Martirena F., *et al.* (2018) "Calcined clay limestone cements (LC^3)" *Cem. Concr. Res.* in press.

6. Lee C. Y., Lee H. K. and Lee K. M. (2003) "Strength and microstructural characteristics of chemically activated fly ash–cement systems" *Cem. Concr. Res.* **33**:425-431.
7. Jueshi Q., Caijun S. and Zhi W. (2001) "Activation of blended cements containing fly ash" *Cem. Concr. Res.* **31**:1121-1127.
8. Velandia D. F., Lynsdale C. J., *et al.* (2016) "Evaluation of activated high volume fly ash systems using Na_2SO_4, lime and quicklime in mortars with high loss on ignition fly ashes" *Constr. Build. Mater.* **128**:248-255.
9. Smaoui N., Berube M. A., *et al.* (2005) "Effects of alkali addition on the mechanical properties and durability of concrete" *Cem. Concr. Res.* **35**:203-212.
10. Sant G., Kumar A., *et al.* (2012) "The influence of sodium and potassium hydroxide on volume changes in cementitious materials" *Cem. Concr. Res.* **42**:1447-1455.
11. Donatello S., Fernandez-Jimenez A. and Palomo A. (2013) "Very high volume fly ash cements. Early age hydration study using Na_2SO_4 as an activator" *J. Am. Ceram. Soc.* **96**[3]:900-906.
12. Li C., Zhu H., *et al.* (2017) "Pozzolanic reaction of fly ashmodified by fluidized bed reactor-vapor deposition" *Cem. Concr. Res.* **92**:98-109.
13. Zhang Y. M., Sun W. and Yan H. D. (2000) "Hydration of high-volume fly ash cement pastes" *Cem. Concr. Comp.* **22**:445-452.
14. Mota B., Matschei T. and Scrivener K. (2015) "The influence of sodium salts and gypsum on alite hydration" *Cem. Concr. Res.* **75**:53-65.
15. Mota B. (2015) "Impact of alkali salts on the kinetics and microstructural development of cementitious systems" *PhD Thesis*, EPFL Switzerland.
16. Collepardi M., Baldini G. and Pauri M. (1978) "Tricalcium aluminate hydration in the presence of lime, gypsum or sodium sulfate" *Cem. Concr. Res.* **8**:571-580.
17. Sanchez-Herrero M., Fernandez-Jimenez A. and Palomo A. (2012) "Alkaline Hydration of Tricalcium Aluminate" *J. Am. Ceram. Soc.* **95**[10]:3317-3324.

Chapter II

CemRS: Fast and efficient modelling platform for the simulation of cementitious systems

2.1. Introduction[a]

Modelling hydration kinetics of ordinary Portland cement (OPC) based binders or cementitious binders in general is of great importance in understanding microstructural development of the paste matrix in concrete. This microstructure development is instrumental for the determination of many of the macroscopic properties of concrete such as strength development, autogenous shrinkage, thermal stresses, durability etc. Cement hydration typically involves complex coupled reactions that take place simultaneously. Primarily, there are three mechanisms which are involved in the hydration reaction. These are dissolution, diffusion, and nucleation and growth[1]. In the dissolution phase, ions are released into the pore solution from the anhydrous grains. Dissolution kinetics is dependent on the saturation level of the pore solution and the active surface area of the anhydrous grains through the formation of etch pits which are in contact with water. These ions diffuse outwards from the surface of the particles and capillary water diffuses inwards to contact with the anhydrous surface. The diffusivity depends on the specific properties of the diffusing species and diffusivity is reduced due to the presence of barriers that arise from the precipitation of hydrates. The diffused ions saturate the pore solution and hydration products are precipitated due to an increase in the supersaturation levels of the hydration products. These hydration products are precipitated heterogeneously on the surface of anhydrous grains/reactants or homogenously in the voids by the process of nucleation and growth. C-S-H, the main hydration product of OPC is nucleated heterogeneously closer to the surface of the anhydrous grains. Each of these mechanisms have different rates of reactions, and the slowest of these reactions is termed as the rate controlling mechanism. In addition, different cementitious materials or cementitious phases have different controlling reaction mechanisms. Even one material can have varying controlling mechanisms with the advancement of hydration, as is the case for C_3S hydration.

There are several models available, which uses a definite simplified set of rules to capture the kinetics of the hydrating materials[2]. Advantages of these models are that with certain levels of calibration with respect to the binder system under study, they can be used to fit the kinetic

[a] Part of this chapter was published as *Joseph S., Van Balen K., Bishnoi S., Cizer Ö. (2016). "CemRS: fast and efficient modelling platform for the simulation of cementitious systems". International RILEM Conference Materials Systems and Structures in Civil Engineering 2016 (MSSCE 2016) on Service Life of Cement-Based Materials and Structures: Vol. 2, Lyngby Denmark (pp. 573-579)*

data. This is further used to predict the mechanical and durability behaviors. On the other hand, the disadvantage is that many of these models are developed on hard wired set of rules and do not give the user the flexibility to tweak the rules to incorporate the latest scientific advancements. This was the basis for development of the microstructural modelling platform µic[3], as the user can develop different reaction mechanisms in accordance with the state of the art and can also test the mathematical validity of a hypothesis. However, requirement for large simulation time for realistic particle size distributions (PSD) limits the use of this modelling platform. Hence, a new microstructural modelling platform CemRS (**Cem**entitious **R**eaction **S**imulator) was developed in this doctoral work, which uses a statistical PSD approach that significantly reduces the time required for simulation without the need of truncation of PSD. This chapter first gives a comparative overview of the existing models of cement hydration and microstructure. This is followed by the new microstructural modelling platform CemRS. To position this model compared to existing models, an overview of the former is given in the next paragraphs.

2.2. Currently available models

2.2.1. Jennings & Johnson model (1986)

Jennings and Johnson[4] first proposed a microstructure-based model (Fig. 2.1) for C_3S hydration based on a vector approach. They used spherical particles to represent C_3S grains where the core shrinks with the advancement of hydration. A concentric growth of C-S-H was assumed to form around the anhydrous C_3S grains and calcium hydroxide (CH) was assumed to form in the capillary pores. The overlap of C-S-H or the impingements from the neighboring particles were calculated in the model and was further used to redistribute the hydration products. The low availability of the computational power at the time of development of the model prevented its further development. Nevertheless, the concepts presented in this model were later used for the development of new models such as HymoStruc and CemHyd3D.

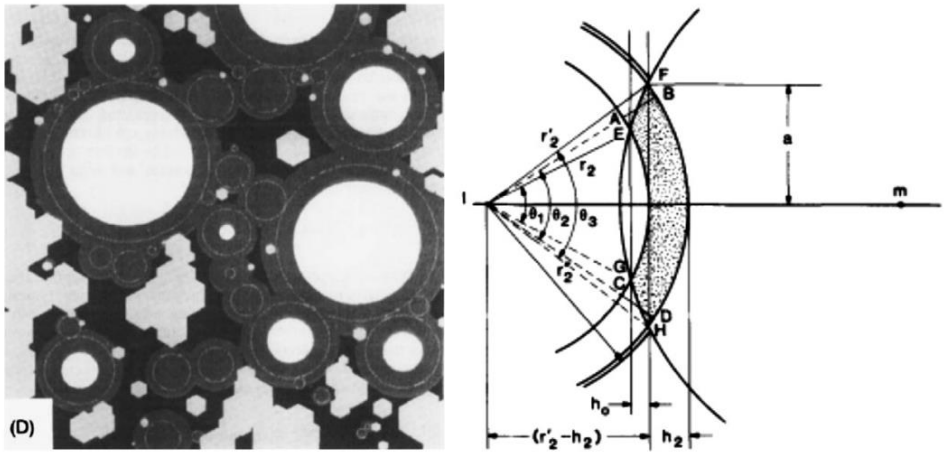

Fig. 2.1: Schematic of hydration in Jennings and Johnson's model; Microstructural image (Left); Adjusting for overlaps (Right)[4]

2.2.2. HymoStruc (1991)

HymoStruc (**Hy**dration, **mo**rphology and **struc**ture development) is a vector-based microstructure model (Fig. 2.2) for the hydration of cement-based materials developed by van Brugel[5,6] at TU Delft. The model is used to predict the strength development, autogenous shrinkage, pore size distribution, etc. The model assumes particles to be spherical. The particle size distribution is modelled using a Rosin-Rammler function and microstructure is modelled on representative elementary volume (REV). The kinetics of reaction is modelled based on a set of empirical equations which are dependent on the composition of cement, w/c, temperature etc., which are not fundamentally based[2]. However, the model does not offer users the flexibility in terms of modifying the kinetic model, which is required to study and to constitute a mathematical validation of the underlying reaction mechanisms in the hydration of the individual phases.

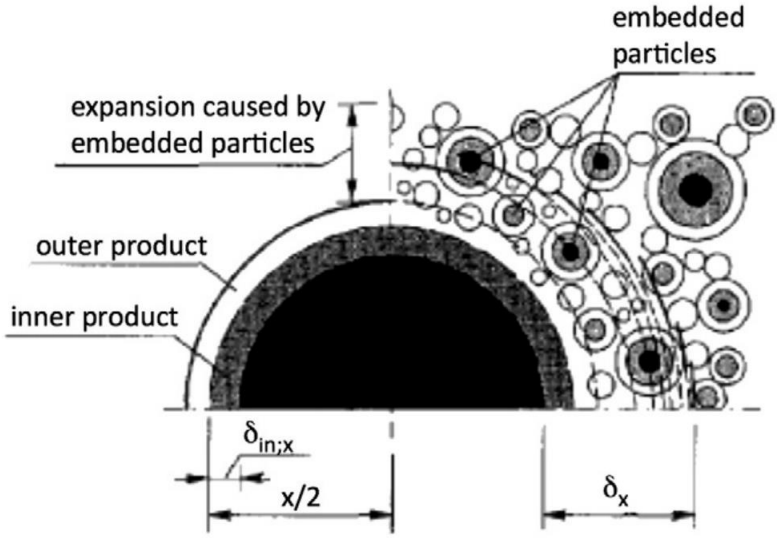

Figure 2.2: Schematic of hydration of cement grains in HymoStruc microstructure model[5]

2.2.3. CemHyd3D (1997)

CemHyd3D was developed by Bentz[7] at NIST, USA. This is a 3D microstructural model (Fig. 2.3) which uses a discrete approach for modelling the microstructure of cement paste. The advantage of using a discrete approach is that random particle shapes can be modelled by storing them in a grid of 3D cubic elements, which is more representative of a typical cement grain. Each of these cubic elements or pixels are represented as an anhydrous phase, hydrated phase or a pore filled with water. It uses a cellular automata approach where the information of the neighboring pixels is taken into account to model the diffusion of ions and dissolution of the phases. As the model uses grid elements for storing the hydrate and unhydrated phases or pores, it is well suited for micromechanical modelling using finite element method. The major limitation of the model is that it has to be calibrated for each experiment for modelling the kinetics of reaction, and thus cannot be used as a tool to predict the hydration due to the lack of a physical time scale parameter[2]. Another drawback is that truncation of PSD is

necessary as the minimum particle size cannot be lower than 1µm. This has a big impact on the modification of the specific surface and therefore a significant effect on modelling the nucleation and growth based mechanisms which is dependent on the initial surface area of anhydrous cement[8].

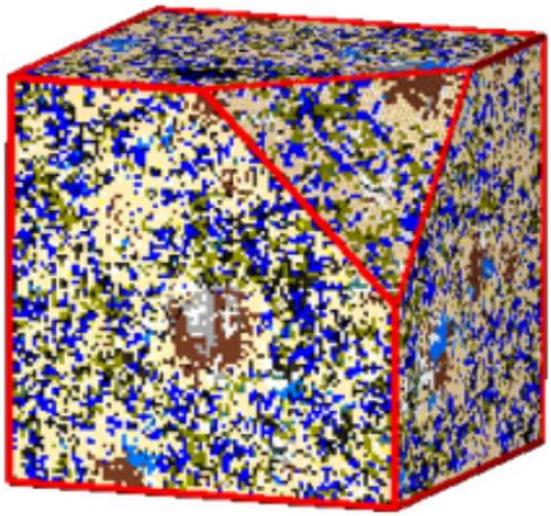

Figure 2.3: Microstructure developed from CemHyd3D for a Type I OPC paste after 14 days of hydration[2]

2.2.4. DuCOM (2003)

DuCOM (**Du**rability **M**odel for **CO**ncrete) was developed by Maekawa et al.[9] at the university of Tokyo, Japan. It uses empirical equations calibrated based on the sensitivity analysis from experimental results to model the reaction kinetics. It does not use the full PSD and uses the mean particle diameter using a single particle modelling approach. The model assumes a metastable barrier to account for the induction period in OPC hydration, and the acceleration period is modelled assuming the disintegration of the barrier layer. The deceleration period is modelled based on the diffusion of species on the layer of C-S-H that is formed on the surface of the cement grain. This model can be used to reasonably fit the kinetics data by varying the parameters and to determine the durability properties. Nevertheless, there is less fundamental basis for the kinetics of such a model and this model is also not useful for studying the mathematical validity of newly developed hypotheses.

2.2.5. HydratiCA (2007)

HydratiCA (**Hydra**tion by **C**ellular **A**utomata) was developed by Bullard[10,11] at NIST, USA (Fig. 2.4). While it uses several basic principles from its predecessor CemHyd3D, HydratiCA is developed on a more fundamental basis of cement hydration. It uses a cellular automata approach to model the mass transport of ions and phase transformations in the cement paste by dissolution, diffusion and nucleation and growth. HydratiCA does not need fitting parameters for calibration of the model as the calculations are based on the thermodynamic data from the literature. Nevertheless, all of these parameters are not available in the literature and hence it

needs to use an educated guess, which could have serious impacts on the simulated kinetics. The major drawback of this model is that it requires high computational power with requirement of multiple processors for simulations due to the requirement of small time steps for numerical stability[2].

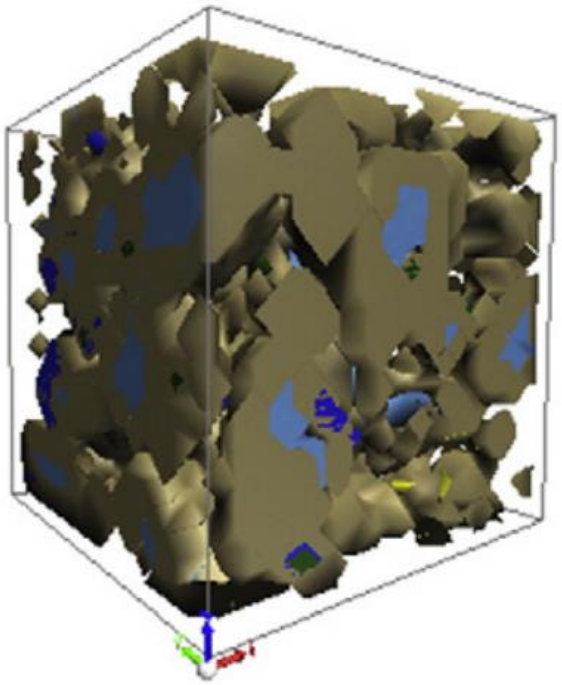

Figure 2.4: Microstructure simulated with HydratiCA for an idealized OPC paste after 180 min hydration[2]

2.2.6. µic (2008)

Microstructural modelling platform µic (pronounced as "mike") (Fig. 2.5) was developed by Bishnoi and Scrivener[3] at EPFL, Switzerland. The modelling platform uses a vector approach. Basic principles incorporated in µic were derived from IPKM (Integrated Particle Kinetics Model) that was developed by Navi and Pignat[12]. The fundamental distinguishing property of µic compared to the other models is that, users can define and modify the reaction mechanisms which control the reaction. This is done by adding a plugin to the program without the need to change the core of the platform. Because of this, debugging is much easier. There are fewer hard wired rules in µic. Hence, there is a certain level of flexibility provided for users to be able to define new rules that need to be followed for the simulation of the reaction kinetics. Therefore, this model is suited for developing models to test or validate new hypotheses for different cementitious binder systems. The platform uses spherical particles to represent cementitious particles, which are randomly distributed in a cubic computational volume. The major strength of this model is that it calculates the impingements occurring due to the growth of hydration products explicitly and efficiently. This is further used to redistribute hydration products and to calculate the free surface area. The platform captures the effect of densification of C-S-H with the progress of hydration. The major drawback of this platform is that it cannot use a statistical particle size distribution. Hence, to capture the effect of PSD, a truncated PSD

should be generated, which contains several millions or billions of particles depending on the computational volume and minimum size of the particles. Such an approach is necessary if one wants to use the microstructural information for simulating the kinetics. However, this has a serious impact on the computational time requirement. Depending on the number of particles that are simulated, it might take few hours or few days for a simulation up to 24 hours in a typical personal computer. Hence, calibration of parameters, which are studied using a trial and error method or refining the parameters for a better fit, will not be ideal.

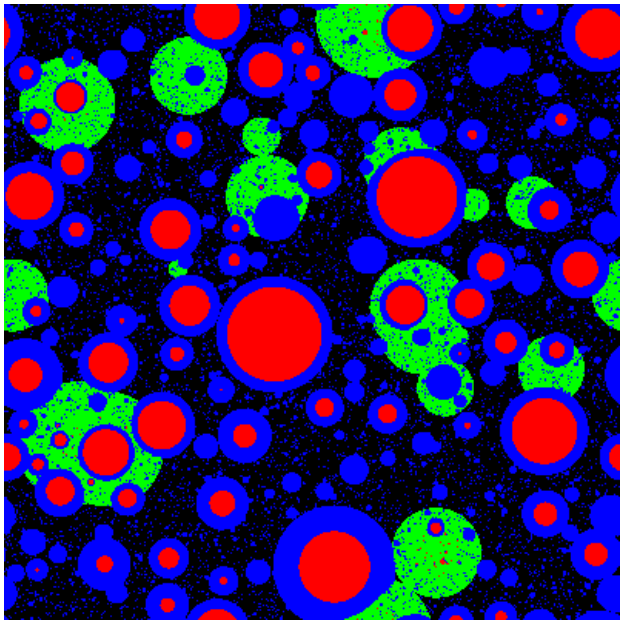

Figure 2.5: Microstructural slice from µic of C_3S at w/c of 0.5 for a degree of hydration of 0.5; Red –C_3S, blue – C-S-H, green – CH, black – pores/water

2.3. Effect of Truncation on degree of hydration

The effect of truncation of PSD on degree of hydration depends primarily on the mechanism of hydration. Assuming a uniform reactive thickness concept, a dissolution or diffusion based mechanism will hardly make significant errors on the numerical modelling scheme[8]. On the other hand, a nucleation and growth based mechanism, which takes into account the surface area of the reactants and products, will significantly have an effect on the degree of hydration.

Fig. 2.6 shows the effect of truncation of alite at 0.2 µm and 0.5 µm. Alite of 17 µm mean diameter and 3600 cm^2/g Blaine surface area is simulated using a modified boundary nucleation and growth (BNG)[13] mechanism. A deviation from the non-truncated PSD can be observed for PSD with truncation. In the modified BNG, it was assumed that individual particles, which are fully hydrated, will not grow further. This assumption in effect reduces the deviation from the original PSD drastically. Hence, this is a very modest account on the effect of truncation.

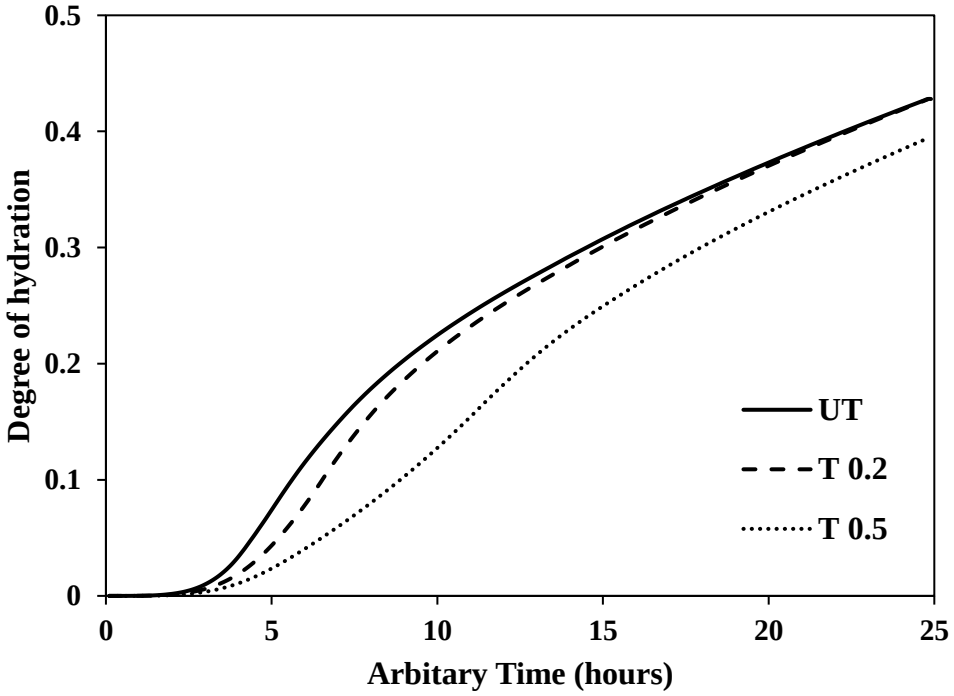

Figure 2.6: Effect of truncation of PSD on the degree of hydration of alite using a modified BNG model. UT - PSD without truncation, T 0.2 - PSD truncated at 0.2µm, T 0.5 - PSD truncated at 0.5µm

The effect of truncation on the number of particles and calculated Blaine surface area is illustrated in Fig. 2.7. It is evident that truncation of PSD can reduce the number of particles significantly and hence the computational cost for traditional modelling platforms (Fig. 2.8). However, at the same time, this truncation has a large effect on the surface area of the particles. As most nucleation and growth models assume uniform growth rate on particles, the difference in the outer surface area of the products will be at a much larger scale.

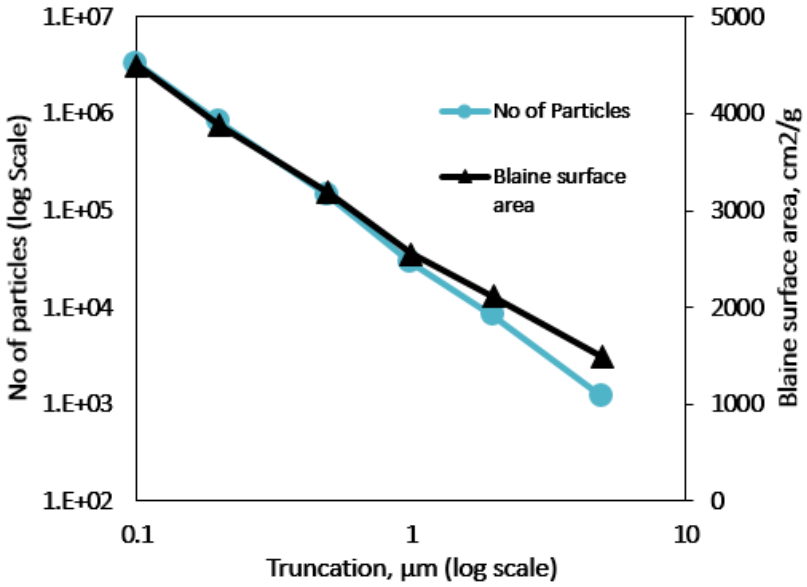

Figure 2.7: Effect of truncation of PSD on the number of simulated particles and numerically calculated Blaine surface area

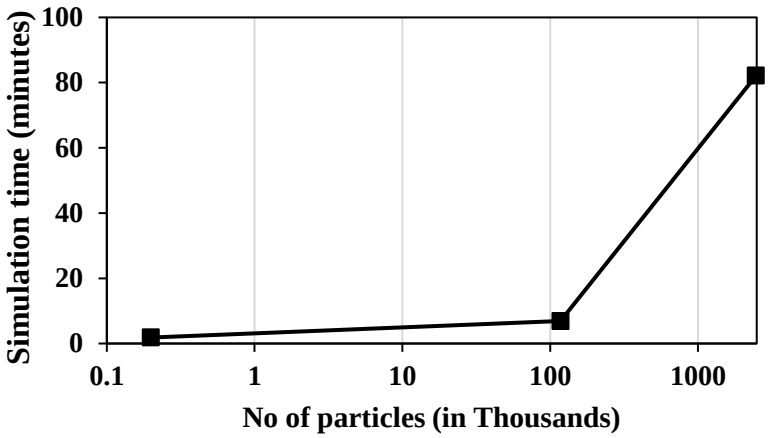

Figure 2.8: Effect of number of particles on the required simulation time[14]

2.4. CemRS modelling platform

CemRS is a microstructural modelling platform developed entirely in C++ using the object oriented approach. Much of the basic principles of this modelling platform are derived from µic[3]. The primary objective of CemRS is to simulate the kinetics of reaction of different cementitious systems without the need for truncation of the PSD for the mathematical validation of the hypothesized reaction mechanism under scrutiny. It should be noted that the ability of the model to capture the hydration kinetics does not automatically prove the hypothesis but aids the experimental evidences. Since the statistical particle modelling approach ensures low computational costs, it is ideal to calibrate and refine parameters using a trial and error approach. The microstructural information available from the model can be further developed in future for micromechanical modelling or for predicting the mechanical properties.

2.4.1. Structure of CemRS

The modelling platform CemRS was developed with different independent classes (modules). The modules were designed to be independent to ensure maximum flexibility to customize each module in the future. The interdependencies of these modules are restricted by using output text files to communicate within these classes. Although this reduces the efficiency of the program, it is easier for users who may not be an expert in programming, to replace or further develop an existing module.

A simplified structure of CemRS is given in Fig. 2.9. Different types of particles could be defined in CemRS (such as C_3S, C_3A, inert fillers etc.) considering the material properties such as specific gravity, PSD, nature of material (such as inert or hydraulic) etc. Each of these particles are modelled using a statistical particle size distribution and a truncated particle size distribution. The statistical PSD is further used for modelling the kinetics of reaction, whereas the truncated PSD is used to model the microstructure. It should be noted that, it is possible to use a truncated PSD for modelling kinetics of reaction as well. However, in the context of this thesis, the cost outweighs the benefits. The user could define the reaction mechanism which

better represents a proposed hypothesis. It is possible to make use of the several predefined functions or completely develop new functions. The reaction mechanism is calibrated with available datasets from the literature or by curve fitting. The kinetics of reaction and the microstructure development are given as outputs. If the user is only interested in simulating the kinetics of reaction, and is not bothered about the microstructure development, it is possible to disable those modules. This would further speed up the simulation.

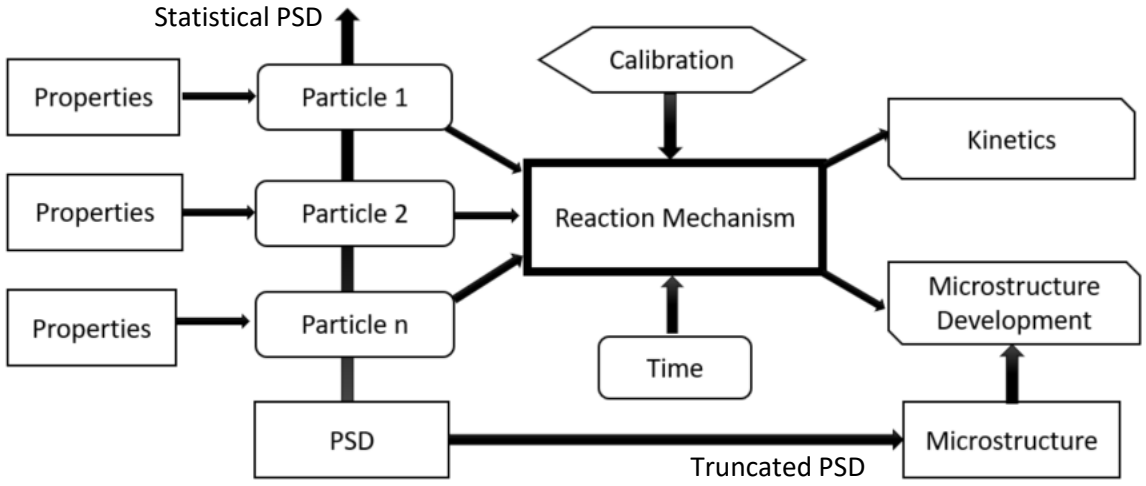

Figure 2.9: Simplified structure of CemRS

2.4.2. Modelling PSD

CemRS uses two approaches to model PSD. A statistical PSD which is used for simulating the kinetics of reaction, and a truncated PSD (which uses a full list of particles that needs to be defined independently) which is primarily used to recreate the microstructure. In both cases, the PSD obtained from laser diffraction is used. An additional standalone module, which uses the Blaine surface area to recreate the cumulative PSD using a Rosin-Rammler equation, is also developed. In this module, an initial median diameter (d_m) of the particles and particle distribution width (w_d) are assumed, and particles are generated according to the Rosin-Rammler equation (Eq. 2.1), where *'f'* is the fraction of particles below diameter *'d'*. The surface area of the particle size distribution is calculated and is reiterated by varying median diameter and/or width until the surface area becomes within the acceptable range with respect to the Blaine surface area.

$$f = 1 - \exp\left(-\left(\frac{d}{d_m}\right)^{w_d}\right) \tag{2.1}$$

The statistical PSD is modelled in CemRS by calculating the number of particles present in a particular range of diameter. This is derived from the cumulative PSD input given to the model from the laser diffraction experiment. The number of points, which are used to measure, and the ranges of particle size used for modelling are determined by the user. By default, the range

of particle diameters are given as 0.01µm for particles < 1µm, 0.1µm for particles >1µm & <10 µm, 0.2 µm for particles > 10 µm & < 100 µm and 1 µm for particles >100 µm. This typically generates 640 particle range (assuming 300 µm maximum diameter) that is much higher than the original PSD input. Fig. 2.10 shows the original PSD from the analysis, the modelled PSD and the number of particles at each particle size. The discontinuity of the number of particles at 0.05µm is because the minimum diameter of particles from the laser diffraction experiments is 0.055µm while the model uses 0.01µm as the minimum particle diameter. The discontinuity at 1µm and 10 µm is due to the variation of the range of particles which is used. The number of particles is calculated assuming a computational volume of $1mm^3$ of paste. It could be noted that several billions of particles occupy in such a computational volume and it is not feasible to simulate billions of particles without a statistical approach. The number of particles for the largest particles are fractions due to the lower size of the computational volume($1mm^3$). Nevertheless, these fractions do not deviate the results on simulations and it represents significantly larger computational volumes. It should be noted that choosing wider ranges for larger particles could avoid the fractions.

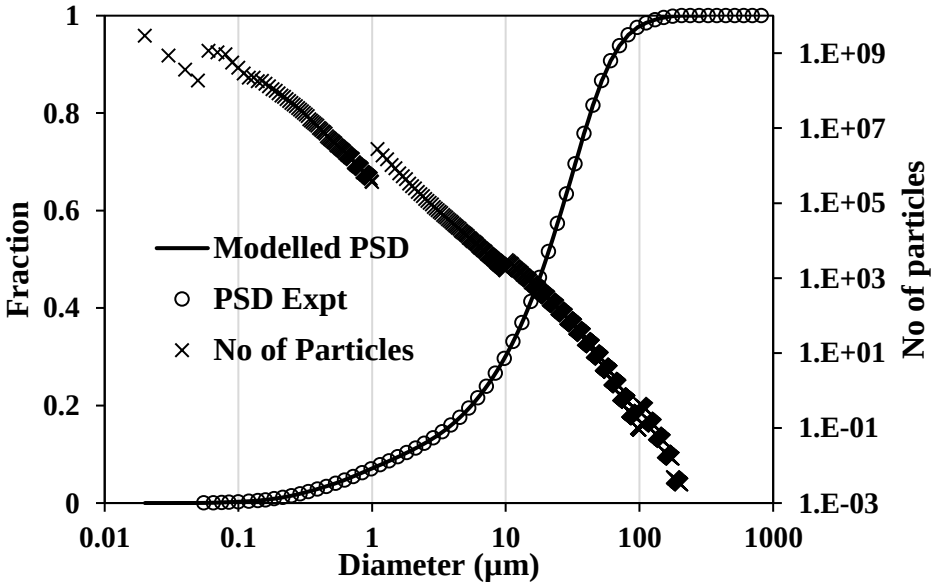

Figure 2.10: Statistical particle size distribution

2.4.3. Modelling kinetics

The most important aspect of CemRS similar to µic is that, the user need to define the kinetic model. This is only logical as different systems have different reaction mechanisms and using a same model for different systems will not have any fundamental basis. Hence, the user can use a predefined model for a particular system or modify the predefined model or create a new model from scratch to capture the hypothesis developed for that system scientifically. The logical flow for such an approach is given in Fig. 2.11. A hypothesis must be developed first based on the experimental evidences. A mathematical model needs to be further developed based on the hypothesis which will be analyzed in CemRS. The next step is to implement the mathematical model in a numerical modelling scheme in CemRS. The parameters are

calibrated based on the experimental data available or from the model using curve fitting. Simulations incorporating the PSD is used for validation. The validation could be based on the kinetic output from the model or from the microstructural information such as the growth rate, dissolution depth, porosity etc. which can be compared against the experimental data if available.

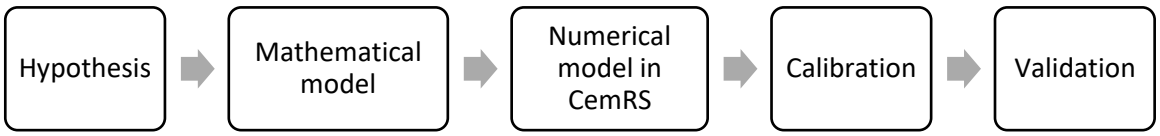

Figure 2.11: Logical overview of modelling and validating a hypothesis in CemRS

Two basic approaches are currently used in CemRS for modelling hydration. These are either dissolution controlled, or precipitation controlled. The dissolution of C_3S and the precipitation of C-S-H at time step *t+dt* are shown in Fig. 2.12. At any particular time step, there is an isotropic dissolution of C_3S (*dr*) and precipitation of C-S-H. C-S-H could be precipitated on the outer surface in C_3S as well as on the surface of a filler grain or in the new void space created due to the dissolution of C_3S or on existing C-S-H layers, thereby further increasing its bulk density. These approaches are further used in the subsequent chapters. In Chapter 3, a precipitation-based mechanism is used for modelling C_3S hydration while in Chapter 5, a dissolution based mechanism is used to model hydration of C_3A.

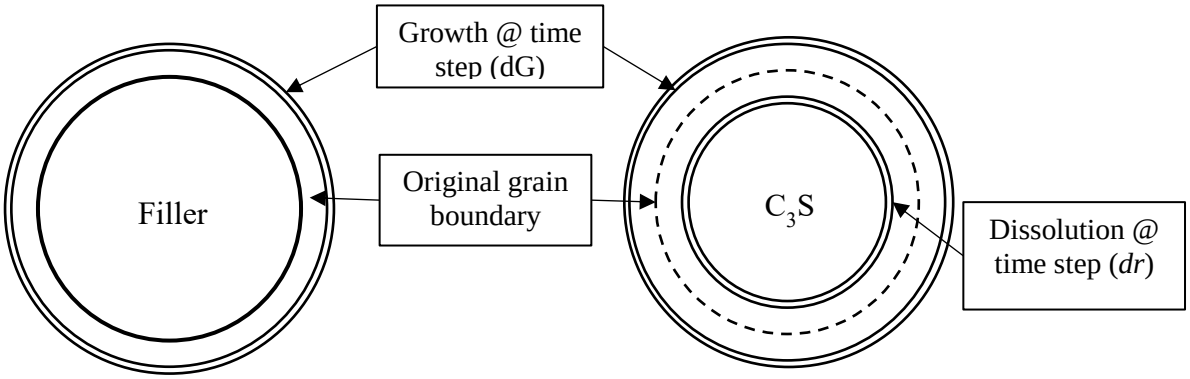

Figure 2.12: Dissolution of C_3S and growth of C-S-H at a particular time step

2.4.3.1. Dissolution-based model

In a dissolution-based model, the kinetics of the reaction is dependent on the isotropic dissolution of anhydrous grains. In such models, the isotropic dissolution rate (*dr/dt*) with respect to time needs to be defined. A same dissolution rate for all the particles or, dissolution rate which is dependent on the particle size are defined. Several rules, which influence *dr/dt* such as availability of water, temperature etc., can be defined. In this approach, assuming the hydration of C_3S, the amount of newly dissolved C_3S is calculated, and the amount of C-S-H determined by the stochiometric ratios are used to calculate the precipitation of C-S-H, and also the other hydration products (in case of C_3S hydration, it would be CH). The rules defined by the user will determine where the hydration products are precipitated in the microstructure.

Such an approach can model dissolution-based mechanisms as well as diffusion-based mechanisms. In a diffusion-based mechanism, the dependence of the rate of dissolution due to the diffusion of barrier layers (in this scenario C-S-H) is defined.

2.4.3.1. Precipitation-based model

In a precipitation-controlled mechanism, the rules are developed by the user which defines the precipitation of new C-S-H with respect to time. It can be the outer C-S-H that grow concentrically (*dG*) or C-S-H that is precipitated in the vacant space due to the dissolution of C_3S in the previous time step or due to the densification of C-S-H. In this approach, the amount of C_3S dissolution corresponding to the stochiometric ratios are calculated. This is calculated in different ways. One way is to assume that all the C-S-H, which is precipitated on the surface of a particular grain of C_3S, is formed from dissolution of C_3S in that particular grain. This can be analytically calculated. However, such an approach does not consider the C-S-H precipitated on a filler particle or on a fully consumed C_3S grains. Hence, CemRS uses two-step method to calculate the dissolution rate. The first step is to calculate the amount of C_3S dissolution occurring due to precipitation of C-S-H on that particular grain analytically. The second step involves calculating total amount of C-S-H that is formed, which is not taken into account in the first step. The second step of dissolution of C_3S grains is calculated by assuming a uniform reactive thickness. In this approach, it is assumed that the depth of isotropic dissolution of all the particles are the same. The dissolution depth is calculated by iterations until it converges to achieve the mass balance of reaction. It should be noted that the precipitation-based model requires higher computational time requirement and such an approach might not be always feasible without a statistical particle size distribution.

2.4.4. Microstructure

Although the current version of CemRS can model the microstructure development, only basic functionalities have been presently developed. Currently the microstructure has been developed only to compare the microstructure developed from different simulations and to present the feasibility of incorporation of microstructure in CemRS. Future versions of the platform will be developed to increase the functionalities and to use the microstructure development for micromechanical modelling. While a statistical PSD is used to simulate the kinetics of reaction, a truncated PSD with the full list of particles are needed for modelling the microstructure. The maximum particle diameter is determined to be *1/2.5* of the size of the length of computational cube (typically 100-250µm) used for the simulation. The minimum particle diameter is chosen by the user. It should be noted that the computational time will drastically increase with the increase in the computational volume and with decrease in the minimum particle diameter.

CemRS generates 2D and 3D microstructure based on the information from the kinetic model. For simulating the 3D microstructure, particles are positioned randomly in the microstructure ensuring that no particles overlap with one another. In case of C_3S hydration, the outer growth of C-S-H, and the dissolution depth of C_3S are obtained from the kinetic model and used for microstructure. To model CH, the user can choose the number of nuclei (typically 100,000)

that are randomly placed, and their diameter is dependent on the total amount of CH. Nevertheless, generating a 3D microstructure is computationally intensive, also, since the model is not further used for micromechanical modelling, a 2D microstructure model is sufficient in the scope of this thesis.

2.4.4.1. 2D microstructure

To create a 2D microstructure, the particles are randomly placed in a 3D computational volume after ensuring no particles are overlapped with one another. To include CH in 2D microstructure, the maximum amount of CH is estimated. This determines the maximum diameter of a CH particle and is added in the 3D microstructure. A two dimensional plane is then chosen by the user. The particles, which have an intercept in the plane, are identified, and the diameter of circles, which intercept on the plane, is calculated. These particles are then stored and the microstructure is developed with respect to time and the data from the kinetic model. This approach drastically reduces the computational time, but the overall porosity of the 2D microstructure is significantly underestimated. This is because, with increase in time, there is a concentric growth of C-S-H which grows outwards of a particle. This would intercept at the plane that was chosen before. However, these interceptions are not included while generating the microstructure. Hence, it should be noted that these 2D microstructural images are not suited for studying the porosity or should not be used for micromechanical modelling. For such purposes, full 3D microstructures should be used. Nevertheless, these 2D microstructural images are used as a visualization tool for different simulations and will aid the user to check for possible bugs in the developed code.

2.4.4.2. Generating a microstructural image

To generate the microstructural image, the 2D vector microstructure or a plane from 3D vector microstructure is used. The microstructure is overlaid with 2D grids where the size of the mesh is determined by the resolution of image selected by user. With higher resolution of image, smaller mesh size is employed. Each voxel is defined with a particular phase (also incorporating the density of C-S-H), similar to a discrete modelling approach and user can determine the color scheme. The image is generated in portable pixmap format (*.ppm).

2.4.4.3. Periodic boundary condition

CemRS uses two types of boundary conditions for modelling microstructure. These are non-periodic microstructure, and periodic microstructure (Fig. 2.13). In the case of a non-periodic microstructure, the particles are not allowed to intercept at the walls of the computational cube. The advantage of such an approach is the reduced computational time, but the disadvantage is that it has a *wall effect*. Most microstructural models use a periodic microstructure, as the computational volume is significantly lower (~0.001mm^3) compared to the volume of real cement paste. This allows the particle to cross boundaries and re-enter from the other side. When these periodic microstructures are clubbed together, it will form a continuous microstructure which will be more representative of larger volumes of pastes by avoiding the wall effect.

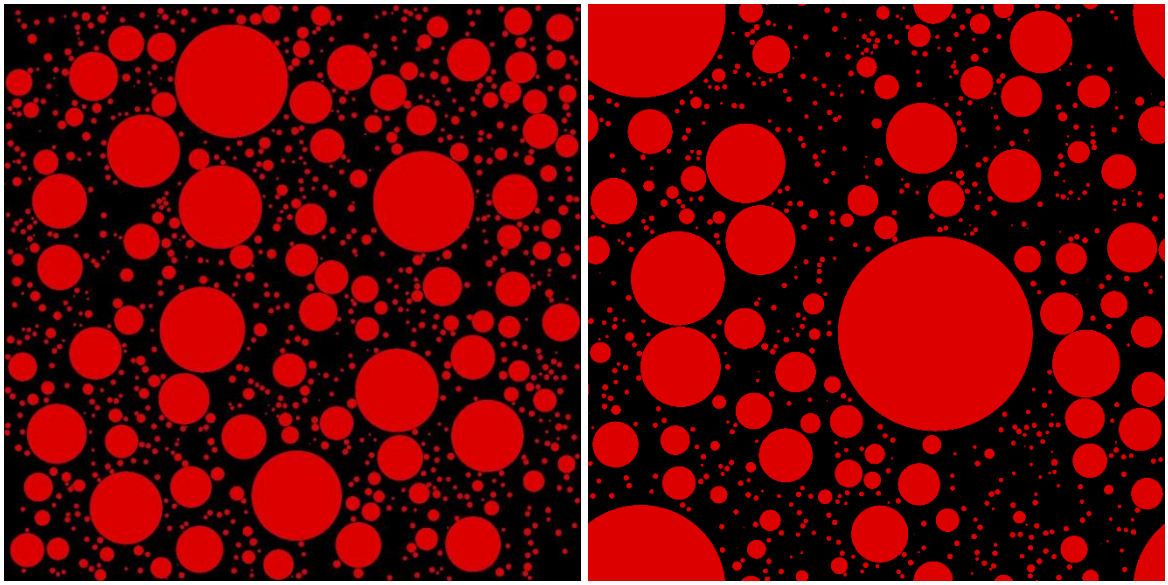

Figure 2.13: 2D image slice of; non-periodic boundary (left), periodic boundary (right).

The downside of using a periodic boundary condition is that it makes the calculations more complex and more computationally intensive. This is because particles can overlap with each other after crossing boundaries. This is schematically represented in Fig. 2.14 for a 2D periodic microstructure. The square '1' is the periodic microstructure with particles A and B with cartesian coordinates (x_1, y_1, z_1) for center of A and (x_2, y_2, z_2) for center of B and radius of particles r_1 and r_2 respectively for A and B. To check the overlap of these particles in a non-periodic boundary condition, it only needs to satisfy the Eq. 2.2 by ensuring that the distance between the center of the circles is larger than the sum of the radius.

$$\sqrt{(x_1 - x_2)^2 + (y_1 - y_2)^2 + (z_1 - z_2)^2} > r_1 + r_2 \tag{2.2}$$

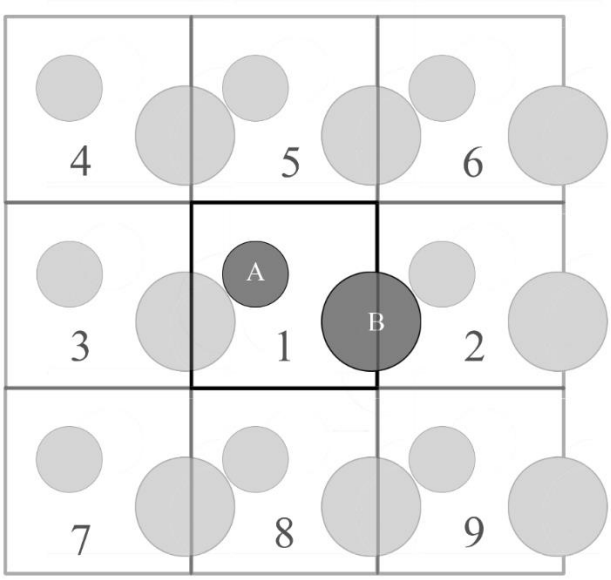

Figure 2.14: Schematic representation of periodic boundary condition in 2D (adapted from[14])

On the other hand, in the case of a periodic boundary condition, one must also check if the particle overlaps from a different side. In Fig. 2.14, it shows 9 positions for which the overlaps should be checked for a 2D microstructure. In a 3D microstructure, it should be checked for 27 different positions. To reduce the computational complexity, the sum of the absolute minimum of the individual components of the vectors is calculated. This value needs to be larger than the sum of the radius of the particles. This is explained in Eq. 2.3 (with 2.3a, 2.3b, 2.3c) where *x*, *y* and *z* are the absolute minimum of the 1D distance between the individual components of the vectors and *a* is the size of the length of computational cube.

$$\sqrt{x^2 + y^2 + z^2} > r_1 + r_2 \tag{2.3}$$

$$x = \min\{\sqrt{(x_1 - x_2)^2}, \sqrt{(x_1 - x_2 - a)^2}, \sqrt{(x_1 - x_2 + a)^2}\} \tag{2.3a}$$

$$y = \min\{\sqrt{(y_1 - y_2)^2}, \sqrt{(y_1 - y_2 - a)^2}, \sqrt{(y_1 - y_2 + a)^2}\} \tag{2.3b}$$

$$z = \min\{\sqrt{(z_1 - z_2)^2}, \sqrt{(z_1 - z_2 - a)^2}, \sqrt{(z_1 - z_2 + a)^2}\} \tag{2.3c}$$

2.4.4.4. Densification of C-S-H

One of the major advantage of CemRS over other models is its capability to model a varying densification of C-S-H on a single particle. Previous studies using transmission electron microscopy have revealed that C-S-H has a varying bulk density in a same particle (Fig. 2.15)[15]. This is employed in CemRS by a layered densification or densification of shells. The outer and inner C-S-H is discretized into several layers (typically around 75-100 to achieve numerical stability) as shown in Fig. 2.16. The density of each layers is governed by rules defined by the user (e.g. dependent on time of formation of that particular layer of C-S-H). The effect of the varying density of C-S-H could be employed on the kinetic model as well as it could be incorporated on the microstructural image. Due to the need for additional discretization of layers for each particle to model the layered densification, this significantly increases the simulation time and memory requirement when the model is developed without a statistical particle size distribution.

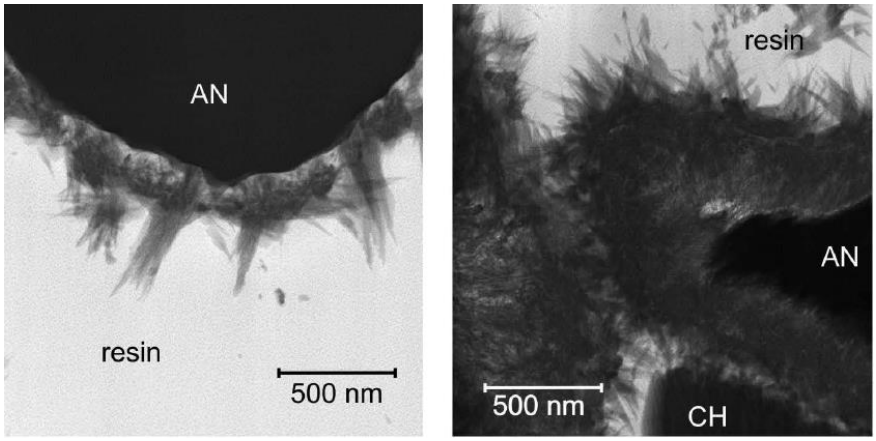

Figure 2.15: Scanning transmission electron microscopy images of C_3S hydration[15]

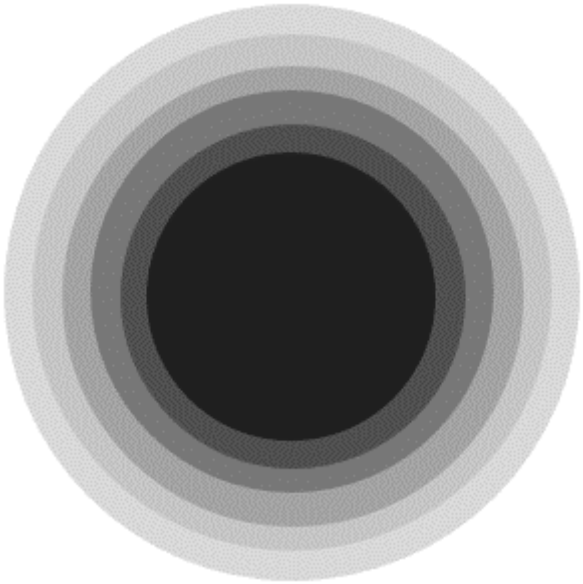

Figure 2.16: Discretization of layers of C-S-H

2.4.4.5. Impingements

Although particles are placed in the computational volume considering the overlaps of the particles, precipitation and growth of hydration products will lead to impingements. During C_3S hydration with fillers, C-S-H impinges with C-S-H formed on another particle, with the other anhydrous C_3S grain or with filler grains. Calculating the impingements analytically is computationally severely intense. CemRS is designed to calculate global impingements but it cannot calculate the local impingements. Global impingements mean the total amount of impingements in the overall microstructure, while local impingements are the impingements from each individual particle. It should be noted that if measurement of local impingements is necessary for the kinetic model, CemRS is not suited for those models, and modelling platform µic shall be used.

To calculate the global impingements, the 3D vector microstructure is overlaid with 3D grid (Fig. 2.17). User could specify the size of the mesh. With increasing the number of grids by

reducing the mesh size, the amount of over-estimated impingements is reduced with an increase in the computational costs. Hence, a balance is needed between the required levels of accuracy and the computational resources. To calculate the amount of impingements, the number of voxels that have more than one phases, is counted. It is possible that more than 2 phases are present in the same voxel. To determine that, each phase is designated with a particular value. For instance, for hydration of C_3S, C-S-H is designated with a value of 1, anhydrous C_3S 10, CH 100.If the value from the voxel is 112, that voxel contains two units of C-S-H, one unit each of C_3S and CH.

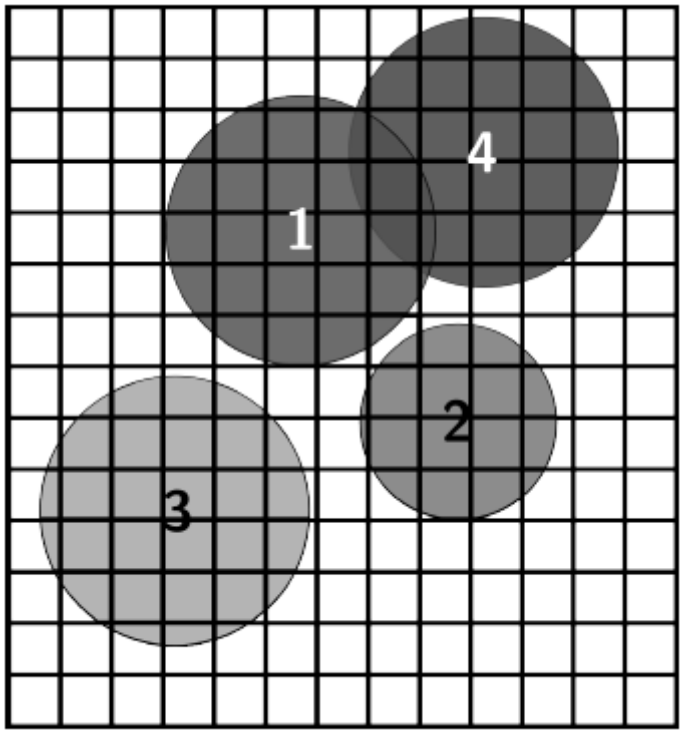

Figure 2.17: Overlaying cubic grid on the vector microstructure (from[15])

2.5. Limitations of the platform

CemRS has several advantages compared to the other existing models with respect to the speed of simulation and flexibility to model new hypothesis to study the mathematical validity of them. Application of a statistical particle size distribution enables the platform to develop more complicated phenomenon such as varying bulk density of C-S-H. On the other hand, CemRS also has some limitations which are given below in comparison with the other models:

- µic: Although the simulation of kinetics is significantly faster in CemRS using a statistical PSD, it is less efficient if microstructural information such as impingements are considered. This is because of the lower efficiency of the algorithms which were used to develop CemRS. Simulation of microstructure itself is significantly inefficient in CemRS compared to µic.
- HydratiCA: CemRS cannot model anisotropic dissolution and cannot model the diffusion of ions considering the concentration gradients in a fundamental level similar to the HydratiCA model.

- HymoStruc: While CemRS offers advancements in the kinetic model, the current version of CemRS cannot model other features such as pore size distribution, modelling strength development, autogenous shrinkage and mechanical properties that are actually out of scope of this doctoral study.

Despite these limitations, future versions of CemRS can be developed to address many of these issues.

2.6. Conclusions

A new microstructural modelling platform named CemRS is introduced in this chapter which could simulate different cementitious systems. New hydration models can be developed and can be simulated for the mathematical validation. The modelling platform is able to simulate a full particle size distribution without the need of truncation using a statistical particle size distribution approach. This approach makes CemRS very computationally efficient with a low requirement of memory space and high speeds. This allows the platform to develop more complex mathematical models which would be better representative of reaction mechanism under investigation.

References

1. Bullard J., Jennings H., *et al.* (2011) "Mechanisms of cement hydration" *Cem. Concr. Res.* **41**:1208-1223.
2. Thomas J., Biernacki J., *et al.* (2011) "Modelling and simulation of cement hydration kinetics and microstructural development" *Cem. Concr. Res.* **41**:1257-1278.
3. Bishnoi S. and Scrivener K. L. (2009) "mic: A new platform for modelling the hydration of cements" *Cem. Concr. Res.* **39**:266-274.
4. Jennings H. M. and Johnson S. K. (1986) "Simulation of microstrucutre development during the hydration of a cement compound" *J. Am. Ceram. Soc.* **69**:790-795.
5. van Breugel K. (1991) "Simulation of hydration and formation of structure in hardening cement-based materials" *PhD Thesis*, TU Delft Netherlands.
6. van Breugel K. (1995) "Numerical simulation of hydration and microstructural development in hardening cement paste (II): applications" *Cem. Concr. Res.* 25:522-530
7. Bentz D. P. (1997) "Three-dimensional computer simulation of cement hydration and microstructure development" *J. Am. Ceram. Soc.* **80**:3-21.
8. Joseph S. and Bishnoi S. (2014) "Study on the effect of particle size distribution and Blaine fineness on the hydration of cement" in *Proceedings of the RILEM International Symposium on Concrete Modeling CONMOD*, Beijing China.
9. Maekawa K., Ishida T. and Kishi T. (2003) "Multi-scale modeling of concrete performance - intergrated material and structural mechanics" *J. Adv. Concr. Technol.* **1**:91-126.
10. Bullard J. W. (2007) "Approxmiate rate constants for nonideal diffusion and their application in a stochastic model" *J. Phys. Chem. A* **111**:2084-2092.

11. Bullard J. W. (2007) “A three-dimensional microstructural model of reactions and transport in aqueous mineral systems” *Modelling Simul. Mater. Sci. Eng.* **15**:711-38.
12. Navi P. and Pignat C. (1996) “Simulation of cement hydration and the connectivity of the capillary pore space” *Adv.Cem. Based Mater.* **15**:58-67.
13. Thomas J. (2007) “A new approach to modelling the nucleation and growth kinetics of tricalcium silicate hydration” *J. Am. Ceram. Soc.* **90**[10]:3282-3288.
14. Bishnoi S. (2008) “Vector modelling of hydrating cement microstructure and kinetics” *PhD Thesis*, EPFL Switzerland.
15. Bazzoni A. (2014) “Study of early hydration mechanisms of cement by means of electron microscopy” *PhD Thesis*, EPFL Switzerland.

Chapter III

Modeling the effect of fineness and filler in early age hydration of tricalcium silicate

Shiju Joseph[i*], Shashank Bishnoi[ii], Koen Van Balen[i], Özlem Cizer[i]

[i] *Department of Civil Engineering, KU Leuven, Leuven - 3001, Belgium*
[ii] *Department of Civil Engineering, Indian Institute of Technology Delhi, New Delhi - 110016, India*

Abstract[a]

Alite (impure C_3S) being the major and most reactive phase in ordinary Portland cement has been studied extensively. This paper focuses on the mathematical modeling of a new hypothesis developed, i.e. densified volumetric growth, applied to the main hydration peak in alite hydration. This hypothesis assumes a time and particle size dependent growth rate and densification rate of C-S-H controlled by its internal surface area. To test this hypothesis a new microstructural modeling platform (CemRS) has been developed. The model was used to calibrate and predict the isothermal calorimetric results from the literature and two sets of original experimental results with alite replaced with different replacement fractions of quartz, fly ash and slag of different fineness. The model is able to capture and predict the effect of fineness and fillers without the need of varying the parameters for the particular set of simulations. The values of the parameters of simulation reflect the current experimental evidence from the literature and thus provide validation of the hypothesis which suggest the main hydration period including deceleration period in the alite hydration is induced by the densification and reducing the outer growth rate of C-S-H.

[*] Corresponding author: shiju.joseph@kuleuven.be, shiju.joseph@live.com
[a] This chapter appears in *J. Am. Ceram. Soc. 100[3]; (2017) pp:1178-1194*

3.1. Introduction

Impure tricalcium silicate (C_3S) or alite is the major phase in ordinary Portland cement (OPC) constituting around 50-75% of its composition. Alite and aluminate are the constituents in OPC, which have high reaction rates in the early ages. As the latter is generally of very lower quantity in OPC, it would be fair to say that alite has the superior role in hydration during the first 24 hours. This is a period of high importance due to its significant effects on the total heat release, shrinkage, microstructure and strength development. This explains the extensive study on this topic and the state of the art has been recently reviewed[1].

Early age hydration of alite is generally divided into 5 stages,

- *Stage 1, Period of high dissolution*: In this period a very rapid rate of reaction is observed as the solution is under-saturated with respect to C_3S ions. The rate of reaction continues to decrease as the concentration of C_3S ions increase in water.
- *Stage 2, Induction period*: This is a period of low rate of reaction. Two hypotheses presently under research explain induction period as the time when solution is under saturated with respect to the dissolving phase[1,2], and as the time required for the stabilization of C-S-H[3].
- *Stage 3, Acceleration period:* The rate of hydration increases significantly for few hours. The working hypothesis regarding this phenomenon is the nucleation and growth mechanism[4, 5].
- *Stage 4, Deceleration period:* The rate of hydration decreases drastically and the reason for the reduction is not well understood and is investigated in this paper.
- *Stage 5, Period of low hydration:* The rate of hydration is reduced and hydration continues very slowly for the rest of the time which is the continuation of the stage 4 and eventually the reaction rate could be controlled by the diffusion of silicate ions or water through C-S-H layer around C_3S grain.

The main focus of interest in this study has been given to the stages 3 and 4 as these two stages contribute considerably to the overall degree of hydration in the early age. There is a growing consensus in recent literature that the acceleration period in the main hydration peak or Stage 3 is controlled by nucleation and growth mechanism. But there is wide disagreement in the literature about the reason for deceleration period namely stage 4. Traditionally a switch to diffusion controlled mechanism[6] was assumed for this stage. This was later challenged by experimental evidences[7] and simulations[4, 8]. Recently Bergold et al.[3] suggested that the switch to deceleration period takes place after the smaller particles are fully consumed. This is highly improbable as narrow particle size distributions of different mean diameters from Costaya[9] showed a similar deceleration period at similar time frames. Although the consumption of particles could reduce the rate of hydration, the deceleration period shall not be solely attributed to it. The possibility of the hydration kinetics of alite being dissolution controlled has been recently argued by Nicoleau and Nonat[10] based on saturation indexes and by Nicoleau and Bertolim[11] based on analytical modeling. However, in these works it is not clear how the presence of inert fillers would affect the rate of hydration of C_3S.

Nucleation and growth models generally assume that initial nucleation materializes on the available surface area of unhydrated particles, and later, concentric outward growth on these nuclei happens. The additional surface area from the growth of nuclei is used to capture the acceleration period and the reduction of surface area due to the impingements attributes to the deceleration period. The classical Johnson Mehl Avrami Kolmogorov (JMAK) model[12, 13, 14, 15] more commonly known as the Avrami model, assumes a homogenous nucleation in the free space. Although the model was able to fit the kinetic data up to 70% of alite hydration reasonably, it did not provide any physical significance[5]. Microscopy images clearly show that the nucleation is primarily taking place on the surface of particles rather than at random positions[16].

A mathematical boundary nucleation and growth (BNG) model, originally developed by Cahn[17], was later proposed by Thomas[18] to model the hydration kinetics of C_3S. This model assumes that nucleation is taking place at the surface of the C_3S grain and nuclei grow at a constant rate outwards with a uniform density. Bishnoi and Scrivener[8] have shown that it is not possible to capture the deceleration period using such a model considering uniform density of C-S-H. This is because there would be enough space for hydration to continue at a very high rate at such high densities of C-S-H, unless water to cement ratio (w/c) is very low. This inspired the authors to propose Nucleation and Densified Growth (NDG) model where a varying density of C-S-H is used. It is assumed that a lower density C-S-H first fills the space, and hydration continues by the densification of C-S-H[8]. As isothermal calorimetry results have hardly any effect on the water to cement ratio, Kirby and Biernacki[19] pointed out that it is not possible to use a space filling mechanism to capture the main hydration peak as the available space changes considerably when the water to cement ratio changes[20]. In other words, deceleration in the stage 4 of the rate of hydration curve cannot be attributed to the impingement of C-S-H. Bazzoni[16] also noted from the STEM imaging that the microstructure is not fully covered even after 24 hours, but reported lower density of C-S-H at early ages.

Maserao et al.[20] have proposed a reaction zone hypothesis to explain the lack of effect of w/c on the rate of hydration. The hypothesis states that the nucleation and growth of C-S-H is confined to a reaction zone around the C_3S particle. This model simulates the effect of particle size distribution (PSD) reasonably by adjusting the reaction zone thickness for each particle fractions of C_3S. However, they were not able to propose a mechanism for the variation of reaction zone thickness for different fractions of same material, and also, a reason for the sudden decline of growth[1].

Although most of these models claim that the effect of fillers could be incorporated, this is not materialized yet. The fillers have a crucial role in alite and OPC hydration. By definition, inert fillers are materials which do not react chemically with water or under alkaline conditions but increase the rate of hydration reactions. Recent experimental results[21] suggest that in the initial 24 hours, supplementary cementitious materials (SCM) act as fillers, atleast at lower temperatures. Although a recent study has suggested that the increased reactivity with the incorporation of fillers is due to the reduction of inter-particle distance[22], literature predominantly reports that it is the effect of surface area. Additionally, the kinetics is not

affected significantly upon changing the water to cement ratio in a blended system which is contrary to the assumption that the inter-particle distance is the major reason for higher hydration rates. We believe that there is an influence of the inter-particle distance on the hydration kinetics although this will not be significant enough to explain the additional hydration due to filler.

In this paper a new hypothesis is proposed which would take into account the available experimental evidences to model the early age hydration kinetics of alite incorporating the effect of fineness and fillers. A new microstructural modeling platform (CemRS), which could be used to model the microstructure and simulate the reaction mechanisms of cementitious binders is developed to test the validity of the proposed hypothesis.

3.2. DVG Hypothesis and mathematical modeling

The **D**ensified **V**olumetric **G**rowth (DVG) hypothesis is a nucleation and growth based mechanism with time and grain size dependent growth rate and densification of C-S-H controlled by its *free internal surface area*. The flowchart of DVG model is illustrated using Fig. 3.1. Pseudo code for DVG model and the list of parameters are given in Appendix I. This hypothesis is a modification of C_3S hydration reaction mechanism proposed by Bazzoni[16].

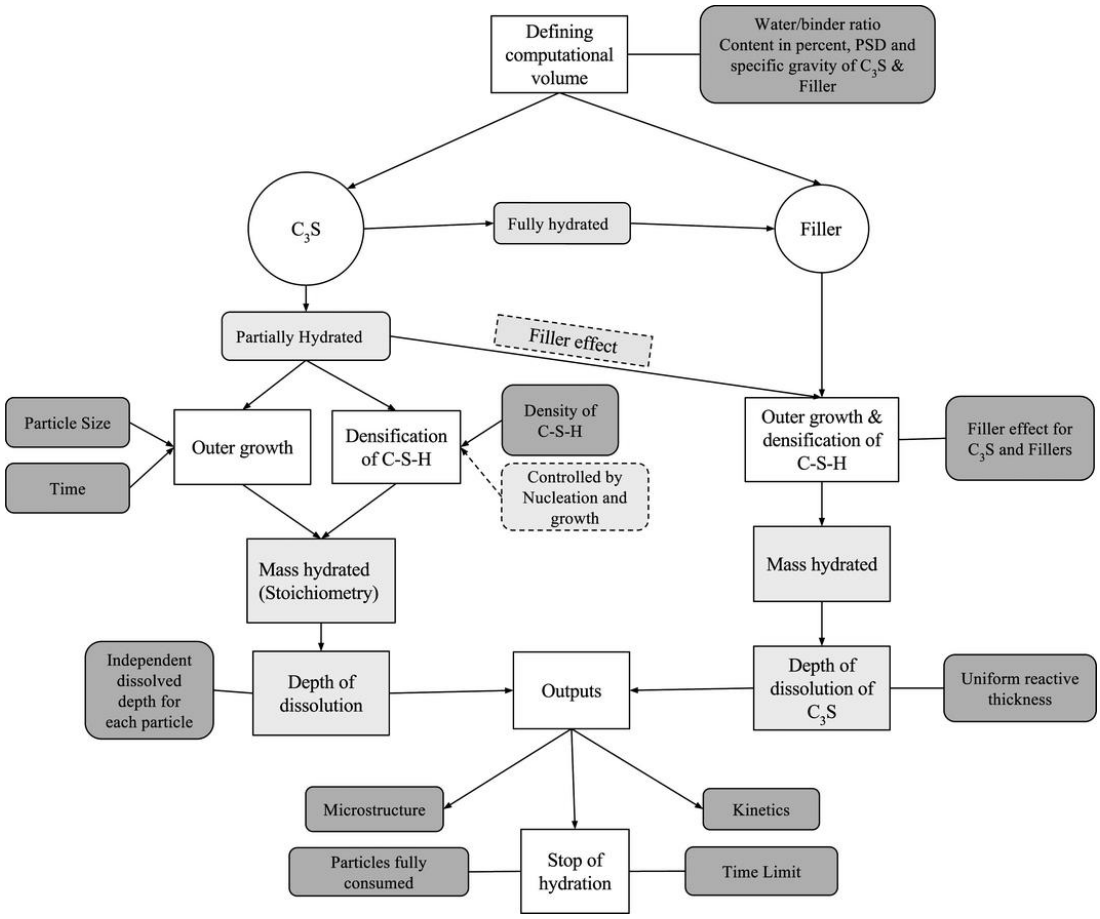

Figure 3.1: Flowchart of DVG model

The C-S-H growth is differentiated between outer growth which grow perpendicular to the surface of the particle and inner growth which fills the voids created by the dissolution of C_3S. This concept is illustrated in Fig. 3.2 (top) assuming that the grain is spherical. The original radius of the particle is r_i and the current radius reduces to r_0 due to dissolution of C_3S. The thickness of outer C-S-H is r_1-r_i and r_i-r_0 is the thickness of inner C-S-H. With increase in time the dissolved depth of C_3S increases along with the outer growth of C-S-H. At the same time, initially when the bulk density of C-S-H increases, the free internal surface area also increases and upon further densification the free internal surface area decreases.

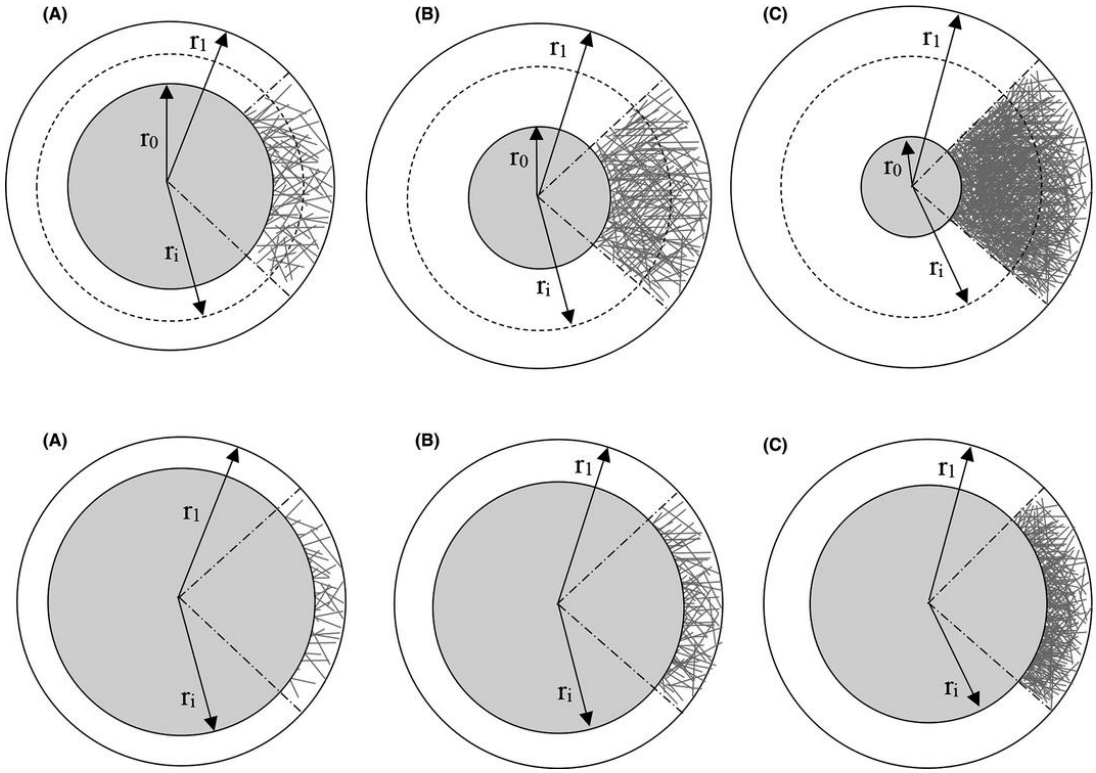

Figure 3.2: Conceptual volumetric densification and growth of C-S-H around C_3S shrinking core grain (top) and filler (bottom), r_0 is the current radius, r_i is the radius of the particle, r_1 is the outer radius: a) Low bulk density C-S-H with lower internal surface area, b) C-S-H densifies and surface area increases, c) C-S-H further densifies and internal surface area decreases due to impingements

Contrary to the traditional models which have a uniform growth rate irrespective of time and particle size, it is assumed that the rate of outward growth reduces drastically during the acceleration period to a much lower growth rate. It is also assumed that the growth rate is also dependent upon the particle radius: i.e. a smaller particle will have a smaller outer growth of C-S-H compared to a larger particle. These assumptions and their implications are further discussed in section 5.

It is assumed that for every individual C_3S grain, all other particles in the system act as a filler as they also provide an extra surface area to for nucleation of C-S-H similar to inert fillers. Hence each C_3S grain acts as a reactant for itself and as a filler for other C_3S particles. In case

of a filler particle, it has only outer C-S-H as the material does not dissolve by definition. Fig. 3.2 (bottom) gives a conceptual representation of C-S-H growth and densification around a filler particle.

Mathematically, the outer growth rate of C-S-H around an alite particle is assumed to follow the empirical Eq. 3.1, which could mimic a steep reduction of growth rate over time and continues at a much lower rate considering the size of particle.

$$\frac{dG(t)_i}{dt} = \left(\frac{G_1}{G_2 + t^{G_3}} + G_4\right)\frac{r_i^{a_1}}{2} \tag{3.1}$$

Where $G(t)_i$ is the outward growth from C_3S reaction at time t around the particle i of radius r_i. The growth parameters G_1, G_2, G_3 and G_4 are used to mimic the reducing growth rate. The total outer growth on a filler grain is assumed to be $G(t)_i * G_f$. Hence the total growth around a C_3S grain including filler effect is $G(t)_i * (1+G_f)$. The parameter a_1 is to control the effect of particle radius on the growth rate. Where Eq. 3.2,

$$a_1 = \begin{cases} a_{11}\ if\ r_i \leq 1\mu m \\ a_{12}\ if\ r_i > 1\mu m \end{cases} \tag{3.2}$$

a_{11} and a_{12} are used when the size of particle is below 1µm and above 1µm respectively and a_{11f} and a_{12f} are used instead of a_{11} and a_{12} for fillers. Two different a_1 are used above and below 1µm, for the mathematical requirement of the simple equation. Additionally it can benefit to get a steeper reduction of growth rate for fines whereas, a flatter increase of growth rate for courser particles. The steeper reduction of growth rate for fines will also take into account of the fines which are rapidly dissolved in the initial dissolution stage of alite hydration which do not act as a nucleation spot. Different a_1 values for fillers were needed as it is assumed that they do not dissolve due to its significantly low solubility and reactivity.

On the other hand, it is assumed that the densification rate is dependent on the instantaneous bulk density of C-S-H which is dependent on the *free internal surface area* of C-S-H. *Free internal surface area* is the surface area of C-S-H which is free to nucleate. Part of the area would not be suitable for nucleation due to the molecular structure of C-S-H. The densification rate of the inner C-S-H is expected to be on a higher side compared to the outer C-S-H as they are much closer to the outer surface of the unreacted grain and has two surfaces to react (the outer surface of the grain and the inner surface of C-S-H hydrated around the grain).

The bulk density of C-S-H at age t is assumed to follow the Eq. 3.3.

$$C-S-H_{den}(t) = D_1(1 - \exp(-D_2 t^{D_3})) \tag{3.3}$$

Where *C-S-H_{den}(t)* is the bulk density of C-S-H at time *t*, D_1, D_2 and D_3 are coefficients of densification. The densification due to filler effect is assumed to be *C-S-H_{den}(t)*D_f*. Hence the total bulk density of C-S-H at time t would be *C-S-H_{den}(t)*(1+D_f).*

To derive a mathematical model with the combination of Eq. 3.1 and Eq. 3.3, consider a small volumetric shell of thickness *dr* at a distance *r* from the center of the C_3S grain *i*. The volume of the shell, dV_i can be written as:

$$dV_i = 4\pi r^2 dr \tag{3.4}$$

And the mass of that shell due to hydration of the individual particle is:

$$dM_i = 4\pi r^2 D_1(1 - \exp(-D_2\tau^{D_3})dr \tag{3.5}$$

Where, τ is the age of the shell at a distance r from the center of the particle,

$$\tau = \begin{cases} t - G^{-1}(r - r_i), if\ r > r_i \\ t, if\ \ r < r_i \end{cases} \tag{3.6}$$

Where G^{-1} is the inverse of the outer C-S-H growth equation as a function of time. For simplification the age of inner C-S-H is assumed to be the same as the age of the initial layer of the outer C-S-H. Hence the inner C-S-H will have a uniform bulk density whereas the outer C-S-H will have a reducing bulk density when moved further away from the surface of the actual particle.

The total mass of C-S-H around the alite particle due to its individual reaction at time *t* could be written as:

$$M_i = \int_{r_0}^{r_i+G(t)} 4\pi r^2 D_1(1 - exp(-D_2\tau^{D_3})dr \tag{3.7}$$

Where r_0 is the inner radius of the alite particle at time t, and taking the filler effect also into account, Eq. 3.7 will become as follows:

$$M_i = \int_{r_0}^{r_i+G(t)(1+G_f)} 4\pi r^2 D_1(1 + D_f)(1 - exp(-D_2\tau^{D_3})dr \tag{3.7a}$$

The equation for the total mass hydrated around a filler particle can be written as:

$$M_i = \int_{r_i}^{r_i+G_f*G(t)} 4\pi r^2 D_1 D_f (1 - exp(-D_2 \tau^{D_3}) dr \tag{3.8}$$

3.3. DVG mechanism in CemRS modeling platform

A new microstructural modeling platform, **Cem**entitious **R**eactions **S**imulator (CemRS), has been developed as part of this research in order to simulate the microstructure for validating DVG hypothesis. The model was developed by adopting some basic concepts of the modeling platform µic [23] to simulate spherical particles. It was completely programmed in C++ incorporating the object oriented approach to make it more efficient and to use it as a standalone program without the need of a third party software. The primary objective of this modeling platform is to test and validate different hypothesis which could give better insights into the hydration kinetics and microstructure development in cementitious systems. Flexibility is the key of CemRS, which could be easily modified to simulate more complex reaction mechanisms. The microstructure so developed could be further implemented for micromechanical modeling and to model transport properties.

3.3.1. Generating the particle size distributions

Particle truncation is a necessity for microstructural modeling for the sake of minimizing computational costs unless a very narrow particle size distribution is modelled. Without truncation the total number of particles could be billions or trillions depending on the minimum and maximum particle sizes and the particle distribution profile. These truncations could have significant effect on the hydration kinetics depending on the reaction mechanism used [24] despite the little effect on the microstructure.

For modeling DVG hypothesis, microstructure is modelled traditionally with truncation while for simulation of hydration kinetics a statistical particle size distribution, which is discretized into steps is used to improve the accuracy and to reduce the computational time by several orders. The growth rate, dissolved depth, bulk density of C-S-H of each particle are fed forward to the microstructure imaging module to generate the microstructure.

3.3.2. Assumptions and simplifications of the model

The DVG hypothesis is simulated in CemRS using some simplifications and assumptions for practical purposes. The first major assumption being that it omits the first two stages of alite hydration. As already pointed out, it is assumed that the impingements do not influence the hydration kinetics which is supported by the results from the literature and hence they are not explicitly calculated. The specific heat of hydration of alite was assumed to be 517 J/g. The hydration of alite is assumed to follow the Eq. 3.9 with assuming a density of 3.15 g/cm^3 for

alite, 1.0 g/ml for water, dry density of 2.6 g/cm^3 [25] for C-S-H and 2.24 g/cm^{3}for *CH.* C/S ratio of 1.7 is assumed for C-S-H throughout the simulations.

$$C_3S + 5.3H \rightarrow C_{1.7}SH_4 + 1.3CH \quad (3.9)$$

Combining the densities and the stoichiometric equation, Eq. 3.9 can be written in volumetric terms as:

$$1.0\, V_{C_3S} + 1.318\, V_H \rightarrow 1.2073\, V_{C-S-H} + 0.593\, V_{CH} \quad (3.10)$$

Mass is conserved with high level of precision[b]. The Portlandite precipitated is assumed not to act as a nucleation spot due to the computational complexity. Smaller particles get consumed fully faster than larger particles, and it is assumed that, even after it is fully consumed, the C-S-H around that particle will act as a filler.

3.3.3. Layered densification

New layers formed due to the outer growth would be having lower bulk density than the older layers. This means that the bulk density of C-S-H is continuously decreasing moving away from the initial surface of the particle. It is therefore important to calculate the densification of each individual layer on every particle. The outer growth is divided into *'n'* number of layers for each time step and the number of layers (current model uses 100 layers) must be sufficiently large enough to avoid any numerical error. The age of each layer is calculated for each time step using numerical integration of Eq. 3.1, and Eq. 3.5 is used to calculate the mass hydrated. The filler effect is also incorporated both in Eq. 3.1 and Eq. 3.5.

The layered densification process is a very computationally expensive calculation and is the prime reason for the requirement of a statistical particle size distribution. The computing cost is directly proportional to the number of layers used.

3.3.4. Depth of dissolution

In the model, growth of C-S-H is taking place in two steps. In the first step the total amount of C-S-H precipitated in that *time step* from filler effect is calculated and the corresponding volume of C_3S dissolved is calculated from Eq. 3.10. A uniform reactive thickness concept [26] is used for finding out the depth of dissolution from this step. It is calculated numerically by iterating the dissolved depth at each time step to achieve the required precision.

[b] In a precipitation-dissolution model a very small error in the mass balance equation is inevitable as the depth of dissolution is solved numerically and not analytically

The second step is the growth and densification of C-S-H on unhydrated grain. The total volume of C-S-H precipitated around that grain at that particular time step is calculated and the depth of dissolution of the particle corresponding is calculated analytically using Eq. 3.11.

$$dod_{i,t} = (r_i - r_{in}) - \sqrt[3]{\frac{3}{4\pi}\left(\frac{4\pi}{3}(r_i - r_{in})^3 - V_{reacted}\right)} \tag{3.11}$$

Where $dod_{i,t}$ is the depth of dissolution of particle i at time t and $V_{reacted}$ is the volume of C-S-H reacted at that time step, r_i is the radius of the particle i and r_{in} is the total depth of dissolution of particle i.

3.4. Simulations in CemRS

Simulations of three different sets of data are performed in CemRS using the DVG model. A calibration – prediction approach was used to fit the experimental data ensuring the total growth and bulk density of C-S-H is in accordance with the values found in the literature. For each individual set of experiments, the value of the parameters does not change with respect to the different mixes used. The parameters used for the simulations are given in Table 3.1.

Table 3.1: Coefficients of simulation

	G_1	G_2	G_3	G_4	D_1	D_2	D_3	G_f	D_f	a_{11}	a_{12}	a_{11f}	a_{12f}
Set #1	10	400	3.5	0.005	0.9	0.0045	2.6	0.55	0.55	1.35	0.38	-	-
Set #2	10	400	3.5	0.0017	0.9	0.006	2.6	0.8	0.9	2.1	0.68	0.3	0.2
Set #3	15	400	3.5	0.002	0.9	0.00325	2.6	1.1	1.1	2	0.3	0.1	0.3

3.4.1. Simulation of published experimental results

Costaya[9] studied the effect of particle size distributions on the hydration kinetics of alite. For this purpose alite was produced in laboratory and narrow particle size distributions were obtained by sieving and the finer particles were further decanted using isopropanol as dispersant matrix. The particle size distributions from this study are shown in Fig. 3.3. Isothermal calorimetry was conducted on these different fractions of alite at 0.4 w/c ratio and 20 °C. The rate of heat evolution from the study is given in Fig. 3.4. The microstructural slices after packing of all the 5 fractions are given in Fig. 3.5. The pores are shown in black and C_3S in grey. It should be noted that the volume of pores in all 5 fractions are the same although visually it could be misleading.

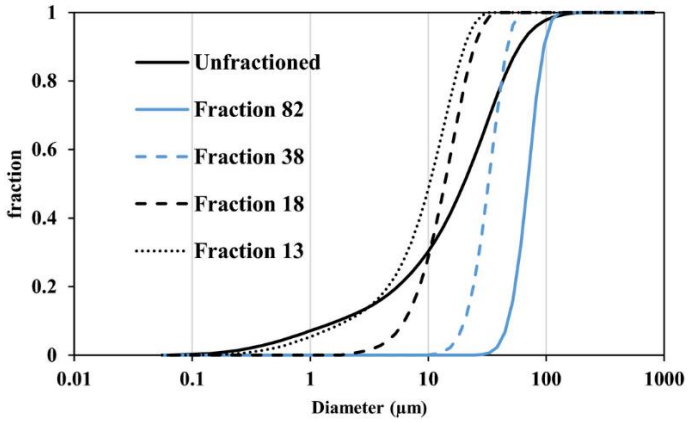

Figure 3.3: Cumulative particle size distributions of alite fractions taken from published experimental results[9] (Set #1)

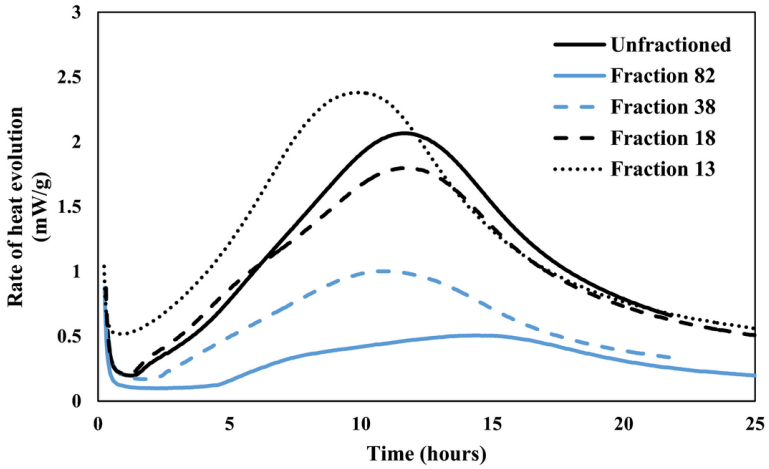

Figure 3.4: Rate of heat release of alite fractions from published experimental results[9] (Set #1)

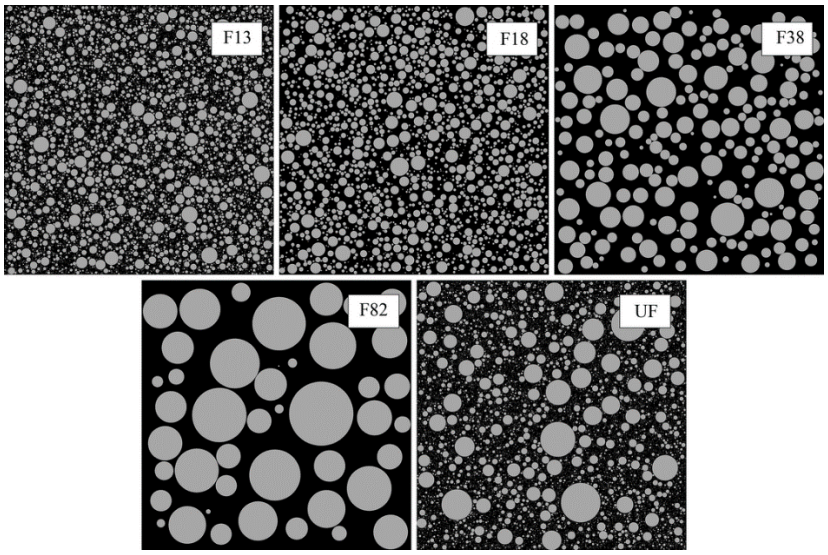

Figure 3.5: Microstructural slices of particle fractions before the start of reaction (Set #1). grey – C_3S particles, black – water.

The four fractions of alite along with the un-fractioned alite are simulated with the parameters given in the Table 3.1. The comparison of model with experimental results after calibration and prediction is given in Fig. 3.6. The parameters are calibrated by fitting the "*unfractioned psd"* and *"fraction 38µm".* These calibrated parameters are used to predict the other three fractions. A small phase shift was adopted to adjust hydration up to the end of the induction period. The predictions match reasonably well with experimental data despite large variations in particle sizes.

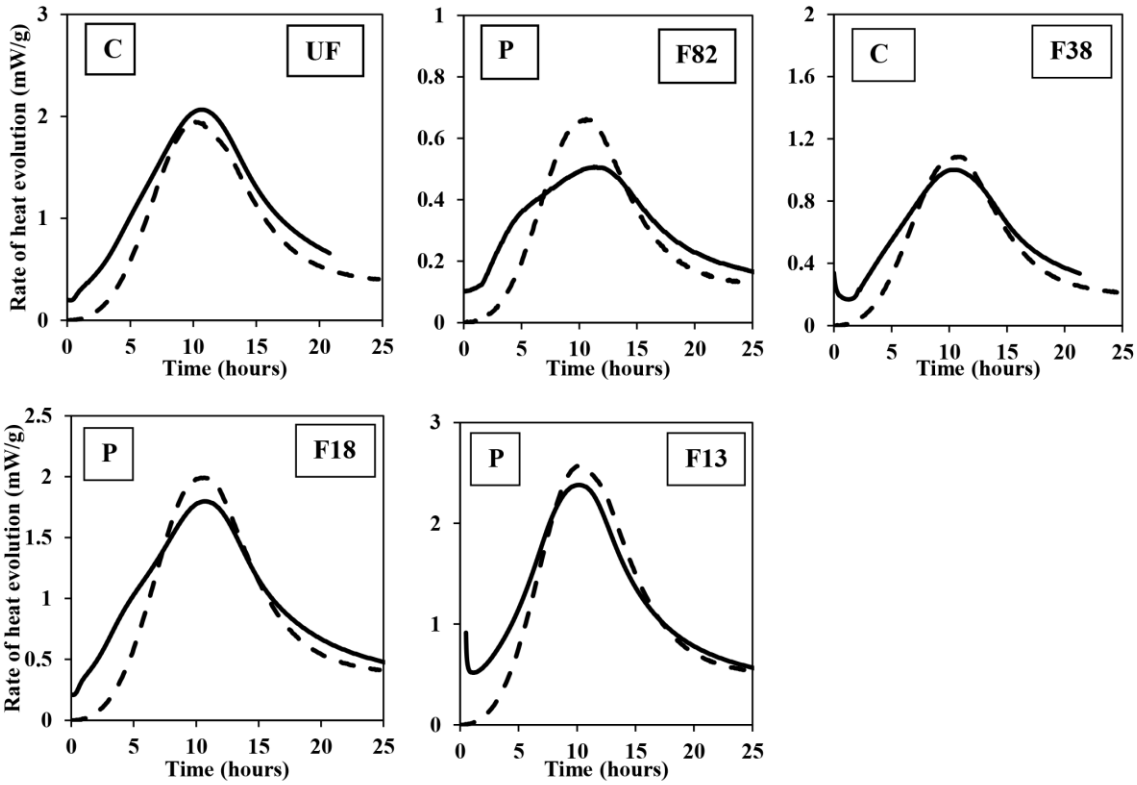

Figure 3.6: Comparison of rate of heat evolution and degree of hydration of different alite fractions on the simulation (dashed line) and published experimental results (solid line)[9]. C - calibrated & P - predicted (Set #1)

3.4.2. Simulation of original experimental results

Two sets of experiments were performed in the laboratory and the details are summarized below.

3.4.2.1. Materials and Characterization

In the first set of experiments (*set #2*) pure triclinic *tricalcium silicate* (SARL Mineral research processing, France) having three different Blaine fineness (3000 cm^2/g, 3600 cm^2/g, 4400 cm^2/g) have been used. The fineness was measured by Blaine technique and alite of three different fineness was produced by sieving through 32 µm and 63 µm sieves, and mixing them. It was named a30, a36 and a44 respectively for the study. Coarse quartz (Merck chemicals) was ground in a ring mill for 10 seconds and 60 seconds. The former was sieved through a 45 µm sieve and the latter through a 28 µm sieve. These quartz fractions are named Qz45 and

Qz28 respectively in the study. *Blast furnace slag*, which was received in granules, was ground in a ball mill for 10000 rotations (sg).

In the second set of experiments (*set #3*) a different batch of triclinic tricalcium silicate (AN) (SARL Mineral research processing, France) was used along with three *quartz* fractions and three fractions of *fly ash*. The three quartz fractions (Qc, Qf and Qcf) were prepared using a similar process described above. Coarse quartz was ground in ring mill for 15 seconds and sieved using a 28µm sieve. The material retained was further ground in the ring mill for another 15 seconds and then sieved with 28µm sieve. The retained quartz fraction was named Qc and finer, Qf, and each of them was mixed thoroughly. Qc and Qf are mixed in equal proportions to get Qcf. Fly ashes of three different fineness were used. The original un-fractioned fly ash is named 'fu' and two fly ash fractions separated using mechanical process were named 'f10' and 'f20'. The variations in oxide compositions of the three fly ashes found using X-ray Florescence (XRF) were not significant.

The particle size distribution of the materials was determined by laser diffraction (Mastersizer 2000) using ethanol as dispersing medium (Fig. 3.7). The specific gravity of alite was found to be 3.15 g/cm^3, quartz 2.65 g/cm^3, slag to be 2.55 g/cm^3 and fly ashes to be 2.17 g/cm^3 at 20 ^{o}C.

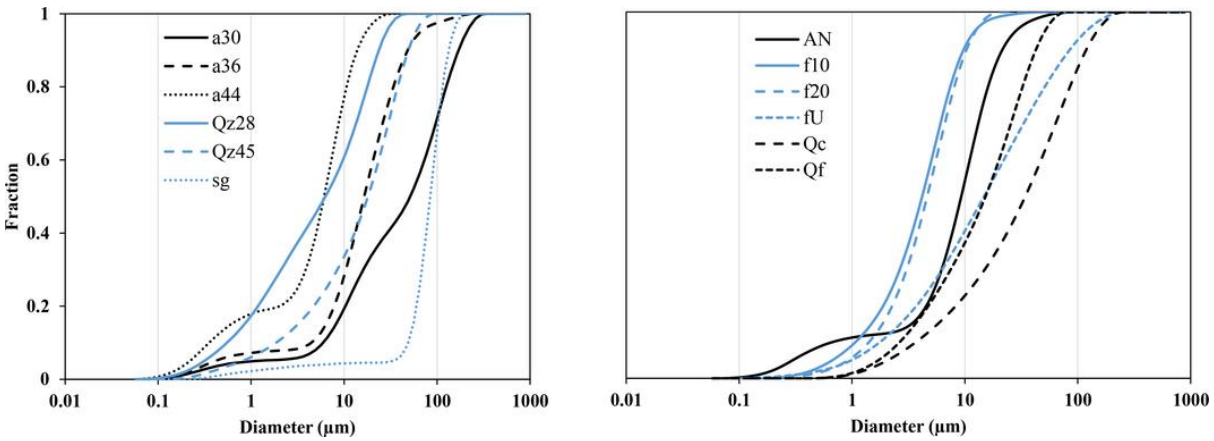

Figure 3.7: Left: Particle size distribution of original experimental results of three different fineness of C_3S (a30, a36, a44) and two quartz powders (Qz28 and Qz45) and slag (sg). (Set #2). Right: Particle size distribution of original experimental results of C_3S (AN) and two quartz powders (Qc and Qf) and three fly ashes (f10, f20 & fU). (Set #3)

3.4.2.2. Experimental procedure

Pastes at water to solid ratio of 0.5 are used in this study. The weight percentage of the composition of each mix for set #2 is given in Table 3.2, for set #3 in Table 3.3. The pastes are prepared under controlled temperature of 20 °C using distilled water. Heat of hydration was continuously monitored using isothermal calorimeter (TAM Air) at 20 °C.

In *set #2*, quartz and slag with two different replacement ratios with alite, 10% and 35% was used to study the effect of replacement of fillers on the kinetics of hydration. In *set #3* quartz and fly ash was replaced with 16.67% and 33.33%.

Pastes prepared with 33.33% replacement for alite with fly ash and quartz along with neat alite were kept in water bath at 20 °C. The reaction was stopped at 2 hours, 24 hours and 48 hours using freeze drying technique at 0.03 millibar pressure after grinding them. Precautions were taken to reduce the effect of carbonation and thermogravimetric analysis (TGA) (Netsch STA 409 PC) was performed at a heating rate of 10 ^{o}C/min to find the total Portlandite content using the tangent method.

Table 3.2: Mix compositions of Set #2 (%)

	a30	**a36**	**a44**	**Qz28**	**Qz45**	**Sg**
#2 M1	100	-	-	-	-	-
#2 M2	-	100	-	-	-	-
#2 M3	-	-	100	-	-	-
#2 M4	-	90	-	10	-	-
#2 M5	-	65	-	35	-	-
#2 M6	-	90	-	-	10	-
#2 M7	-	65	-	-	35	-
#2 M8	-	90	-	-	-	10
#2 M9	-	65	-	-	-	35
#2 M10	-	-	90	-	10	-

Table 3.3: Mix compositions of Set #3 (%)

	AN	**f10**	**f20**	**fU**	**Qc**	**Qf**	**Qcf**
#3 M1	100	-	-	-	-	-	-
#3 M2	83.333	16.666	-	-	-	-	-
#3 M3	66.666	33.333	-	-	-	-	-
#3 M4	83.333	-	16.666	-	-	-	-
#3 M5	66.666	-	33.333	-	-	-	-
#3 M6	83.333	-	-	16.666	-	-	-
#3 M7	66.666	-	-	33.333	-	-	-
#3 M8	83.333	-	-	-	16.666	-	-
#3 M9	66.666	-	-	-	33.333	-	-
#3 M10	83.333	-	-	-	-	16.666	-
#3 M11	66.666	-	-	-	-	33.333	-
#3 M12	66.666	-	-	-	-	-	33.333

3.4.2.3. Results

The results of the isothermal calorimetry are presented in Fig. 3.8 for *set #2* and Fig. 3.9 for *set #3*. The rate of hydration was normalized to *per gram of C_3S* instead of per gram of solid (C_3S + filler). C_3S with higher fineness is giving a higher rate of heat release compared to C_3S with a coarser C_3S which is expected. C_3S mixes with finer fillers are giving slightly higher heat of hydration than the fillers with lower fineness. Also with increased replacement of C_3S with fillers, higher heat is released from the C_3S. This is in accordance with the literature reporting that with increase in fineness the available surface area also increases which will increase the nucleation rate that is dependent upon the available surface area. Fig. 3.10 shows the amount of portlandite calculated from isothermal calorimetry assuming only C_3S hydration (reaction enthalpy of -517 J/g) compared to the portlandite content from TGA. As already reported[20], this confirmed that the reaction of fly ash is rather limited and it acts only as a filler in the initial 24 hours. Nevertheless there is a slight reduction in the amount of Portlandite in the initial 24 hours. This could be assumed to be compensated in the simulations as a small dissolution of fly ash which corresponds to lower surface area to act as nucleation spots.

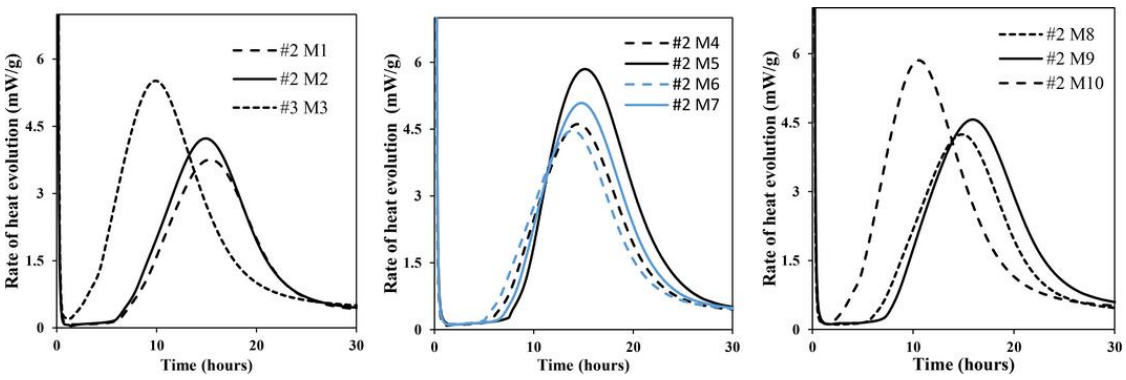

Figure 3.8: Isothermal calorimetry data for the original experimental results for different mix compositions given in Table 3.2 (Set #2)

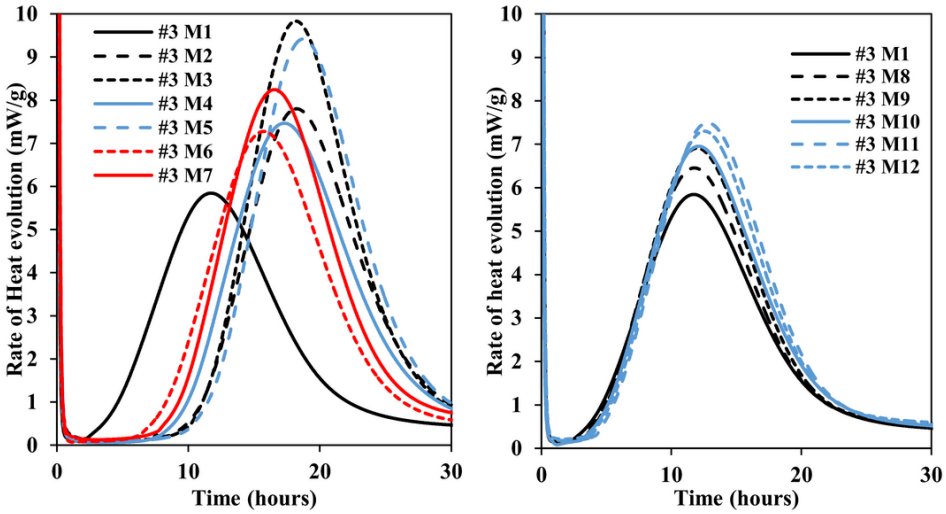

Figure 3.9 : Isothermal calorimetry data for the original experimental results for different mix compositions given in Table 3.3 (Set #3)

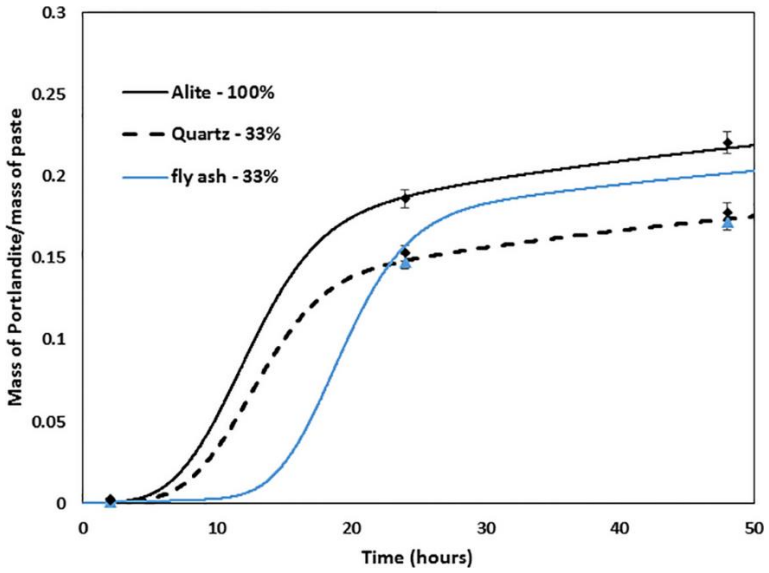

Figure 3.10: Portlandite content from isothermal calorimetry (line) and TGA (marker) for pastes with 100% alite, and 33% of alite replaced with fly ash and quartz

3.4.2.4. Simulations

Similar to section 4.1, DVG model was simulated for the two sets of mixes in CemRS. The comparison of the model with the experiments and simulations are given in Fig. 3.11 and Fig. 3.12 for *Set #2* and *Set #3* respectively. As the first two stages are omitted a phase shift was adopted for every sample for removing the induction period. The parameters used for the simulations are given in Table 3.1. In *set #2* mixes M1, M3, M4 and M7 were used for calibration and the rest of them were predicted without changing the parameters. On the other hand, for *set #3*, mixes M1, M2 and M5 were calibrated and the other 9 mixes were predicted keeping the parameters fixed. The simulation results show good correlation of the experimental results with the simulations.

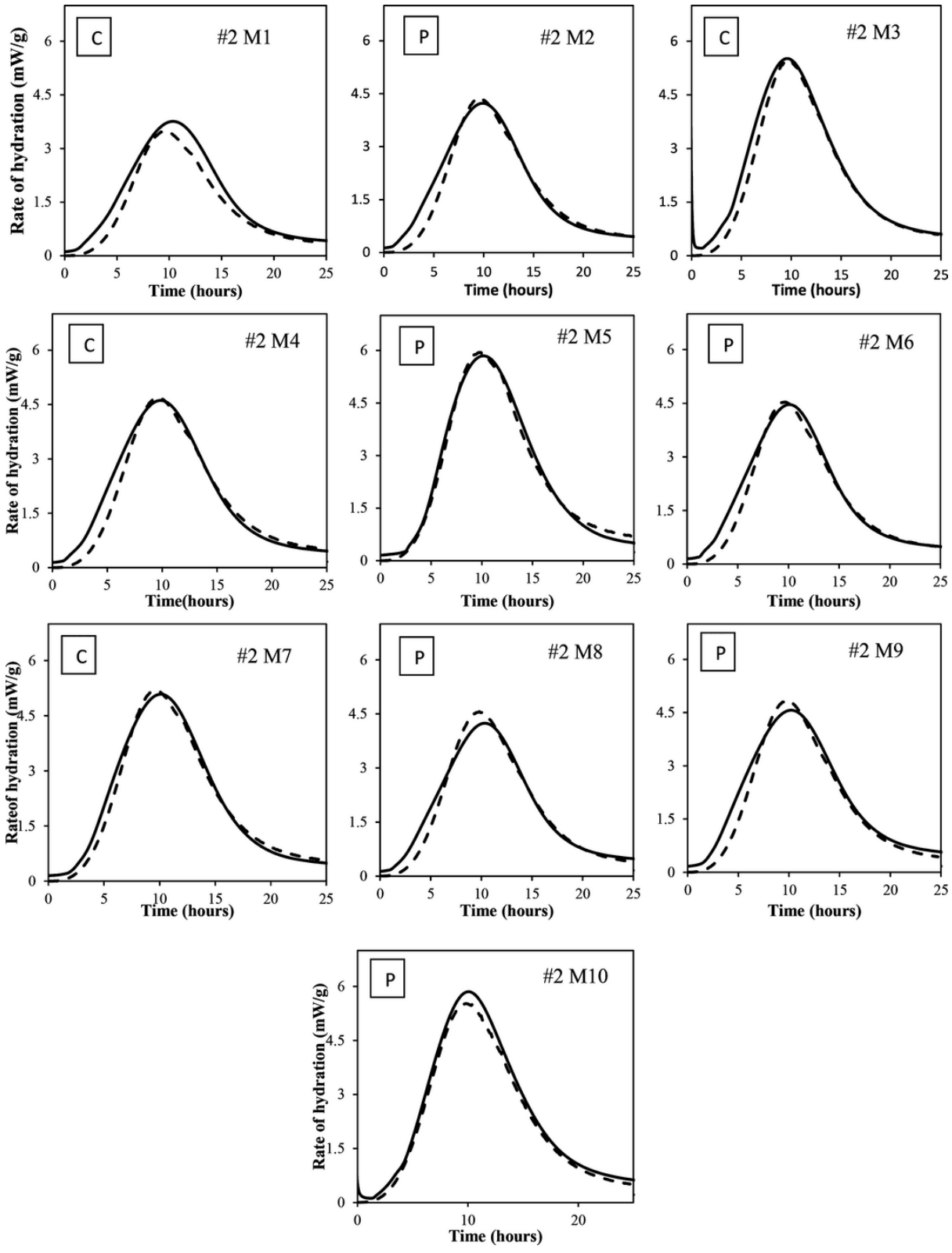

Figure 3.11: Comparison of rate of heat evolution and degree of hydration of different mixes from simulation (dashed line) and results from original experimental data (solid line), C – calibrated, P – predicted (Set #2)

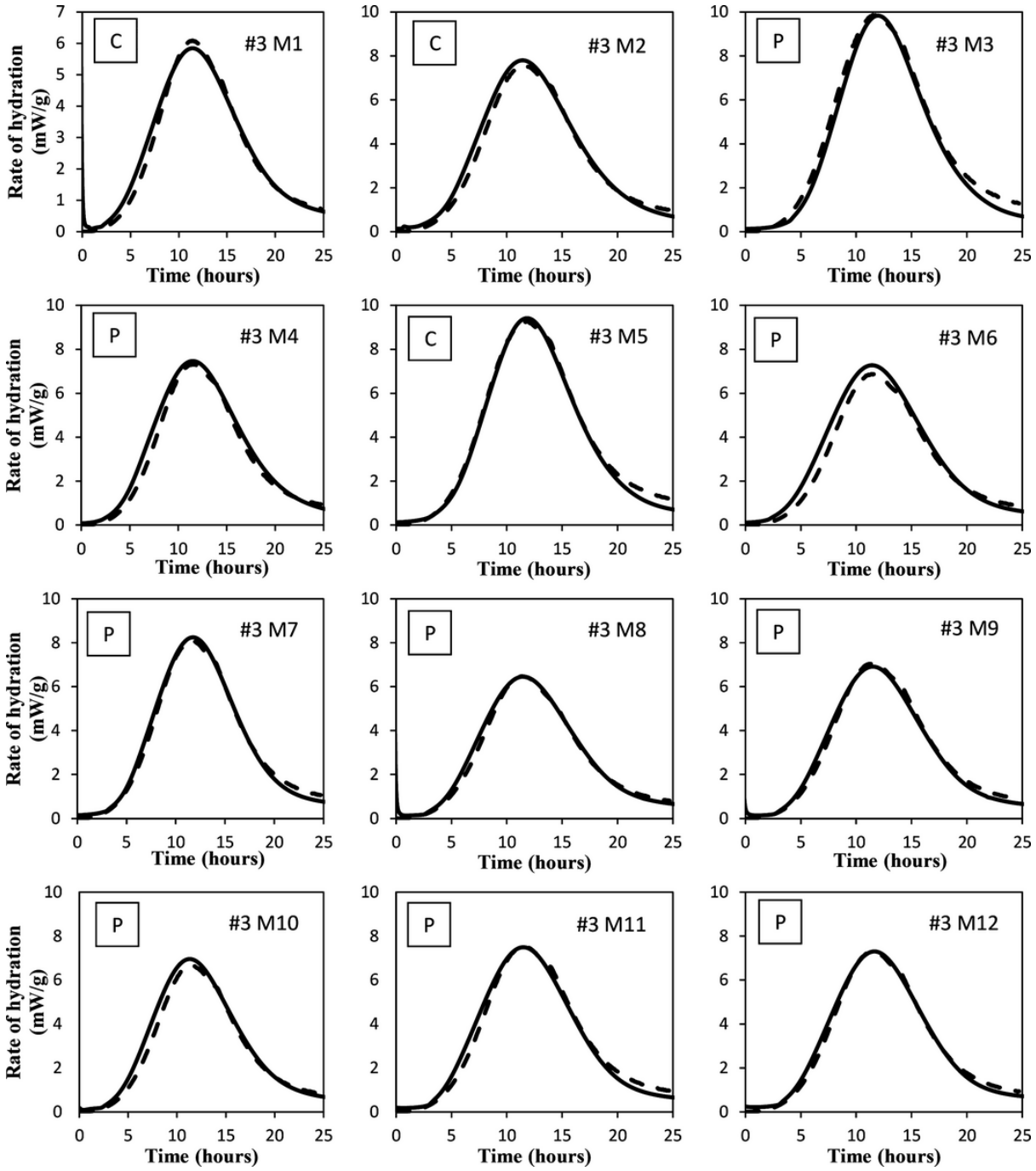

Figure 3.12: Comparison of rate of heat evolution and degree of hydration of different mixes from simulation (dashed line) and results from original experimental data (solid line), C – calibrated, P – predicted (Set #3)

Fig. 3.13 shows the microstructural slices for M1 and M3 (*set #2*) before reaction and after 20 hours of reaction. Black shows the pores, grey shows the unreacted C_3S and white shows the hydration products. Fig. 3.14 shows the microstructural slices for M4 and M5 (*set #3*) before reaction and after 20 hours of reaction. Darker shade of grey indicates the fly ash. Portlandite is precipitated homogenously. The C-S-H around fillers are much lower compared to C-S-H around C_3S as in the latter case there would be extra thickness, as the original particle size reduces due to dissolution.

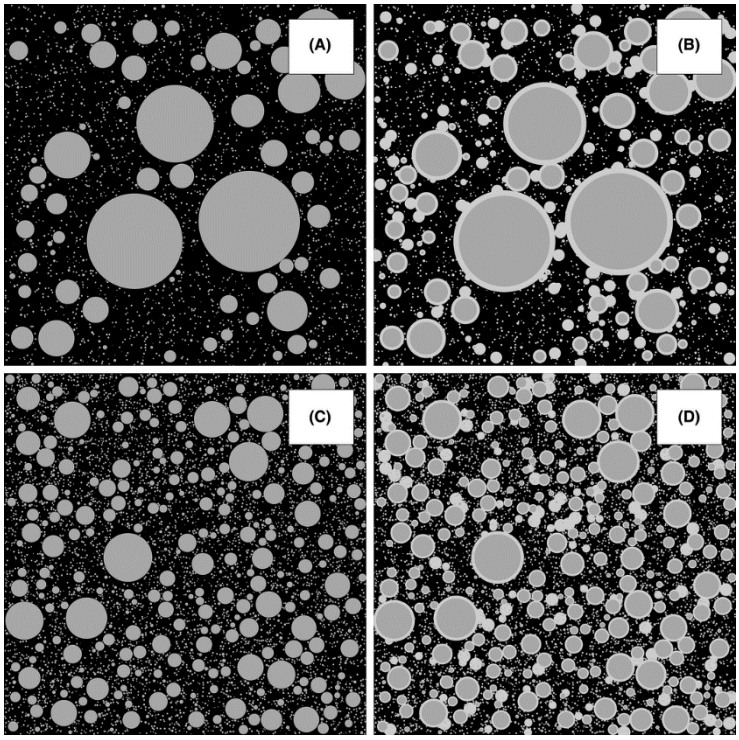

Figure 3.13: Microstructural slices of simulation from Set #2. a) #2 M1 at time=0, b) #2 M1 at time=20hr, c) #2 M3 at time=0, d) #2 M3 at time=20h. grey – alite, white – hydration products.

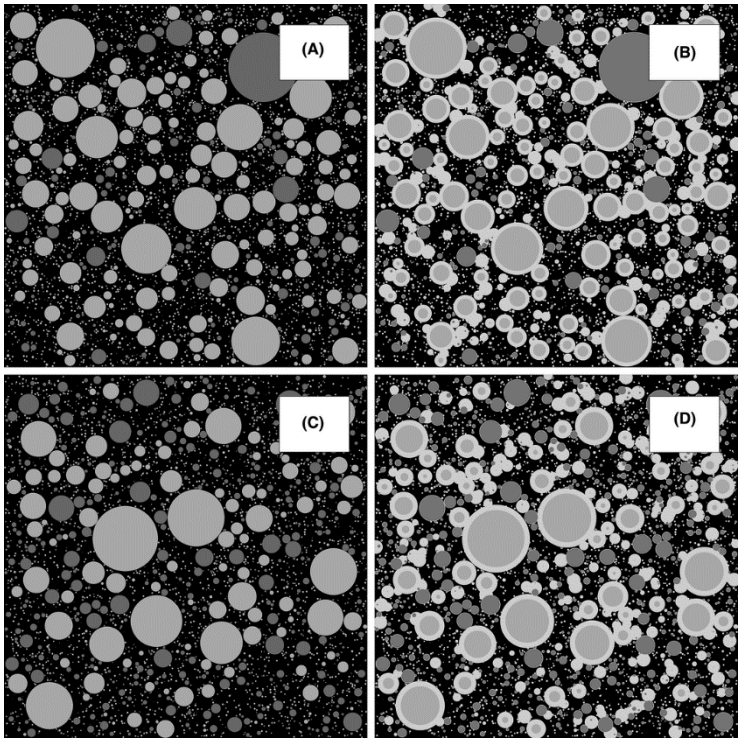

Figure 3.14: Microstructural slices of simulation from Set #2. a) #3 M4 at time=0, b) #3 M4 at time=20hr, c) #3 M5 at time=0, d) #3 M5 at time=20h. grey – alite, white – hydration products.

3.5. Discussion

3.5.1. C-S-H densification

The composition, morphology and density of C-S-H are still under active research in the literature[5, 25, 27, 28]. The current state of the art identifies C-S-H as a type of gel composed of solid layers with chemically and physically combined water. A lower and denser form of C-S-H was identified which was attributed to the inner and outer C-S-H[27, 28]. Recent STEM images of high resolution suggest that C-S-H grows as needle like structures and the bulk density is increased with time[1, 29]. Work from Muller et al.[25] suggests that even though the solid density of C-S-H hardly changes during the hydration, the bulk density of C-S-H increases with the increase in the degree of hydration which is in accordance with the basic idea of DVG model. It was also found in that work that, the bulk density increases with a decrease in water to cement ratio at 28 days. Besides, water to cement ratio is found to have a significant impact on the degree of hydration at later ages[1, 21]. This could lead to a conclusion that in the early ages the impingements are less pronounced and those impingements even though might increase the C-S-H bulk density marginally, they would not reduce the rate of hydration, as the internal surface area does not change significantly, and may even increase marginally in such a case. But in the later ages, the impingements would be higher and a higher bulk density at an already dense C-S-H could mean lowering of the internal surface area. Also, this dense layer of C-S-H could lead to a diffusion controlled hydration kinetics in the later ages. It should be also noted that the maximum bulk density of the simulations used were similar to the bulk density (~1.5 – 1.8 after 24 hours) found using ^{1}H NMR relaxometry[25]. Fig. 3.15 shows a slice of microstructure simulation of unfractioned C_3S (*set #1*) before hydration and after 8 hours and 20 hours. This shows the densification of C-S-H. Red is the unreacted C_3S particle, black is the pores, shades of grey is C-S-H, lighter the denser and white is the Portlandite precipitated.

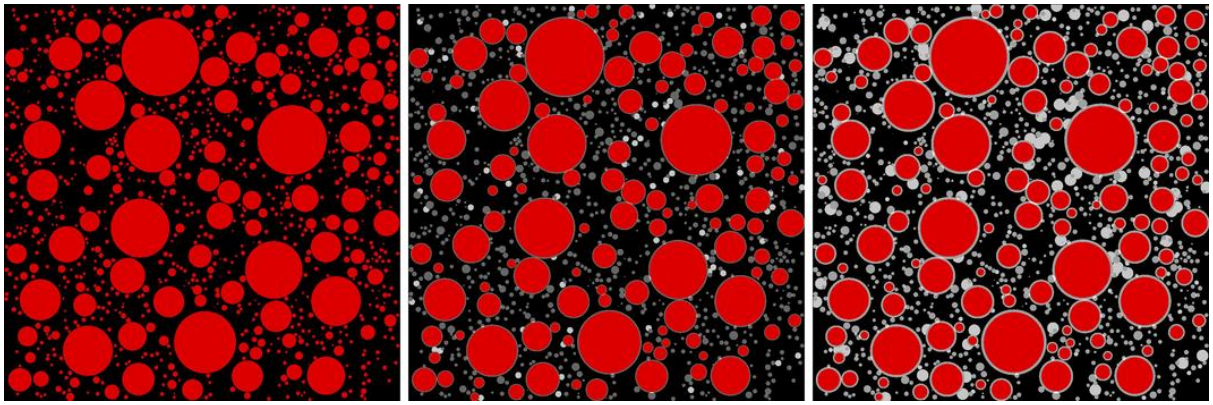

Figure 3.15: Densification of C-S-H, Unfractioned C_3S (Set #1), for time 0, 8hrs and 20hrs (left to right). Black – pores, red – C_3S, shades of grey – C-S-H, darker the grey lower the bulk density

3.5.2. Outer growth rate

Uniform growth rate of C-S-H perpendicular to the surface of the particle is assumed in most of the available models. This is attributed to the acceleration regime in the main hydration peak

of alite. A deceleration was simulated assuming the impingements between particles[8, 18]. As impingements are low in the early ages, the uniform growth rate will lead to unrealistic degree of reaction. The assumption of uniform growth rate was supported by the assumption that the concentration of ions throughout the system is constant. But once the dissolution takes place, there would be higher concentration of ions near to surface of the particle. These ions would be transported to the rest of the system through diffusion and hence there will be a concentration gradient normal to the surface of particle. This concentration gradient and slower diffusion of silicate ions can impact the outer growth of C-S-H. The rate of diffusion of ions would be much slower if the concentration gradient is flatter.

This reduction in growth rate could be also because of the blocking of C_3S surface due to moderately opaque C-S-H as proposed by Bullard et al.[30] which reduces the dissolution rate and hence the supersaturation and growth rate of C-S-H. Their simulations in HydratiCA [31] showed a reducing growth rate over time depending on the opacity of C-S-H. Blocking of surface also means that the diffusivity is decreased due to a less permeable layer outside.

3.5.2.1. Effect of particle size on the growth rate

If the growth rate is controlled by dissolution, then the growth rate will be also dependent on the size of C_3S grain. This could be explained with simple geometry. Consider two spheres of radius r_1 and r_2, where $r_1 > r_2$. The outer surface area of the two spheres would be $4\pi r_1^2$ and $4\pi r_2^2$ respectively. If the ions from these surfaces diffuse an outward distance dr normal to the surface, the surface area of the new spheres would be $(4\pi r_1+dr)^2$ and $(4\pi r_2+dr)^2$ respectively. If we assume that the concentration at the outer surface of the particle was same for both the spheres, the concentrations of the outer surface with respect to the inner surface of the particles could be written as $1/(1+dr/r_1)^2$ and $1/(1+dr/r_2)^2$ respectively. As $r_1 > r_2$ the concentration would be higher at an equal radial distance for a larger particle compared to a smaller particle. This could influence the growth rate as described in the section above. This shall not be the only reason, but also because the C_3S surface of the smaller particle will be covered with C-S-H more opaquely than of a larger particle and hence a lower growth rate on smaller particle. A similar concept was applied by Garrault et al.[32] for modeling the effect of particle size distribution on the hydration kinetics. In their model, it was assumed that the outer growth stops when C-S-H covers the surface completely. With constant growth rate parallel to the surface, smaller particles would be covered by C-S-H much faster than on a larger particle.

It could be also argued that if growth rate was dependent on particle size, it would not have been unnoticed by the electron imaging. This could be explained by the Noyes-Whitney equation[33] which suggests that rate of dissolution is dependent on the concentration at the surface of the particle. Hence smaller particles would have higher dissolved depth compared to larger particles and as by electron imaging it is impossible to exactly identify the original grain boundary, it looks like all the particles are having similar growth. From the microstructural images of the simulations, it could be also noted that the total thickness of C-S-H does not vary much with particle size. That is because, for individual C_3S hydration Eq. 3.11 is used for finding the depth of dissolution, which would be higher for smaller particles compared to larger particles. It should be also noted that the growth rate did not change

drastically using the simulation parameters in the model, but rather reduced the growth rate of fines. Even if the total volume of fines is less than 2-5% in a particle size distribution, the number of particles would be huge. Assuming a uniform outer growth rate for each of these particles would not be realistic. The growth rate would have to be varied on a significantly high order to capture the hydration kinetics in those cases [8].

3.5.3. Filler effect

The model was able to capture the filler effect with a replacement ratio of 10% and 35% for *set #2* and 16.66% and 33.33% for *set #3*. As correctly pointed out by Berodier and Scrivener, filler effect cannot be modelled just by considering it as extra surface area similar to the surface area of C_3S[22]. Hence a lower growth rate and lower densification rate was applied for filler effect in this model. This is in accordance with the explanations given in the above sections as concentration of ions would be higher near to the surface of the C_3S particle. So a lower rate has to be assumed for the filler effect. The fitting parameters indicate that with increase in the particle radius, there is an increase in the growth rate. This could be in reality the effect of a combination of factors such as, the effect of nucleation rate on the size of the particle, the effect of shearing[22] and agglomeration. In this model it is assumed that only growth rate varies with the effect of particle sizes, and nucleation density remains the same.

3.5.4. Calibration and prediction

The results from the simulation of all three data sets are in good agreement with the experimental results without the need for changing the parameters for effect of fineness or fillers. The coefficients do not change drastically with in three sets of parameters of simulation. Some deviations of the simulations from the experimental results are expected because of the assumptions used in the model, and the errors from the experimental results. As there are many other factors which affect the kinetics of the system from the shape of the particles, agglomeration, morphology, impurities of C_3S[29] to thermal treatment of C_3S production[34], it is assumed that these effects would be captured in the calibration making prediction possible without considering those effects.

Although the number of parameters used in the model is on the higher side compared to the existing models, it should be noted that the increased number of parameters were used to compensate for some of the assumptions which contradict experimental evidences. In this model, four parameters are used to model the growth rate, whereas traditional models used a constant outward growth. Also three parameters are used to model the effect of densification of C-S-H instead of a uniform density. Additional parameters are used to capture the filler effect and to model the effect of fineness. Although a different set of parameters are in fact necessary for capturing the filler effect more efficiently, the current model just used filler effect to be a fraction of the main hydration reaction to make it more simple and to reduce the number of particles. The ability of the model to capture hydration kinetics without contradicting the experimental evidences and to predict for different particle size distributions and different replacement of fillers validates the model. Nevertheless, this model could be used as a tool to predict the effect of fineness and fillers.

3.6. Conclusions

A new hypothesis named densified volumetric growth (DVG) model has been developed and tested using the newly developed microstructural modeling platform for hydration of cementitious systems, CemRS. The hypothesis assumes that even though the main hydration peak is controlled by nucleation and growth mechanism, dissolution and diffusion also have a significant effect on it. This model uses a time and particle size dependent reducing outer growth rate of C-S-H which could be attributed to dissolution and diffusion. The kinetics of the system is dependent on the internal surface area of C-S-H which varies with the instantaneous bulk density of C-S-H of each layer and the total thickness of C-S-H around each particle.

The results from simulations confirm that the main hydration peak including the deceleration period in C_3S hydration is dependent on the densification of C-S-H and reducing growth rate. It could be also confirmed that filler effect is due to the additional surface area provided by the fillers to nucleate C-S-H although its effect is not as prominent as the surface area of alite, as nucleation ideally tends to take place closer to the hydrating particle.

The model also displays its ability to capture and predict the effect of fineness and fillers without the need for varying the parameters and without contradicting the available evidences from the literature which gives the validation of the model. The microstructure so obtained is more realistic with varying bulk density of C-S-H and it could be further used for micromechanical modeling, studying transport properties and to achieve one step closer to model hydration of OPC-SCM systems.

References

1. Scrivener K. L., Juilland P. and Monteriro P. J. (2015) "Advances in understanding hydration of Portland cement" *Cem. Concr. Res.* **78**:38-56.
2. Juilland P., Gallucci E., *et al.* (2010) "Dissolution theory applied to the induction period in alite hydration" *Cem. Concr. Res.* **40:**831-844.
3. Bergold S. T., Goetz-Neunhoeffer F. and Neubauer J. (2015) "Mechanically activated alite: New insights into alite hydration" *Cem. Concr. Res.* **76**:202-211.
4. Bullard J., Jennings H., *et al.* (2011) "Mechanisms of cement hydration" *Cem. Concr. Res.* **41:**1208-1223.
5. Thomas J., Biernacki J., *et al.* (2011) "Modeling and simulation of cement hydration kinetics and microstructural development" *Cem. Concr. Res.* **41**:1257-1278.
6. Gartner E. M., Young J. F., *et al.* (2002) “Hydration of Portland cement”, in *Structure and Performance of Cements*, London: Taylor, Francis.
7. Thomas J. J. (2012) "The instantaneous apparent activation energy of cement hydration measured using a novel calorimetry-based method" *J. Am. Ceram. Soc.* **95**[10]:3291–3296.
8. Bishnoi S. and Scrivener K. L. (2009) "Studying nucleation and growth kinetics of alite hydration using mic" *Cem. Concr. Res.* **39**:849-860.

9. Costaya M.(2008) "Kinetics and microstructural investigation on the hydration of tricalcium silicate," *PhD Thesis*, EPFL Switzerland.
10 Nicoleau L., Nonat A. (2016) “A new view on the kinetics of tricalcium silicate hydration” *Cem. Concr. Res.* **86**:1-11.
11. Nicoleau L., Bertolim M. A. (2016) “Analytical model for the alite (C_3S) dissolution topography”, *J. Am. Ceram. Soc.* 99[3]:773-786
12. Avarami M. (1939) "Kinetics of phase change I" *J. Chem. Phys.* **7**:1103-1112.
13. Avarami M. (1940) "Kinetics of phase change II" *J. Chem. Phys.* **8**:212-224.
14. Johnson W. and Mehl R. (1939) "Reaction kinetics in processes of nucleation and growth," *T. Am. I. Min. Metall. Eng.* **135**:416-458.
15. Kolmogorov A. (1937) "A statistical theory for the recrystallization of metals," *B. Acad. Sci. USSR. Ch.*, **3**:355-359.
16. Bazzoni A. (2014) "Study of early hydration mechanisms of cement by means of electron microscopy" *PhD Thesis*, EPFL Switzerland.
17. Cahn J. W. (1958) "The kinetics of grain boundary nucleated reactions" *Acta. Metall.* **4**:449-457.
18. Thomas J. (2007) "A new approach to modeling the nucleation and growth kinetics of tricalcium silicate hydration" *J. Am. Ceram. Soc.* **90[**10]:3282-3288.
19. Kirby D. and Biernacki J. J. (2012) "The effect of water to cement ratio on the hydration kinetics of tricalcium silicate cements: testing the two step hydration hypothesis" *Cem. Concr. Res.* **42**[8]:1147-1156.
20. Masoero E., Thomas J. J. and Jennings H. M. (2014) "A reaction zone hypothesis for the effects of particle size and water to cement ratio on the early hydration kinetics of C_3S" *J. Am. Ceram. Soc.* **97[**3]:967-975.
21. Berodier E. and Scrivener K. (2015) "Evolution of pore structure in blended systems" *Cem. Concr. Res.* **73**:25-35.
22. Berodier E. and Scrivener K. (2014) "Understanding the filler effect on the nucleation and growth of C-S-H" *J. Am. Ceram. Soc.* **97**[12]:3764-3773.
23. Bishnoi S. and Scrivener K. L. (2009) "µic: A new platform for modeling the hydration of cements" *Cem. Concr. Res.*, **39**:266-274.
24. Joseph S. and Bishnoi S. (2014) "Study on the effect of particle size distribution and Blaine fineness on the hydration of cement" in *Proceedings of the RILEM International Symposium on Concrete Modeling CONMOD*, Beijing China.
25. Muller A. C. A., Scrivener K. L., *et al.* (2012) "Densification of C-S-H measured by ^{1}H NMR Relaxometry," *J. Phys. Chem.* **117**:403-412.
26 Termkhajornkit P. and Barbarulo R. (2012) "Modeling the coupled effects of temperature and fineness of Portland cement on the hydration kinetics in cement paste" *Cem. Concr. Res.* **42**[3]:526-538.
27. Jennings H. (2008)” Refinements to colloid model of C-S-H in cement: CM-II” *Cem. Concr. Res.* **38**:275-289.
28. Richardson I. (2008) “The calcium silicate hydrates” *Cem. Concr. Res.* **38**:137-157.
29. Bazzoni A., Ma S., *et al.* (2014) "The effect of magnesium and zinc ions on the hydration kinetics of C_3S" *J. Am. Ceram. Soc.* **97**:3684-3693.

30. Bullard J. W., Scherer G. W. and Thomas J. J. (2015) "Time dependent driving forces and the kinetics of tricalcium silicate hydration" *Cem. Concr. Res.* **74**:26-34.
31. Bullard J. W., Enjolras E., *et al.* (2010) "A parallel reaction-transport model applied to cement hydration and microstructure development" *Model. Simul. Mater. Sci. Eng.*, **18**:16.
32. Garrault S., Nicoleu L. and Nonat A. (2010) "Tricalcium silicate hydration modeling and numerical simulations" in *Proceedings of the RILEM International Symposium on Concrete Modeling CONMOD*, Lausanne Switzerland.
33. Noyes A. A. and Whitney W. R. (1897) "The rate of solution of solid substances in their own solutions" *J. Am. Chem. Soc.* **19**:930–934.
34. Fierens P., Tirlocq J. and Verhaegen J. P. (1973) "Luminescence et hydration du sukucate tricalcique" *Cem. Concr. Res.* **3**[5]:549-560.
35 Juilland P., Kumar A., *et al.* (2012) "Effect of mixing on the early hydration kinetics of alite and OPC systems" *Cem. Concr. Res.* **42**[9]:1175-1188

Chapter IV

Effect of the densification of C-S-H on hydration kinetics of tricalcium silicate

Shiju Joseph [i]*, Shashank Bishnoi [ii], Koen Van Balen [i], Özlem Cizer [i]

[i] *Department of Civil Engineering, KU Leuven, Leuven – 3001, Belgium*
[ii] *Department of Civil Engineering, IIT Delhi, New Delhi – 110016, India*

Abstract[a]

Effect of water to cement (w/c) ratio and temperature profiles on the densification of C-S-H (calcium silicate hydrate gel) and hydration kinetics of triclinic tricalcium silicate (C_3S) is studied beyond the first day of hydration. Calorimetry and quantitative X-ray diffraction/Rietveld analysis show that the degree of hydration is unaffected by w/c up to seven days and marginally thereafter. Coupling the degree of hydration with the portlandite content measured from thermal analysis indicate that C/S ratio of C-S-H decreases with increasing w/c. There is a clear increase in the portlandite content with increasing w/c, even though the degree of hydration is unchanged, due to the variations in C/S ratio of C-S-H. On the other hand, when C_3S is initially cured at a lower temperature (20°C) and then at a higher temperature (40°C), there is a significant increase in the reactivity even until 28 days and vice versa. These experimental results were explained using the densified volumetric growth (DVG) hypothesis, which assumes that hydration kinetics are dependent on the internal surface area of C-S-H.

[a] *Chapter adapted from article published in J. Am. Ceram. Soc.(2018);101:2438-2449, DOI: 10.1111/jace.15390*
* *Corresponding Author: shiju.joseph@kuleuven.be, shiju.joseph@live.be*

4.1. Introduction

Even though tricalcium silicate (C_3S [b])/alite, the major phase in the ordinary Portland cement (OPC), has been studied extensively, the focus of most research is limited to the first 24 hours of hydration. Little research has been carried out beyond 24 hours of hydration, as the rate of hydration is significantly lower in this period. However, hydration thereafter is critical as it contributes to the major proportion of the overall strength and microstructural development in concrete.

The hydration kinetics of C_3S are broadly divided into five stages: period of rapid dissolution, induction period, acceleration period, deceleration period and the slow hydration period. Extensive research has been carried out primarily on the induction period and the main hydration peak (acceleration and deceleration period) using several experimental techniques[1, 2] and numerical modeling[3]. The different hypotheses that potentially explain the induction period are geochemical dissolution[4], presence of a metastable barrier[5, 6], and stabilization of C-S-H[7]. Although the controlling mechanism behind the main hydration peak is still under active debate, it is generally attributed to nucleation and growth (N&G) based mechanisms for which several models have been developed[8-10.] Some researchers point out that it could be a dissolution-controlled mechanism as well which are based on etch pit formation and surface coverage[11, 12].

4.1.1. Densification of C-S-H

Taplin[13] first classified C-S-H broadly into "inner" and "outer" C-S-H depending on its formation inside or outside the original grain boundary. It was further observed from SEM micrographs that a densely packed C-S-H was found near the unhydrated cements grains and loosely packed C-S-H was found away from the surface[14, 15]. The different densities are attributed to the volume of the saturated nanoscale gel pores that are present around the C-S-H sheets in the bulk volume of C-S-H. A high and low density C-S-H (HD C-S-H & LD C-S-H) have also been proposed to explain the surface area measurements from nitrogen adsorption[16, 17]. These high and low densities of C-S-H are further used for micromechanical and transport modeling[18, 19]. TEM[20] and STEM[21] images show a progressive densification of C-S-H over time. According to ^{1}H NMR relaxometry results the bulk density of C-S-H increases with the progress of hydration although its dry density remains the same[22]. Recent studies using *X-ray absorption contrast* clearly shows a densification of the hydration products on the three-dimensional microstructure[23, 24]. Although it used a very high w/c, a harsh hydration stopping process was not needed for the measurement compared to the other imaging techniques. These results validated Powers' assumption of a progressive densification of C-S-H[25].

The effect of the bulk density of C-S-H on hydration kinetics was mostly attributed only to the diffusion-controlled mechanisms, where the denser medium reduces the flow of species[26, 27]. Although many of the models[28, 29] based on nucleation and growth mechanism assume a

[b] Cement chemistry notations: C (CaO); S (SiO_2); H (H_2O)

uniform density of C-S-H, the nucleation and growth of C-S-H around the grain boundaries indeed leads to an increase in the bulk density of C-S-H. Bishnoi and Scrivener[30, 31] proposed a two-step mechanism of Nucleation and Densifying growth (NDG), which assumes that a C-S-H of low bulk density fills the available space in the microstructure, followed by the densification of C-S-H. This view on the hydration kinetics was challenged by Kirby and Biernacki[32] as the maximum heat released remains practically the same even after 24 hours, despite varying w/c, which would change the available space for hydrate formation. Joseph et al.[10] proposed and mathematically modelled a densifying volumetric growth (DVG) hypothesis that assumes that the acceleration period and deceleration period in the main hydration peak are controlled by the densification of C-S-H. The DVG model is also a nucleation and growth based mechanism with an assumption that the densification of C-S-H is related to the internal surface area of C-S-H and assumes a time dependent outer growth rate.

The two major factors that could affect the densification of C-S-H apart from time are water to cement ratio(w/c) and temperature. Tennis and Jennings[17] reported the reduction of mass ratio of low density C-S-H in the overall C-S-H with increase in time and reduction in w/c from regression analysis on the nitrogen sorption measurements[33]. These results imply densification of C-S-H with respect to the degree of hydration and reduction in w/c. Other researchers have also found that the density of hydration product increases with decreasing w/c[34-37]. Recent studies using ^{1}H NMR clearly demonstrated that bulk density of C-S-H increases with the reduction in w/c in white Portland cement. It was proposed that the densification is dependent on the available space[22, 38].

Verbeck and Helmuth[26] have proposed that owing to the time required for the diffusion, hydration products are formed more homogeneously in the paste matrix when cured at a lower temperature and it is heterogeneously formed closer to the surface of the particle when cured at a higher temperature. Experimental evidence from other researchers have also indicated an increased heterogeneity of hydration products and increased porosity upon curing at higher temperature[39-41]. The increased heterogeneity in hydration products was generally attributed to a denser C-S-H[42, 43] and the stability of ettringite[44]. Jennings et al.[45] have reported that the C-S-H gel densifies with increased temperature based on small angle neutron scattering (SANS) measurements. Gallucci et al.[46] have calculated the density of C-S-H gel from backscattered electron image analysis and found it to be increasing with respect to the increase in temperature. Although many other factors such as doping of ions, addition of inert fillers and SCMs, alkalis etc. could also vary the density of C-S-H, their influence is still not conclusively understood.

In this paper, the effect of densification of C-S-H on the hydration kinetics of tricalcium silicate of different fineness are investigated by varying parameters that are known to change the bulk density of C-S-H in Portland cement systems, such as w/c and temperature. To reaffirm the results, the effect of w/c is studied for two different temperatures (20 and 40°C) and the effect of temperature profiles are studied for three different fineness. Also, the reaction mechanism that controls the hydration kinetics of C_3S beyond the first day of hydration is identified and validated. It must be noted that there are several other factors that influence the hydration of C_3S such as addition of inert fillers[10, 47], relative humidity[48], impurities[49], presence of alkalis[50]

or sulfates[51], mixing rates[52] etc. These factors remain out of scope of this study and have been kept constant.

4.2. Experimental Protocol

4.2.1. Materials

Pure triclinic *tricalcium silicate* (SARL Mineral Research Processing, Meyzieu, France) of three different particle size distributions (PSD) '*Ac*', '*An*' and '*Af*' was used in this study. The different grades of fineness were obtained by sieving through 32 and 63 µm sieves and mixing the retained fraction from each sieve and the pan. The particle size distributions (PSD) were determined using laser diffraction technique (Malvern Mastersizer 2000, Hoeilaart, Belgium) and using ethanol as dispersing medium (Fig. 4.1).

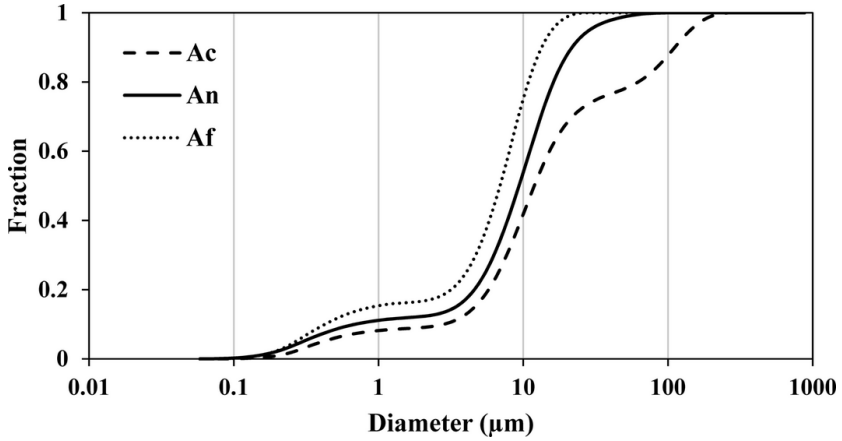

Figure 4.1: Particle size distribution obtained from laser diffraction for the three particle fineness of C_3S used in the study

4.2.2. Temperature profiles

Eight different temperature profiles using a combination of 20°C and 40°C were used to study the effect of temperature on the hydration kinetics of alite at w/c of 0.5. The different temperature profiles used are shown in Fig. 4.2. Here, 20 and 40 refer to the temperatures (°C) under which the samples were cured.. 201 indicates that the sample is first cured at 20°C for 1 day, and then is cured at 40°C. Similarly, 403 indicates that the sample is cured at 40°C for the first 3 days and is afterwards cured at 20°C.

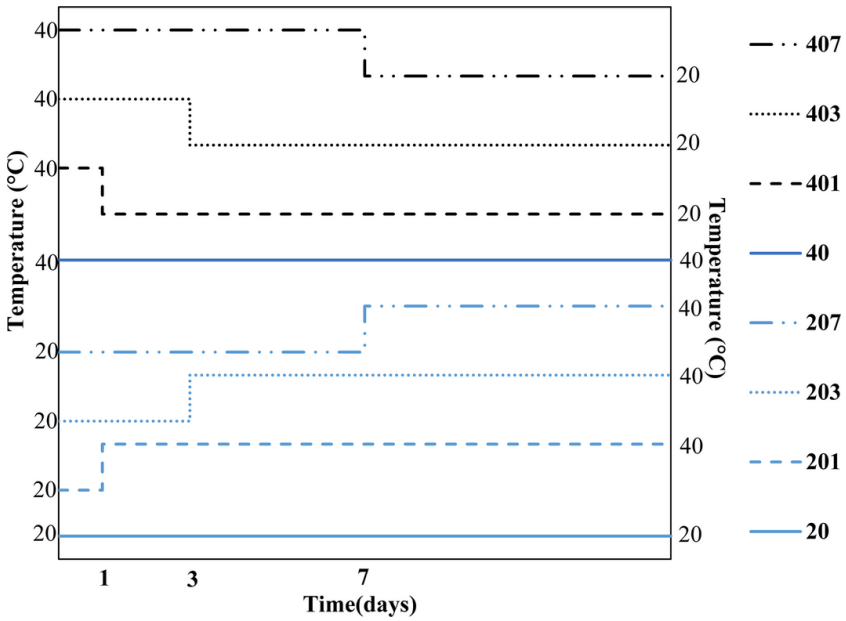

Figure 4.2: Temperature regimes used in the study (in °C). 201, 203 and 207 refer to curing temperatures at 20°C for 1, 3 and 7 days respectively. 401, 403 and 407 refer to curing temperatures at 40°C for 1, 3 and 7 days respectively.

4.2.3. Isothermal calorimetry

C_3S pastes were prepared in a temperature controlled room at 20°C using deionized water at their respective w/c. Heat of hydration was continuously monitored using TAM Air isothermal calorimeter at 20°C and 40°C for up to 7 days for most samples and up to 28 days for limited number of samples. The calorimeter was installed at a temperature controlled room at 20°C and hence could be used for measurement of heat release for a longer period at 20°C. To study the effect of pre-curing on the heat of hydration, the samples were stored at the respective temperature profiles before performing the calorimeter measurements. To ensure that the lower precision of temperature controlled chambers compared to isothermal calorimeter does not affect the accuracy of the results, the samples were first cured at 20°C and 40°C for one day and three days in temperature controlled chambers before keeping them in the calorimeter at the respective temperatures. These results were compared with the measurements for which the samples had been continuously kept at those temperatures. No deviation from the original results was found. The degree of hydration was obtained by dividing the cumulative heat release measured using isothermal calorimetry by the reaction enthalpy 517 J/g[53].

4.2.4. Thermogravimetric analysis

Pastes prepared using the above-mentioned protocols were transferred to 1.5ml plastic tubes that were sealed to avoid evaporation and water leakage. These tubes were then cured at the designated curing temperature profiles for 28 days. Hydration was stopped using a freeze drier (2 hours at 0.03 mbar) after hand crushing the sample using a mortar agate at ages 1, 3, 7 and 28 days. Approximately 25-40 mg of the samples were used to perform thermogravimetric analysis (TGA) to quantitatively determine the portlandite content. NETZSCH STA 409 PC was used at a controlled heating rate of 10°C /min for a temperature range of 20°C - 600°C and

at nitrogen atmosphere with a flow rate of 60mL/min. Some of the samples were also tested until 1000°C to ensure that no carbonation had occurred. The portlandite content was determined by measuring the mass loss due to portlandite decomposition using the tangent method[54]. This was further used in Eq. 4.1, where M_{CH} is the mass loss in percentage due to decomposition of portlandite and 74 and 18 are the molecular masses (g/mol) of portlandite and water respectively.

$$CH_{measured} = M_{CH} \times \frac{74}{18} \tag{4.1}$$

The portlandite content(g) per 100 grams of paste was calculated using Eq. 4.2 [55] where *BW* is the total bound water content (based on mass loss up to 600°C). Portlandite content per 100 grams of anhydrous C_3S is calculated using Eq. 4.3. The degree of hydration of C_3S from TGA is calculated by incorporating the portlandite content in the balanced stoichiometric equation Eq. 4.4 assuming an average C/S ratio of 1.7 and H/S ratio of 2.6, considering the initial anhydrous C_3S content in the paste.

$$CH_{per\ 100g\ paste} = \frac{100 * CH_{measured}}{\left(1 + \frac{w}{c}\right) * (100 - BW)} \tag{4.2}$$

$$CH_{per\ 100g\ anhydrous} = \frac{100 * CH_{measured}}{(100 - BW)} \tag{4.3}$$

$$C_3S + 3.9H \rightarrow C_{1.7} - S - H_{2.6} + 1.3CH \tag{4.4}$$

4.2.5. Quantitative X-ray diffraction

Freeze-dried samples at 7 days and 28 days were further analyzed by X-ray diffraction with Rietveld method to quantitatively determine the degree of hydration of C_3S. Scans were performed using Phillips diffractometer (PW1830, Cu-Kα radiation) and Bruker diffractometer (D2 phaser, Cu-Kα radiation). Two different diffractometers were used due to the breakdown of the first diffractometer after first uses. All these specimens could not be repeated on the second diffractometer due to the insufficient quantities of specimens for analysis. Three hydrated paste samples and one unhydrated C_3S were measured in both diffractometers.

Phase quantification by Rietveld analysis was performed with Topas (Academic) using a combination of external standard method[56] and scale factor approach[57, 58], and by using anhydrous C_3S as the standard. The mass attenuation coefficient (MAC) of the sample was calculated from the oxide composition of C_3S. The bound water content calculated from the thermal analysis for hydrated paste was also incorporated for the calculation of MAC. The crystallinity of C_3S used in this study, calculated against corundum standard is around 91%.

The bound water content and w/c were also considered to calculate the degree of hydration of C_3S, using Eq. 4.5, similar to Eq. 4.2. The ICSD numbers of C_3S and portlandite used for the refinement were 4331 and 20220 respectively.

$$C_3S_{per\ 100g\ paste} = \frac{100 * C_3S_{Reitveld}}{\left(1 + \frac{w}{c}\right) * (100 - BW)} \quad (4.5)$$

4.2.6. X-ray compositional micro analysis

EDS (energy dispersive spectrometry) and WDS (wavelength dispersive spectrometry) techniques were used to obtain elemental and oxide composition of C-S-H. For this purpose, C_3S pastes with w/c 0.4, 0.5 and 0.66 were prepared, and hydration was stopped using solvent exchange method (isopropanol) after 7 days of hydration. Around 100ml of isopropanol was used for stopping hydration of around 1ml of paste. Isopropanol was replaced after 24 hours of immersion and the specimens were kept immersed for another 7 days. The specimen was then impregnated in resin and was polished after keeping in vacuum for 24 hours. Platinum coating of 5nm was applied for increasing conductivity. EDS measurement was carried out at 10kV using FEI-Nova Nanosem 450 and WDS measurement at 15kV using Jeol JXA-8530F EPMA (electron probe microanalyzer).

4.3. Experimental Results

4.3.1. Effect of water to cement ratio

Fig. 4.3 shows the effect of w/c on the cumulative heat release for 20°C up till 28 days and for 40°C up till 7 days for *'An'*. The measurement of heat release for 20°C has been repeated for 7 days and no considerable deviations have been observed. Although previous researches have already indicated that w/c has a limited influence on hydration kinetics at early ages (until 24 hours)[29, 32], there are limited studies on the effect at later ages for C_3S. It is clearly seen in Fig. 4.3 that the w/c does not have a significant effect on the kinetics of C_3S hydration even at later ages. This result is contrary to the effect of w/c on the hydration of Portland cement, in which increasing w/c increases its overall heat release at the later ages[47]. Fig. 4.4 shows the comparison of the chemically bound water associated with the decomposition of C-S-H for w/c 0.5 and 0.66 at respective ages. This is calculated by subtracting the mass loss due to portlandite decomposition from the mass loss between 105-600°C in TG measurement and is normalized to per 100g of paste. The results show that there is no significant difference in the mass loss due to decomposition of C-S-H for w/c 0.5 and 0.66 for both 20°C and 40°C. This implies that the degree of hydration of C_3S does not significantly vary with w/c. This must be treated with caution because, there could be an overlap of physically bound water, chemically bound water and adsorbed water within the temperature range. Additionally, it has been reported that changes in C/S ratio could also vary the chemically bound water per mol of C-S-H[59].

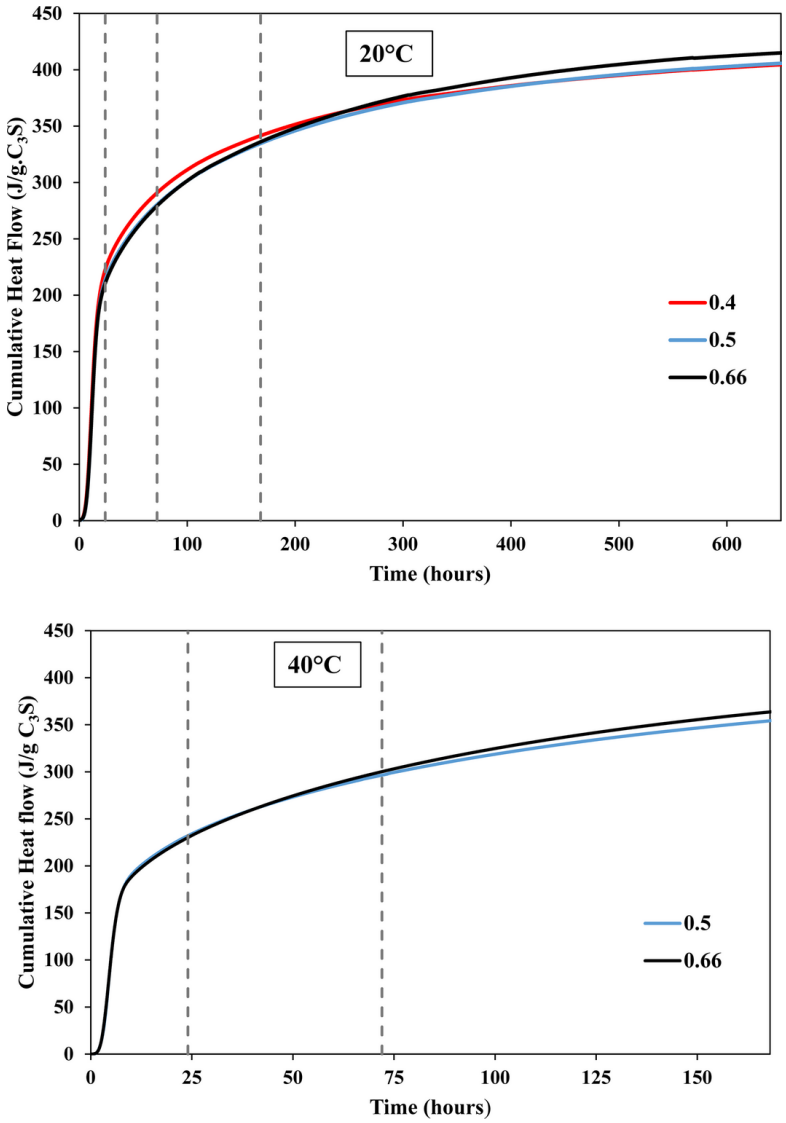

Figure 4.3: Effect of w/c on cumulative heat release of 'An' at 20°C up to 28 days (top). Heat release up to 7 days for w/c 0.5 and 0.6 at 40°C (bottom). Dashed vertical lines indicate 1, 3 and 7 days.

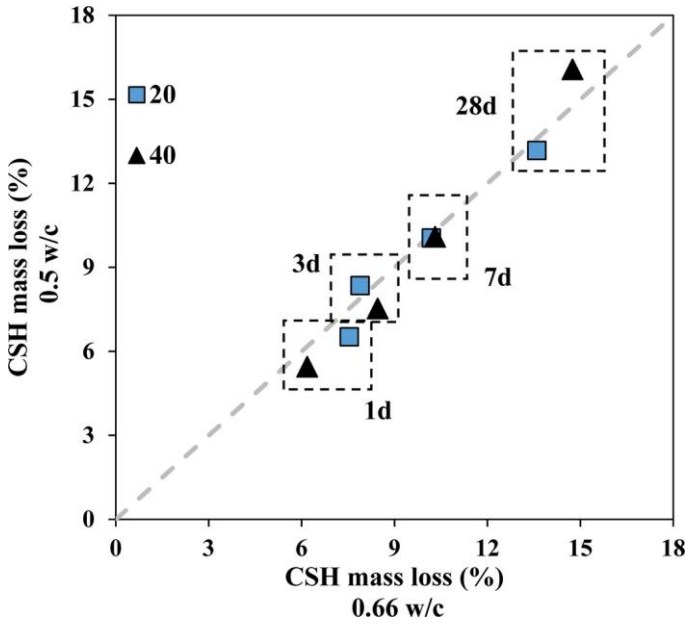

Figure 4.4: Comparison of the chemically bound water associated with the decomposition of C-S-H measured from thermal analysis for '*An*' *at* w/c ratio 0.5 and 0.66 at 20°C (1, 3, 7 and 28 days) and 40°C (1, 3, 7, 28 days)

To further confirm that the degree of C_3S hydration is not affected by w/c, samples from 7 days and 28 days of hydration were analyzed with quantitative X-ray diffraction (QXRD) using Rietveld method. Comparison of the degree of hydration of C_3S quantified using Rietveld refinement and isothermal calorimetry is given in Fig. 4.5. The difference in the degree of hydration for different w/c is low when measured by QXRD as well. This trend is very similar to the results from calorimetry. This further confirms that the w/c has very limited influence on the hydration kinetics of C_3S even at later ages.

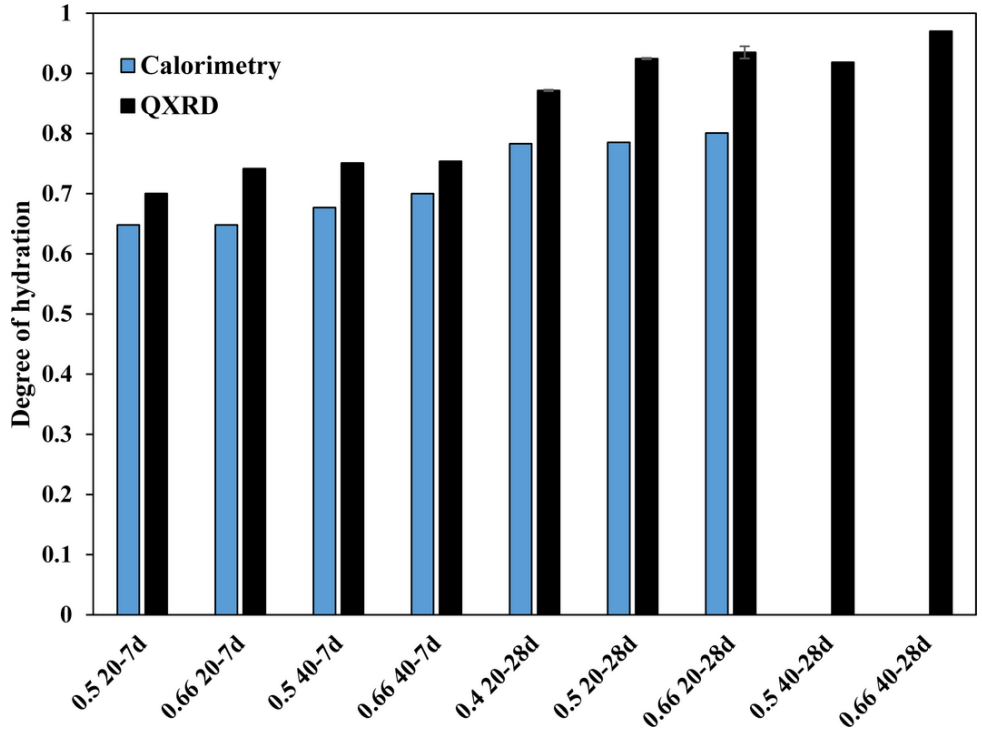

Figure 4.5: Comparison of the degree of hydration of 'An' calculated from isothermal calorimetry and quantitative X-ray diffraction. Labels indicate w/c ratio (0.4, 0.5, 0.66), temperature (20 and 40) and age (7d and 28d) respectively. Error bars calculated for three XRD samples from measurements by two different diffractometers.

The degree of hydration is consistently lower when it is measured by isothermal calorimeter and the difference is more pronounced at 28 days. Nevertheless, this is expected because the initial heat flow is omitted to calculate the cumulative heat flow and at the later ages there would be more loss of heat from the calorimeter due to considerably low output heat rate. Note that the isothermal calorimetry is inferior to QXRD for measurement of degree of hydration and it is more suited to measure the rate of hydration. This is because, when the cumulative heat release is calculated from calorimetry, the errors associated (such as the heat loss) with the calorimeter is accumulated over time. Also, the values for the enthalpy of reaction of C_3S that are used to calculate the degree of hydration are found to vary in the literature and range from 500 to 564J/g[8, 9, 54, 60].

To study the effect of C/S ratio on w/c, EDS and WDS measurements were performed on polished samples of w/c 0.4, 0.5 and 0.66 after 7 days for hydration that had been cured at 20ºC (Fig. 4.6). Both EDS and WDS measurements indicate an increase in C/S ratio with a decrease in w/c. The trend corresponds well with the literature where the variations in w/c are significantly high[61]. However, our results are not conclusive owing to the large standard deviation. The error primarily arises from the intermixing of portlandite with C-S-H[62] and due to the large interactive volume (of the order few microns) of the X-rays compared to the much smaller C-S-H shells. The uneven surface due to imperfect polishing could also cause the deviations. Similar large standard deviations in measurement of C/S ratio are generally seen in the literature[63, 64].

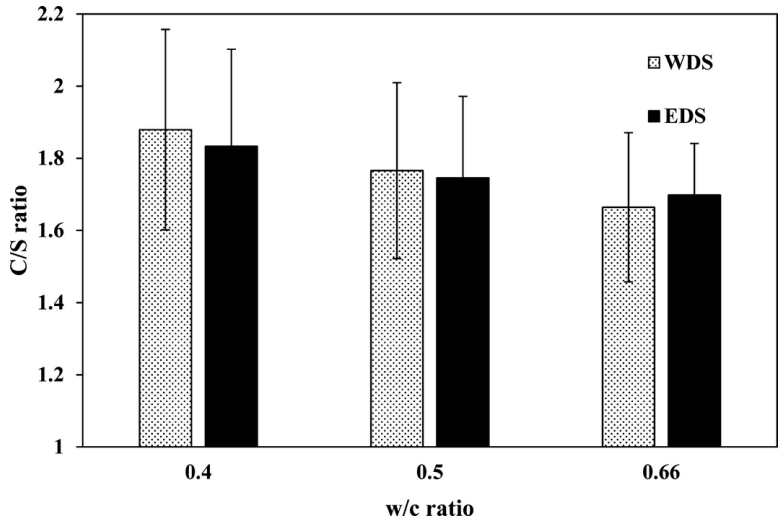

Figure 4.6: Effect of w/c on C/S ratio measured using EDS (10kV) and WDS (15kV) on polished samples of *'An'* after 7 days of hydration. The error bar represents the standard deviation

In order to validate the effect of C/S ratio on the w/c, the portlandite content was calculated from the thermal analysis using the tangent method (Fig. 4.7). The error bar represents the standard deviation obtained from nine repeated measurements on hydrated C_3S pastes. The results consistently show an increase in the portlandite content with increasing w/c ratio for both 20°C and 40°C. If there is a reduction in the C/S ratio with increasing w/c, the portlandite content would be on a higher side even though the degree of hydration is the same. This clearly indicates that the C/S ratio is decreasing with an increasing w/c. It must be noted that a wide range of C/S ratios are reported in the literature, which ranges from 1.2 to 2.3 [15, 59, 65].

When C/S ratio changes, the number of moles of precipitating portlandite would change, but the number of moles of C-S-H remains the same according to the stoichiometric equation, Eq. 4.6, where '*x'* is the C/S ratio and '*b*' is the moles of chemically bound water in C-S-H (substituting *x=1.7 & b=2.6*, Eq. 4.6 becomes Eq. 4.4).

$$C_3S + (3 - x + b)H \rightarrow C_x - S - H_b + (3 - x)CH \quad (4.6)$$

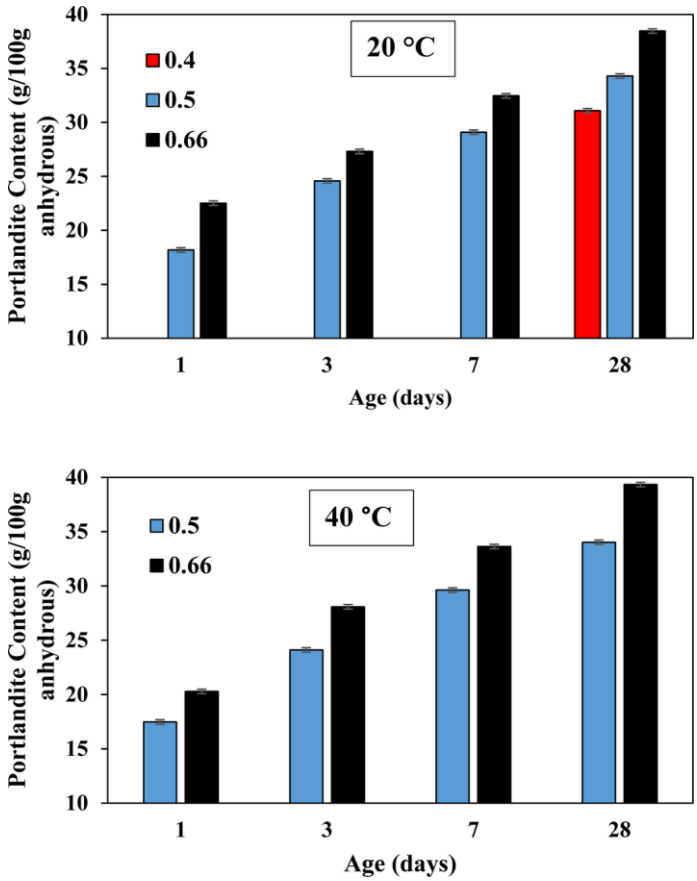

Figure 4.7: Effect of w/c (0.4, 0.5, 0.66) on the portlandite content (per 100g anhydrous) calculated from thermal analysis for 'An' at 20 °C (top) and 40 °C (bottom)

Fig. 4.8 shows the C/S ratio calculated by coupling the degree of hydration and portlandite content from isothermal calorimetry and TGA (Fig. 4.8: top) and from QXRD and TGA (Fig. 4.8: bottom). The differences in the top and bottom figure arises due to the variations of the degree of hydration measured using QXRD and calorimeter. The C/S ratios calculated are in the range reported in the literature and also follow the same trend as in Fig. 4.6. This confirms that C/S ratio decreases with increasing w/c, thereby increasing the amount of precipitated portlandite. There is no definite trend that could be drawn from the current result on the C/S ratio with respect to the degree of hydration and temperature.

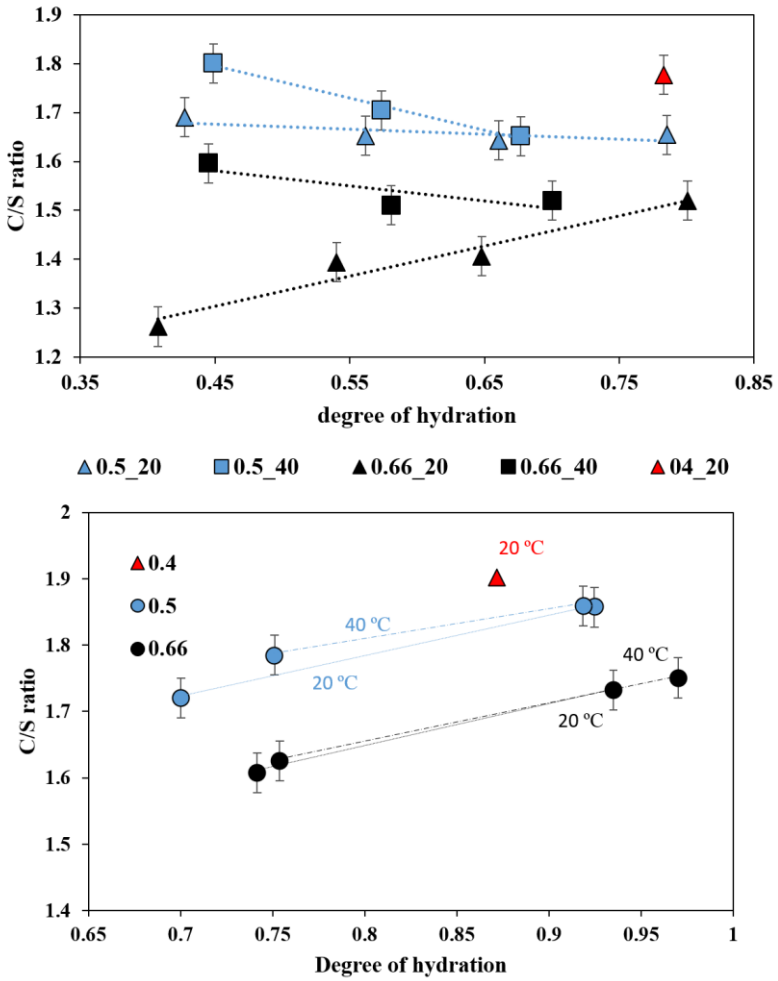

Figure 4.8: C/S ratio calculated for 'An' by coupling the degree of hydration and portlandite content from isothermal calorimetry and TGA (top) and from QXRD and TGA (bottom). Labels indicate w/c ratio (0.4, 0.5, 0.66) and temperature (20 and 40) respectively.

4.3.2. Effect of temperature profile

Fig. 4.9 shows the rate of heat release and the degree of hydration with respect to the cumulative heat for the three-different fineness of C_3S cured at 20°C and 40°C. Increased fineness leads to a higher heat release, and the main peak appears earlier and higher at the higher temperature. As also reported in the literature, the degree of hydration of '*Ac*' and '*Af*,' at 40˚C becomes lower than that at 20˚C after a certain age of hydration[66, 67]. The decrease in the degree of hydration is marginal and does not happen for '*An'*.

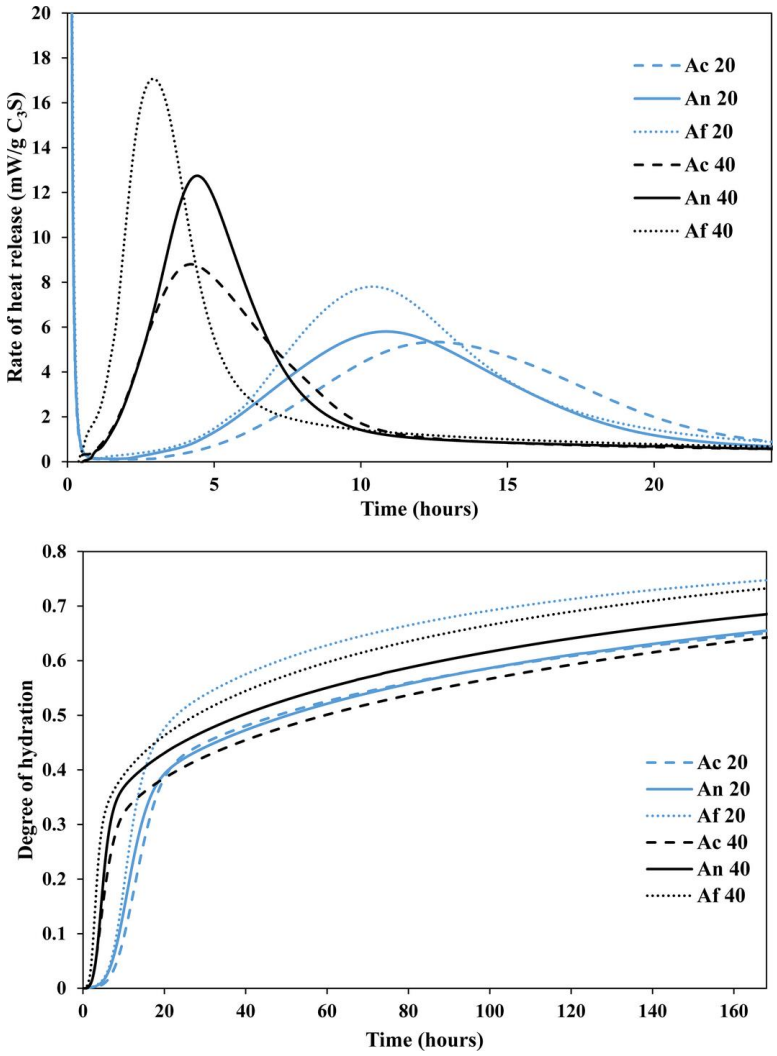

Figure 4.9: Isothermal calorimeter results at 20°C and 40°C for three particle fineness Ac, An and Af (w/c: 0.5). Rate of heat release up to 1 day (top) and degree of hydration calculated from the cumulative heat release up to 7 days (bottom).

Fig. 4.10 shows the cumulative heat release measured in an isothermal calorimeter for the different temperature profiles until seven days of hydration on the three particle fractions. For the sample 'An', the degree of hydration calculated using the portlandite content, measured from thermal analysis, assuming a C/S ratio of '*1.7*' is also shown in the graph. The results show that the cumulative release from C_3S is not much different after 1 day of hydration when cured at 20°C or 40°C. On the other hand, when C_3S is pre-cured at a lower temperature and then cured at a higher temperature, there is a substantial increase in the overall heat release. On the other hand, if it is pre-cured at a higher temperature and then cured at a lower temperature the overall heat release is significantly lower. This phenomenon is observed for all three-different fineness of C_3S. Additionally, after one day, more than half of the degree of hydration achieved after seven days is reached. Fig. 4.10 also shows that there is a good agreement between the degree of hydration measured from isothermal calorimeter (assuming a reaction enthalpy of 517J/g) and that calculated from thermal analysis.

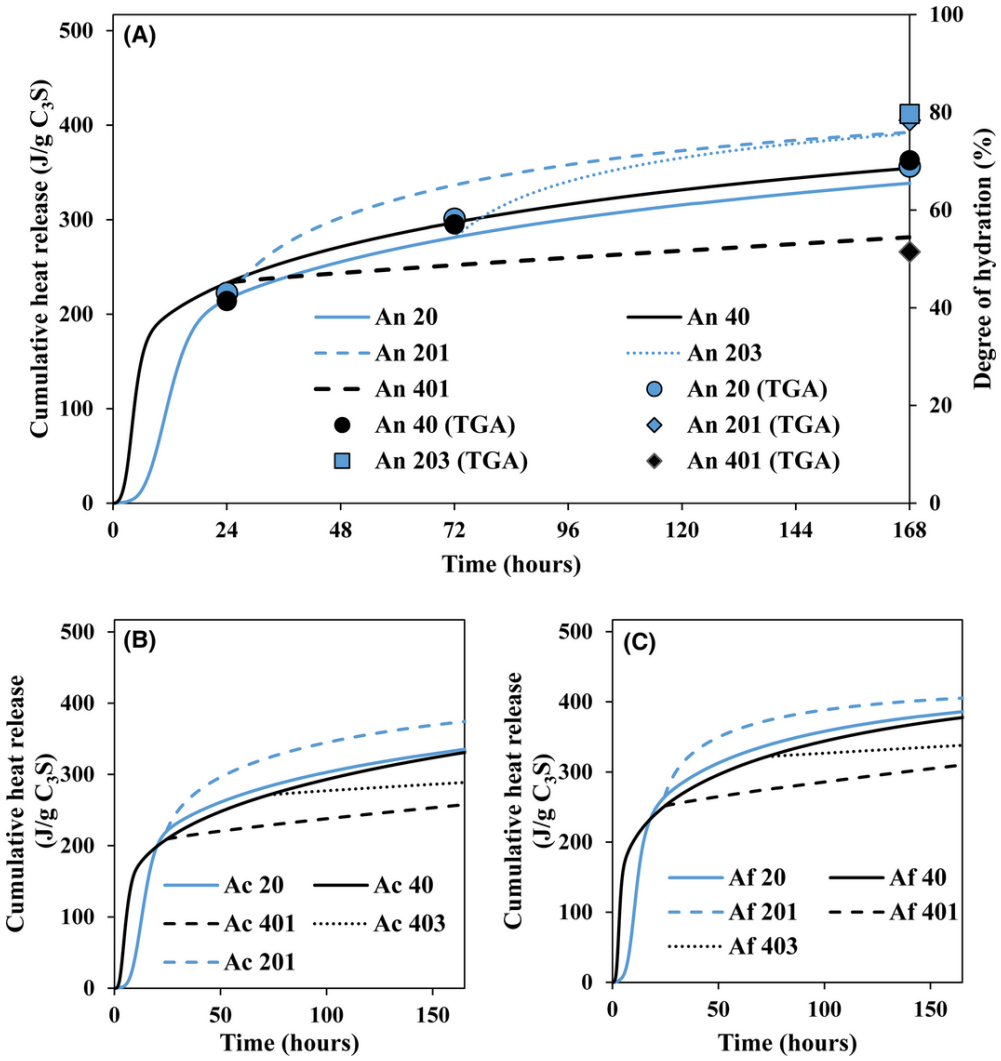

Figure 4.10: Effect of different temperature profiles (Fig. 4.2) on the hydration kinetics of three particle fineness (w/c: 0.5); (A) An (calorimeter data and TGA data indicated by blue and black markers referring to the degree of hydration calculated using portlandite content); (B) Ac (calorimeter data); (C) Af (calorimeter data).

Fig. 4.11 shows the portlandite content per 100 g of paste for all the temperature profiles until 28 days. This corresponds well with the results of the isothermal calorimetry, further confirming that this is not just an early age behavior, and that this trend continues at the later ages as well. Isothermal calorimetry was limited to seven days as beyond that period the results would be more prone to error as indicated in the previous sections.

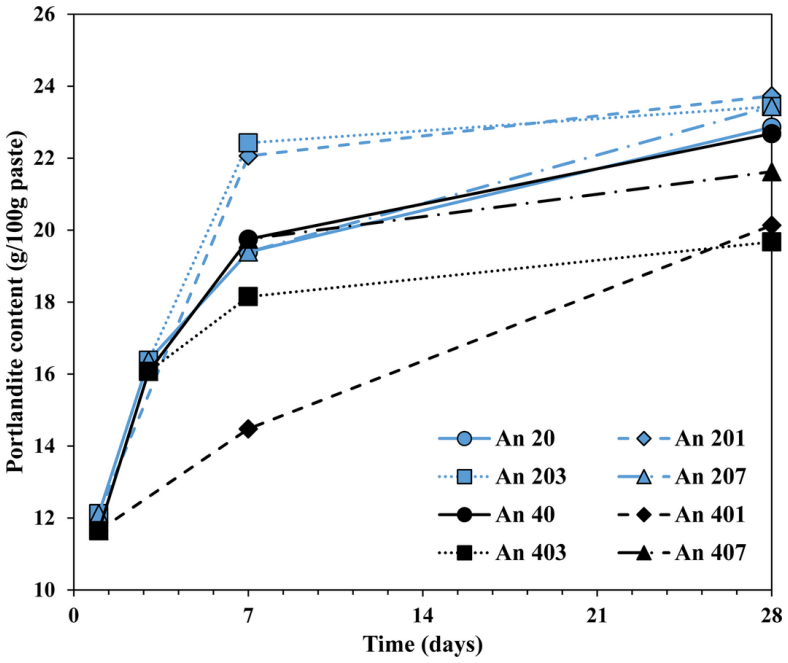

Figure 4.11: Portlandite content (per 100 g of paste) in 'An' at all temperature profiles (Fig. 4.2) up to 28 days (w/c: 0.5).

4.4. Activation Energy

The concept of an "apparent" activation energy has been used for decades to model the effect of temperature on hydration kinetics and strength development in cement-based materials using a maturity method[68]. The activation energy was calculated making linear plots from the isothermal data for different curing temperatures. The calculated activation energy was generally seen to vary during the progress of hydration[67, 69, 70]. This change in the activation energy was attributed to change in the reaction mechanism in cement. The ground-breaking paper from Thomas[71] concluded based on results from differential scanning calorimetry that the activation energy of C_3S does not change with time even up to 70% hydration. This shows that the rate controlling mechanism does not change over the course of hydration. The objective of this section is to reaffirm this finding using the experimental data presented in the preceding section.

Fig. 4.12 shows the rate of heat release versus degree of hydration (α). When α > 0.25-0.35 (depending upon the PSD), the rate of hydration for 40°C is lower than that of 20°C. This would have a significant impact on the calculation of the activation energy because it is dependent on the rate of hydration for different temperatures at the same degrees of hydration. The activation energy, *Ea*, can be calculated from Eq. 4.7 [69], where T_1 and T_2 are the absolute temperature of curing, R the universal gas constant and k_1, k_2 are the rates of hydration at the same degree of hydration.

$$E_a = R\left[\frac{T_1 T_2}{T_1 - T_2}\ln\left(\frac{k_1}{k_2}\right)\right] \tag{4.7}$$

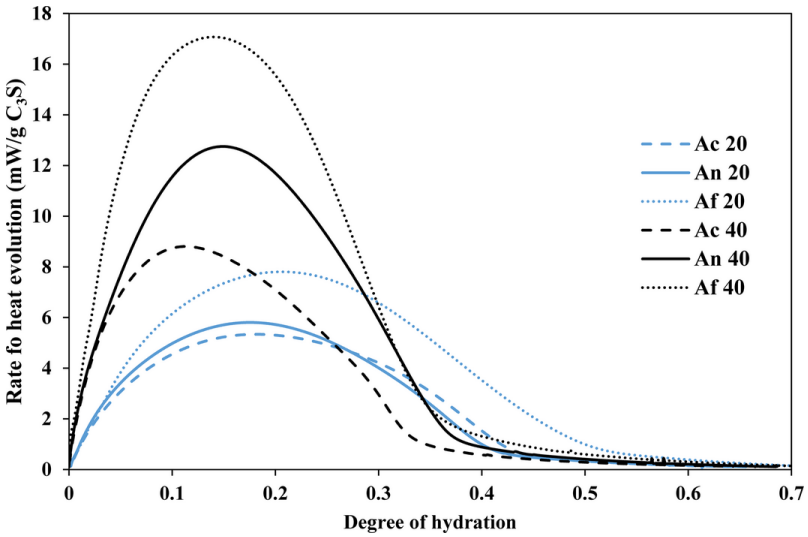

Figure 4.12: Rate of heat release vs degree of hydration at 20°C and 40°C (w/c: 0.5)

Fig. 4.13 shows the variation of the calculated activation energy for the three fineness of C_3S using Eq. 4.7. The results show the same trend which was seen in the results of Thomas[71] and Kejellsen and Detwiler[67]. The calculated activation energy reduces and even goes below zero which is theoretically not possible for the system. According to Thomas[71] this should be expected because of the microstructural changes when it is cured at different temperatures. Fig. 4.14 shows the instantaneous activation energy calculated by measuring the change in the rate of hydration when a specimen was moved from 20˚C to 40˚C in the isothermal calorimeter after 1 day and 3 days of hydration. While this method of calculating the activation energy is similar to that reported by Thomas[71], the preconditioning of the specimen, before keeping it in the calorimeter, was carried out in an oven maintained at the other temperature. Despite all experimental care, the readings within the first 30 minutes of changing the temperature had to be discarded because the temperature of the calorimeter did not stabilize during this period of time. The results further confirm the finding of Thomas[71] that the activation energy does not change during hydration, atleast at 1 and 3 days. The average activation energy was calculated as 46723 J/mol, which is close to the value reported (~51.1 kJ/mol) by Thomas[71]. It may be noted that the method used in this work will be simpler to use with normal isothermal calorimeters, since it requires only one calorimeter and does not require changing of temperature in the equipment during the measurement.

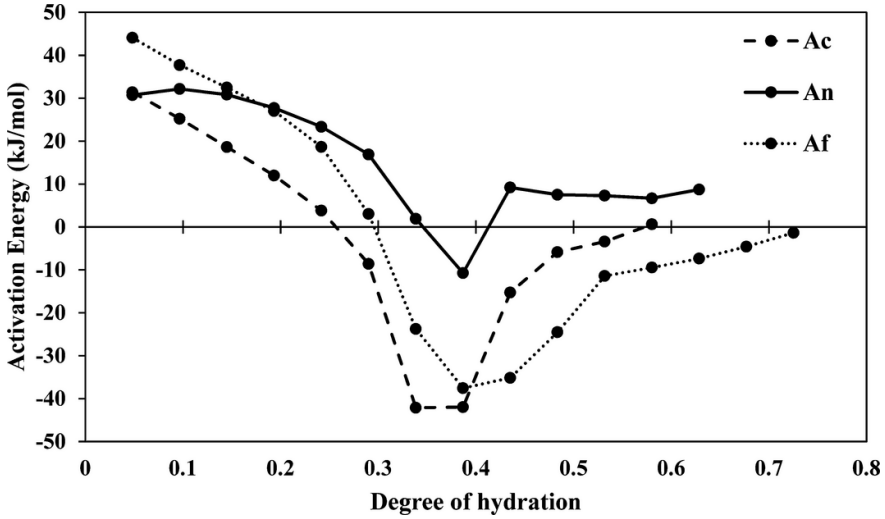

Figure 4.13: Activation energy calculated for the three-different fineness at w/c 0.5 using Eq. 4.7

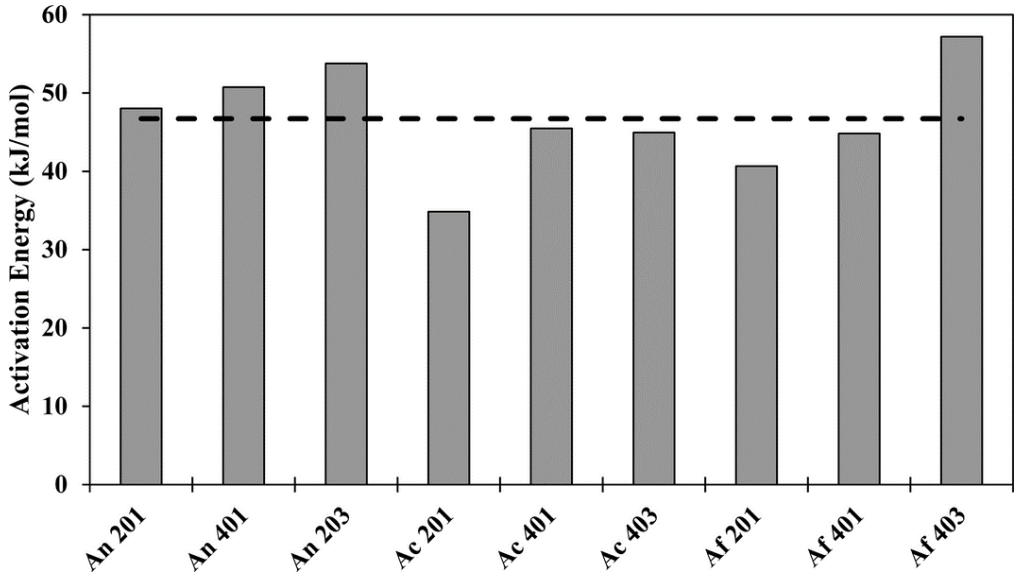

Figure 4.14: Instantaneous activation energy calculated for '*Ac*', '*An*' and '*Af*' for w/c 0.5. Dashed line indicates the calculated average activation energy

4.5. Proposed Mechanism

The mechanism intending to explain the results of this study is an extension of the densified volumetric growth (DVG) hypothesis[10], which is a variant of the nucleation and growth mechanism. As per this hypothesis the rate of hydration of C_3S is dependent on the total internal surface area of C-S-H. The internal surface area is assumed to be controlled by the densification of C-S-H. When C-S-H nucleates and grows on its own surface, the bulk density increases, which initially increases the internal surface area. However, after an initial peak, it will decrease due to impingements of C-S-H in layers and from C-S-H from other particles. At the same time, while C-S-H grows from its initial surface, new low-density layers increase the surface area available for C-S-H to nucleate. It is assumed that the outer growth rate of C-S-H

will be reduced with time as nucleation would be preferable along the internal edges than on the surface owing to the lower energy requirement[72].

When C_3S is cured initially at a higher temperature and thereafter at a lower temperature, the denser C-S-H formed due to the increased temperature will have a lower internal surface area. Followed by curing at a lower temperature, the rate of reaction will be also lower as the C-S-H layers are already dense, and there will be less available surface for C-S-H to nucleate. Similarly, when C_3S is cured initially at a lower temperature and then at a higher temperature, the C_3S with lower bulk density of C-S-H, owing to its higher internal surface area, will have an even higher reaction rate with the increased temperature. While C_3S is cured constantly at a lower or a higher temperature, the densification is compensated with the temperature of curing, which in turns gives similar degrees of hydration.

With respect to the effect of w/c, as the kinetics of hydration hardly changes, this would imply that the densification is also not affected significantly. This is contrary to the specific bulk density measured using ^1H NMR by Muller[22] which was found to decrease with increasing w/c. This could be either due to or combination of:

i. Hadley grains: Hadley grains[73], which are the hollow shells closer to the original particle boundary(Fig. 4.15), are seen more commonly in Portland cement systems and are insignificant in C_3S systems in the later ages[74, 75]. This would lead to an increase in bulk density of C-S-H due to the interparticle impingements as there would be higher amounts of outer C-S-H.
ii. C/S ratio: The change in C/S ratio with respect to the w/c could influence the calculated specific bulk density or the internal surface area as the molecular mass of C-S-H is also changing.

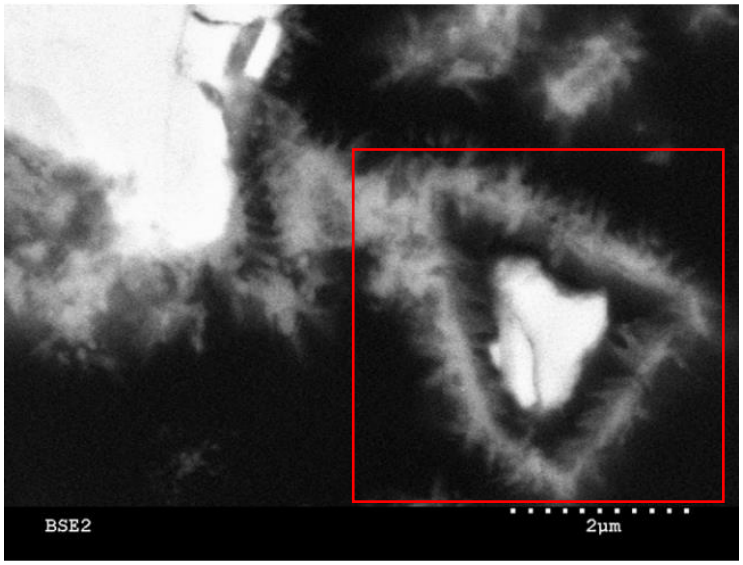

Figure 4.15: Backscattered electron image of cement paste hydrated for 13 hours which shows Hadley grains[75]

Hadley grains could also explain why there is an effect of w/c on the rate of hydration of Portland cement at the later ages[47], even though it is not seen in C_3S. More importantly, as the rate of hydration hardly changes with changing w/c, this would imply that kinetic models could be used for studying C_3S hydration without the need of calculating complex interparticle impingement of C-S-H even at later ages.

4.6. Conclusion

This study presents the effect of water to cement ratio(w/c) and temperature profiles, the factors that are expected to influence the densification of C-S-H, on the hydration kinetics of triclinic tricalcium silicate (C_3S) beyond the initial day of hydration. The major conclusions of this study are as follows:

i. Results from isothermal calorimetry show that there is a minimal effect on the studied w/c (0.4, 0.5, and 0.66) on the hydration kinetics of C_3S. This is further supported by chemical bound water content of C-S-H determined with thermal analysis and degree of hydration of C_3S calculated using quantitative X-ray diffraction(QXRD).
ii. By coupling the degree of hydration measured from isothermal calorimetry and QXRD and the portlandite content calculated from thermal analysis, it was found that C/S ratio decreases with increasing w/c. Hence there would be an increased precipitation of portlandite with increasing w/c, even though the degree of hydration is hardly changing.
iii. When C_3S is pre-cured at a lower temperature (20°C) and then cured at a higher temperature (40°C), a higher degree of hydration is obtained. On the other hand, when C_3S is pre-cured at a higher temperature and then cured at a lower temperature, there is a significant reduction in the overall degree of hydration. This is probably because, with an increase in temperature, although the rate of hydration increases, simultaneously the bulk density of C-S-H is also increasing. This increase in the bulk density will hinder the overall degree of reaction due to the reduction in the internal surface area of C-S-H.
iv. The results in the work reaffirm the previous study that there is no change of instantaneous activation energy at least at 1 and 3 days of hydration.

These experimental results reaffirm the previously proposed densified volumetric growth (DVG) hypothesis, which is essentially a nucleation and growth controlled mechanism in which the rate of hydration depends on the internal surface area of C-S-H.

References

1. Scrivener K.L, Juilland P and Monteriro P.J.(2015) “Advances in understanding hydration of Portland cement” *Cem. Concr. Res.*; **78**:38-56.
2. Bullard J, Jennings H, *et al.* (2011) “Mechanisms of cement hydration” *Cem. Concr. Res.* **41**:1208-1223.
3. Thomas J, Biernacki J, *et al.* (2011)“Modelling and simulation of cement hydration kinetics and microstructural development” *Cem. Concr. Res.* **41**:1257-1278.

4. Juilland P, Gallucci E, *et al.*(2010) “Dissolution theory applied to the induction period in alite hydration” *Cem. Concr. Res.***40**:831-844.
5. Stein H.N and Stevels J.M. (1964) “Influence of silica on the hydration of 3CaO, SiO2.” *J. appl. Chem.* **14**[8]:338-346.
6. Jennings H.M and Pratt P.L. (1979) “An experimental argument for the existence of a protective membrane surrounding portland cement during the induction period” *Cem. Concr. Res.* **9**:501-506.
7. Bergold S.T, Goetz-Neunhoeffer F and Neubauer J. (2015) “Mechanically activated alite: New insights into alite hydration” *Cem. Concr. Res.* **76**:202-211.
8. Bishnoi S and Scrivener K.L. (2009) “Studiying nucleation and growth kinetics of alite hydration using μic” Cem. Concr. Res. **39**:849-860.
9. Masoero E, Thomas J.J and Jennings H.M. (2014) “A reaction zone hypothesis for the effects of particle size and water to cement ratio on the early hydration kinetics of C_3S” *J. Am. Ceram. Soc.* **97**[3]:967-975.
10. Joseph S, Bishnoi S, *et al.* (2017) “Modeling the effect of fineness and filler in the early-age hydration of tricalcium silicate” *J. Am. Ceram. Soc.* **100**[3]:1178-1194.
11. Nicoleau L and Nonat A. (2016) “A new view on the kinetics of tricalcium silicate hydration” *Cem. Concr. Res.* **86**:1-11.
12. Nicoleau L and Bertolim M.A. (2016) “Analytical model for the Alite (C3S) dissolution topography” *J. Am. Ceram. Soc.* **99**[3]:773-786.
13. Taplin J.H. (1959) “A method for following the hydration reaction in Portland cement paste” *J. Appl. Sci.* **10**:329-345.
14. Scrivener K.L. (1989) “Microstructure of Concrete” *Materials science of concrete Vol I,* Westerville, Ohio, American Ceramic Society; 127-161.
15. Richardson I.G. (1999) “The nature of C-S-H in hardened cements” *Cem. Concr. Res.* **29**:1131-1147.
16. Jennings H.M. (2000) “A model for the microstructure of calcium silicate hydrate in cement paste” *Cem. Concr. Res.* **30**:101-116.
17. Tennis P.D, Jennings H.M. (2000) “A model for two types of calcium silicate hydrate in the microstructure of Portland cement pastes” *Cem. Concr. Res.***30**:855-863.
18. Jennings HM. (2004) “Colloid model of C-S-H and implications to the problem of creep and shrinkage” *Mater. Struct.* **37**:59-70.
19. Patel R.A, Phung Q.T, *et al.* (2016) “Diffusivity of saturated ordinary Portland cement-based materials: A critical review of experimental and analytical modelling approaches” *Cem. Concr. Res.* **90**: 52-72.
20. Mathur P.C. (2007) “Study of cementitious materials using transmission electron microscopy” *PhD Thesis*, EPFL Switzerland.
21. Bazzoni A. (2014) “Study of early hydration mechanisms of cement by means of electron microscopy” *PhD Thesis*, EPFL Switzerland.
22. Muller A.C.A, Scrivener K.L, *et al.* (2012) “Densification of C-S-H measured by ^1H NMR Relaxometry” *J. Phys. Chem.* **117**:403-412.
23. Hu Q, Aboustait M, *et al.* (2016) “Direct measurements of 3D structure, chemistry and mass density during the induction period of C_3S hydration” *Cem. Concr. Res.* **89**:14-26.

24. Hu Q, Aboustait M, *et al.* (2016) "Direct three-dimensional observation of the microstructure and chemistry of C_3S hydration" *Cem. Concr. Res.* **88**:157-169.
25. Powers T.C. (1960) "Physical properties of cement paste" in *Proceedings of the fourth international symposium on the chemistry of cement*, Washington DC United States of America.
26. Verbeck G.J and Helmuth R.H. (1968) "Structure and physical properties of cement paste" in *Proceedings of the 5th International Congress on the Chemistry of Cement*, Tokyo Japan.
27. Escalante-Garcia J.I and Sharp J.H. (1998) "Effect of temperature on the hydration of the main clinker phases in portland cements: part I, neat cements" *Cem. Concr. Res.* **28**[9]:1245-1257.
28. Garrault S, Nicoleu L and Nonat A. (2010) "Tricalcium silicate hydration modeling and numerical simulations" in *Proceedings of the RILEM International Symposium on Concrete Modeling CONMOD*, Lausanne Switzerland.
29. Thomas J. (2007) "A new approach to modelling the nucleation and growth kinetics of tricalcium silicate hydration" *J. Am. Ceram. Soc.* **90**[10]:3282-3288.
30. Bishnoi S. (2008) "Vector modelling of hydrating cement microstructure and kinetics" *PhD Thesis*, EPFL Switzerland.
31. Bishnoi S and Scrivener K.L. (2009) "μic: A new platform for modelling the hydration of cements" *Cem. Concr. Res.* **39**:266-274.
32. Kirby D and Biernacki J.J. (2012) "The effect of water to cement ratio on the hydraion kinetics of tricalcium silicate cements: testing the two step hydration hypothesis" *Cem. Concr. Res.* **42**[8]:1147-56.
33. Hunt C.M. (1966) "Nitrogen sorption measurements and surface areas of hardened cement pastes" in *Proc of a Symp on the Structure of Portland Cement Paste and Concrete*, Washington DC United States of America.
34. van Breugel K. (1991) "Simulation of hydration and formation of structure in hardening Cement-Based materials" *PhD Thesis*, TU Delft Netherlands.
35. Koster H, and Odler I. (1986) "Investigations on the structure of fully hydrated Portland cement and tricalcium silicate pastes. I. Bound water, chemical shrinkage and density of hydrates" *Cem. Concr. Res.* **16**:207-214.
36. Relis M and Soroka I. (1977) "Variation in density of Portland cement hydration products" *Cem. Concr. Res.* **7**:673-680.
37. Feldman R.F. (1972) "Helium flow and density measurement of the hydrated tricalcium silicate-water system" *Cem. Concr. Res.* **2**:123-136.
38. Königsberger M, Hellmich C and Pichler B. (2016) "Densification of C-S-H is mainly driven by available precipitation space, as quantified through an analytical cement hydration model based on NMR data" *Cem. Concr. Res.* **87**:170-183.
39. Skanly J and Odler I. (1972) "Pore structure of calcium silicate hydrates" *Cem. Concr. Res.* **2**:387-400.
40. Radjy F and Richards C.W. (1973) "Effect of curing and heat treatment history on the dynamic mechanical response and the pore structure of hardened cement paste" *Cem. Concr. Res.* **3**:7-21.

41. Sellevold E.J. (1974) "Mercury porosimetry of hardened cement paste cured or stored at 97°C" *Cem. Concr. Res.* **4**:399-404.
42. Kjellsen K.O, Detwiler R.J and Gjorv O.E. (1990) "Backscattered electron imaging of cement pastes hydrated at different temperatures" *Cem. Concr. Res.* **20**:308-311.
43. Scrivener K.L. (1992) "The effect of heat treatment on inner product C-S-H" *Cem. Concr. Res.* **22**:1224-1226.
44. Lothenbach B, Winnefeld F, *et al.* (2007) "Effect of temperature on the pore solution, microstructure and hydration products of Portland cement pastes" *Cem. Concr. Res.* **37**[4]:483-491.
45. Jennings H.M, Thomas J.J, *et al.* (2007) "A multi-technique investigation of the nanoporosity of cement paste" *Cem. Concr. Res.* **37**:329-336.
46. Gallucci E, Zhang X and Scrivener K.L. (2013) "Effect of temperature on the microstructure of calcium silicate hydrate (C-S-H)" *Cem. Concr. Res.* **53**:185-195.
47. Berodier E. (2015) "Impact of the supplementary cementitious materials on the kinetics and microstructural development of cement hydration" *PhD Thesis*, EPFL Switzerland.
48. Jensen O.M, Hansen P.F, *et al.* (1999) "Clinker mineral hydration at reduced relative humidities" *Cem. Concr. Res.* **29**[9]:1505-1512.
49. Bazzoni A, Ma S, et al. (2014) "The effect of magnesium and zinc ions on the hydration kinetics of C_3S" *J. Am. Ceram. Soc.* **97**:3684-3693.
50. Sant G, Kumar A, et al. (2012) "The influence of sodium and potassium hydroxide on volume changes in cementitious materials" *Cem. Concr. Res.* **42**:1447-1455.
51. Mota B, Matschei T and Scrivener K.L. (2015) "The influence of sodium salts and gypsum on alite hydration" *Cem. Concr. Res.* **75**:53-65.
52. Juilland P, Kumar A, et al. (2012) "Effect of mixing on the Early hydration kinetics of alite and OPC systems" *Cem. Concr. Res.* **42**[9]:1175-1188.
53. Costaya M. (2008) "Kinetics and microstructural investigation on the hydration of tricalcium silicate" *PhD Thesis*, EPFL Switzerland.
54. Taylor H (1997) "Cement Chemistry. Second Edition", London: Thomas Telford.
55. Lothenbach B., Durdzinski P and De Weerdt K. (2016) "Thermogravimetric analysis" *A practical guide to microstructural analysis of cementitious materials*, Scrivener KL, Snellings R, Lothenbach B. Eds. CRC Press, 177-212.
56. Jansen D, Goetz-Neunhoeffer F *et al.* (2011) "A remastered external standard method applied to the quantification of early OPC hydration" *Cem. Concr. Res.* **41**:602-608.
57. Hesse C, Goetz-Neunhoeffer F and Neubauer J. (2011) "A new approach in quantitative in-situ XRD of cement pastes: Correlation of heat flow curves with early hydration reactions" *Cem. Concr. Res.* **41**[1]:123-128.
58. Merlini M, Artioli G, *et al.* (2008) "Tricalcium aluminate hydration in additivated systems. A crystallographic study by SR-XRPD" *Cem. Concr. Res.* **38**[4]:477-486.
59. Allen A.J, Thomas J.J and Jennings H.M (2007) "Composition and density of nanoscale calcium-silicate-hydrate in cement" *Nat. Mater.* **6**[4]:311-316.
60. Bergold S.T, Goetz-Neunhoeffer F and Neubauer J. (2013) "Quantitative analysis of C-S-H in hydrating alite pastes by in-situ XRD" *Cem. Concr. Res.* **53**:119-126.

61. Scrivener K, Bazzoni A, *et al.* (2016) “Electron Microscopy” *A Practical Guide to Microstructural Analysis of Cementitious Materials*, Scrivener KL, Snellings R, Lothenbach B. Eds. CRC Press, 351-418.
62. Chen J, Sorelli L, *et al.* (2010) “A coupled nanointendation/SEM-EDS study on low water/cement ratio Portland cement paste: Evidence for C-S-H/$Ca(OH)_2$ nanocomposites” *J. Am. Ceram. Soc.* **93**[5]:1484-1493.
63. Richardson I.G and Cabrera J.G. (2000) “The nature of C-S-H in model slag cements” *Cem. Concr. Comp.* **22**:259-266.
64. Richardson I.G. (1999) “The nature of C-S-H in hardened cements” *Cem. Concr. Res.* **29**:1131-1147.
65. Pelleneq R.J.M, Kushima A, *et al.* (2009) “A realistic molecular model of cement hydrates” in *Proceedings of the National Academy of Sciences of the United States of America* **106**[38]:16102-16107.
66. Zacak M, Garrault S, *et al.* (2007) “Effect of temperature on the developement of C-S-H during early hydration of C_3S” in *Proceedings of the 12th International congress on the chemistry of cement*, Montreal Canada.
67. Kjellsen K.O and Detwiller R.J. (1992) “Reaction kinetics of portland cement mortars hydrated at different temperatures” *Cem. Concr. Res.* **22**:112-120.
68. Freisleben H, Pedersen E.J. (1977) “Maturity computer for controlling curing and hardening of concrete” *Nordisk Betong* **1**:21-25.
69. Kada-Benameur H, Wirquin E and Duthoit B. (2000) “Determination of apparent activation energy of concrete by isothermal calorimetry” *Cem. Concr. Res.* **30**:301-305.
70. D'Aloia L and Chanvillard G. (2002) “Determining the "apparent" activation energy of concrete Ea - numerical simulations of the heat of hydration of cement” *Cem. Concr. Res.* **32**:1277-1289.
71. Thomas J.J. (2012) “The Instantaneous Apparent Activation Energy of Cement Hydration Measured Using a Novel Calorimetry-Based Method” *J. Am. Ceram. Soc.* **95**[10]:3291–3296.
72. Cahn J.W. (1958) “The kinetics of grain boundary nucleated reactions” *Acta Metallurgica* **4**:449-457.
73. Hadley D.W. (1972) “The nature of the paste-aggregate interface”. West Lafayette, Purdue University.
74. Kjellsen K.O, Justnes H. (2004) “Revisiting the microstructure of hydrated tricalcium silicate - a comparison to Portland cement” *Cem. Concr. Comp.* **26**:947-956.
75. Kjellsen K.O and Lagerblad B. (2007) “Microstructure of tricalcium silicate and Portland cement systems at middle periods of hydration-development of Hadley grains” *Cem. Concr. Res.* **37**:13-20.

Chapter V

A quantitative study of the C_3A hydration

5.1. Introduction

Tricalcium aluminate (C_3A) is one of the four major constituents of an ordinary Portland cement (OPC) clinker. Although typically it is of relatively low quantity (2-10 %), it has a significant effect on the setting of cement and largely contributes to the early age heat release due to its very high reactivity. When C_3A directly reacts with water, it sets instantly, which is commonly known as flash set. To control the setting time, gypsum ($C\$H_2$) is typically added in cement by inter-grinding with clinker. Due to elevated temperature due to grinding, gypsum is generally decomposed into bassanite ($C\$H_{0.5}$) and anhydrite (C$).

The mechanisms, which control the hydration of C_3A, are still under active debate which are discussed in detail in the subsequent sections. An improved scientific understanding on the mechanisms of hydration of C_3A is crucial for different fields of research and application. One such application is the development of admixtures which could effectively control the setting time. Another one is the development of microstructural models[1] which could more accurately and precisely predict the kinetics of hydration of OPC and thereby predicting the early-age heat release and microstructural development with respect to time.

5.1.1. Hydration of C_3A

Hydration of C_3A in the absence of gypsum results in the precipitation of Al_2O_3-Fe_2O_3-mono (AFm) phases which have a general formula of $C_4(A,F)X_2.nH_2O$, where X is a monovalent anion or $C_4(A,F)X.nH_2O$ in case of a divalent anion. Typically, in OPC, OH^-, SO_4^{2-} and CO_3^{2-} anions can act as X to form AFm phases (hydroxy-AFm, monosulphate and monocarboaluminate respectively)[2]. AFm phases that belong to lamellar double hydroxide (LDH) family, are composed of positively charged main layers ($[Ca_2Al(OH)_6]^+$) and negatively charged interlayers ($[X\cdot nH_2O]^-$) [2].

In the absence of gypsum, OH-AFm (hydroxy-AFm or h-AFm) phases such as C_4AH_{13} and C_2AH_8 are formed (Eq. 5.1). C_4AH_{19} can be formed instead of C_4AH_{13} depending on the relative humidity (RH)[2,3]. Nevertheless, these metastable h-AFm phases are later converted into more stable C_3AH_6 (hydrogarnet) (Eq. 5.2) through an endothermic reaction[4,5] with the release of additional water to the system[6,7].

$$2C_3A + 21H \rightarrow C_4AH_{13} + C_2AH_8 \quad (5.1)$$

$$C_4AH_{13} + C_2AH_8 \rightarrow 2C_3AH_6 + 9H \quad (5.2)$$

When C_3A hydrates in the presence of calcium sulphates, an Al_2O_3-Fe_2O_3-tri (AFt) phase, ettringite ($C_6A\$_3H_{32}$), is formed (Eq. 5.3). In such conditions, although thermodynamic calculations predict only the formation of ettringite as the solution is generally saturated or super-saturated with respect to gypsum[8], many researchers have reported the presence of h-AFm[8-12]. The quantity of h-AFm formed is found to be dependent on the type of calcium sulphate used[8]. It is reported that more h-AFm phases are produced while gypsum is added compared to similar amount of bassanite[8]. Also, with the addition of small amounts of ettringite, there is a considerable reduction in the amount of h-AFm that precipitates in this stage[8].

$$C_3A + 3C\$H_2 + 26H \rightarrow C_6A\$_3H_{32} \quad (5.3)$$

With the exhaustion of gypsum, C_3A reacts with ettringite to form monosulphoaluminate AFm (m-AFm or monosulphate) (Eq. 5.4). The general formula of m-AFm is denoted as $C_4A\$H_{6+x}$, where *x* is the interlayer water[3]. Depending on the RH and temperature, *x* can vary from 2 to 10 [2,3,13]. $C_4A\$H_{12}$ and $C_4A\$H_{14}$ are the most commonly seen m-AFm phases in C_3A systems.

$$2C_3A + C_6A\$_3H_{32} + 4H \rightarrow 3C_4A\$H_{12} \quad (5.4)$$

With the depletion of ettringite, C_3A continues to react with water to form h-AFm phases, which could occur as separate crystals or as solid solution along with m-AFm[2].

5.1.2. Kinetics of reaction

In the absence of gypsum, C_3A reacts very quickly with water. Hence, a very high amount of C_3A reacts in the initial hours of hydration[14]. Although h-AFm phases are expected to form initially from this reaction, crystalized C_3AH_6 has been detected from XRD analysis even at the beginning of the hydration reaction[5,15]. This is because, when the w/c is not very high, the high heat release upon the contact of water with C_3A surface will increase the temperature of the mixture, which will accelerate the conversion of h-AFm to C_3AH_6[5]. It has been proposed that water-transport to the surface of C_3A particles is the rate determining step of the hydration of C_3A with water[5,15].

The reaction of C_3A in the presence of gypsum can be divided into three stages, as depicted in Fig. 5.1. Stage 1 corresponds to the reaction between C_3A and gypsum. It consists of an initial dissolution peak followed by a stage of low heat release. This stage continues until the

depletion of gypsum in the system. The reason for low heat release region in the first stage was widely debated. Initially, it was attributed to the presence of a barrier layer on C_3A surface. The barrier layer was thought to be ettringite formed by topochemical reaction between C_3A and $CaSO_4$[16]. Impermeability of ettringite was thought to hinder the hydration of C_3A until the depletion of SO_4^{2-}, which leads to the recrystallisation of ettringite into m-AFm[16]. The end of low reactivity stage is ensued by disruption of barrier layer due to the osmotic pressure between the solution in contact with cement grains and that outside the barrier layer or crystallization pressure of topochemically formed ettringite[17]. From electron microscopy studies, it has been concluded that ettringite is formed from a through-solution mechanism and not from a topochemical mechanism[18]. It was debated that although ettringite crystals are formed through a through-solution mechanism, they form on the surface of C_3A preferentially due to the catalytic action of C_3A and thus inducing a barrier layer[14]. It was later reported that the needle like crystalline morphology of ettringite makes it unsuitable to be a barrier layer[19]. Several authors also proposed that h-AFm could also be the barrier layer which retards the C_3A hydration[11,19,20]. However, it was noted that formation of h-AFm in systems without gypsum did not retard the hydration of C_3A, or in the presence of hemihydrate, where h-AFm was not formed there was retardation[8,10].

The activation energy of the first stage of reaction was found to be around 40-80 kJ/mol[10]. If the activation energy is above 20 kJ/mol, the mechanism is very unlikely to be diffusion controlled[21]. It has been also observed that the rate of hydration is dependent on the specific surface area of C_3A, which further disproves the theory of a barrier layer. The rate of C_3A hydration is constant after accounting for the effect of decrease in particle size. If the hydration is controlled by a barrier layer, the rate of hydration should reduce over time as the barrier layer thickens[9,10].

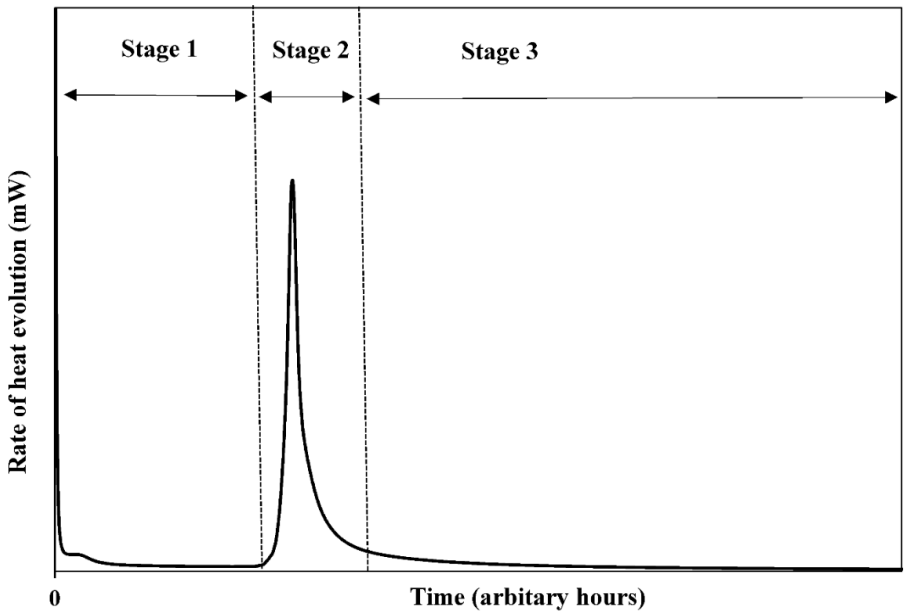

Figure 5.1: A typical heat release curve of C_3A hydration

Suppression of dissolution of C_3A by the adsorption of calcium or sulphate ions is the other major hypothesis for the low heat release. It was considered that the adsorption of sulphates on the active sites of C_3A is responsible for the retardation[22]. However, it was later refuted as other sulphates such as Na_2SO_4 did not yield a retardation[14]. The theory was further modified by Skanly et al.[16,23] claiming the effect to be due to the chemisorption of Ca^{2+} ions on the aluminum rich surfaces of C_3A, thereby producing a positive charge on which the negatively charged sulphate ions could adsorb. This would further retard C_3A hydration by reducing the available dissolution sites by a blocking effect of sulphate ions on the coordination sites[24]. This theory was later supported by several authors who reported that the C_3A hydration is effectively controlled by the specific surface area of C_3A, which implies that it is controlled by surface mechanisms[8-10,25,26]. Myers et al.[27,28] recently reported a lack of evidence for the specific adsorption of sulphate ions onto the partially dissolved C_3A particles and thereby proposed a modification for the existing mechanism. They proposed that Ca-sulfur ion pair complexes are adsorbed onto the Al-rich surface of C_3A, thereby increasing the local saturation and thereby retarding the dissolution of C_3A[27,28].

Stage 2 of C_3A hydration is the hydration peak with an acceleration and deceleration period. With respect to the ettringite barrier theory proposed for the first stage, early studies have indicated that the increase in the reaction rate results from the removal of ettringite barrier due to the recrystallization to m-AFm, while the deceleration period arises from the barrier formed due to the AFm phases[29]. Minard et al.[9] proposed that this stage is controlled by dissolution, and enhanced heat release is due to the desorption of the calcium and/or sulphate ions. This was challenged by Quennoz and Scrivener[10] who stated that the characteristic shape of the hydration peak is not representative of a dissolution-controlled mechanism, particularly for systems which are not severely diluted. They observed that the peak broadens with increase in gypsum content[30] and attributed this to be due to the nucleation and growth of AFm phases similar to what was observed for C_3S hydration[31]. The authors have reported that while the acceleration is controlled by the specific surface area of C_3A, the deceleration period is also dependent upon the available space for the hydrates to form[10]. Bergold et al.[32] noted that the broadening of the peak could be due to the increased time requirement for the removal of blockage of C_3A surface with an increase in the sulphate content. However, further research is needed for a better understanding of this second stage of C_3A hydration.

Stage 3 of C_3A hydration is a period of low heat release which continues until complete consumption of the reactants. Pommersheim[29] proposed that this period follows a similar reaction mechanism to a hydrating C_3A without gypsum addition. Minard et al.[9] and Quennoz and Scrivener[10] postulated this period to be the continued effect of the dissolution mechanism or nucleation and growth mechanism respectively as proposed for the second stage of hydration.

The main objective of this chapter is to improve the fundamental understanding of the mechanisms which are involved during the hydration of C_3A-gypsum systems. In this chapter, C_3A hydration was quantitatively studied with two different fineness of C_3A, varying gypsum content and w/c at 20°C using a combination of experimental techniques such as isothermal

calorimetry, TGA, ^{27}Al NMR and XRD until 7 days of hydration. Reaction mechanisms that control the reaction are revisited for different stages of hydration, and further investigated using numerical simulations in CemRS.

5.2. Experimental protocol

5.2.1. Materials

Synthetic C_3A (SARL minerals, France) from two different batches with different fineness, coarse (Ac) and fine (Af) fractions, were used for this study (Fig. 5.2). While Ac was found to have a comparable fineness compared to a typical OPC, Af was significantly finer. C_3A was produced by mixing pure Al_2O_3 and lime (Merck) and heating it up to 1400ºC using a muffle furnace. Characterization using X-ray diffraction technique has inferred that C_3A has a cubic crystal structure with minor impurities from mayenite ($C_{12}A_7$) and portlandite (CH). Gypsum ($CaSO_4.2H_2O$, calcium sulphate dihydrate) was purchased from Merck. The fineness of these powders was determined by laser diffraction technique, using Malvern Mastersizer 2000, with ethanol as dispersing medium (Fig. 5.2).

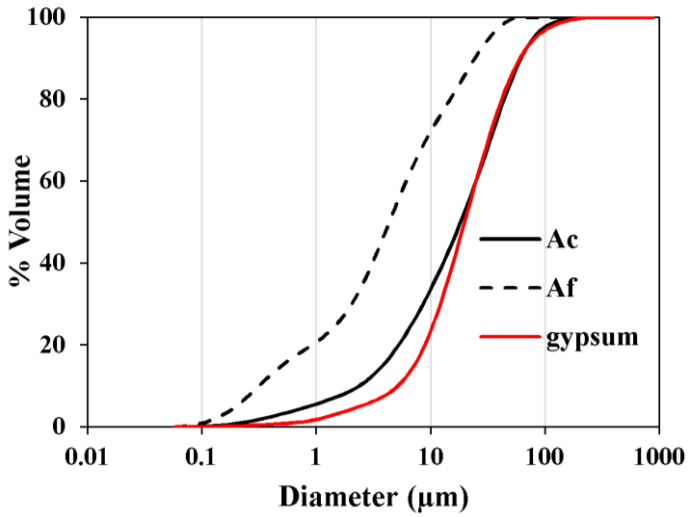

Figure 5.2: Particle size distributions of gypsum and different fineness of C_3A (Ac, Af)

5.2.2. Sample preparation

Unless otherwise specifically mentioned, all the sample preparations followed the standard procedure described below. For systems with gypsum, C_3A and gypsum were mixed in a 100ml bottle and was mixed thoroughly using a Turbula shaker for around 24 hours. Pastes were prepared with deionized water and mixed at 750rpm for two minutes in a 20ºC temperature-controlled room. Freeze dry technique was used to arrest hydration (2 hours, 0.03mbar pressure) of samples which were cured at 20ºC in a sealed 1.5ml plastic tube. It should be noted that freeze-drying or any hydration stoppage method in general would partially deteriorate ettringite and AFm phases[33-36]. Care was taken to avoid unnecessary exposure to atmosphere to minimize carbonation. The freeze-dried samples were then stored in a vacuum desiccator.

5.2.3. Experimental techniques

Isothermal calorimetry: TAM Air 8 channel isothermal microcalorimeter was used to measure the heat release until 7 days at 20ºC. Calorimeter being stored in a temperature controlled room at 20ºC makes it ideal for measuring for longer periods with minimum heat loss. To study the instantaneous activation energy, the protocol developed in a previous study (Chapter IV) has been used[37]. Prepared pastes were transferred to the bottles and are sealed before curing them in 20 ºC or 30 ºC. They are then measured using the calorimeter after appropriate curing time at 20 ºC or 30 ºC.

Thermal analysis: NETZSCH STA 409 PC was used to perform the thermogravimetric analysis (TGA). This technique measures the mass loss due to dehydroxylation at different temperatures and it enables to quantitatively measure the bound water content and qualitatively asses the hydration products. Heating rate was kept at 10ºC/min under N_2 atmosphere. Around 25-40mg of the sample was used for each measurement.

X-ray diffraction: Bruker diffractometer (D2 phases with CuKα radiation) was used to perform X-ray diffraction (XRD). The measurements were performed from 5 to 70 º2θ on the hydrated samples after hydration stoppage. The samples were finely crushed in an agate mortar before loading. Samples were top loaded hence some phases, especially gypsum, are prone to preferred orientation. XRD was used in this study for qualitative phase analysis as the crystal structures of AFm phases are not well defined.

Solid state NMR: A 600MHz (magnetic field strength: 14.09T) Varian NMR spectrometer was used to perform ^{27}Al Magic Angle Spinning (MAS) Nuclear Magnetic Resonance (NMR) spectroscopy with proton decoupling. This technique was used to quantitatively measure the degree of hydration and to estimate the amount of hydration phases. Samples were finely ground in an agate mortar and a measured mass of around 0.07-0.09 g was transferred to a 4mm partially sintered zirconia (PSZ) rotor. The samples were spun at 13kHz at 2.8bar bearing pressure. A single pulse experiment was performed with 0.5 µs excitation pulse for rf field strength, $\gamma B1/2\pi \approx 60$ kHz and a relaxation delay of 2s. Typically around 4096 scans were performed with a measurement time around 2 hours. 1M aqueous $AlCl_3.6H_2O$ was used for referencing. A quadruple[38] peak from 85-20ppm was detected for anhydrous C_3A (Fig. 5.3). Quadrupole peak arises due to the 5/2 nuclear spin of ^{27}Al. In the hydrated samples, ettringite was detected at 13.2 ppm[39], C_3AH_6 at 12.3ppm[39,40] and AFm phases at 9.5-11.5ppm[39,41]. Estimation of m-AFm and h-AFm from the total AFm content is extremely difficult due to the similar chemical shifts and broader peaks. The degree of hydration was measured by integrating the central bands of anhydrous and hydrated phases also taking into account of the spinning side band. Deconvolution for the hydrated phases was performed using gaussian and Lorentzian peak shapes. While VNMRJ software was used for integration, dmfit[42] was used for deconvolution.

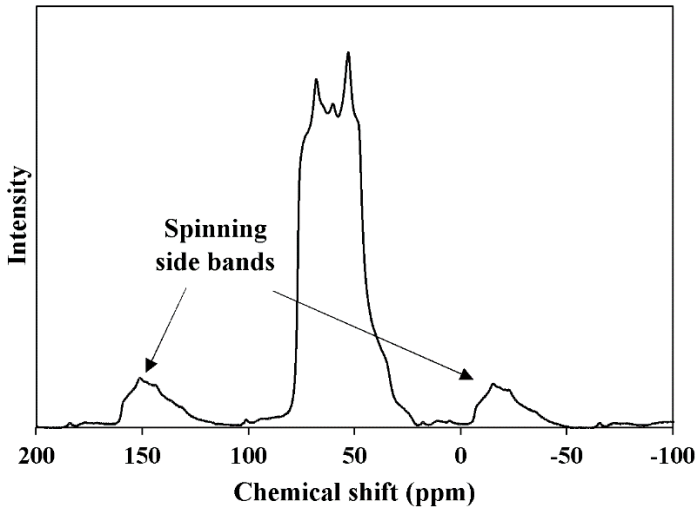

Figure 5.3: ^{27}Al MAS NMR spectra of anhydrous C_3A

5.3. Experimental results

5.3.1. Hydration of C_3A without gypsum

Fig. 5.4 shows the effect of w/c on the degree of hydration of C_3A (Ac) without gypsum. The degree of hydration is measured from ^{27}Al MAS NMR at 1 and 7 days, and from isothermal calorimetry. The degree of hydration measured by isothermal calorimetry was shifted along the *y* axis to coincide with the NMR result after 1 day of hydration. This was done as C_3A has high heat release initially right when water comes in contact with the surface of C_3A particles, some of which is lost during mixing and placing in calorimeter. It is observed that approximately half of C_3A is hydrated within an hour. A clear difference in the degree of hydration with respect to w/c is also observed. This shows that w/c does play an important role in the hydration kinetics without addition of gypsum. It is interesting to note that this effect of w/c is also displayed for calcium aluminate cements[43].

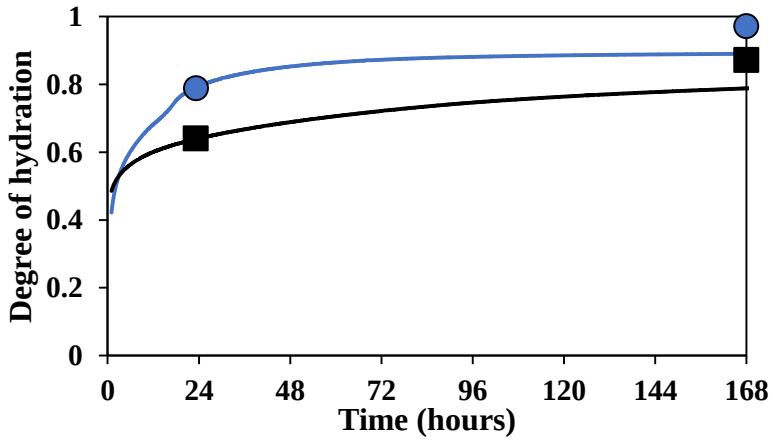

Figure 5.4: Degree of hydration of C_3A (Ac) without gypsum at 0.5 and 1 w/c; Blue: w/c 1, Black: w/c 0.5; Marker: Degree of hydration measured from ^{27}Al MAS NMR, Line: degree of hydration measured from isothermal calorimetry shifted vertically to coincide 1-day degree of hydration measured using NMR.

Fig. 5.5 shows the percentage of Al present in different phases in the hydrated sample. An increase in the total hydrated phases at higher w/c is expected due to higher w/c. By 7 days, although the amount of C_3AH_6 is similar for both w/c 0.5 and 1, the amount of h-AFm is significantly higher in w/c = 1 than that in w/c = 0.5. This should be because of the higher amount of water available in the case of w/c = 1. These results are also consistent with the thermal analysis (Fig. 5.6). An increase in the total mass loss is attributed to the increased bound water content with increase in the degree of hydration. The DTG curve showing the mass loss due to the dehydroxylation from C_3AH_6[44] is also consistent with the C_3AH_6 quantities measured from NMR results (Fig. 5.5). The results from ^{27}Al MAS NMR measurements are further supported by the qualitative analysis of XRD patterns (Fig. 5.7). There is a definite increase in the amount of h-AFm phase (peak at 7.92Å) at 7 days with w/c 1 compared to the other samples.

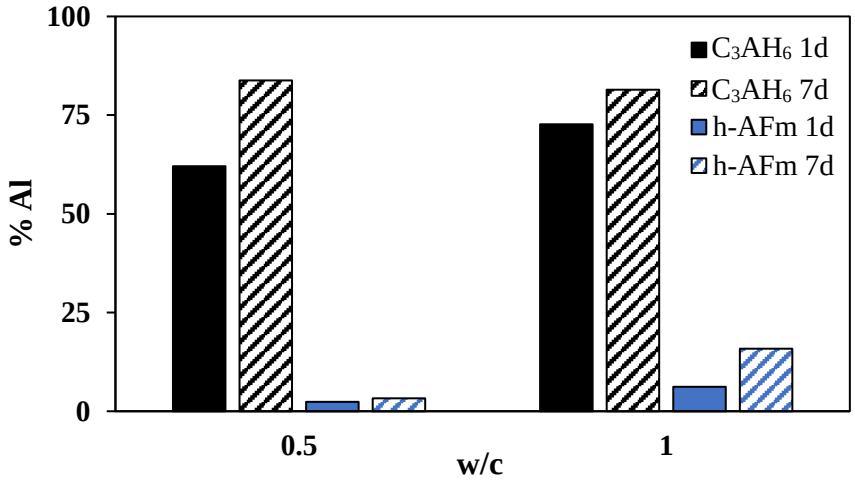

Figure 5.5: Quantification of phases in hydrated C_3A without gypsum measured from ^{27}Al MAS NMR

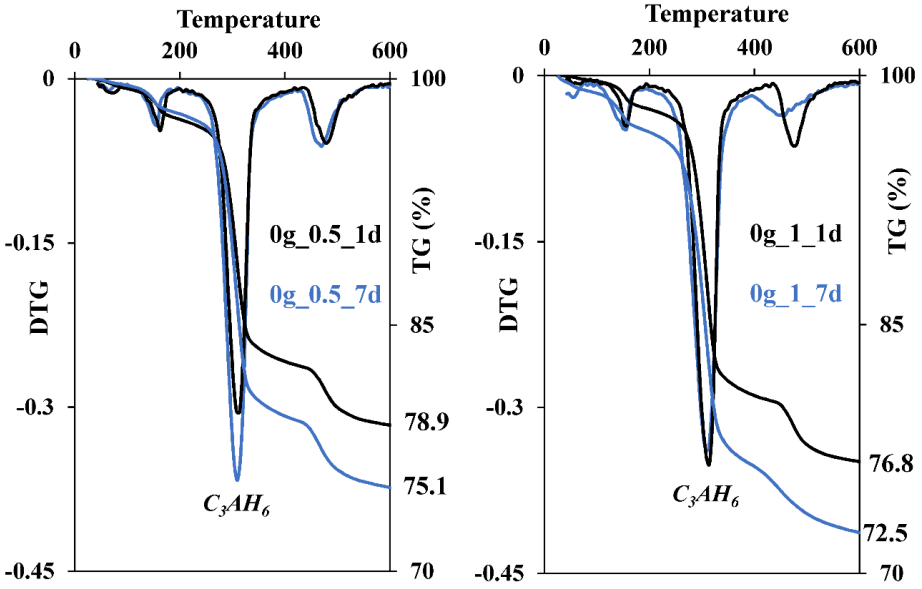

Figure 5.6: TG and DTG curves for C_3A (Ac) without gypsum at 1 & 7 days for w/c 0.5 & 1.

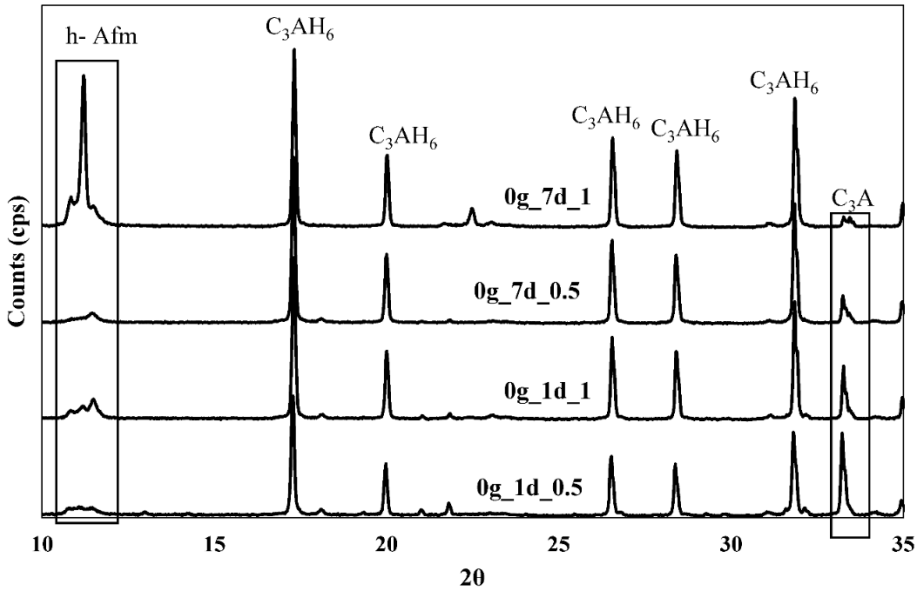

Figure 5.7: XRD (CuKα) patterns of C_3A (Ac) without gypsum at 1 & 7 days with w/c 0.5 and 1

5.3.2. Hydration of C_3A with added gypsum

5.3.2.1. Effect of gypsum content

Fig. 5.8 shows the effect of gypsum content on the fine C_3A with respect to the rate of heat release and the cumulative heat release measured from isothermal calorimetry. With increase in the gypsum content, there is a prolongation in the first stage of C_3A hydration[26]. The main peak of C_3A hydration (stage 2) is clearly broadened and intensity is shortened with increasing amount of gypsum[10]. There is an increase in the overall heat release with an increase in the addition of gypsum, which is due to the higher enthalpy of formation of ettringite compared to the formation of AFm phases[2].

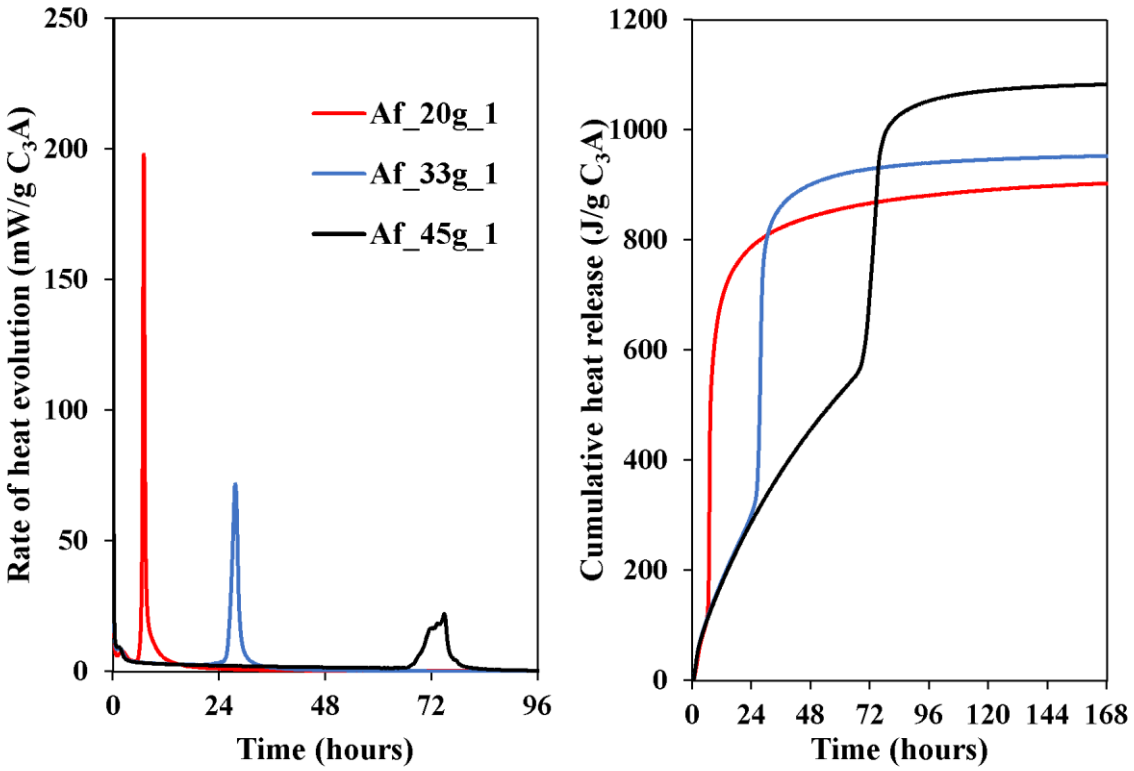

Figure 5.8: Rate of heat release (left) and cumulative heat release (right) measured from isothermal calorimetry for C3A(Af) with different amounts of gypsum

5.3.2.2. Effect of fineness of C_3A

Fig. 5.9 shows the effect of fineness on the rate of heat release and the cumulative heat release measured from isothermal calorimeter at 20ºC with w/c of 1. There is a significant effect on the fineness both in stage 1 and stage 2. Stage 1 is significantly increased with a reduction in fineness, which is attributed to the increased time for the consumption of gypsum[8,9]. Stage 2 shows a broadening of the peak and significant reduction in the maximum peak intensity with the reduction in fineness[10]. While isothermal calorimetry indicates that the overall degree of hydration is the same for Ac and Af, ^{27}Al MAS NMR measurements (Fig. 5.10) show that there is an increase in the degree of hydration by 7 days. This difference is attributed to the increase in C_3AH_6 content in the fine C_3A (Af). As the second stage of C_3A occurs much earlier for Af, there is more time for the stabilization of the metastable h-AFm to C_3AH_6. As this conversion is an endothermic reaction[4,5], the isothermal calorimeter detects only lower heat release. The increase in the degree of hydration for C_3A could also be due to the additional water released from the h-AFm to C_3AH_6 conversion (Eq. 5.2). An increase in the total C_3AH_6 content was also detected from DTG for Af and increased bound water content from TG (Mass loss at 600º C; Af: 34%, Ac: 32%). A lower heat release measured for Af could be also from higher reaction during initial minutes of mixing, as previous studies have indicated a higher amount of h-AFm formation in the early minutes with finer C_3A[8,9].

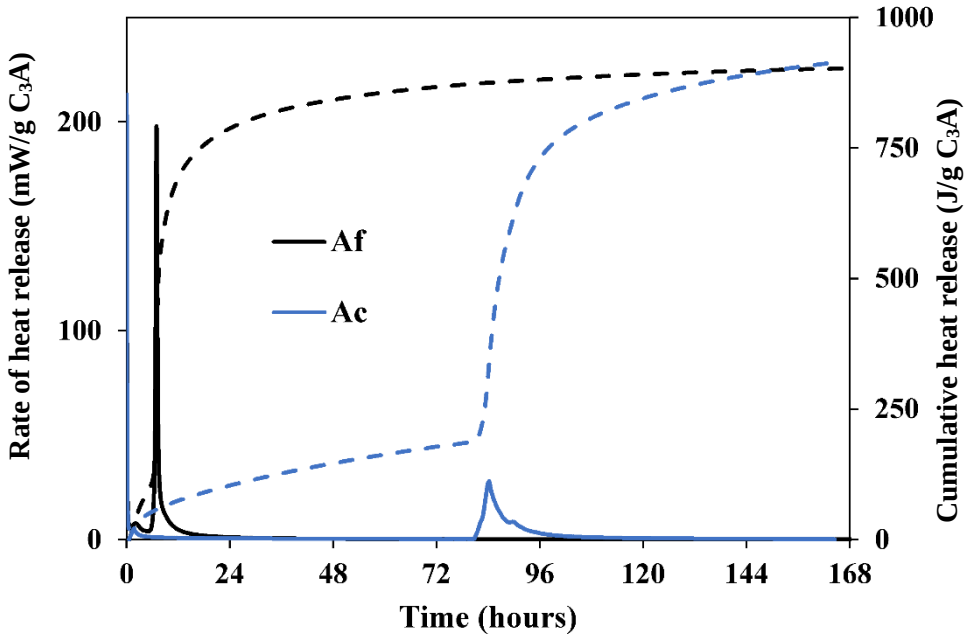

Figure 5.9: Effect of fineness on the rate of heat release and cumulative heat release until 7 days as measured from isothermal calorimeter

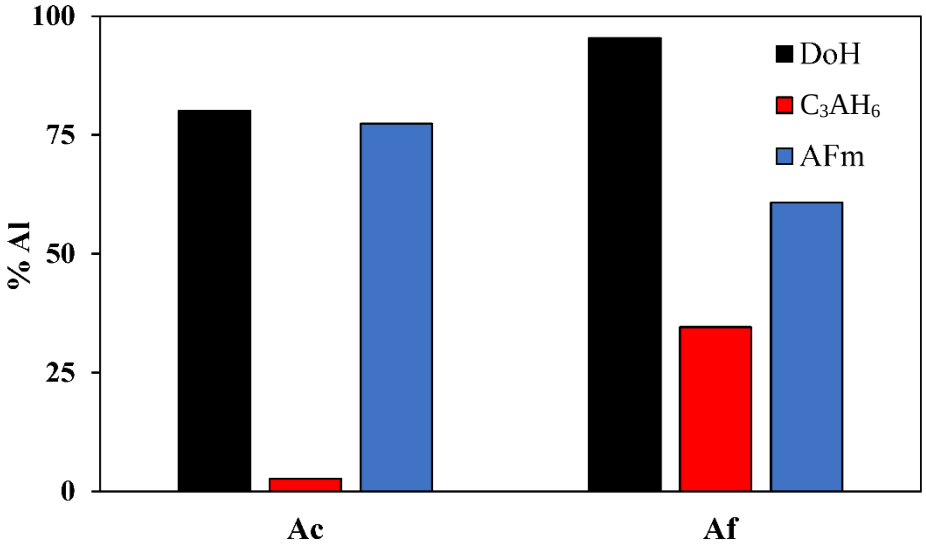

Figure 5.10: Al in total hydrates(DoH), C_3AH_6 and AFm as measured from ^{27}Al MAS NMR on Ac and Af at 7 days with w/c 1.

5.3.2.3. Effect of w/c

Fig. 5.11 shows the effect of w/c on the rate of hydration and cumulative heat release measured from isothermal calorimetry. Experiments were performed in coarse C_3A (Ac) which allowed to reduce the w/c to even 0.36 ensuring proper workability. These results verify the previous findings[10] that there is no effect of w/c on stage 1 of C_3A-gypsum reaction. Also, the maximum heat release in the main hydration peak is also unaffected with w/c[10]. A small deviation in the duration of stage 1 and height of peak of stage 2 is typical for the same samples upon

repetition[45]. However, there is a significant increase in the total heat released with an increase in w/c for both 10% as well as 20% gypsum addition. Although this was expected as per previous work[10] based on the rate of heat release, the effect was not quantitatively estimated before. Also, that investigation was limited to less than one day of hydration and was also limited to one gypsum content (12% gypsum).

The increase in the degree of hydration is further validated with ^{27}Al MAS NMR measurements. There is a higher amount of C_3AH_6 in 10% gypsum samples compared to 20% gypsum. This is expected as there is more time for the transformation of h-AFm to C_3AH_6, and the fact that more h-AFm is produced in 10% gypsum due to lower sulphate content. Fig. 5.13 shows the qualitative study of the AFm phases in 10% and 20% gypsum at w/c 0.5 and 1 after 7 days of curing[3]. An increase in the quantity of m-AFm12 ($C_4A\$H_{12}$) was detected with increasing gypsum content, which should be expected as more ettringite is transformed into monosulphate. There is an increase in m-AFm12 with an increase in w/c. The reason of this is not very clearly understood. It could be because there is higher crystallization at higher w/c or transformation of m-AFm12 to m-AFm with lower interlayer water, e.g. m-AFm10.5($C_4A\$H_{10.5}$). With 10% gypsum and w/c 1, h-AFm19 (C_4AH_{19}) was detected. It should be noted that the hydration stoppage process could partially deteriorate AFm phases by removing part of the interlayer water.

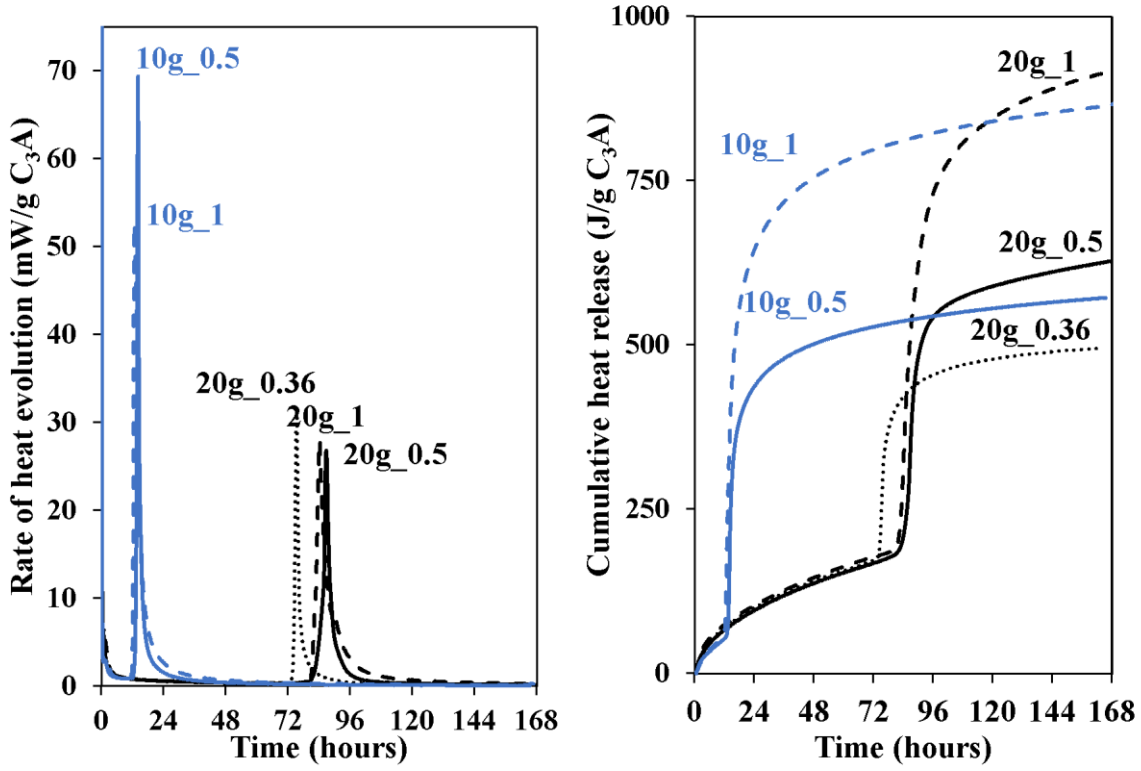

Figure 5.11: Effect of w/c ratio on the rate of heat release (left) and cumulative heat release (right) of C_3A (Ac) measured from isothermal calorimetry for 10% gypsum (w/c 0.5 & 1) and 20% gypsum (w/c 0.36, 0.5 & 1) content.

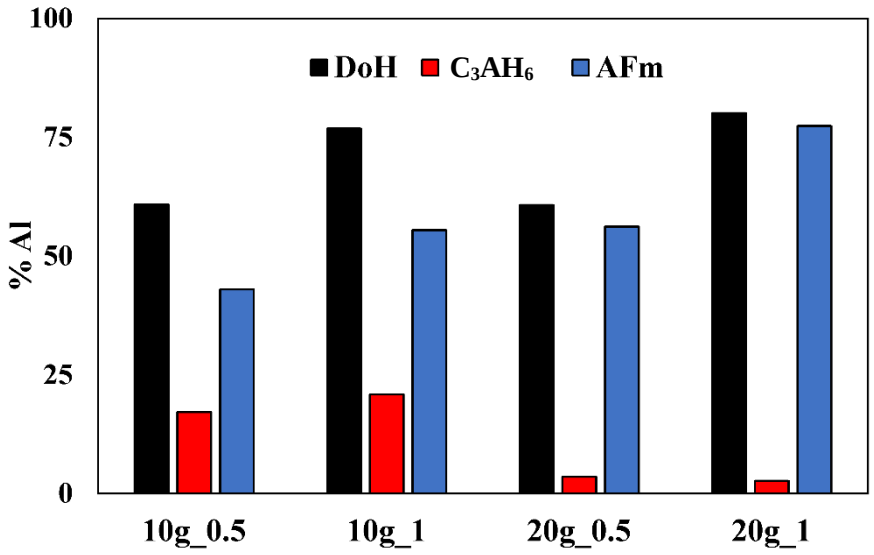

Figure 5.12: Al in total hydrates (DoH), C_3AH_6 and AFm as measured from ^{27}Al MAS NMR on 10% gypsum and 20% gypsum at 7 days with w/c 0.5 & 1.

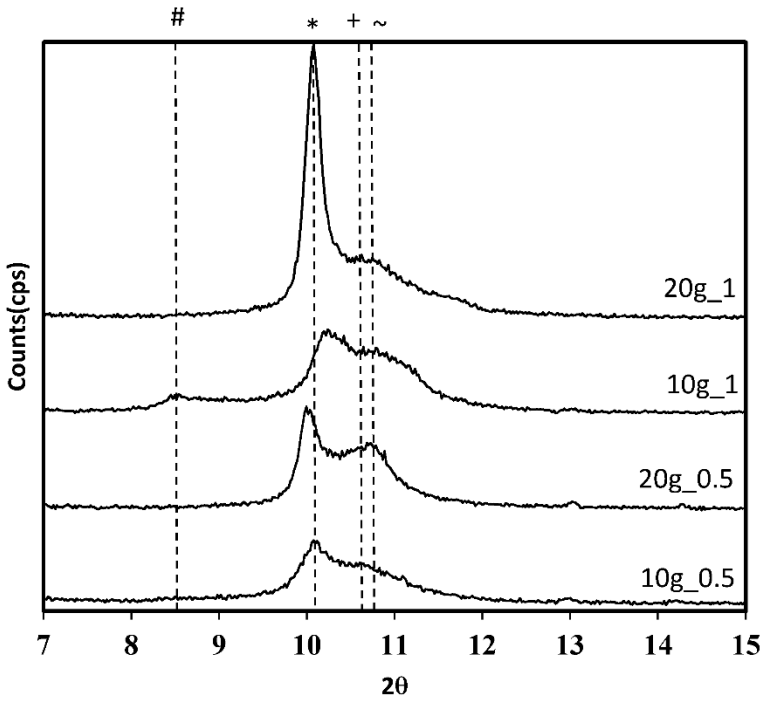

Figure 5.13: Qualitative analysis from XRD (CuKα) of AFm phases with 10% and 20% gypsum at w/c 0.5 and 1 at 7 days. ($^{\#}C_4AH_{19}$; $^{*}C_4A\$H_{12}$; $^{+}C_4AH_{13}$; $^{\sim}C_4A\$H_{10.5}$[3])

Fig. 5.14 shows the effect of additional water on the heat release. For this measurement, the admix ampoule (TAM Air) set was used. 2ml of water was measured and stored in the syringe and paste was prepared at 0.36 w/c and was weighed (3.285g) and transferred to the bottle. This whole set up was then transferred to the calorimeter and the measurement was started. After 24 hours, the water in the syringe was injected into the bottle slowly. As the water was already inside the calorimeter, this would not affect the signal due to a change in temperature.

This procedure is similar to the experimental protocols developed for the measurement of chemical shrinkage[46] where additional water is added on top of the cement paste for the measurement of degree of hydration. From Fig. 5.14, it is observed that there is a significant increase in the overall heat release with the addition of extra water. The overall heat release with the extra water is even higher than the overall heat release with w/c 1.

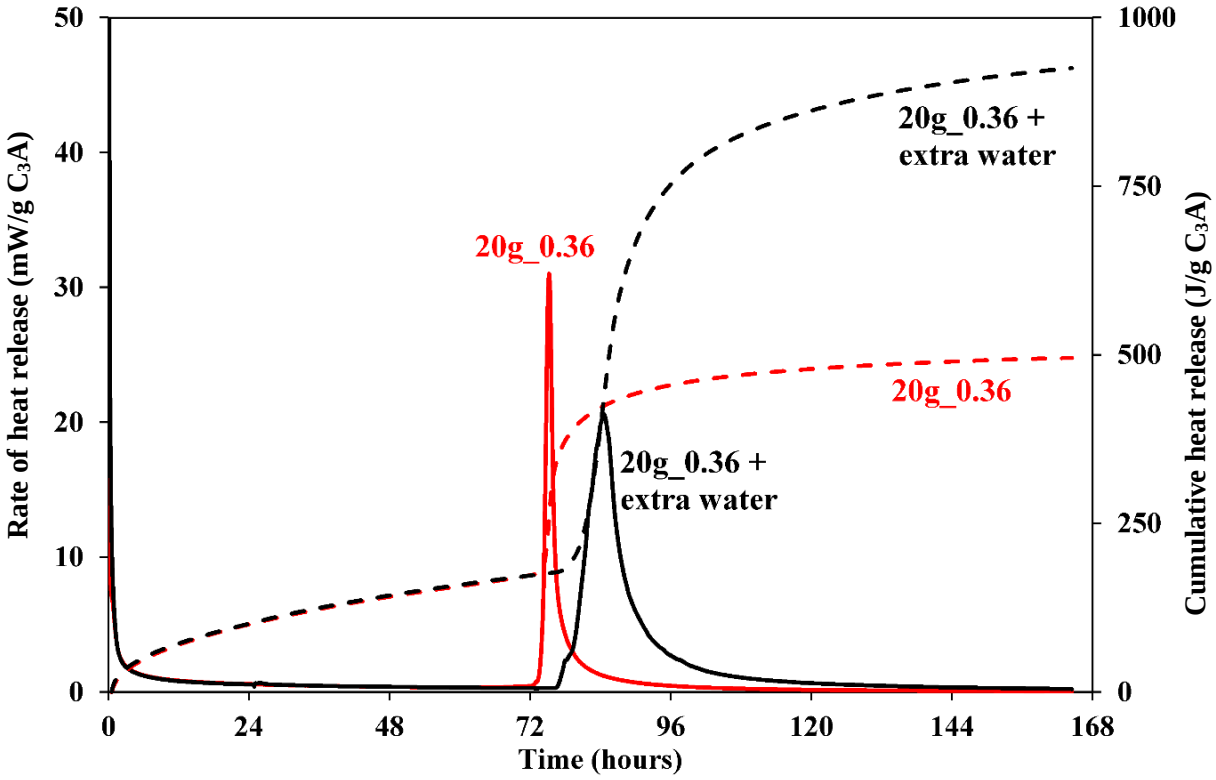

Figure 5.14: Effect of additional water injected during the calorimetry measurement after 24 hours

5.3.2.4. Instantaneous activation energy

The instantaneous activation energy was measured using the methodology previously developed for C_3S[37], which itself is a modification of the method developed by Thomas[47] (Fig. 5.15). The measurement was carried out at 20ºC and 30ºC for both Ac and Af that were replaced with 20% gypsum at w/c 1. The instantaneous activation energy during stage 1 and stage 3 for Ac, and the stage 2 and stage 3 for Af, were measured. The instantaneous activation energy was calculated using the Eq. 5.5, where, E_a is the activation energy, R is the universal gas constant, T_1 and T_2 are the temperatures in Kelvin, k_1 and k_2 the rate of heat releases.

$$E_a = R\left[\frac{T_1 T_2}{T_1 - T_2}\ln\left(\frac{k_1}{k_2}\right)\right] \tag{5.5}$$

The instantaneous activation energy has a fairly constant value of around 75±6 kJ/mol at stage 1 and 69±3 kJ/mol at stage 2. As it is difficult to determine and highly prone to error for

changing the temperature during the narrow peak of C_3A hydration, the rate at maximum peak was used to measure the instantaneous activation energy. While integrating the acceleration period, a similar cumulative heat release was measured by the end of the acceleration period at 20ºC as well as for the measurements at 30ºC. This ensured that the rate of heat release at the tip of the hydration peak was at the same degree of hydration. In addition, in stage 3, there is a steep reduction of instantaneous activation energy to around 21-29 kJ/mol. The instantaneous activation energy during the stage 1 is similar to the activation energy reported in the literature (79±1 kJ/mol for 20% gypsum)[10] by superimposing calorimetry curves. As more h-AFm is precipitated in stage 3, it is possible that an error arises from underestimation of the activation energy. This is because, the endothermic reaction (Eq. 5.2), is also accelerated with increase in temperature.

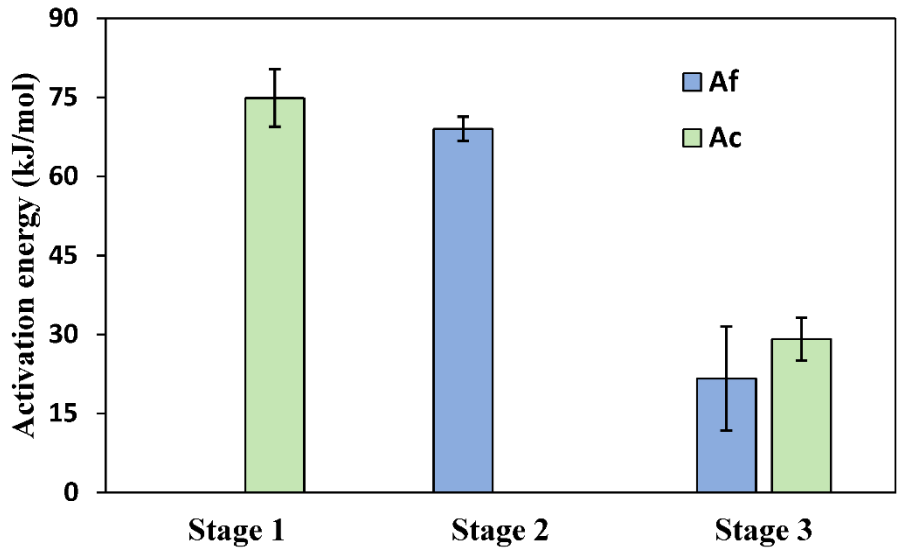

Figure 5.15: Instantaneous activation energy

5.4. Numerical modelling

The main objectives of numerical modelling of C_3A hydration are twofold. Primarily, it is aimed to check the mathematical feasibility of a proposed new mechanism. Secondly, this contributes to advancing the existing models for Portland cement hydration by incorporation of a more scientifically sound C_3A hydration module. This will lead to a better prediction of early-age properties and evolution of heat from cement-based materials. While a significant number of numerical models is available for C_3S hydration[31,48,49], very few models exist for C_3A hydration. Most of the earlier models assume a barrier layer hypothesis for C_3A hydration[5,29,50]. Other models, which are currently available for modelling cement hydration, use kinetic data from experiments of C_3A hydration and are fitted using empirical equations[1,51-53]. Although more complex models exist, they are unsuitable for simulating higher number of particles which are representative of a typical Portland cement due to computational limitations[54].

5.4.1. Theory & Assumptions

A new numerical model was developed on the microstructural modelling platform CemRS[48,55]. The complete particle size distribution is incorporated from the laser diffraction in the model without the need of truncation and using a statistical particle modelling approach[55]. The particles are assumed to be spherical in shape to reduce the complexity involved, which is a typical approach used in most models and modelling platforms[49]. Although it is known that C_3A dissolution is anisotropic with the formation of etch pits[56], the current model assumes an isotropic dissolution based on a uniform reactive thickness concept[57,58]. According to this concept, it is assumed that the depth of dissolution is uniform for all particles irrespective of the size. Thus, the degree of hydration at any particular time could be calculated using Eq. 5.6.

$$\alpha_t = \sum_{i=0}^{n-1} N \frac{{r_{i0}}^3 - {r_i(t)}^3}{{r_i}^3} \begin{cases} if\ r(d) < r_i\ , & r_i(t) = r_i - r_d(t) \\ else, & r_i(t) = 0 \end{cases} \tag{5.6}$$

Where, α_t is the degree of hydration at time *t*, *n* is the number of particle sizes, *N* is the number of particles in each particle size, r_{i0} is the initial radius of particle *i*, $r_i(t)$ is the radius of the particle *i* at time *t*, $r_d(t)$ is the dissolution depth at time *t*.

For simplicity, the formation of h-AFm platelets in the stage 1 of hydration is neglected. It is assumed that only C_3A-gypsum reaction, which leads to ettringite formation, takes place during this period (Eq. 5.3). The enthalpy of this reaction is assumed to be -1674.1 J/g_{C3A}[2]. During this period, C_3A is assumed to be controlled by pure isotropic dissolution with a low dissolution rate. This low dissolution rate compensates the reduction of the reactive surface due to the adsorption of calcium and/or sulphate ions[9] on the surface of C_3A. In the model, the rate of change of dissolved depth with respect to time '*t*' is assumed to be a constant (c_1) as shown in Eq. 5.7. This period continues until the depletion of gypsum as indicated by τ_1 in Fig. 5.16. The parameter c_1 is fitted with respect to the calorimetry curve for the end of stage 1.

$$dr_d/_{dt} = c_1 \tag{5.7}$$

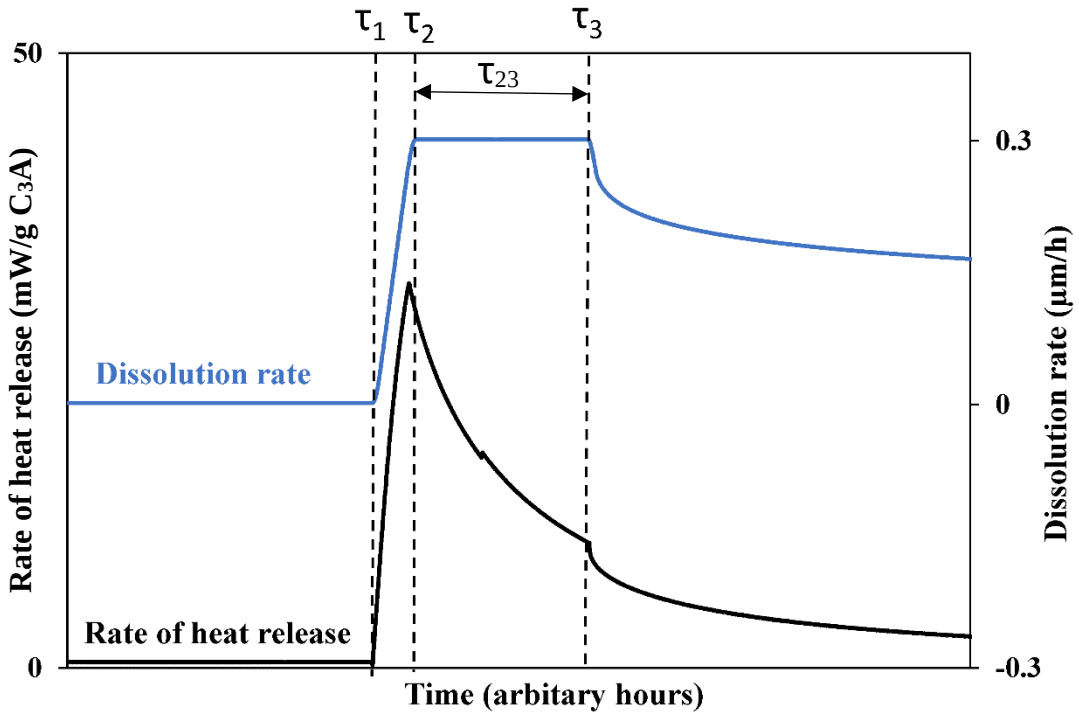

Figure 5.16: Effect of dissolution rate on rate of heat release

Once gypsum is completely depleted in the system, the model advances to stage 2. In the second stage, the dissolution rate is increased from τ_1 (calculated by the model based on the depletion of gypsum) until τ_2, when it reaches the maximum dissolution limit (c_3) and continues at that rate till τ_3 (Eq. 5.8). The slow increase in the dissolution rate until τ2 is attributed to the release of the adsorbed calcium and/or gypsum ions from the active surface of C_3A particles. In this period, C_3A first reacts with ettringite to form m-AFm (Eq. 5.4) assuming the enthalpy of heat release to be -881.5 J/g_{C3A}[2]. This reaction is assumed to continue till the complete depletion of ettringite, after which C_3A reacts with water to form h-AFm (Eq. 5.1) that would partially transform to C_3AH_6 (Eq. 5.2). The enthalpies of heat release for these reactions are assumed to be -1162J/g_{C3A} and +254.6 J/g_{C3A} respectively[2]. For mixes of which ^{27}Al MAS NMR are performed, the amount of h-AFm and C_3AH_6 are calculated from those measurements. This is done by calculating the theoretical maximum amount of m-AFm and reducing that from the total AFm content measured from NMR measurement. For mixes that do not have NMR measurements, the amount of h-AFm and C_3AH_6 are interpolated from the mixes for which NMR is performed, based on the time of complete consumption of gypsum. A linear increase in C_3AH_6 is assumed with respect to time. These are also further used to calculate the evaporable water in the system.

$$dr_d/_{dt} = \min\{ c_1 + c_2(t - \tau_1), c_3 \} \tag{5.8}$$

In the model, stage 3 is defined as the period after which the kinetics is not controlled purely by the isotropic dissolution of C_3A. Stage 2 (Eq. 5.8) continues for user defined time (τ_{23}), and beyond the rate of dissolution of C_3A is controlled by Eq. 5.9. The reduction in the dissolution rate could be either due to the reduction in free water or due to the lower availability of space for advancement of hydration or a diffusion barrier layer. For reducing the growth rate, an equation, which is similar to the classical Avrami equation[59,60] was used.

$$dr_d/dt = c_3 - k_1\left(1 - e^{-k_2\left(\frac{t-\tau_3}{k_3}\right)^n}\right) \tag{5.9}$$

It should be noted that k_2, k_3 and n are kept constant at 0.15, 0.01 and 0.415 respectively after calibrated from few initial fits. This equation was used to get a reducing profile. Better profile shapes could be developed using alternate equations, but that would involve increasing the number of fitting parameters, thereby making it difficult to get trivial values.

Thus, the variable parameters used for fitting are c_1, c_2, c_3, τ_{23} and k_1. When c_1 is increased, τ_1 decreases implicating a faster reaction of C_3A and gypsum. Fig. 5.17 shows that when c_2 is decreased, τ_2 increases and the peak of stage 2 of hydration broadens with a lower peak intensity. When c_3 is increased, τ_2 increases and the intensity of the main peak increases (Fig. 5.18). When τ_{23} is increased or when k_1 is decreased, the cumulative heat release increases. The decrease in the spike followed by the main peak in Fig. 5.17 compared to Fig. 5.18 is due to the difference in the reaction enthalpies used after the consumption of ettringite (the spike appears with the complete consumption of ettringite). In Fig. 5.17, the enthalpy of reaction is assumed to be -1162 J/g_{C3A} (corresponding to formation of h-AFm) and in Fig. 5.18, the enthalpy was assumed to be -907.4 J/g_{C3A} (corresponding to complete instantaneous transformation of h-AFm to C_3AH_6). As -907.4J/g_{C3A} is closer to the enthalpy reaction in Eq. 5.4 (-881.4 J/g_{C3A}), the spike is lower. In reality, these spikes do not occur, as the transition between two reactions occur more smoothly. Due to the simplicity of the current model, it could be easily modelled in more sophisticated microstructural modelling platforms such as µic[1].

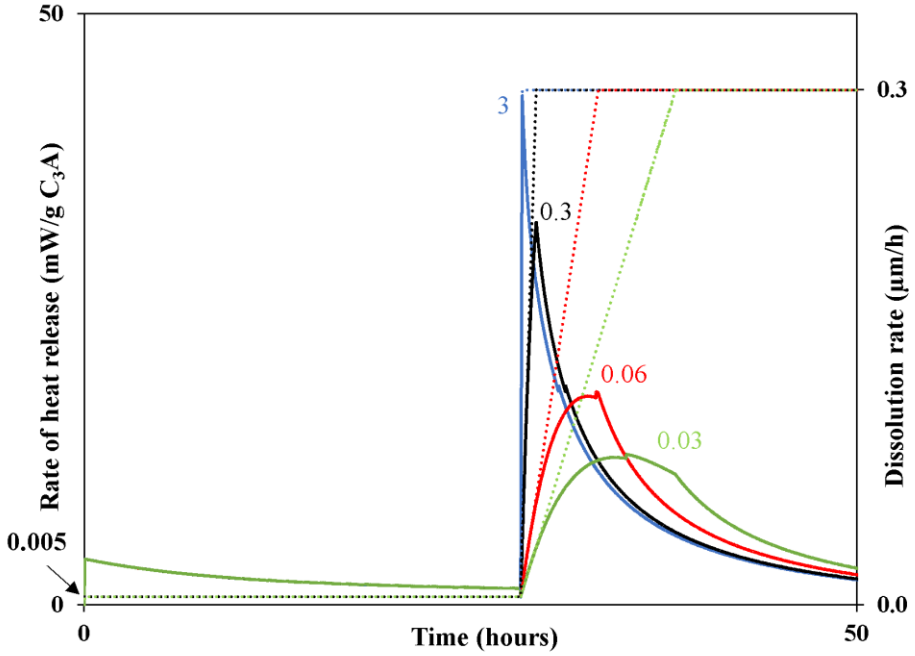

Figure 5.17: Effect of the parameter c_2 on the dissolution rate and on the rate of heat release

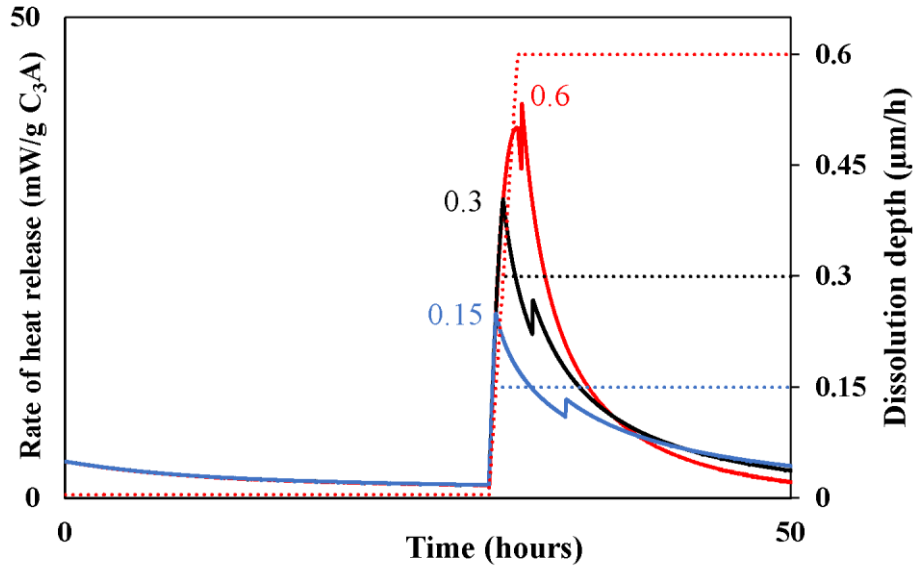

Figure 5.18: Effect of the parameter c_3 on the dissolution rate and on the rate of heat release

5.4.2. Numerical simulations & Validation

The mathematical model described above was incorporated in the microstructural modelling platform CemRS. The particle size distribution measured from laser diffraction experiment was used as user input and incorporated in CemRS using a statistical modelling approach without the need of truncation. Nevertheless, as a uniform reactive thickness concept is used in this

model, truncation does not significantly deviate the results[61]. The time step for the simulation was kept constant at 0.01 hours and it was simulated until 7 days. Each simulation took around 10 seconds in a laptop computer with modest configurations. The microstructure was not modelled owing to the lack of quantitative data of densification of hydrates. Nevertheless, once there is available data, this part should be straightforward. As the model does not require microstructural information (e.g. impingements), this would not affect the results in any way.

In this model, the initial high heat release in the start of measurement as seen from calorimetry measurements (e.g. Fig. 5.1) is not captured. This is because, this heat release is partially due to the formation of h-AFm phases[8]. Additionally, as this model assumes an isotropic dissolution on spherical particles, the initial rapid dissolution, which occurs due to the irregular shape of C_3A particles and drastically increases the surface area[62], is not captured by the model.

Table 5.1 shows the parameters that were used for all the simulations, and the effect of increase of fineness, gypsum content and w/c on these parameters are shown in Table 5.2. Table 5.1 also shows the degree of hydration calculated from the model and is compared against the degree of hydration which was measured from ^{27}Al MAS NMR after 7 days of hydration. The parameters of simulations were fitted to replicate both the heat release curve measured from isothermal calorimetry, and the overall degree of hydration with that was measured from ^{27}Al MAS NMR. ^{27}Al MAS NMR was preferred over isothermal calorimetry because the latter is an inferior method to measure the degree of hydration due to some loss of heat while measuring the overall heat release. The degree of hydration calculated from the model is very close to the values that were measured from NMR. The maximum isotropic dissolution rate of C_3A (c_3) was kept unchanged at 0.3 µm/h. While this does not mean that the maximum dissolution rate is 0.3 µm/h for all C_3A systems, this was done to check if it is possible to replicate the experimental results without changing this value.

Table 5.1: Simulation parameters for the different mixes and the degree of hydration calculated from model and ^{27}Al MAS NMR after 7 days of hydration

Mix	Simulation Parameters					Degree of hydration	
	c_1 (µm/h)	c_2 (µm/h^2)	c_3 (µm/h)	τ_{23} (h)	k_1	Model	NMR
Af_20g_1	0.0044	1.5	0.3	2	0.28	0.947	0.941
Af_33g_1	0.00325	0.6	0.3	5	0.28	0.956	-
Af_45g_1	0.0037	0.06	0.3	20	0.28	0.989	-
Ac_20g_1	0.0018	0.3	0.3	7.5	0.275	0.803	0.8
Ac_20g_0.5	0.0017	0.3	0.3	1.5	0.292	0.6	0.607
Ac_20g_0.36	0.002	0.3	0.3	0.2	0.299	0.472	-
Ac_10g_1	0.0037	1.2	0.3	5	0.285	0.77	0.768
Ac_10g_0.5	0.0036	1.2	0.3	1.75	0.295	0.6	0.609
Ac_0g_0.5	-	-	0.3	5	0.27	0.87	0.871
Ac_0g_1	-	-	0.3	15	0.23	0.97	0.973

Table 5.2: Effect of increase in fineness, gypsum content and w/c on simulation parameters in Table 5.1. – indicates no change, ↓ indicates a decrease and ↑ indicates an increase

	c_1	c_2	c_3	τ_{23}	k_1
Fineness	—	↓	—	↓	—
Gypsum	—	↓	—	↑	—
w/c	—	—	—	↑	↓

Fig. 5.19 shows the comparison of simulation results and results from isothermal calorimetry on Af (fine C_3A) which has w/c of 1. The results show that the model is able to fit the experimental results well, including both rate of heat release and cumulative heat release. The time of occurrence of the peak of hydration was fitted by changing the parameter c_1. The dissolution rate was found in the range of 0.00325-0.0044 µm/h. As these variations are of the same order, they are found satisfactory. It should be noted that the rate of dissolution in this stage is around 100 times lower that the maximum dissolution rate (c_3). This shows the impact of surface coverage with the addition of gypsum. While c_3 was kept constant, c_2 was found to decrease substantially with the increase in gypsum content. This shows that when the gypsum content is higher, it takes longer time for the desorption of species from the active sites of C_3A grains. The time the model continues in pure dissolution (τ_{23}) was also found to increase with the increased gypsum content. As the heat release in the initial minutes (until 45 minutes) was not included (due to the time for mixing, measuring, placing the samples in the calorimeter and the time for stabilization of calorimeter) in the cumulative curve, the *y* axis of the measurement was shifted so that the cumulative heat release at the end of stage 1 coincides.

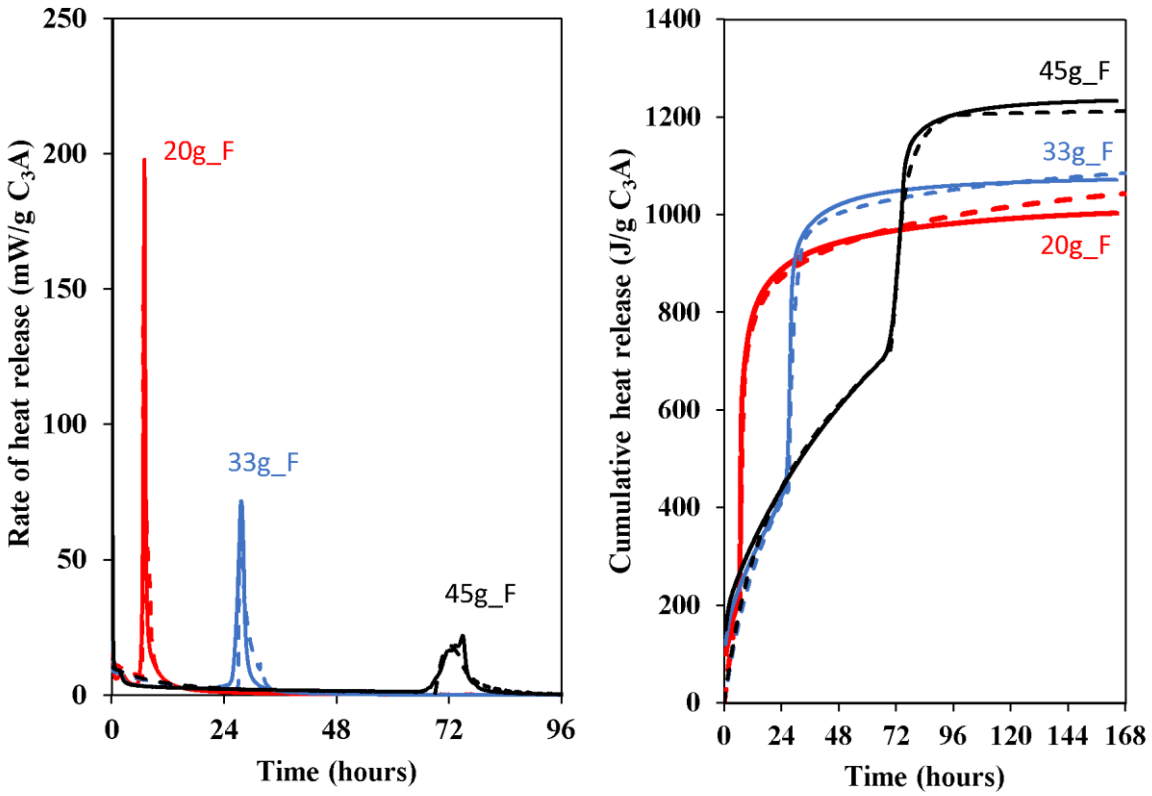

Figure 5.19: Comparison of results from model and experiments for Af at 20%, 33% and 45% gypsum; Rate of heat release (left); Cumulative heat release (right); Straight line indicate result from isothermal calorimetry and dashed lines indicate results from simulations.

Fig. 5.20 shows the comparison of simulation results and results from isothermal calorimetry on Ac (coarse C_3A) with 10% and 20% gypsum with variable w/c (0.36, 0.5, 1). This figure further validates the model as it is able to capture the effect on the coarser C_3A as well without the need of a drastic change in the parameters (Table 5.1). The parameter c_2 is decreased with increase in gypsum content, which is similar to the trend on Af. While there is a reduction in τ_{23} at w/c 1 with the decrease in gypsum content, this is not the case at w/c of 0.5. With the decrease in w/c, there is a significant decrease in τ_{23} and an increase in k_1.

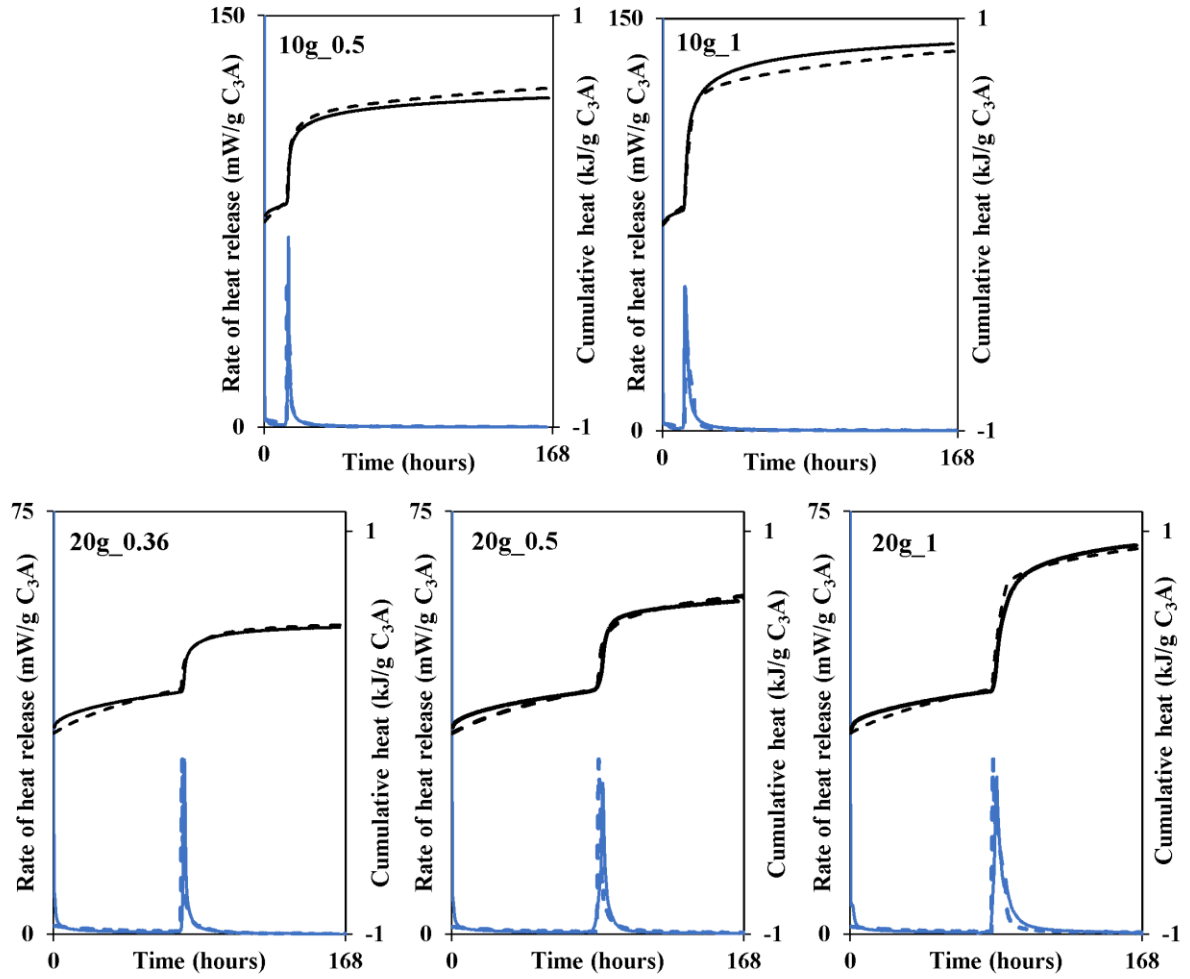

Figure 5.20: Comparison of results from model and experiments for Ac at 10% and 20% gypsum; Rate of heat release (blue); Cumulative heat release (black); Straight line indicate result from isothermal calorimetry and dashed lines indicate results from simulations.

Fig. 5.21 compares the degree of hydration of C_3A hydration without the addition of gypsum with experiments and modelling. As there is no retarding effect due to the addition of gypsum, parameters c_1 and c_2 are not needed for this simulation. The constant maximum dissolution rate (c_3) of 0.3 µm/h can also fit the degree of hydration in the system without adding gypsum. The red line in Fig. 5.21 shows continuous pure isotropic dissolution without a reduction in the rate of dissolution from Eq. 5.9. This implies the evolution of degree of hydration if the sample is infinitely diluted.

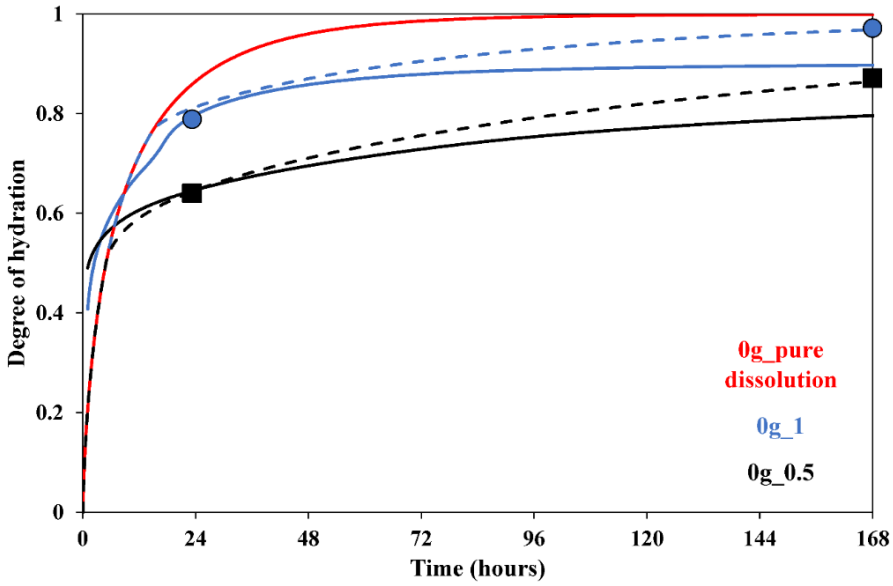

Figure 5.21: Degree of hydration measured from isothermal calorimetry (line), ^{27}Al MAS NMR (marker); y axis is shifted (0g_0.5: 0.49, 0g_1: 0.41) for isothermal calorimetry results to superimpose with NMR after 1 day; Dashed lines are model. Red line is the theoretical curve with pure isotropic dissolution with a dissolution rate of 0.3µm/hr.

Fig. 5.22 compares the dissolution rates of Ac and Af calculated from the model with respect to the degree of hydration. This figure clearly shows the capability of the model to capture the effect of fineness. Up to around 65% of hydration, there is no significant deviation between the dissolution rates of Ac and Af. Beyond that, the dissolution rate of Ac is lower than that of Af. This confirms the robustness of the model, as it is clearly seen in Fig. 5.9 that the variation of the rate of hydration and cumulative heat release of Ac and Af is drastic.

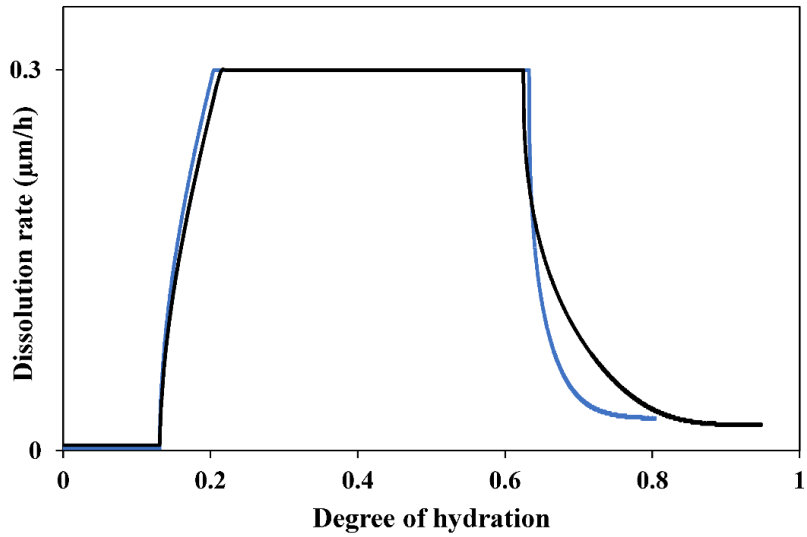

Figure 5.22: Comparison of variation of dissolution rate with respect to degree of hydration calculated from the simulations for Ac (blue) and Af (black) at w/c 1.

Fig. 5.23 shows the amount of evaporable water calculated from the model and measured from TGA and NMR (for Ac). The model calculates the amount of evaporable water from the w/c and the stoichiometric equations (Eq. 5.1 –5. 4) that is used to model the hydration of C_3A. The bound water was measured from TGA and the evaporable water was calculated based on the amount of gypsum and the w/c of the mixture[63]. The degree of hydration measured from ^{27}Al MAS NMR was used to plot the evaporable water against the degree of hydration. Clearly, the model is able to capture the amount of water in the hydrates well. This further validates the model. Some discrepancies are expected due to the effect of hydration stoppage on the interlayer water of hydrates. The evaporable water is slightly underestimated by the model in all mixes except 10g_1. This is consistent with the detection of C_4AH_{19} in 10g_1 (Fig. 5.13). As the model assumes the formation of C_4AH_{13} and C_2AH_8, this would underestimate the amount of bound water.

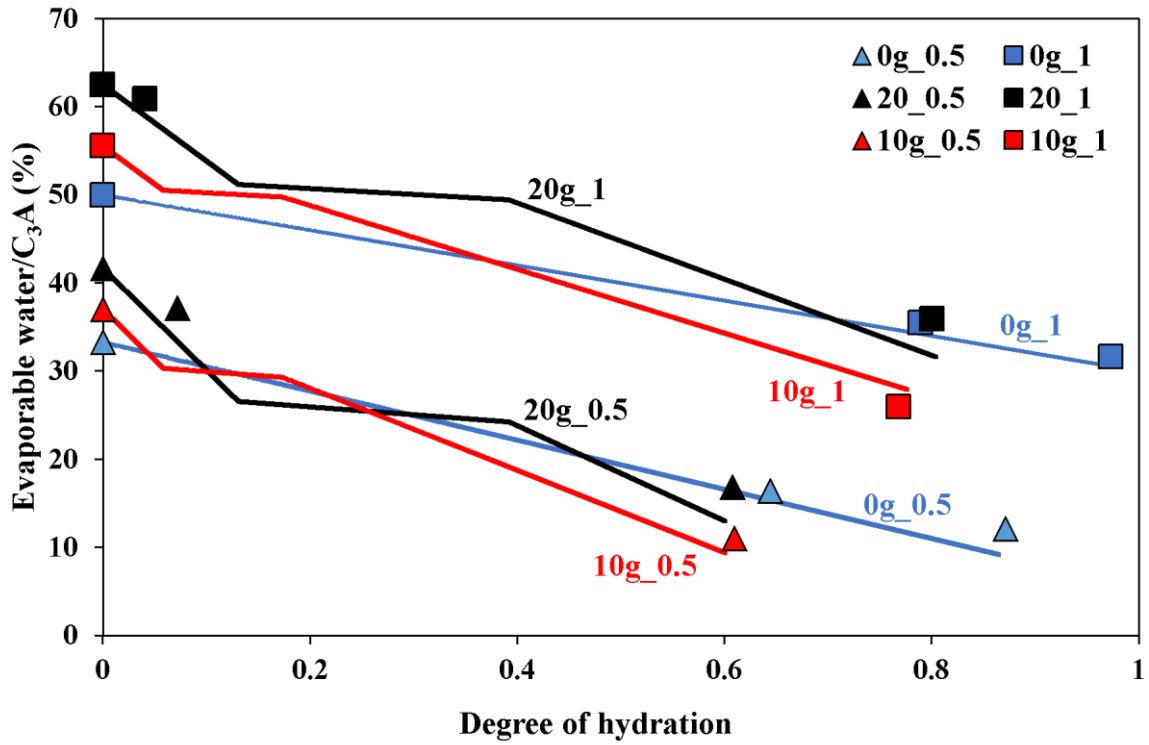

Figure 5.23: Evaporable water as measured from model and experiments (TGA and NMR) for coarse C_3A (Ac); Lines: Model, Marker: Experiments

5.5. Discussion

5.5.1. Before depletion of gypsum

In accordance with the previous findings[8-10,25,26], current results reaffirm that, in the first stage of C_3A hydration in the presence of gypsum, the hydration is retarded by surface mechanisms. The measured instantaneous activation energy of 75±6 kJ/mol (Fig. 5.15) is in agreement with the activation energy measured by Quennoz & Scrivener[10] (40-80 kJ/mol) based on the maturity method. As they pointed out, with such high values of activation energy, it is unlikely

that a diffusion-controlled mechanism is controlling the heat release. Hence, the barrier layer theory should be downright rejected.

Retardation by surface reduction is further supported by the numerical model. The parameter c_1, within a same order of magnitude, is able to capture the increase in the time of stage 1 with reduction in fineness and increase in gypsum. This suggests that the dissolution rate is constant throughout this period. A variation is expected as an isotropic dissolution is assumed in this model with a uniform reactive thickness concept. However, in reality, the dissolution is anisotropic with the formation of etch pits[56], and finer particles have a higher dissolution depth compared to the coarser particles[48]. As the shape of the particle is assumed to be spherical, the effects due to the irregular shape of C_3A grains could also lead to a variation in the dissolution depth[62], particularly in the early stages of hydration. This is because, the irregular surface becomes smoother over the course of dissolution. The amount of h-AFm phases, which are formed during the time of mixing, could also influence the time duration of stage 1, as these h-AFm phases could consume gypsum to form ettringite[64]. If the retardation is caused due to the barrier layer, c_1 should further decrease with time as during the course of hydration, the barrier layer would thicken[9,10].

Although retardation due to the adsorption of calcium and/or sulphate ions could explain the current results, an alternate hypothesis is proposed in this work. This hypothesis assumes that the retardation is due to the surface coverage of the active sites of C_3A hydration due to the precipitation of ettringite. This is similar to the hypothesis proposed by Nicoleau & Bertolim[65] for surface coverage of C_3S particles by deposition of C-S-H on its active sites. Minard et al.[9] and Quennoz and Scrivener[10] concluded that the retardation is due to the adsorption of calcium, and/or sulphate ions was based on the undersaturation of C_3A ions, and due to the effect of particle fineness on the time for consumption of gypsum. If the precipitated ettringite is blocking the active sites of C_3A, same effects should be expected on the undersaturation of C_3A ions and the effect of particle fineness, as dissolution of C_3A is still the controlling mechanism. This hypothesis could explain why Na_2SO_4 is not retarding the C_3A hydration[14]. When C_3A is hydrated solely in the presence of Na_2SO_4, ettringite is not formed[14] but monosulphate is formed later[66]. Ettringite is known to precipitate preferentially on the surface of C_3A although the hydration occurs through a solution mechanism[16,29]. Bullard et al.[54] predicted from simulations of reaction-transport modelling that ettringite is formed closer to the C_3A particles compared to gypsum or C_3S. Although C_3A and ettringite have positive zeta potential[67], ettringite could still potentially adsorb on the surface of the negatively charged aluminium layer of C_3A similar to the adsorption of positively charged calcium ions. Earlier hypothesis, which assumed ettringite to be the barrier layer, was disproved, as those models postulated that ettringite would hinder diffusion of ions, while the current hypothesis postulates that ettringite precipitation hinders the dissolution of C_3A. Nevertheless, further study is required to confirm the validity of this hypothesis.

5.5.2. After gypsum depletion

Currently, two hypotheses exist for the revived dissolution of C_3A. First theory proposed by Minard et al.[9] argues that this stage is controlled by a dissolution control mechanism. They

attributed the enhancement of heat release to the desorption of the calcium and/or sulphate ions. This was supported by the high undersaturation of C_3A ions during this period[9]. On the other hand, Quennoz and Scrivener[10] argued that in a non-diluted system, the characteristic shape of hydration peak is not representative of a dissolution-controlled mechanism as they expect a sharp increase and afterwards a fairly constant rate. Hence, they proposed that this period is controlled by nucleation and growth of AFm phases similar to the nucleation and densifying growth (NDG) mechanism proposed by Bishnoi and Scrivener[31] for C_3S hydration.

5.5.2.1. Arguments for a dissolution controlled mechanism

In the second stage, a high instantaneous activation energy (69±3kJ/mol), which was close to the instantaneous activation energy at stage 1 was found. This confirms that a change in the reaction mechanism does not occur during this period as such a change would be accompanied by a change in activation energy[47]. This value was found to be slightly higher than the activation energy measured by Quennoz and Scrivener[10] (59±8kJ/mol). It should be noted that they used a different approach using maturity method for the measurement of activation energy. With respect to the similar activation energy, it could be hypothesized that the second stage of hydration is also controlled by the dissolution of C_3A.

Results from numerical modelling also clearly show that a dissolution-based mechanism could explain the acceleration and deceleration period in the main hydration peak. It is proposed that the slope of the acceleration period is dependent on the rate at which the blocked active sites are available for hydration again. This could explain the broadening of the main peak of C_3A hydration with the reduction of fineness and increase in gypsum content as can be seen in Fig. 5.17. When c_2 is decreased, the slope of the acceleration period decreases and broadens the entire peak with the intensity of the main peak being reduced. If the retardation in stage 1 occurs due to adsorption of calcium and/or sulphate ions, this would be the time required for the desorption of the ions[32]. Although it is not clear why the desorption takes longer time when there is an increased amount of gypsum in the system. On the other hand, if we assume ettringite is blocking the active surface of C_3A, this could explain the increased time requirement very well. When gypsum content is higher, more ettringite is formed, which blocks the active surface. With the exhaustion of gypsum, C_3A reacts with ettringite to form m-AFm. In this process, the ettringite, which is blocking the surface of C_3A, is removed. When there is an increased amount of ettringite blocking the surface, this would take longer period to remove them. When the effect of fineness is considered, in fine C_3A (Af), the removal of ettringite occurs faster, because faster reaction to form m-AFm takes place which consumes ettringite faster. This is consistent with the parameter that controls the slope of acceleration in the model, c_2, which increases with increase in fineness (when compared to Ac_20g_1 and Af_20g_1). The deceleration period in the main hydration peak should be attributed to the reduced surface area due to the consumption of particles. This is validated by the similar dissolution depth which reasonably fits both the acceleration period and the deceleration period for the fine and coarse C_3A (Fig. 5.22). The reduction in the dissolution rate as seen in Fig. 5.22 is after the start of the deceleration regime.

The narrower peaks in diluted systems[8,9] compared to the current systems should be attributed to the continuous stirring that has been used in former systems and the large liquid to binder ratio of 25. The current model was able to fit the calorimetry curves published by Minard et al.[9], taking into consideration the particle size distribution which was plotted in the article (Appendix II). The value of c_1 was found to be around 0.023-0.029 which is one order of magnitude higher than the values of simulation in the present study (Table 5.1). This implies that the adsorption of calcium and/or sulphate ions are lower, or if surface coverage of ettringite is considered to be the rate limiting step, blockage of ettringite is lower on the active sites of C_3A. This could be due to the continuous stirring and/or higher liquid content, which would reduce the quantity of adsorbed ions or ettringite is less formed on the surface of C_3A particles. With the consumption of gypsum, these adsorbed ions will be released more quickly into the solution or ettringite from the surface is removed by recrystallization into m-AFm.

Although the dissolution rate remains unchanged till around 65% of hydration (Fig. 5.22), there is a significant drop in the dissolution rate beyond that period. In mixes with lower w/c, the retardation occurs earlier. This drastic reduction in the dissolution rate could be due to Eq. 5.9, which is used to model the heat release curve. A smoother retardation of the dissolution rate could also gain similar results. Future researches could potentially solve this problem by developing better equations for this model. In any case, the final total dissolution depth at 7 days of hydration is not affected.

This retardation of the dissolution rate, or the reduction of cumulative heat release (Fig. 5.11) and degree of hydration (Fig. 5.12) with reduction in w/c should be attributed to the reduced amount of free water content in the microstructure. With the increase in w/c, there is more water available at the surface of C_3A that enhances the reaction. Although the amount of evaporable water is low when the w/c is 0.5, there is significant amount of water remaining at w/c of 1 (Fig. 5.23). It should be noted that these measurements and calculations took into account only the chemically bound water, but not physically bound water. Additionally, more water could be present in the interlayers which would have reduced due to the hydration stoppage. As water is a wetting liquid, it would have a tendency to prefer the finer gel pores than the capillary pores. This could reduce the availability of water on the surface of C_3A. This hypothesis is further supported by Fig. 5.14, where additional water after 1 day of hydration leads to significantly higher heat release. The reduction in the available water would only retard the kinetics and does not stop the hydration. The hydration continues until whole water is depleted in the system. It has been observed that, Ac with 20% gypsum mixed with w/c 0.4 cured at 20ºC measured a degree of hydration of 0.91 after 45 days of hydration. This is almost 50% higher than the degree of hydration of Af_20g_0.5 after 7 days of hydration. With the transformation of h-AFm to more stable C_3AH_6, further water will be released into the system, which would also contribute to increasing degree of hydration in the later stage. This retardation in stage 3 is similar to the hydration of C_3A without gypsum (Fig. 5.4). In pure C_3A-water systems, the hydration advances very fast in the initial hours and then slows down. With an increase in w/c, there is an acceleration in the rate of hydration. Note that the reduction in the instantaneous activation energy measured in stage 3 is not conclusive. This reduction could be due to the transformation of h-AFm to C_3AH_6 (Eq. 5.2), which is favorable to be occurred

at higher temperature[5]. As this reaction is endothermic[5], this would underestimate the rate of reaction takes place, as isothermal calorimetry only measures the heat release.

5.5.2.2. Arguments against nucleation and growth-based mechanism

Although some of the current results could be explained by a nucleation and growth of AFm phases, there remains some unanswered questions. Similar instantaneous activation energy is measured in stage 1 and stage 2. Although it could be argued that both dissolution and nucleation and growth mechanism have similar activation energies, this is unlikely[26]. One of the major arguments in favor of a nucleation and growth mechanism put forward by Quennoz and Scrivener[10] is the characteristic shape of the hydration peak, which they stated was unlikely to occur in a dissolution controlled mechanism. However, the numerical model in the current study shows that it is clearly possible to have such a characteristic shape with dissolution-controlled mechanism as well, owing to high dissolution rates.

If the acceleration is induced by the surface area of C_3A and deceleration is induced by the available space as Quennoz and Scrivener[10] proposes, one would expect a higher peak with an increase in w/c as explained by Kirby and Biernacki[68]. However, calorimetry results showed no increase in the hydration peak with increase in w/c (Fig. 5.11). An explanation for this effect is not very clear. Quennoz and Scrivener[10] attributed this to the platy morphology of AFm phases. As increase in the w/c does not significantly increase the grain spacing, the distance a crystal must grow before they impinge is also not affected significantly[10]. Although the inter-particle distance between the particles is not significantly increased by the increase in w/c, there is a significant increase in volume. This would contribute to a lower bulk density and hence an increased internal surface area[37,48], which should therefore have a higher peak.

Furthermore, if the decrease in overall degree of hydration with decrease in w/c is due to the space constraints, one would not see a significant increase in the heat release when addition of water is added after 24 hours. Although it could be argued that this addition of water after 1 day could increase the space, this is unlikely as such an increase in volume is not seen in Portland cement paste, when they are subjected to chemical shrinkage measurements. On the contrary, even in the plastic state, a reduction in volume is observed owing to the coupled chemical and autogenous shrinkage[46].

5.6. Conclusions

The effect of fineness of C_3A, gypsum content and w/c were quantitatively studied using experimental techniques such as isothermal calorimetry, X-ray diffraction, thermal analysis, ^{27}Al MAS NMR. The experimental results show that an increase in fineness leads to a faster depletion of gypsum, and the peak of main hydration peak narrower and of higher intensity. The overall degree of hydration is also higher with fine C_3A after 7 days of hydration. With increase in gypsum content, it takes longer time for the consumption of gypsum and the peak of hydration becomes broadened with a lower intensity. These results are in accordance with the previous findings. When the w/c is increased, although first stage of hydration is not affected, there is a significant increase in the overall degree of hydration after 7 days of

hydration. This is also seen for C_3A systems without addition of gypsum. These results are further used to validate a new numerical model for C_3A hydration developed in this doctoral study on the new microstructural modelling platform CemRS. The model is able to capture the rate of heat release from isothermal calorimetry, the degree of hydration measured from ^{27}Al MAS NMR and the total bound and evaporable water found from TGA.

The major findings of this work are summarized as follows:

- Current study further validates that the hydration before the consumption of gypsum is controlled by surface mechanisms. Although adsorption of calcium and/or sulphate ions could potentially explain the current experimental results, a new hypothesis has been proposed. According to this hypothesis, the hydration in the presence of gypsum is hindered by the surface coverage of ettringite on the active surface of C_3A. This is significantly different from the ettringite barrier layer hypothesis, as in the current hypothesis, the retardation is proposed to be still controlled by a dissolution controlled mechanism but not by a diffusion controlled mechanism, which is the case for the theories on ettringite barrier layer.
- After the gypsum is depleted, the hydration continues to be controlled by dissolution of C_3A. The revived rate of hydration after the consumption of gypsum is attributed to the desorption of calcium and/or sulphate ions or the removal of the ettringite which blocks the active surface.
- The broadening and the lowering intensity with decreasing fineness of C_3A and increase in the gypsum content is attributed to the increased time for desorption of calcium and/or sulphate ions or increased time for the removal of the ettringite which covers the active surface of C_3A.
- With a decrease in w/c the overall hydration is retarded by 7 days. This is attributed to the lower availability of free water with the reduction in w/c and increase in degree of hydration of C_3A.

References

1. Bishnoi S. and Scrivener K. L. (2009) “mic: A new platform for modelling the hydration of cements” *Cem. Concr. Res.* **39**:266-274.
2. Taylor H. (1997) “Cement Chemistry: Second Edition”, London: Thomas Telford.
3. Baquerizo L., Matschei T., *et al.* (2015) “Hydration states of AFm cement phases” *Cem. Concr. Res.* **73**:143-157.
4. Corstanje W., Stein H. and Stevels J. (1973) “Hydration reactions in pastes $C_3S+C_3A+CaSO_4.2aq+H_2O$ at 25ºC” *Cem. Concr. Res.* **3**:791-806.
5. Pommersheim J. (1986) “Kinetics of hydration of tricalcium aluminate” *Cem. Concr. Res.* **16**:440-450.
6. Jupe A., Turrillas X., *et al.* (1996) “Fast in situ X-ray-diffraction studies of chemical reactions: a synchrotron view of the hydration of tricalcium aluminate” *Phys. Rev. B* **53**:R14697-R14700.

7. Black L., Breen C., *et al.* (2006) "Hydration of tricalcium aluminate (C3A) in the presence and absence of gypsum—studied by Raman spectroscopy and X-ray diffraction" *J. Mater. Chem.* **16**:1263-1272.
8. Pourchet S., Regnaud L., *et al.* (2009) "Early C_3A hydration in the presence of different kinds of calcium sulfate" *Cem. Concr. Res.* **39**:989–996.
9. Minard H., Garrault S., *et al.* (2007) "Mechanisms and parameters controlling the tricalcium aluminate reactivity in the presence of gypsum" *Cem. Concr. Res.* **37**:1418-1426.
10. Quennoz A. and Scrivener K. (2012) "Hydration of C_3A–gypsum systems" *Cem. Concr. Res.* **42**:1032–1041.
11. Brown P. W., Libermann L. O. and Frohnsdorff G. (1984) "Kinetics of the early hydration of tricalcium aluminate in solutions containing calcium sulfate" *J. Am. Ceram. Soc.* **67**:793-795.
12. Eitel W. (1957) "Recent investigations of the system lime–alumina–calcium sulfate–water and its importance in building research problems" *J.Am. Res. Inst.* **28**:679-698.
13. Baquerizo L., Matschei T., *et al.* (2014) "Methods to determine hydration states of minerals and cement hydrates" *Cem. Concr. Res.* **65**:85-95.
14. Collepardi M., Baldini G. and Pauri M. (1978) "Tricalcium aluminate hydration in the presence of lime, gypsum or sodium sulfate" *Cem. Concr. Res.* **8**:571-580.
15. Stein H. N. (1963) "Mechanism of the hydration of $3CaO,Al_2O_3$" *J. appl. Chem.* **13**:228-232.
16. Skalny J. and Tadros M. (1977) "Retardation of Tricalcium Aluminate Hydration by sulfates" *J. Am. Ceram. Soc.* **60**:174-175.
17. Powers T. (1961) "Some Physical Aspects of the Hydration of Portland Cement" *J. Res. Dev. Lab., Portland Cem. Assoc.* **3**[1]:47-56.
18. Mehta P. (1976) "Scanning Electron Microscopic Studies of Ettringite Formation" *Cem. Concr. Res.* **6**[2]:169-182.
19. Scrivener K. and Pratt P. (1984) "Microstructural studies of the hydration of C_3A and C_4AF independently and in cement paste" *Proc. Brit. Ceram. Soc.* **35**:207-219.
20. Gupta P., Chatterji S. and Jeffrey W. (1973) "Studies of the effect of different additives on the hydration of tricalcium aluminate: part 5—a mechanism of retardation of C_3A hydration" *Cem. Technol.* **4**:146-149.
21. Lasaga A. (1998) "Kinetic Theory in the Earth Sciences" Princeton: Princeton University Press.
22. Feldman R. and Ramachandran V. (1966) "The influence of $CaSO_4.2H_2O$ upon the hydration character of $3CaO.Al_2O_3$" *Mag. Concr. Res.* **18**:185-196.
23. Skalny J., Jawed I. and Taylor H. (1978) "Studies on hydration of cement—recent developments" *World Cem. Technol.* **9**[6]:183-191.
24. Bensted J. (1983) "Hydration of Portland Cement" *Adv. Cem. Technol.* , Pergamon Press 306-347.
25. Bullard J., Jennings H., et al (2011) "Mechanisms of cement hydration" Cem. Concr. Res. **41**:1208-1223.
26. Scrivener K. L., Juilland P. and Monteriro P. J. (2015) "Advances in understanding hydration of Portland cement" *Cem. Concr. Res.* **78**:38-56.

27. Myers R., Geng G., *et al.* (2017) "Role of adsorption phenomena in cubic tricalcium aluminate dissolution" *Langmuir* **33**:45-55.
28. Myers R., G. Geng, *et al.* (2017) "Solution chemistry of cubic and orthorhombic tricalcium aluminate hydration" *Cem. Concr. Res.* **100**:176-185.
29. Pommersheim J. (1988) "Kinetics of hydration of tricalcium aluminate in the presence of gypsum" *Cem. Concr. Res.* **18**:911-922.
30. Tenoutasse N. (1968) "The hydration mechanism of C3A and C3S in the presence of calcium chloride and calcium sulfate" in *The 5th International Symposium on the Chemistry of Cement*, Tokyo Japan.
31. Bishnoi S. and Scrivener K. L. (2009) "Studiying nucleation and growth kinetics of alite hydration using µic" *Cem. Concr. Res.* **39**:849-860.
32. Bergold S. T., Goetz-Neunhoeffer F. and Neubauer J. (2017) "Interaction of silicate and aluminate reaction in a synthetic cement system: Implications for the process of alite hydration" *Cem. Concr. Res.* **93**:32-44.
33. Zhang L. and Glasser F. P. (2000) "Critical examination of drying damage to cement pastes" *Adv. Cem. Res.* **12**[2]:79-88.
34. Zhang J. and Scherer G. W. (2011) "Comparison of methods for arresting hydration of cement" *Cem. Concr. Res.* **41**:1024-1036.
35. Snoeck D., Velasco L. F., *et al.* (2014) "The influence of different drying techniques on the water sorption properties of cement-based materials" *Cem. Concr. Res.* **64**:54-62.
36. Knapen E., Cizer O., *et al.* (2009) "Effect of free water removal from early-age hydrated cement pastes on thermal analysis" *Constr. Build. Mater.* 23:3431-3438.
37. Joseph S., Bishnoi S., *et al.* (2018) "Effect of the densification of C-S-H on hydration kinetics of tricalcium silicate" *J. Am. Ceram. Soc*. **101**[6]:2438-2449
38. Skibsted J., Bildsoe H. and Jakobsen H. (1991) "High-Speed Spinning versus High Magnetic Field in MAS NMR of Quadrupolar Nuclei. ^{27}A1 MAS NMR of 3CaO. $A1_2O_3$" *J. Magn. Reson.* **92**:669-676.
39. Skibsted J., Henderson E. and Jakobsen H. (1993) "Characterization of Calcium Aluminate Phases in Cements by ^{27}Al MAS NMR Spectroscopy" *Inorg. Chem* **32**:1013-1027.
40. Jakobsen H., Skibsted J., *et al.* (1989) "Magic-angle spinning NMR spectra of satellite transitions for quadrupolar nuclei in solids" *J. Magn. Reson.* 85:173-180.
41. Skibsted J., Henderson E. and Jakobsen H. J. (1993) "Characterization of Calcium Aluminate Phases in Portland Cements by ^{27}Al MAS NMR Spectroscopy" *Inorg. Chem.*, **32**:1013-1027.
42. Massiot D., Fayon F., *et al.* (2002) "Modelling one- and two-dimensional Solid State NMR spectra" *Magn. Reson. Chem.* **40**:70-76.
43. Gosselin C., Gallucci E. and Scrivener K. (2010) "Influence of self heating and Li_2SO_4 addition on the microstructural development of calcium aluminate cement" *Cem. Concr. Res.* **40**:1555–1570.
44. Collier N. (2016) "Transition and decomposition temperatures of cement phases- A collection of thermal analysis data" *Ceramics-Silikáty* **60**[4]:338-343.
45. Quennoz A. (2011) "Hydration of C_3A with calcium sulphate alone and in presence of calcium silicate" *PhD Thesis*, EPFL Switzerland.

46. Geiker M. (2016) "Characterisation of development of cement hydration using chemical shrinkage," in *A Practical Guide to Microstructural Analysis of Cementitious Materials*, K. Scrivener, R. Snellings and B. Lothenbach, Eds., CRC Press 75-106.
47. Thomas J. J. (2012) "The Instantaneous Apparent Activation Energy of Cement Hydration Measured Using a Novel Calorimetry-Based Method" *J. Am. Ceram. Soc.*, **95**[10]:3291–3296.
48. Joseph S., Bishnoi S., et al. (2017) "Modeling the effect of fineness and filler in early-age hydrationof tricalcium silicate" *J Am Ceram Soc.* **100**[3]:1178-1194.
49. Thomas J., Biernacki J., *et al.* (2011) "Modelling and simulation of cement hydration kinetics and microstructural development" *Cem. Concr. Res.* **41**:1257-1278.
50. van Breugel K. (1991) "Simulation of hydration and formation of structure in hardening cement-based materials" *PhD Thesis*, TU Delft Netherlands.
51. Bullard J. (2014) "Virtual cement and concrete testing laboratory" National Institute of Standards and Technology, User guide v. 9.5, Special Publication (NIST SP) - 1173
52. Bentz D. (1997) "Three-dimensional computer simulation of cement hydration and microstructure development" *J. Am. Ceram. Soc.* **80**[1]:3-21.
53. Bullard J. and Stutzman P. (2006) "Analysis of CCRL Portland cement proficiency samples number 151 and number 152 using the virtual cement and concrete reference laboratory" *Cem. Concr. Res.* **36**:1548-1555.
54. Bullard J., Enjolras E., et al. (2010) "A Parallel Reaction-Transport Model Applied to Cement Hydration and Microstructure Development" *Modell. Simul. Mater. Sci. Eng.* **18**:025007.
55. Joseph S., Bishnoi S., *et al.* (2016) "CemRS: fast and efficient modelling platform for the simulation of cementitious systems" in *International RILEM Conference Materials Systems and Structures in Civil Engineering 2016 (MSSCE 2016)*, Lyngby Denmark.
56. Brand A. and Bullard J. (2017) "Dissolution Kinetics of Cubic Tricalcium Aluminate Measured by Digital Holographic Microscopy" *Langmuir* **33**[38]:9645-9656.
57. Termkhajornkit P. and Barbarulo R. (2012) "Modeling the coupled effects of temperature and fineness of Portland cement on the hydration kinetics in cement paste" *Cem. Concr. Res.* **42**[3]:526-538.
58. Osbaeck B. and Johansen V. (1989) "Particle size distribution and rate of strength development of Portland cement" *J. Am. Ceram. Soc.* **72**[2]:197-201.
59. Avarami M. (1939) "Kinetics of phase change I" *J. Chem. Phy.* **7**:1103-1112.
60. Avarami M. (1940) "Kinetics of phase change II" . *Chem. Phy.* **8**:212-224.
61. Joseph S. and Bishnoi S. (2014) "Study on the effect of particle size distribution and Blaine fineness on the hydration of cement" in *Proceedings of the RILEM International Symposium on Concrete Modeling CONMOD*, Beijing China.
62. Bullard J. and Garboczi E. (2006) "A model investigation of the influence of particle shape on portland cement hydration" *Cem. Concr. Res.* **36**[6]:1007-1015.
63. Lothenbach B., Durdzinski P. and De Weerdt K. (2016) "Thermogravimetric analysis" in *A practical guide to microstructural analysis of cementitious materials*, CRC Press, 177-212.
64. Janotka I. and Mojumdar S. C. (2007) "Degree of hydration in cement paste and C_3A-sodium carbonate-water systems" *J. Therm. Anal. Calorim.* **90**:645-652.

65. Nicoleau L. and Bertolim M. A. (2015) “Analytical Model for the Alite (C_3S) Dissolution Topography” *J. Am. Ceram. Soc.* **99**:773-786.
66. Sanchez-Herrero M., Fernandez-Jimenez A. and Palomo A. (2012) “Alkaline Hydration of Tricalcium Aluminate” *J. Am. Ceram. Soc.* **95**[10]:3317-3324.
67. Yoshioka K., Tazawa E., *et al.* (2002) “Adsorption characteristics of superplasticizers on cement component minerals” *Cem. Concr. Res.* **32**:1507-1513.
68. Kirby D. and Biernacki J. J. (2012) “The effect of water to cement ratio on the hydraion kinetics of tricalcium silicate cements: testing the two step hydration hypothesis” *Cem. Concr. Res.* **42**[8]:1147-56.

Chapter VI

Hydration of polyphase C_3S-C_3A model cements in the presence of Na_2SO_4

6.1. Introduction

New alternatives for the conventional ordinary Portland cement (OPC) is under investigation for the past few decades due to sustainability and environmental concerns. Cement industry is currently responsible for around 10%[1] of total man-made CO_2 emissions due to the production of 4.6 billion tonnes of cement per year[2]. This would further increase with the projected increase in demand for cement to around 5.8 billion tonnes[3] by 2050. Blended cements which partially replaces OPC with supplementary cementitious materials (SCMs) are found to be one of the most feasible alternative for OPC as a general-purpose cement. These SCMs are mostly industrial by-products such as coal combustion fly ash, blast furnace slag from iron industry, silica fume etc.

The maximum replacement levels of most of the SCMs, barring highly reactive blast furnace slag, are generally limited to around 35% (CEM II). This is because higher replacement levels have a negative impact on the early age strength development and durability (due to reduced pH and higher porosity). For better utilization of these SCMs, the way forward should be to increase their replaceability limits by further activating the blended system, compensating for early-age strength reduction and the increase in porosity.

Sodium sulphate (Na_2SO_4) is found to be a potential activator to increase the mechanical properties of systems with higher replacement levels. Previous studies have demonstrated a significant increase in the overall reactivity and mechanical properties, when high volume fly ash blends are activated with Na_2SO_4[4-6]. This was also verified by the experiments in our lab (unpublished, Chapter 1, Fig. 1.1), which showed a higher strength with 50% replacement of fly ash when the blended cement was activated with Na_2SO_4 than the control OPC mix at 28 days. Nevertheless, the current understanding on the effect of Na_2SO_4 on the hydration of Portland cement systems is rather limited. A better understanding of how Na_2SO_4 influences the individual phases of OPC is necessary for studying the fundamental mechanism, potentials and limitations of such systems.

The advantage of studying polyphase C_3S-C_3A model systems is that they could mimic the early age hydration of OPC, while reducing the complexity involved within OPC hydration. This provides results with better clarity for qualitative and quantitative determination of the

hydrated phases using analytical techniques. Hydration in the early ages of Portland cement systems has been a major focus in this field of research due to high reaction rates. The significance of this period lies in being the time at which various important phenomena such as setting, hardening, strength development etc. takes place. This is a period that can also cause cracking risk in concrete due to thermal expansion, shrinkage, ettringite formation etc.

6.1.1. C_3S hydration

Alite/tricalcium silicate (C_3S) is the major phase which constitutes around 50-70% of OPC. C_3S hydration is instrumental in the setting and hardening process and contributes a major part of the strength development. C_3S reacts with water to form calcium silicate hydrate (C-S-H) gel and portlandite. In a blended cement system, C_3S hydration provides most of the amount of portlandite which increases the pH of the pore solution and reacts with SCMs in a pozzolanic reaction to form additional C-S-H. C_3S hydration is typically a fast reaction where most of the reaction finishes by around 7 days. Its hydration is typically divided into 5 stages[7] as shown in Fig. 6.1

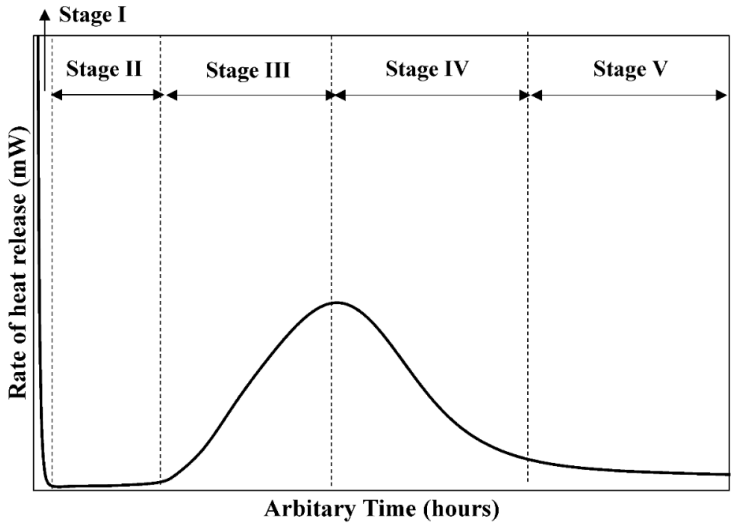

Figure 6.1: Typical heat release curve and stages of C_3S hydration

- *Stage I: Dissolution period* – Typically a period with very short duration, which occurs due to the under-saturation of C_3S ions in the added water and ends when the solution is saturated.
- *Stage II: Induction period* - After the end of the dissolution period, the hydration of C_3S approaches a dormant period or an induction period with very little heat release.
- *Stage III: Acceleration period* – The induction period is succeeded by the acceleration period characterized by a very fast increase in the rate of heat release.
- *Stage IV: Deceleration period* – After the rate of heat release reaches a maximum, the rate starts to decrease over time, which is termed as the deceleration period.
- *Stage V: Period of low hydration* – With the end of the deceleration period, the rate of heat release continues at a very slow rate for a very long time, during which the rate slowly and gradually reduces over time.

Significant studies have been previously carried out on the induction period (Stage II) and the main peak of C_3S hydration (Stage III & Stage IV)[7,8]. The induction period has a high significance in setting time, thereby giving ample time for the transportation and placing of concrete. Juilland et al.[9] proposed that the induction period is controlled by a geochemical dissolution mechanism where the kinetics is dependent on the under-saturation levels of C_3S ions. Although most publications support this hypothesis[10-12], some discrepancies are also reported[13]. Other prominent hypotheses that tried to explain this period are based on stabilization of C-S-H[16] and presence of a metastable barrier[14,15]. Lack of experimental evidence reduced the popularity of metastable barrier hypothesis[8].

The main peak of C_3S hydration, which consists of an acceleration period and a deceleration period, was also studied in detail as it has significant impact on the early age strength development in concrete. This period is generally thought to be controlled by nucleation and growth (N&G) based mechanisms[7,8] which is in turn controlled by the available surface area for the nucleation seeding and growth of C-S-H needles[17]. More recent studies hypothesize that the densification of C-S-H is influential on the N&G mechanism, as it induces changes in the internal surface area of C-S-H which will act as reaction surface for N&G[18]. It has been further proposed that the N&G mechanism continues to control the hydration kinetics in the later ages based on the effect of C_3S reaction kinetics with variable temperature profiles[19]. While the literature predominantly points out that the C_3S reaction during this period is controlled by N&G, some researchers point out the possibility of a dissolution-controlled mechanism[20,21]. According to their hypothesis, the acceleration period is due to the increased reaction surface as a result of etch pit formations. The deceleration period and beyond are due to the reduction in the reactive surface area due to the coagulation of etch pits and the surface coverage of C-S-H which blocks the active reaction front, and thereby retarding the kinetics of hydration[20,21].

It has been reported that although triclinic C_3S hydration does not have much effect on gypsum addition[22], monoclinic C_3S shows an enhanced hydration on the addition of gypsum[22,23]. Mota et al.[23,24] studied the effect of Na_2SO_4 on C_3S in considerable detail. They reported that Na_2SO_4 accelerates the hydration kinetics of C_3S in pure pastes, resulting in a higher degree of hydration in the early ages and similar degrees of hydration at later ages. They also noted that the morphology of the C-S-H changed from convergent fibrils without sulphate addition to divergent bundles of fibrils with sulphates. The dry density of C-S-H was found to be lower with addition of Na_2SO_4, while the bulk density of C-S-H was similar, meaning that Na_2SO_4 has an influence on the incorporation of water in the C-S-H gel.

6.1.2. C_3A hydration

Although the amount of C_3A is generally low in a typical Portland cement, it has a high significance in the early age heat release and is instrumental in controlling the setting time[7]. When C_3A is hydrated in the absence of gypsum, hydration proceeds very fast leading to formation of hydroxy-AFm (C_4AH_x, h-AFm) or/and hydrogarnet (C_3AH_6)[25-27] which would induce flash setting. Hence, gypsum is added into the system to regulate the setting time. The hydroxy-AFm would later convert to thermodynamically stable C_3AH_6 releasing additional water[26,27]. As the enthalpies of reaction of C_3A hydration is much higher compared to C_3S or

C_2S (Belite)[28], its contribution in the early age heat release in Portland cement systems is significant.

C_3A hydration is typically divided into three stages in the presence of gypsum (Fig. 6.2). The first stage is the period of low heat release, where C_3A reacts with gypsum to form ettringite (AFt). Literature generally agrees that the kinetics is controlled by a dissolution-controlled mechanism[7,8]. The low reactivity of this period is primarily attributed to the adsorption of sulphates or/and calcium ions on the surface of C_3A[25,29]. In Chapter 5, it was proposed that the reduction in the dissolution rate of C_3A could be also due to the surface blockage effect derived from the preferential formation of ettringite on the C_3A surface. The second stage includes a narrow, but a high peak of heat release which occurs after the consumption of gypsum. With increasing amount of gypsum[25] or other calcium sulphates (bassanite, anhydrite)[30], the second stage is delayed, and the peak broadens with a reduction in the peak height[29]. The increased delay in the formation of hydration peak is due to the requirement of longer time for the consumption of gypsum. In the second stage, the dissolution is enhanced by the removal of adsorbed Ca^{2+} and/or SO_3^- ions with the consumption of gypsum[25] or as stated in Chapter 5, due to removal of ettringite from C_3A surface due to recrystallization of ettringite to monosulphate. It was shown through numerical modelling in Chapter 5 that broadening and lowering of the main peak with increased gypsum content could be explained with the dissolution-controlled mechanism. An alternative hypothesis[29] explains that the reaction in this period is controlled by a nucleation and growth process of AFm phases and further controlled by the available space in the microstructure. Once the ettringite is fully consumed, C_3A hydration will proceed by the release of h-AFm phases. The third stage of C_3A hydration succeeds the main peak of C_3A reaction and this is a slow reacting stage. The heat release in this period is quite low due to the lower availability of the specific surface area due to the partial consumption of C_3A and Chapter 5 showed that available water in the capillary pores have a significant effect on the kinetics during this stage. It was found that, with increasing the w/c ratio, the degree of hydration is significantly enhanced. The addition of Na_2SO_4 in pure C_3A systems does not seem to react similar to the addition of gypsum, as the heat release is not reduced and although ettringite is not precipitated, formation of monosulphate was identified[31,32].

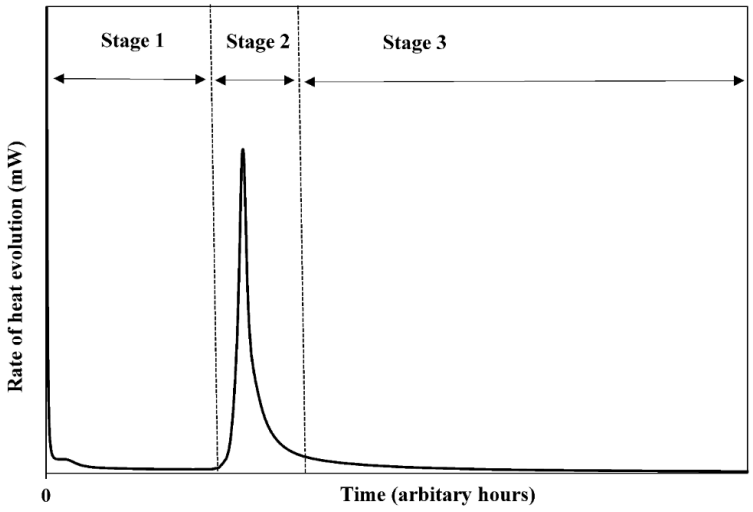

Figure 6.2: Typical heat release curve and stages of C_3A-gypsum hydration

6.1.3. Hydration of C_3S-C_3A model systems

Experimental studies have been conducted previously on mixing monophase C_3S and C_3A[22,33] and on polyphase C_3S-C_3A systems[22,34] in the presence of added calcium sulphates ($CaSO_4.xH_2O$, C$.xH). With increasing amounts of gypsum or calcium sulphates in general, the formation of the main peak of C_3A hydration is delayed as with the C_3A-gypsum systems[22,33]. With varying amounts of gypsum, the main peak of C_3A hydration could occur before the start of acceleration period, in the acceleration period, in the deceleration period or after the deceleration period of the main peak of C_3S hydration. If the gypsum content is too high compared to the total C_3A content, it is also possible that the main hydration period of C_3A does not occur. In this study, this is classified as:

- *Under-sulphated (U$)*: Main peak of C_3A hydration precedes the C_3S hydration peak (C_3A hydration peak forms at the Stage II of C_3S hydration).
- *Slightly-under-sulphated (sU$)*: Main peak of C_3A hydration will appear during the acceleration period (Stage III) of C_3S hydration.
- *Properly-sulphated (P$)*: In this system, which is most commonly seen in commercial OPC, the main peak of C_3A hydration will occur during the deceleration period (Stage IV) of C_3S hydration.
- *Over-sulphated (O$)*: In this system the peak of C_3A hydration will succeed the C_3S hydration peak (C_3A hydration peak forms at the Stage V of C_3S hydration).
- *Severely-over-sulphated (sO$)*: When the sulphate content is too high compared to the total C_3A content, stage 1 of C_3A hydration does not end and there will be a lack of peak from C_3A hydration.

It has been previously observed in both monophase and polyphase model systems[22,33] that the reaction of C_3A and the sulphate content have significant influence on the hydration of C_3S. In the case of under-sulphated systems, the induction period appears to be longer and the rate of C_3S hydration which succeeds the induction period is retarded and broadened[22,33,35]. In slightly-

under-sulphated systems, after the C_3A hydration peak, the rate of C_3S hydration tends to decelerate and reaccelerates from a lower rate level and further decelerates leading to a double peak of C_3S hydration[33]. It was noted that although the kinetics is severely affected, the cumulative heat release from the under-sulphated, slightly-under-sulphated and properly-sulphated systems are not significantly different after 48 hours[33].

Quennoz[22] attributed the retardation of C_3S after the C_3A hydration peak to be the hindering effect of Al ions in the solution on the hydration of C_3S. It is proposed that with the depletion of sulphates, Al ions released from the C_3A hydration are not completely bounded in the hydrated phases. This increase in the Al ions in the solution could lead to precipitation of C-A-S-H instead of C-S-H[36]. It has been previously found that the C-A-S-H has limited effect as a nucleation seed compared to C-S-H[37]. This implies that C-A-S-H is not an efficient nucleation surface compared to C-S-H, which would lead to a retardation of C_3S hydration. Pustovgar et al.[38] studied the inhibiting effect of Al on C_3S hydration by using $NaAlO_2$ solutions and found that Al could retard the hydration of C_3S causing an increase in the induction period in the early hours of hydration. They suggested that this is due to the surface adsorption of Al and occurs only at lower pH (<13) which was also suggested by Nicoleau et al.[39]. Bergold et al.[33] have a different view on the retardation of C_3S after the C_3A hydration, as they propose that precipitation of the AFm phases on the reactive surface of the C-S-H inhibits the N&G of C-S-H and thereby retarding C_3S hydration.

Although the effect of Na_2SO_4 is not specifically studied for C_3S-C_3A model systems, it has been previously studied on white Portland cements. With its addition in white cement, there is a reduction in the degree of hydration beyond 1 day of hydration although the degree of C_3S hydration is enhanced up to 24 hours[23]. On the other hand, the hydration of C_3A is significantly retarded with the addition of Na_2SO_4[23]. It is interesting to note that hydration of pure C_3A with the addition of Na_2SO_4 systems does not yield any ettringite, blended cements when activated with Na_2SO_4 (in the absence of gypsum) yield ettringite[40].

In this chapter, polyphase C_3S-C_3A model systems with variable additions of gypsum in combination with and without Na_2SO_4 is studied. More focus is given on over-sulphated systems (O$ & sO$) due to the limited number of studies on such systems in C_3S-C_3A model cements. This also aims at understanding of the effect of additional sulphate content by means of Na_2SO_4 addition. The effect of fineness of polyphase C_3S-C_3A model systems and the synergy between the reactions of C_3S and C_3A are also investigated. Analytical techniques such as isothermal calorimetry, QXRD, TGA, ^{27}Al & ^{29}Si MAS NMR were used to gather quantitative information about the hydration kinetics and to characterize the hydration products.

6.2. Experimental protocol

6.2.1. Materials

Polyphase C_3S-C_3A model cements (C_3S and C_3A are present in same grain, similar to Portland cement clinker), with two different compositions of C_3S and C_3A with two different fineness each are purchased from SARL minerals (France). The polyphase C_3S-C_3A model cements are

produced by mixing appropriate fractions of CaO, Al_2O_3 and SiO_2 and burning it at 1450ºC considering the Al_2O_3 that will be dissolved in C_3S. ^{29}Si MAS NMR confirmed that the polymorph of C_3S is monoclinic M1, while XRD confirmed that the polymorph of C_3A is cubic.

The composition, fineness and abbreviation used in this study for the polyphase C_3S-C_3A are given in Table 6.1. The particle size distribution of all these materials measured from laser diffraction (Malvern Mastersizer 2000) after dispersing in ethanol is given in Fig. 6.3. Analytical grade gypsum ($CaSO_4.2H_2O$) and technical grade sodium sulphate (Na_2SO_4, N$) purchased from Merck was used. Table 6.2 shows the mix compositions used in this study with the addition of different percentages of gypsum and sodium sulphate solution of 0.75M. The different parameters that are focused in this study are: Composition of C_3S-C_3A, gypsum content, fineness and addition of Na_2SO_4.

Table 6.1: Polyphase C_3S-C_3A model cements used in the study

Abbreviation	Composition	Fineness	Blaine (cm^2/g)
p90	C_3S 90%, C_3A 10%	Fine	3956
p90_C	C_3S 90%, C_3A 10%	Coarse	2337
p93	C_3S 93%, C_3A 7%	Fine	3096
p93_C	C_3S 93%, C_3A 7%	Coarse	2019

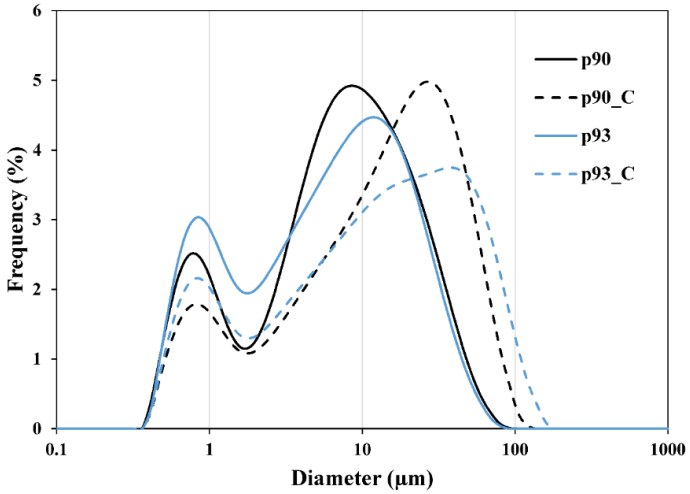

Figure 6.3: Particle size distributions of different polyphase C_3S-C_3A model cements used in this study

Table 6.2: Identification of mixes used in this study

Cement	Gypsum	Na_2SO_4	Age (days)	Abbr.
p90	4%	-	1	p90_4g_1d
		-	7	p90_4g_7d
		Yes	1	p90_4g_N$_1d
		Yes	7	p90_4g_N$_7d
	6%	-	1	p90_6g_1d
		-	7	p90_6g_7d
	8%	-	1	p90_8g_1d
		-	7	p90_8g_7d
		Yes	1	p90_8g_N$_1d
		Yes	7	p90_8g_N$_7d
p90_C	6%	-	1	p90_C_6g_1d
		-	7	p90_C_6g_7d
		Yes	1	p90_C_6g_N$_1d
		Yes	7	p90_C_6g_N$_7d
p93	4%	-	1	p93_4g_1d
		-	7	p93_4g_7d
		Yes	1	p93_4g_N$_1d
		Yes	7	p93_4g_N$_7d
	8%	-	1	p93_8g_1d
		-	7	p93_8g_7d
		Yes	1	p93_8g_N$_1d
		Yes	7	p93_8g_N$_7d
p93_C	4%	-	1	p93_C_4g_1d
		-	7	p93_C_4g_7d
		Yes	1	p93_C_4g_N$_1d
		Yes	7	p93_C_4g_N$_7d
	8%	-	1	p93_C_8g_1d
		-	7	p93_C_8g_7d
		Yes	1	p93_C_8g_N$_1d
		Yes	7	p93_C_8g_N$_7d

6.2.2. Methodology

Appropriate amount of gypsum was mixed with the polyphase C_3S-C_3A systems by dry mixing using a Turbula blender for 8 hours. The pastes were prepared in a temperature-controlled room at 20ºC with deionized water. A w/c ratio of 0.5 was used throughout the study. The pastes were mixed using a mechanical mixer at 750 rpm for 2 minutes to ensure homogenous mixing.

6.2.2.1. Isothermal calorimetry:

A TAMair 8 channel isothermal microcalorimeter was used to monitor the heat release for 7 days. All the measurements were carried out at 20 ºC. Around 3 g paste was transferred into an ampoule before transferring to the calorimeter. The calorimeter was installed in a temperature-controlled room of 20ºC which ensures minimum heat loss. The cumulative heat release was calculated by integrating the rate of heat release after ignoring the first 30 mins of measurements. The initial period was omitted as this is a period with a potential of high error which could occur from the temperature difference of the sample and the calorimeter.

6.2.2.2. Hydration stoppage:

To further study the hydrated phases using other quantitative techniques such as X-ray diffraction, Thermal analysis and NMR, the hydration of the pastes at 20ºC was stopped after 1 and 7 days using freeze-drying technique. In the freeze dryer, the sample was exposed to 25 mbar pressure and -60ºC. In these conditions the evaporable water would achieve the triple point and would be sublimated to water vapour. It has been previously reported that freeze drying partially deteriorate the hydration phases such as ettringite and monosulphate etc[41]. It has to be noted that although different drying techniques exist for arresting hydration, none of these techniques are free from damaging the system with respect to physical or chemical properties[42-44].

6.2.2.3. Thermogravimetric analysis:

TGA was performed using NETZSCH STA 409 PC on the samples after the hydration stoppage. A heating rate of 10ºC/min was used with approximately 25-40mg sample for each measurement. The measurement was performed from 20ºC to 600ºC under N_2 environment. Random samples were measured until 1000ºC to ensure that there is no carbonation involved. The portlandite content was calculated using the tangent method[28] and was recalculated per 100g anhydrous cement using the Eq. 6.1[45]

$$CH_{per\ 100g\ anhydrous} = \frac{100CH_{measured}}{100 - BW} \quad (6.1)$$

where, BW is the bound water content (mass loss at 600ºC[45]).

6.2.2.4. Quantitative X-ray diffraction:

X-ray diffraction (XRD) was performed from 5 to 70º 2θ on the hydrated samples after hydration stoppage using a Bruker D2 phaser diffractometer with CuK anode. The samples were front loaded, and hence a significantly high preferred orientation for the (0 2 0) peak of gypsum and moderate preferred orientation for (0 0 2) peak of portlandite were identified. The quantification of phases was done using Rietveld analysis using Topas (Academic) software by using a combination of scale factor method[34] and external standard method[46]. This method

was used in samples after hydration stoppage by considering the mass absorption coefficient (MAC) of the sample, which is calculated combining the bound water content measured from TGA, and using corundum as an external standard. One of the major challenges for using XRD in this particular study was the M1 polymorph of C_3S. Lacking a well-tested crystal structure, the crystal model proposed by de Noirfontaine et al.[47] was used in this study. The crystallinity of the phases in the polyphase C_3S-C_3A systems were not particularly high as there was approximately 15% of amorphous/not detected content as measured against the corundum standard. Which is why a scale factor approach in combination with external standard method was used for the determination of degree of hydration, while external standard method was used for estimating ettringite and portlandite content. The degree of hydration of C_3S and C_3A, the ettringite and portlandite content were further recalculated incorporating the bound water content measured from TGA as described in [48].

6.2.2.5. ^{29}Si MAS NMR:

^{29}Si Magic Angle Spinning (MAS) Nuclear Magnetic Resonance (NMR) spectroscopy was used in the present study to measure the degree of hydration of C_3S and to characterize the C-S-H in pastes by calculating the mean chain length (MCL) and Al/Si ratio using deconvolution of the spectra. The solid-state ^{29}Si MAS NMR measurements were recorded at 59.6 MHz on a Varian INOVA 300MHz (7.05T) spectrometer using a home-built CP/MAS probe at Aarhus University, Denmark. A 7 mm outer radius partially sintered zirconia (PSZ) rotor (220µl sample volume) was used with around 0.2-0.3 g samples with a spinning speed of 6.0 kHz and bearing pressure of 2.6 bar. A single pulse experiment with 30 µs pulse width (~45º flip angle) at radio frequency field strength of $\gamma B1/2\pi \approx 40.0$ kHz was used. A 60s repetition delay was used and 2816 scans (total measurement time ~24 hours) were recorded, which was enough to achieve a good enough signal to noise (S/N) ratio. Neat tetramethyl silane was used as reference to account for the ^{29}Si chemical shifts. The deconvolutions were performed using the dmfit program[49] and the relative intensities from the Si sites were measured (which are denoted as Q^0, Q^1, $Q^2(1Al)$ and Q^2). The Q^0 peaks (which indicates the unhydrated C_3S) for the deconvolution model were fixed with respect to the position and line width based on the ^{29}Si MAS NMR spectra of the anhydrous model cement. The equations (Eq. 6.2, Eq. 6.3, Eq. 6.4) to calculate the average chain length of aluminosilicate tetrahedra (MCL), average chain length of pure silica tetrahedra (MCL_{Si}) and the molar ratios of Al incorporated in the C-S-H (Al/Si) are described below[50-53].

$$MCL = \frac{2[Q^1 + Q^2 + \frac{3}{2}Q^2(1Al)]}{Q^1} \quad (6.2)$$

$$MCL_{Si} = \frac{2[Q^1 + Q^2 + Q^2(1Al)]}{Q^1 + Q^2(1Al)} \quad (6.3)$$

$$Al/Si = \frac{Q^2(1Al)}{2[Q^1 + Q^2 + Q^2(1Al)]} \quad (6.4)$$

6.2.2.6. ^{27}Al MAS NMR:

Solid state ^{27}Al MAS NMR measurements were recorded at 156.3 MHz on a 600MHz Varian Direct-Drive VNMR-600 (14.09T) spectrometer using a home-built CP/MAS probe at Aarhus University, Denmark. A 4mm o.d. PSZ rotor was used with around 0.07- 0.09 g samples with a spinning speed of 13.0 kHz and bearing pressure of 2.8 bar. A single pulse experiment with 0.5 µs excitation pulse was used with proton decoupling. The rf field strength, $\gamma B_1/ 2\pi \approx 60.0$ kHz and a relaxation delay of 2s was used. Typically, 4096 scans were performed, which provided a good enough S/N. 1M aqueous solution of $AlCl_3.6H_2O$ was used for referencing. Deconvolution was performed using dmfit program, using gaussian and Lorentzian peak shapes. Decoupling is particularly difficult for ^{27}Al MAS NMR spectra with the gaussian and Lorentzian shapes as ^{27}Al has a nuclear spin of 5/2, which induces quadrupole coupling. Estimation of degree of hydration for C_3A in a model C_3S-C_3A system is difficult due to the broad peaks of Al(4) in the silicate chain[54,55] and Al(5) sites on the interlayer C-S-H[56,57] at around ~70 and 35 ppm which overlaps with the Al sites of anhydrous C_3A (~90 −17ppm)[53].

6.3. Results

6.3.1. Studying hydration kinetics using isothermal calorimetry

6.3.1.1. Effect of sulphates on the hydration kinetics

Fig. 6.4 shows the rate of heat release measured from isothermal calorimeter at 20ºC on p90 with 4%, 6% and 8% of gypsum with and without Na_2SO_4. With increasing amount of gypsum, the heat release peak from aluminate reaction is consistently delayed and there is a broadening of the peak which is consistent with the previous studies[22]. The height of the aluminate peak is also reduced with the increase in gypsum content. This is not very clear with 6% gypsum (p90_6g) as the aluminate peak is superimposed with the main peak of hydration of C_3S reaction. These results remain consistent with the effect of increasing gypsum content on the hydration of pure C_3A systems[29] (also seen in Chapter 5) and hydration of C_3A in C_3S-C_3A model systems[22,33]. The system with 4% gypsum (p90_4g) is under-sulphated, as the aluminate peak occurs before the main peak of C_3S reaction. It is observed that there is an increase in the induction period, and the peak of C_3S hydration is much broader and less intensified compared to the higher gypsum contents which were also reported in [22] and [33]. With 6% gypsum content (p90_6g), the system is slightly-under-sulphated as the C_3A peak is in the acceleration stage of C_3S hydration. A broad second peak of C_3S hydration is also visible[33]. In the case of 8% gypsum (p90_8g), the system is over-sulphated as a small and broad peak of C_3A is observed after the C_3S hydration peak. With the addition of Na_2SO_4 (p90_4g_N$, p90_8g_N$), instead of two distinct peaks of C_3S and C_3A hydration, only a single peak appears, which is narrower and with higher intensity compared to the peak of C_3S. Although it could not be solely concluded based on isothermal calorimetry that the peak probably derives from C_3S hydration,

as with the addition of Na_2SO_4, the main peak of C_3A could be further delayed and broadened owing to the higher sulphate content.

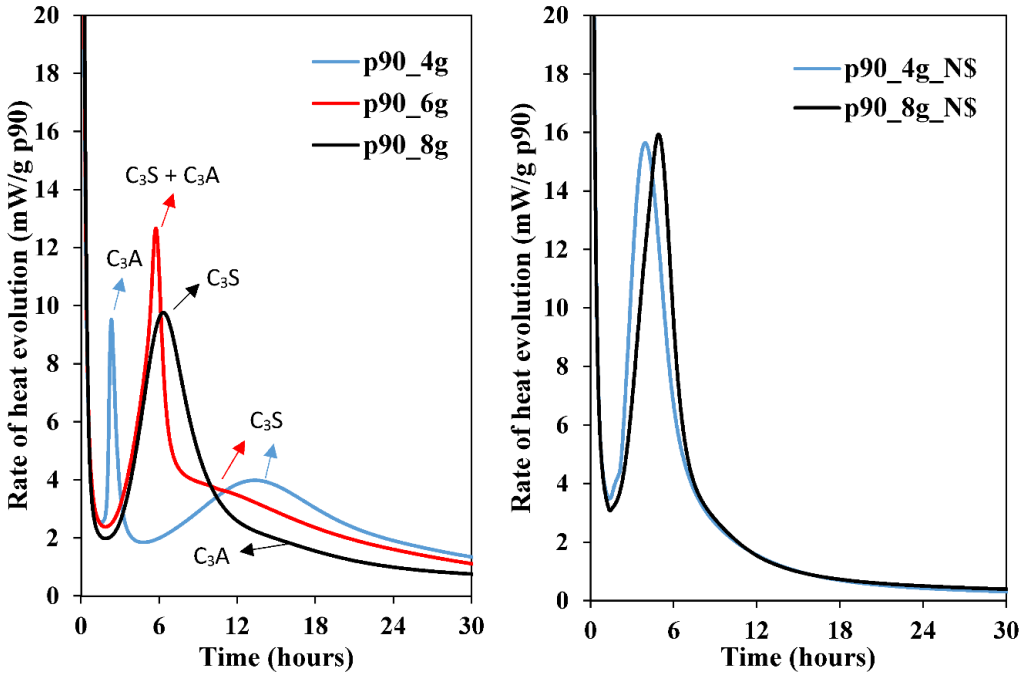

Figure 6.4: Effect of gypsum content and Na_2SO_4 on the rate of heat release for p90 systems until 30h; Without Na_2SO_4 (left), with Na_2SO_4 (right)

Fig. 6.5 shows the cumulative heat release up to 7 days for the mixes studied in Fig. 6.4. Even though the under-sulphated (U$ and sU$) systems (p90_4g and p90_6g) exhibited a lower heat release in the early ages, the measured overall heat release is similar[33]. With the addition of Na_2SO_4, there is a clear increase in the heat release in the early hours, but after that, there is a significant drop in the total heat release. However, with the addition of Na_2SO_4, both 4% gypsum and 8% gypsum systems show similar cumulative heat release by 7 days. The variations between the cumulative heat release by 7 days for mixes p90_4g, p90_6g, p90_8g and mixes p90_4g_N$, p90_8g_N$ are within the expected error range of the calorimeter.

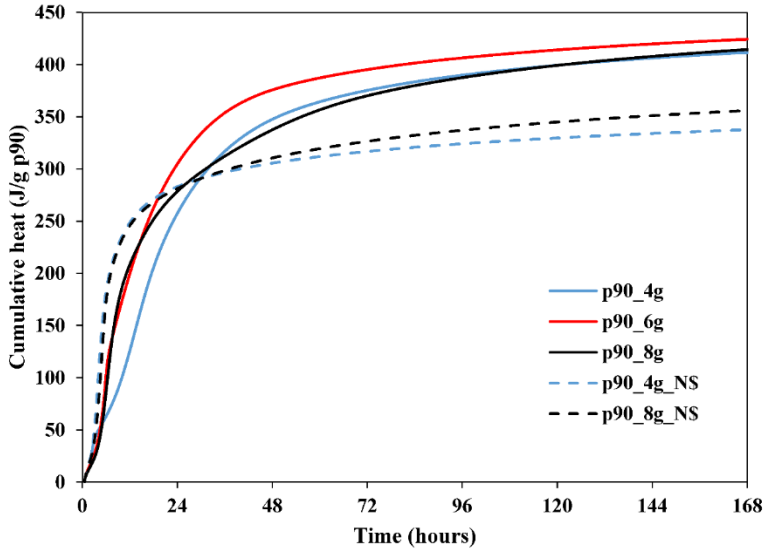

Figure 6.5: Effect of gypsum content and Na_2SO_4 on the cumulative heat release of hydration of p90 until 7 days of hydration

To further study the effect of sulphates on the hydration of C_3S and C_3A, the experiments were repeated on a different system with 93% C_3S and 7% C_3A (p93). Fig. 6.6 (left) shows that with 4% gypsum (p93_4g), the system is properly-sulphated while with 8% gypsum is severely-over-sulphated. This should be expected when compared to p90, because p93 has a lower amount of C_3A content, the C$/$C_3A$ ratio is further increased in this system. It is clearly seen that with p93_8g, a peak of C_3A hydration does not exist as the gypsum content is too high compared to the amount of C_3A. This also means that gypsum is not fully consumed even after 7 days. Cumulative heat release of p93 systems (Fig. 6.6, right) reveals a significant reduction in the overall heat release for p93_8g compared to p93_4g. There is a significant reduction in the overall heat release for p93_8g_N$ as well while compared to p93_4g_N$. It should be noted that the cumulative heat release of p93_8g is similar to p93_8g_N$ after 7 days. These results show that severely-over-sulphated systems have reduced degree of hydration after the initial hydration.

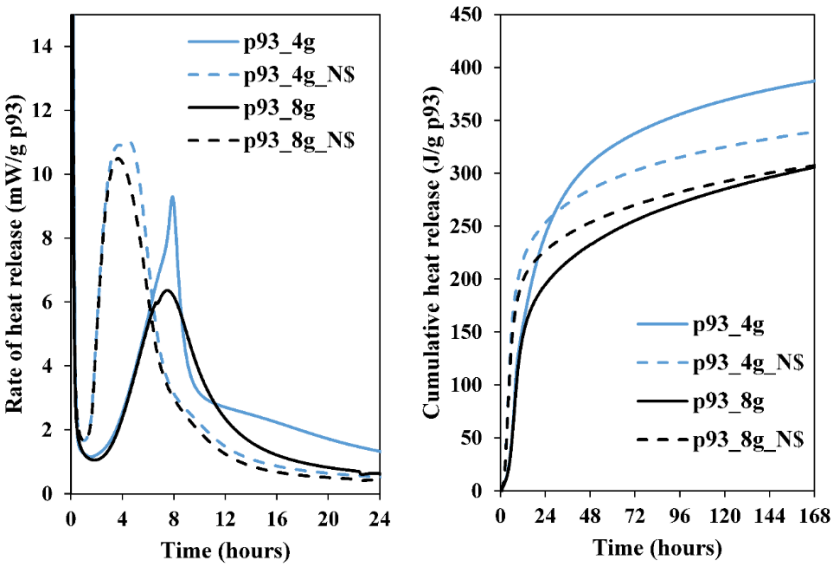

Figure 6.6: Effect of gypsum content and Na_2SO_4 on p93 systems; the rate of heat release until 24h (left); cumulative heat release until 7 days (right);

6.3.1.2. Effect of fineness on the hydration kinetics

Coarse fractions of p90 (p90_C) and p93 (p93_C) were used to study the effect of fineness on the hydration kinetics. Fig. 6.7 shows the effect of fineness on the hydration rate of p90 system (both fine and coarse). When the fineness is low, p90_C_6g becomes over-sulphated (main hydration peak of C_3A positioned around 33hrs), while p90_6g is slightly under-sulphated. This implies that apart from C$/$C_3A$ ratio, fineness also plays an important role in the peak position of C_3A hydration. With the reduction in fineness, the induction period has been also increased which is in agreement with the previous results with pure C_3S[18]. Fig. 6.7 further shows that the overall heat release is consistently lower with coarser materials, and there is a reduction in the heat release with the addition of Na_2SO_4 following the similar trend which is seen in Fig. 6.5.

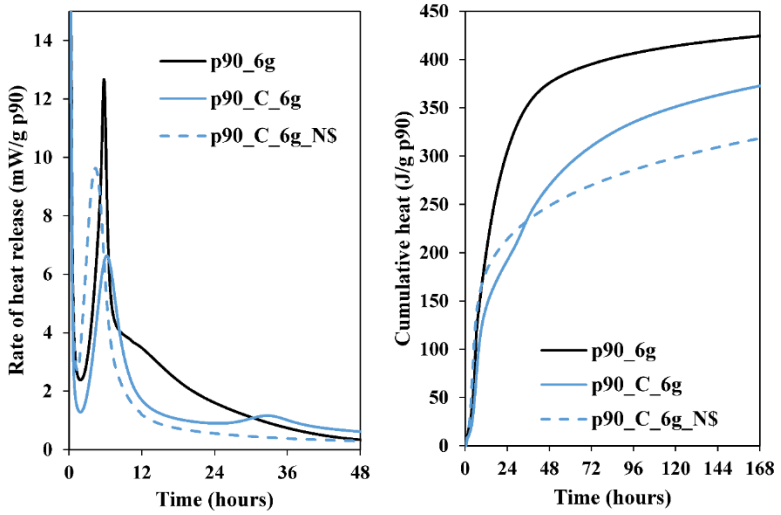

Figure 6.7: Effect of fineness of p90 on rate of heat release Effect of fineness of p90 on the cumulative heat release

p93_C systems (Fig. 6.8) exhibit similar trends when compared to the previous results (Fig. 6.6 and Fig. 6.7). The peak of C_3A hydration in p93_C_4g is positioned further in the deceleration period of C_3S compared to p93_4g due to lower fineness. With 8% gypsum (p93_C_8g), it is still severely-over-sulphated and the C_3S hydration peak resembles with that of p93_C_4g although the intensity is slightly on the lower side. With Na_2SO_4 addition, the rate of hydration is practically the same for both 4% and 8% gypsum content upto 24 hours. While comparing the cumulative heat release, although the heat release is similar for the two pairs of results in the early hours, there is a considerable difference between them in the later ages. There is a significant reduction in the cumulative heat release with 8% gypsum, both with and without Na_2SO_4 (p93_C_8g & p93_C_8g_N$), with p93_C_8g significantly lower than all other mixes in Fig. 6.8.

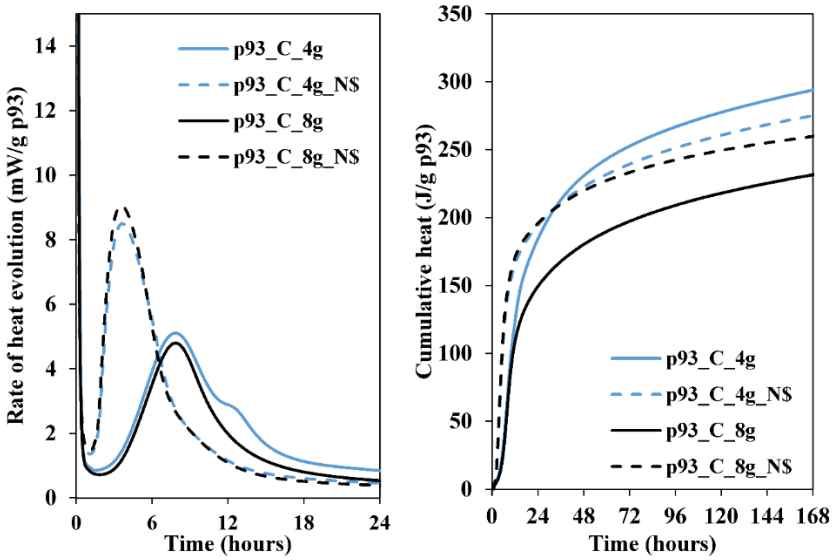

Figure 6.8: Effect of p93_C on rate of heat release Effect of p93_C on cumulative heat release

6.3.2. Study on paste after hydration stoppage

Although isothermal calorimetry is an excellent experimental technique to follow the kinetics of reaction, its inability to quantify the individual reactions in the whole system makes it necessary to use it in combination with other analytical techniques such as TGA, XRD and NMR. Hence, to gather further quantitative information regarding the hydration of C_3S-C_3A system, hydration was stopped using freeze drying technique after 1 and 7 days of hydration. These samples are then stored in a vacuum desiccator before and after performing the experiments.

6.3.2.1. ^{29}Si MAS NMR

^{29}Si MAS NMR spectroscopy is particularly useful in studying model systems with C_3S-C_3A compared to a Portland cement system. This is because there is an overlapping of Q^0 sites from C_2S (belite) which could affect the quality of the quantification in Portland cement systems. An example of the deconvolutions from ^{29}Si MAS NMR is given in Appendix III. From the

deconvolutions 6 Q^0 sites are identified at -69.1, -70.4, -71.4, -72.6, -73.6, -74.8 ppm. Two Q^1 sites were detected at -77.1 and -78.9 ppm. Site of Q^2(1Al) was detected at -80.9 ppm. Two peaks of Q^2 were detected at -83.1 and -85.1 ppm. These sites are in the same range as previously reported[53]. The deconvolution of all the ^{29}Si MAS NMR measurements are further given in Appendix III. Table 6.3 shows the average chain length of aluminosilicate tetrahedra (MCL), the average chain length of pure silica tetrahedra (MCL_{Si}) and the molar ratios of Al incorporated in the C-S-H (Al/Si) calculated from Eq. 6.2, Eq. 6.3 and Eq. 6.4 respectively and the degree of hydration of C_3S, as measured from ^{29}Si MAS NMR.

Table 6.3: Results from ^{29}Si MAS NMR and ^{27}Al MAS NMR for all the samples.

Sample	^{29}Si MAS NMR				^{27}Al MAS NMR		
	MCL	MCL_{Si}	Al/Si	C_3S DoH	AFt	AFm	C_3A DoH
p90_4g_1d	4.03	2.69	0.1	0.4	0.8	34.8	0.8
p90_4g_7d	4.41	3.02	0.08	0.73	0.3	40.2	0.94
p90_4g_NS_1d	3.82	2.58	0.1	0.5	13.6	21.7	0.76
p90_4g_NS_7d	3.74	2.55	0.1	0.59	13.7	24.3	0.83
p90_6g_1d	4.56	2.54	0.14	0.47	1.5	42.2	0.97
p90_6g_7d	4.39	2.66	0.12	0.71	2.9	41.4	1
p90_C_6g_1d	4.49	2.68	0.12	0.3	0.1	17.0	0.39
p90_C_6g_7d	4.33	2.7	0.11	0.61	4.8	34.2	0.89
p90_C_6g_NS_1d	3.81	2.62	0.09	0.37	4.5	21.0	0.5
p90_C_6g_NS_7d	3.75	2.74	0.08	0.52	20.9	8.7	0.63
p90_8g_1d	4.74	2.6	0.14	0.45	0.9	38.3	0.87
p90_8g_7d	4.71	2.79	0.12	0.73	1.8	36.8	0.97
p90_8g_NS_1d	3.89	2.51	0.11	0.47	9.2	24.2	0.73
p90_8g_NS_7d	3.93	2.64	0.1	0.65	29.7	8.1	0.83
p93_4g_1d	3.97	2.51	0.12	0.27	5.5	30.2	0.81
p93_4g_7d	4.01	2.58	0.11	0.58	6.9	29.3	0.96
p93_4g_NS_1d	3.8	2.41	0.12	0.37	1.6	25.3	0.59
p93_4g_NS_7d	3.67	2.61	0.09	0.55	25.3	7.1	0.7
p93_8g_1d	4.2	2.48	0.13	0.24	7.0	16.2	0.47
p93_8g_7d	4.06	2.63	0.11	0.44	15.9	18.3	0.65
p93_8g_NS_1d	4.36	2.52	0.14	0.33	9.1	24.2	0.61
p93_8g_NS_7d	4.1	2.58	0.12	0.47	19.0	18.1	0.68
p93_C_4g_1d	3.92	2.5	0.12	0.19	17.1	18.5	0.74
p93_C_4g_7d	4.37	2.66	0.12	0.41	16.0	14.7	0.81
p93_C_4g_NS_1d	3.96	2.57	0.11	0.27	4.4	16.5	0.49
p93_C_4g_NS_7d	3.88	2.73	0.09	0.44	18.7	9.2	0.61
p93_C_8g_1d	3.81	2.46	0.11	0.14	13.6	4.0	0.39
p93_C_8g_7d	4.2	2.63	0.11	0.29	20.2	5.6	0.56
p93_C_8g_NS_1d	3.96	2.52	0.12	0.22	0.6	18.4	0.55
p93_C_8g_NS_7d	3.93	2.68	0.09	0.35	26.9	2.8	0.66

6.3.2.2. ^{27}Al MAS NMR

An example for the deconvolution of the ^{27}Al MAS NMR spectra is given in Appendix III. The ^{27}Al MAS NMR spectra of anhydrous model cement, which has quadrupole coupling due to the 5/2 nuclear spin of ^{27}Al, was deconvoluted using 7 Al sites having gaussian and Lorentzian peak shapes. The sites were at 87.1, 82.2, 74.7, 71.1 60.9, 51.4, 35.4 ppm. In hydrated samples, assuming p90_6g_7d is fully hydrated with respect to C_3A, the deconvolution detected two Al sites for Al(4) (Al incorporated in C-S-H) at 72.1 and 67.3 ppm which corresponded well with the literature[53-55]. The fivefold-coordinated Al in the C-S-H interlayer, Al(V) was detected at 33.4 ppm[55-57]. Third aluminate hydrate (TAH), an X-ray amorphous phase, which is expected to form at the surface of C-S-H, is detected at 4.6ppm[56,57]. Depending on the age and gypsum composition, different samples detected ettringite at 13.2ppm and AFm phases at around 9.5-10.5ppm, which is consistent with the literature[58]. It must be noted that differentiating the different AFm phases (m-AFm and h-AFm) is extremely difficult with ^{27}Al MAS NMR as they have chemical shifts very close to one another. As the estimation of degree of hydration is difficult due to the overlapping Al (4) and Al (5) sites on the anhydrous C_3A, the degree of hydration was estimated factoring the relative total of ettringite + AFm + TAH content (<14ppm) with these quantities of p90_6g_7d. This is indeed a crude method for estimating the degree of hydration. Table 6.3 reports the degree of hydration of C_3A, % of Al in ettringite (AFt) and % Al in AFm phases (AFm).

6.3.2.3. TGA

Table 6.4 shows the portlandite content per 100g anhydrous and the total bound water content. The bound water is estimated as the total mass loss until 600ºC[45]. The portlandite content is quantified from the tangent method[28]. The mass losses from de-hydroxylation of C-S-H, ettringite and AFm phases are not quantifiable in nature as they tend to overlap with each other, and the peaks from these phases also shifts depending on the degree of reaction, mass of sample etc.[45].

6.3.2.4. X-ray diffraction

Table 6.4 shows the degree of hydration of C_3S, C_3A measured from XRD and the quantity of portlandite and ettringite present per 100g anhydrous based on the scale factor method in combination with the external standard method. For the Rietveld refinement, a model suggested in [47] was used for refining M1 polymorph of C_3S, ICSD 202220 for Portlandite, 1841 for C_3A cubic, ICSD 409581 for gypsum, ICSD 155395 for ettringite, ICSD 100138 for kuzelite. Hydrogarnet (C_3AH_6) was not detected in any of the systems. The estimation of gypsum is not reported as it is extremely erroneous due to the preferred orientation. AFm phases, being poorly crystalline and lacking crystal structure files, are not refined but the broad peaks are refined using PONKCS method[59].

Table 6.4: Results from TGA measurements and QXRD/Rietveld analysis; Bound water (%), Portlandite content (CH, per 100g anhydrous), Ettringite (AFt, per 100g anhydrous);

Sample	TGA		XRD			
	Bound water	CH	C_3S DoH	C_3A DoH	CH	AFt
p90_4g_1d	12.9	18.0	0.49	0.76	18.7	0.2
p90_4g_7d	20.1	29.2	0.91	0.97	29.5	0.3
p90_4g_NS_1d	16.5	15.4	0.57	0.77	18.9	4.1
p90_4g_NS_7d	16.1	17.1	0.68	0.83	22.2	4.3
p90_6g_1d	16.4	21.4	0.62	0.96	18.4	0.2
p90_6g_7d	21.4	28.9	0.88	1	26.2	0.5
p90_C_6g_1d	10.7	16.2	0.47	0.37	12.0	0
p90_C_6g_7d	19.8	28.2	0.78	0.9	22.7	2.1
p90_C_6g_NS_1d	12.4	13.8	0.49	0.47	12.0	0.2
p90_C_6g_NS_7d	15.6	18.0	0.66	0.46	19.7	7.4
p90_8g_1d	15.0	21.3	0.62	0.93	18.6	0.1
p90_8g_7d	20.8	26.9	0.89	0.97	22.6	0.2
p90_8g_NS_1d	13.6	14.3	0.59	0.58	14.3	2.4
p90_8g_NS_7d	18.8	21.3	0.74	0.68	20.2	10.8
p93_4g_1d	13.4	17.7	0.46	0.9	11.9	0.6
p93_4g_7d	20.3	28.2	0.76	0.98	25.0	3.7
p93_4g_NS_1d	14.0	15.2	0.52	0.6	13.6	0.5
p93_4g_NS_7d	18.1	20.3	0.69	0.71	21.5	7.7
p93_8g_1d	12.9	15.0	0.34	0.2	9.8	0.5
p93_8g_7d	17.0	21.6	0.62	0.36	20.8	4.7
p93_8g_NS_1d	13.6	14.3	0.45	0.46	10.8	1.6
p93_8g_NS_7d	16.1	17.5	0.66	0.54	16.7	5.8
p93_C_4g_1d	11.4	12.7	0.41	0.82	8.1	6.2
p93_C_4g_7d	16.3	22.7	0.62	0.89	18.0	6.3
p93_C_4g_NS_1d	11.4	11.7	0.45	0.52	10.6	0.7
p93_C_4g_NS_7d	16.2	17.1	0.65	0.65	18.2	6.7
p93_C_8g_1d	9.1	11.2	0.36	0.49	8.2	3.8
p93_C_8g_7d	13.8	16.8	0.56	0.41	11.3	7.9
p93_C_8g_NS_1d	10.7	12.0	0.49	0.56	9.9	0.3
p93_C_8g_NS_7d	15.4	16.2	0.6	0.57	14.1	10.4

6.3.3. Comparison of the results from the different experimental techniques

6.3.3.1. Degree of hydration

Fig. 6.9 compares the degree of hydration of C_3S and C_3A measured using QXRD and ^{27}Al and ^{29}Si MAS NMR. The degrees of hydration of C_3A are indeed comparable with XRD and NMR and the variations are expected due to the lower amount of C_3A in the system, and due to the

crude method which was used for quantification of degree of hydration of C_3A with ^{27}Al MAS NMR. The difference is small at higher degrees of hydration. With respect to C_3S, there is a clear increase in the degree of hydration when measured with XRD compared to that of NMR. This could arise due to a combination of different factors including:

- *Crystallinity of C_3S:* The anhydrous powders of p90 and p93 have crystallinity of around 90% for C_3S, based on the total undetected/amorphous content in the anhydrous sample. A similar crystallinity value was found for triclinic C_3S previously[19]. As quantitative XRD only calculates the crystalline phases, this could potentially lead to an error in quantification.
- *Model crystal structure of C_3S:* There is potential for errors that could arise from the choice of the crystal structure of C_3S M1 for Rietveld refinement. It is possible that additional atomic refinements could improve the results.
- *Q^0(h) overlapping:* There could be small overlapping of hydroxylated Q^0(h) species on the Q^0 (6) site in the ^{29}Si MAS NMR spectra, which leads to an underestimation in the degree of hydration measured through ^{29}Si MAS NMR.

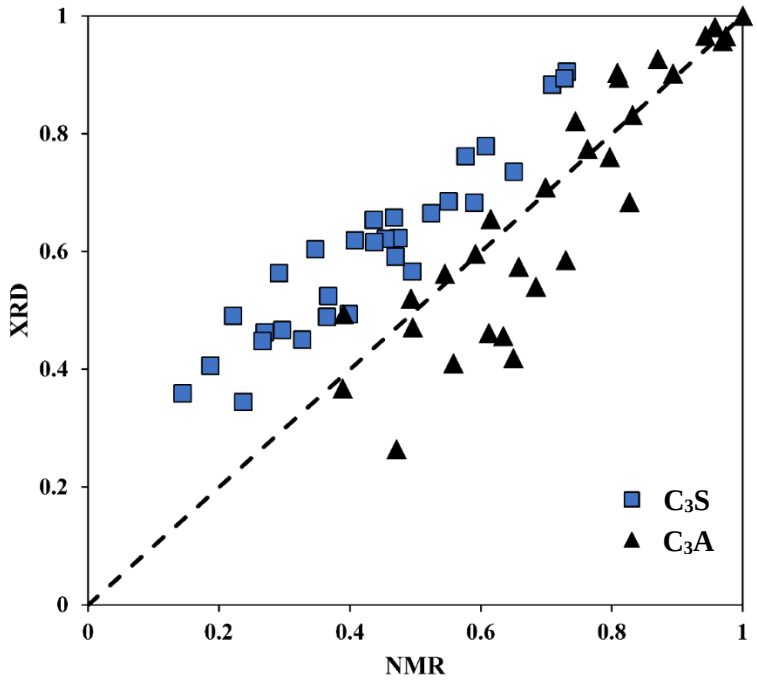

Figure 6.9: Degree of hydration of C_3S and C_3A measured from QXRD and ^{27}Al and ^{29}Si MAS NMR

Fig. 6.10 compares the measured heat release from isothermal calorimetry at 1 and 7 days with the heat release calculated from XRD and NMR. For the calculation of the theoretical heat release, the measured degrees of hydration of C_3S and C_3A are multiplied with the respective enthalpies of reaction. It is assumed that the enthalpy of reaction of C_3S is *517 J/g* and C_3A as *1453 J/g*[28]. The enthalpies of reaction of C_3A are different for the formation of ettringite, monosulphate and other hydroxy-AFm phases and the values are an average value found in literature[28,60]. It could be seen from Fig. 6.10 that calculated heat from the NMR measurements

are closer to the heat measured from the calorimetry. This would imply that XRD is over estimating the C_3S hydration in the system. At higher heat release, the calculated heat release is higher than the measured one. This could be due to the heat loss from the isothermal calorimetry measurements[19]. The discrepancies from the measured and calculated heat release could be also due to the enthalpies of hydration which are used for calculation[19]. As an average enthalpy from C_3A hydration is used, with increasing degree of hydration of C_3A, the enthalpy reaction would be lower because the reaction with ettringite formation possess the highest heat release and vice versa. As most of the heat release is contributed from C_3S due to the higher composition, it could be concluded that degree of hydration of C_3S measured using ^{29}Si MAS NMR is more reliable compared to QXRD for the current set of results.

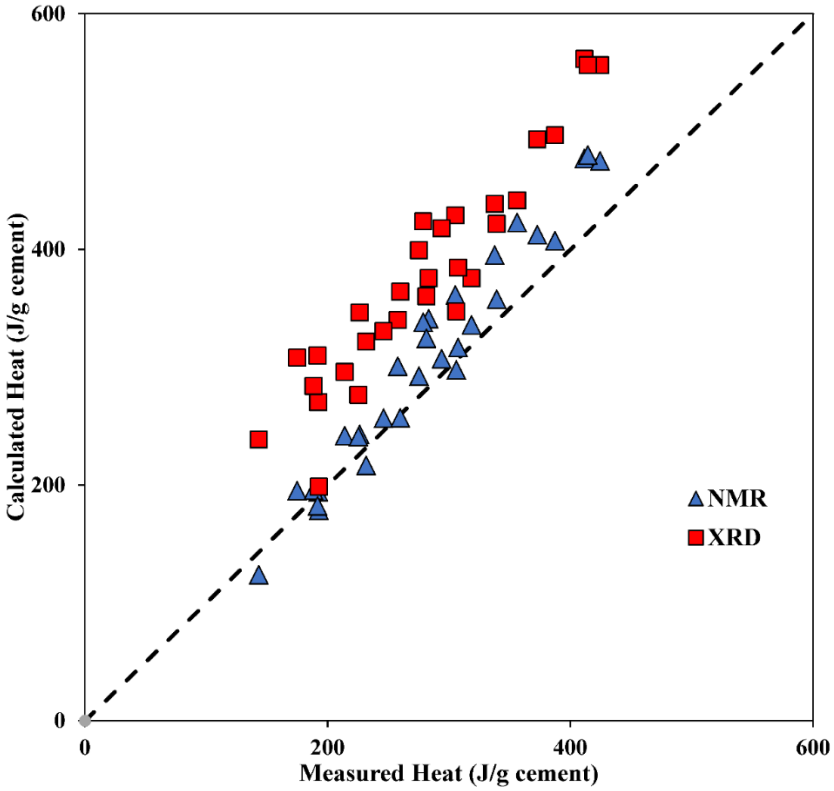

Figure 6.10: Measured heat from isothermal calorimetry vs calculated heat from XRD and NMR

Fig. 6.11 compares the degree of hydration of C_3S and C_3A with and without Na_2SO_4. The degree of hydration of both C_3S and C_3A when mixed with the Na_2SO_4 is consistently higher at lower degree of hydrations and vice versa. This is also consistent with the measurements from isothermal calorimetry, where the cumulative heat release with Na_2SO_4 is accelerated in the early age, while there is a reduction in the overall heat release at later ages.

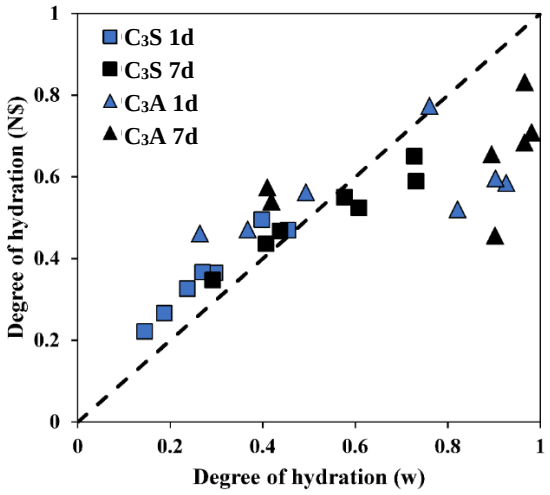

Figure 6.11: Effect of Na_2SO_4 on degree of hydration of C_3S and C_3A at 1 and 7 days; N$ (Na_2SO_4); w (water); Degree of hydration of C_3S (^{29}Si MAS NMR); Degree of hydration of C_3A (QXRD)

6.3.3.2. Portlandite content

Fig. 6.12 compares the portlandite content measured per 100 g of anhydrous model cement from QXRD and TGA. The measured portlandite content is consistently on the lower side at lower degrees of hydration of C_3S (from ^{29}Si MAS NMR) while it is more comparable at higher degrees of hydration. It has been previously reported that the portlandite content is often underestimated from XRD analyses[33,61]. They propose that this could be due to the random orientation of few large crystals of portlandite precipitated during hydration, which apparently could not be corrected by preferred orientation correction in Rietveld analysis[61].

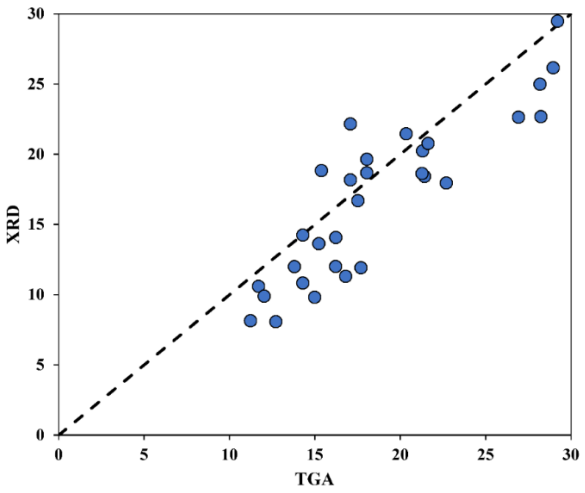

Figure 6.12: Portlandite content from TGA and XRD

Fig. 6.13 shows the portlandite content measured from TGA with respect to the degree of hydration of C_3S (^{29}Si MAS NMR). The figure shows that the portlandite content is lower with Na_2SO_4 addition at similar degrees of hydration. This could be due to the consumption of portlandite by Na_2SO_4 to form NaOH and $CaSO_4$ as described in Eq. 6.5.

$$Na_2SO_4 + Ca(OH)_2 \rightarrow 2NaOH + CaSO_4 \quad (6.5)$$

It is also possible that this difference in portlandite content with the addition of Na_2SO_4 derives from varying C/S ratio. If the C/S ratio is higher for C_3S reaction in the presence of Na_2SO_4, this could lead to a decrease in the measured portlandite content. This is supported by Fig. 6.14, as there is a decrease in the MCL value with the addition of Na_2SO_4. This could be interpreted as an increasing C/S ratio in the presence of Na_2SO_4 as it has been often reported that a lower C/S ratio of C-S-H increases the MCL[36,53]. Nevertheless, with a possibility of consumption of portlandite due to Eq. 6.5 would be unwise to measure the C/S ratio for the current system from the degree of hydration and portlandite content as described in a previous study[19]. Furthermore, C_3A could also react with portlandite to form h-AFm in the absence of gypsum[28], or h-AFm could precipitate portlandite after consuming gypsum[62]. These would make it harder to calculate the C/S ratio accurately.

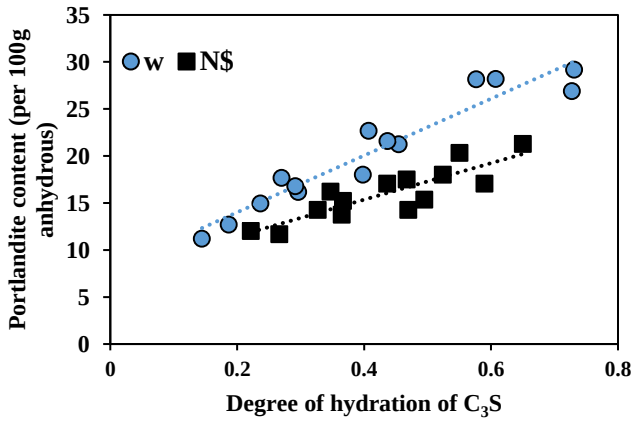

Figure 6.13: Degree of hydration of C_3S vs portlandite content for N$ and water (w)

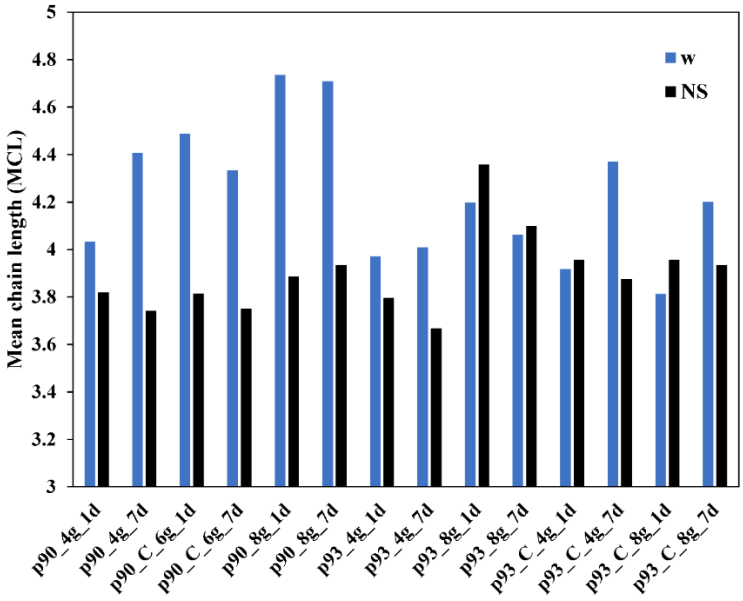

Figure 6.14: Comparison of the mean chain length with (N$) and without (w) Na_2SO_4, calculated using Eq. 6.2

6.3.3.3. Ettringite content

Fig. 6.15 compares the ettringite content measured from ^{27}Al MAS NMR and QXRD. A good linear relationship exists between the two, suggesting that there are no major errors or biases in measurement of ettringite content from both methods. The ettringite content measured from ^{27}Al MAS NMR is in relative percentage of Al present as ettringite, while from XRD, it is the mass content per 100 g anhydrous cement.

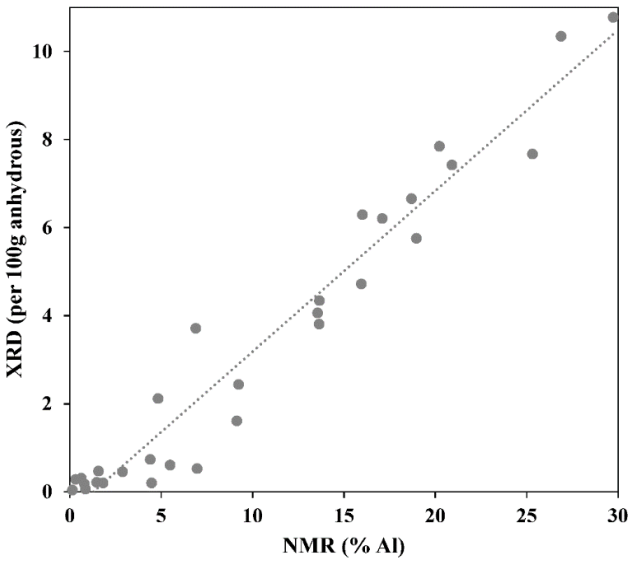

Figure 6.15: Ettringite content from NMR and XRD

Fig. 6.16 shows the relative amount of aluminium in unhydrated C_3A, ettringite and AFm measured from ^{27}Al MAS NMR at 1 and 7 days. These results should be interpreted with caution as there could be deviations, especially on the amount of ettringite and AFm due to the hydration stoppage technique used[42,43]. The total ettringite content in p90_4g, p90_6g and p90_8g is low (<3%) at both 1 and 7 days. This is in agreement with the results from Fig. 6.4, as the main peak of C_3A finishes well before 24 hours for these mixes and hence the ettringite content should be expected to be low. The degree of hydration of C_3A is also high in these mixes. Therefore, most of the ettringite would be already converted to monosulphate, which is why there is a very high percentage of AFm in these mixes. It is observed that there is a small increase of ettringite from 1day to 7 days for p90_6g and p90_8g. Literature suggests that this small increase originates from the ettringite formation which occurs due to the release of the adsorbed sulphates from C-S-H[22,33,34]. Similar trend is also observed with p93_4g as there is a low level of AFt content at 1day and there is a slight increase as well by 7 days. In the case of the properly sulphated system of p93_C_4g, a slight reduction in the ettringite content is recorded at 7 days compared to 1 day. The difference in the distribution of the hydration products compared to p93_4g could be attributed to the lower fineness. The amount of unhydrated C_3A is particularly high at 1 and 7 days in the case of severely-over-sulphated systems (p93_8g, p93_C_8g). An increase in the ettringite content is also clearly visible in these cases. This is expected as the gypsum is not depleted, and therefore, there would not be a reduction in the ettringite content. While analysing p90_C_6g, much of the hydration occurs

during 1 to 7 days. As the main peak of C_3A occurs between 30 and 36 hours, a higher amount of ettringite would be excepted by 1 day. A lower amount of ettringite content is also measured from QXRD (Table 6.4). This could be due to the harsh drying condition derived from the hydration stoppage. With the use of Na_2SO_4, for all samples except p90_4g_NS, there is an increase in the ettringite content at 7 days compared to 1 day. The increase in ettringite content is compensated with a reduction in AFm content. Thus it shall inferred that a recrystallization of ettringite occurs, which is similar to delayed ettringite formation[63]. There is a significant increase in the ettringite content after 1 day, while there is a drastic reduction in the AFm content. It should be noted that p90_4g was an under-sulphated system.

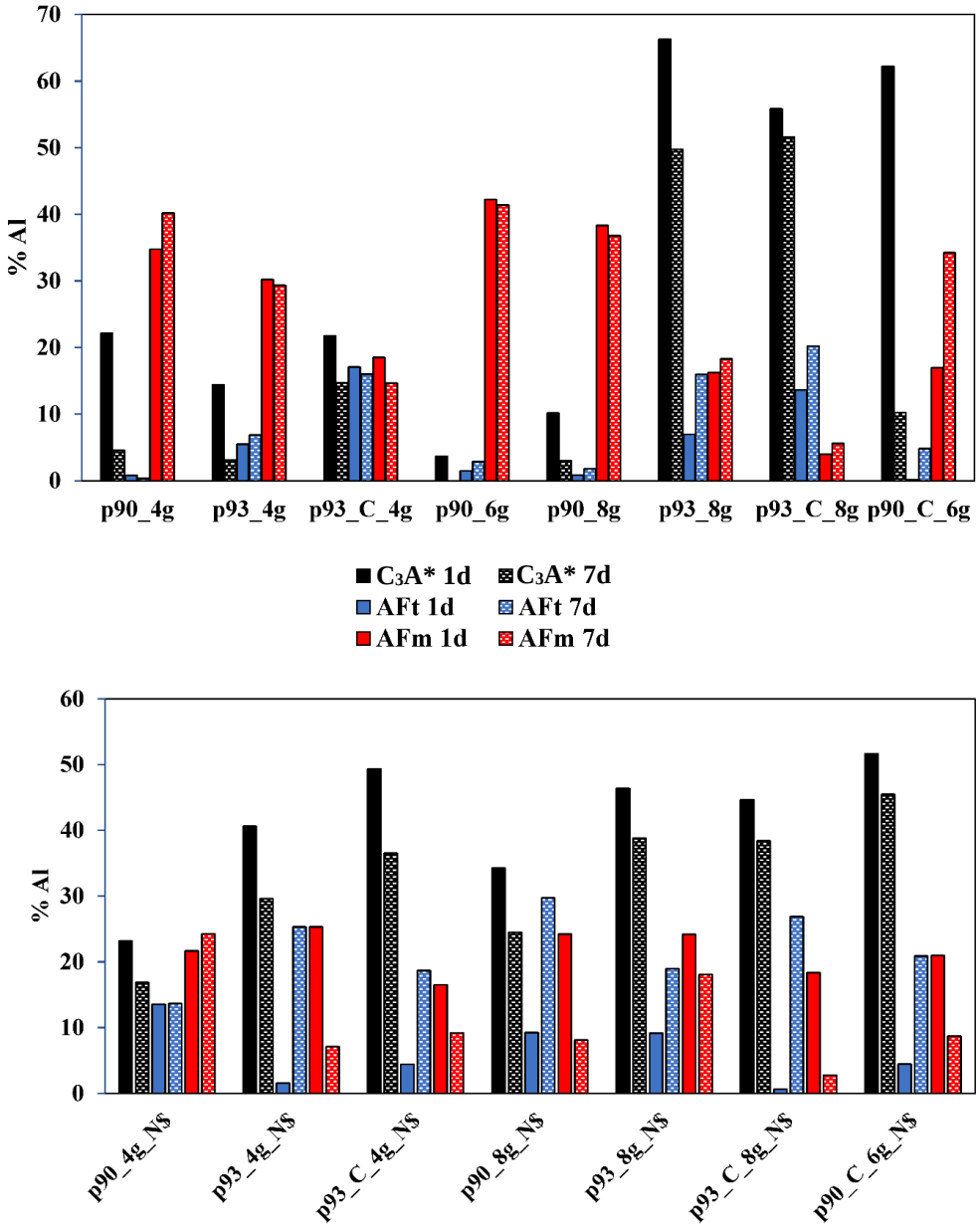

Figure 6.16: Percentage of aluminates present as AFt, AFm in 1 and 7 days and percentage of aluminate involved in the C_3A reaction during 1 to 7 days

6.4. Discussion

6.4.1. Hydration kinetics of C_3S

Fineness is identified as one of the key parameters, which influences the hydration kinetics of C_3S in the model system. Results clearly show that with a decrease in the fineness of C_3S, there is a reduction in the degree of hydration, both in the early and later ages. This agrees well with the previous studies on the effect of fineness in OPC[60,64,65] as well as in pure C_3S[18,66,67]. The increase in the reaction rate with the increase in fineness is attributed to the higher surface area available for the heterogenous nucleation of C-S-H in N&G mechanisms[17,18]. On the other hand, in dissolution-controlled mechanisms, the increase in reactive surface due to the increase in the fineness of the material is attributed to the increase in the rate of hydration[21,68].

Results indicate that the C_3S hydration is also significantly influenced by the hydration of C_3A-gypsum. When C_3S hydration is followed by the peak of C_3A reaction, a significant retardation is observed in the rate of heat release (Fig. 6.4). In an under-sulphated system, the induction period is increased and the peak of C_3S hydration is broadened and retarded[22,33]. With slightly-under-sulphated systems, there appears to be two peaks of C_3S hydration (Fig. 6.4), with the deceleration of the C_3S hydration peak after the C_3A hydration, and reacceleration from a lower point[33]. In properly sulphated systems (Fig. 6.6), after the C_3A hydration, the rate of hydration of C_3S is broadened and retarded[22,33,34]. In over-sulphated and severely-over-sulphated systems, the C_3S hydration peak is unaffected. However, except severely-over-sulphated systems, other systems (under-sulphated, slightly-under-sulphated, properly-sulphated, over-sulphated) achieve similar degrees of hydration by 7days. However, in the case of severely-over-sulphated systems, there is a clear reduction on the degree of hydration beyond 1 day which has not been previously reported on model systems.

With the addition of Na_2SO_4, while there is an acceleration in the early hours, there is a significant reduction of the degree of hydration by 7 days. Mota et al.[24] reported that with addition of Na_2SO_4, the reaction rate is enhanced in the early ages as well as in the later ages in pure C_3S systems. At the same time, although C_3S hydration is enhanced with addition of Na_2SO_4 in the early ages, there is a considerable reduction in the overall degree of hydration in white Portland cements[23].

A major hypothesis that addresses the retarding effect of C_3A on C_3S hydration is the inhibiting effect of Al ions in the solution. It is proposed that, when there is gypsum in the system, the Al ions are bound in the form of ettringite, and once gypsum is completely consumed, Al could be freely available in the solution[22]. One explanation for the inhibiting effect of Al on C_3A hydration could be the reduction of active site of dissolution of C_3S surface by adsorption of Al ions[38,39]. However, this adsorption of Al on C_3S surface will only occur at lower pH (<13)[38,39]. Pustovgar[38] also reported that, with the addition of $NaAlO_2$ solution, while there is an increase in the induction period of C_3S reaction, the main hydration peak is significantly enhanced. Hence, for the current results, although prolongation of the induction period could in fact be explained in under-sulphated systems, the retardation of the C_3S hydration peak could not be explained using this hypothesis.

A second explanation for the inhibiting effect of Al could be the formation of C-A-S-H instead of C-S-H[36]. Formation of C-A-S-H could indeed hinder the reaction kinetics of C_3S hydration as C-A-S-H does not have a similar seeding effect compared to C-S-H[37]. Hence, C-A-S-H probably cannot act as a substrate for the precipitation of C-S-H. Quennoz[22] reported an increase in Al/Ca ratio measured from EDS analysis after the hydration peak of C_3A reaction. However, the Al/Si ratio calculated in the present study (Table 6.3) measured from ^{29}Si MAS NMR clearly shows that there is no significant difference in the incorporated Al in C-S-H with different gypsum compositions. It should be also noted that, EDS measurements performed at high voltages (15kV)[22] are subjected to higher interaction volumes and hence could lead to significant errors and hence is not a conclusive evidence[19].

Bergold et al.[33] proposed the coagulation of C-S-H with AFm phases to be the reason for the retardation of C_3S reaction. As a result, the free surface area of C-S-H reduces, which in turn hinders the N&G process. This is plausible as the zeta potential is positive for AFm[69] and could coagulate with the negatively charged silicate surfaces of C-S-H. A reversal of zeta potential for C-S-H has been reported with increased Ca^{2+} concentration in the solution and thereby an increased adsorption of Ca^{2+} on C-S-H surface[70-72]. Bergold et al.[33] also proposed that the initial nano-sized ettringite crystals formed could also act as a seeding agent for faster nucleation of C-S-H. This also explains why addition of gypsum accelerates alite but not pure C_3S[22] and explain the increased induction period after peak of C_3A hydration (Fig. 6.4).

In an under-sulphated system (p90_4g), as the C_3A hydration peak occurs before C_3S hydration, hence ettringite is consumed. This would increase the induction period compared to the systems with higher sulphate content, as ettringite will provide additional nucleation surface area for an accelerated precipitation of C-S-H. When additional AFm phases are produced over the course of hydration, this further retards C_3S hydration by reducing the internal surface area of C-S-H by its coagulation with AFm. In the slightly-under-sulphated system (Fig. 6.4, p90_6g), C_3A hydration peak occurs near the end of the acceleration period. It removes the ettringite surface which aids N&G by replacing them with AFm thereby reducing the surface area and hindering the N&G process of C-S-H. As the C_3A hydration peak occurs near the end of the acceleration period, a second peak of C_3S[33] is not clearly visible in the current results (Fig. 6.4). In the properly sulphated systems (p93_4g, p93_C_4g), the reaction proceeds like the slightly-under-sulphated system. As in the case of p93_C_4g, the hydration peak of C_3A is occurring more down the deceleration curve, the effects are minimized. In the over-sulphated systems (p90_8g, p90_C_6g), C_3S hydration peak is not tampered as the hydration peak of C_3A succeeds it. The retardation due to C_3A in these cases is not affected in the long term, as with the precipitation of additional C-S-H, N&G process will continue to thrive.

While this hypothesis could very well explain the current results with respect to the under-sulphated, slightly-under-sulphated, properly-sulphated and over-sulphated systems, this could not explain the reduced degree of hydration of severely-over-sulphated systems and systems with Na_2SO_4. In severely-over-sulphated systems and systems with Na_2SO_4, there is significantly higher amounts of ettringite, and less AFm which according to the theory

proposed by Bergold et al.[33] should further accelerate due to the additional nucleation surface area provided by ettringite.

A possible explanation for the retarding effect on the severely-over-sulphated system and systems with Na_2SO_4 addition is the partial blockage of reactive surface of C_3S due to ettringite precipitation. As the zeta potential of ettringite is even higher (positive) than that of AFm[69] and C_3S has a negative zeta potential[73], ettringite could be adsorbed on the surface of C_3S. While ettringite precipitates on the surface of C-S-H or portlandite increases the reaction rate following a N&G process, adsorption of ettringite on the C_3S surface can hinder the dissolution of C_3S, thereby shifting to a dissolution-controlled mechanism[20]. Small amounts of ettringite adsorption in early hours of hydration is not likely to shift to a dissolution-controlled mechanism due to the fast reaction and increasing etch pit formation. However, when more and more ettringite is adsorbed in the period of low reaction, this could have an inhibiting effect on the overall C_3S reaction. This mechanism is similar to the mechanism proposed in Chapter 5 for explaining the retardation of C_3A in presence of gypsum. The reduction in hydration rate in C_3S due to ettringite formation is not as efficient compared to the retardation of ettringite on C_3A. This can be explained with the preferential precipitation of ettringite, which according to simulations from reaction-transport modelling, prefers C_3A surface than C_3S surface[74].

6.4.2. Hydration kinetics of C_3A

The gypsum content has a significant effect on the hydration of C_3A in model systems as in the case of pure C_3A systems. When gypsum is added in the system, calcium or/and sulphate ions are adsorbed on the surface of C_3A grains, thereby hindering the dissolution process[25]. As explained in Chapter 5, it could also be due to the blockage of active surface by precipitation of ettringite or due to a combination of these two factors. When the gypsum is consumed by the system, the dissolution process is retrieved and hence the main hydration peak of C_3A appears[25]. This explains the delaying of the hydration peak of C_3A with an increase in gypsum addition. The broadening of the peak of C_3A hydration has been explained in Chapter 5, as this is a consequence of the higher degree of reaction achieved by C_3A before the start of the peak of hydration.

With similar fineness of p90 compared to the coarse C_3A in Chapter 5, there is a significant acceleration of C_3A-gypsum reaction in the model C_3S-C_3A systems. For instance, p90_4g, p90_6g and p90_8g is equivalent to 29%, 39% and 47% by weight of gypsum respectively for a C_3A-gypsum system. While, in Chapter 5, in pure C_3A-gypsum system, 10% of gypsum took around 12 hours for gypsum depletion, while 20% gypsum took around 80 hours. However, in p90_4g, p90_6g and p90_8g, the main peak of C_3A hydration occurred at around 2 hours, 6 hours and 15 hours respectively. While comparing systems with similar C_3S/C_3A ratios of Hesse et al.[34] and Bergold et al.[33], it could be seen that the monophase system used by Bergold[33] needed much lower sulphate content to be properly sulphated compared to the polyphase system used by Hesse[34]. This effect was not seen between polyphase systems and monophase systems studied by Quennoz[22], as gypsum depletion occurred faster in the monophase C_3S-C_3A-gypsum model systems compared to C_3A-gypsum. However, the fineness of C_3A was

significantly higher than the fineness of the polyphase system, which obviously reduces the time for gypsum depletion[29].

Quennoz[22] attributed the faster formation of the C_3A hydration peak in monophase C_3S-C_3A systems, compared to pure C_3A systems, to the sulphate adsorption of C-S-H. With the reduction of available sulphates for the precipitation of ettringite, the adsorbed sulphates on C_3A are desorbed, thereby leading to the hydration peak of C_3A. Although this could explain the marginal decrease in the gypsum depletion between monophase C_3S-C_3A systems and pure C_3A systems, this cannot explain the difference in the occurrence of C_3A peak between polyphase C_3S-C_3A systems and monophase C_3S-C_3A systems. Also, in the current results, it is unlikely that adsorption of sulphate alone could explain the faster depletion of gypsum.

A possible explanation is that in polyphase systems, C_3S and C_3A are mixed in a single grain. Hence, although the adsorbed sulphates could hinder the dissolution of C_3A, when C_3S is reacted, it opens new reactive surfaces for C_3A to further advance its reaction. Hence, in these polyphase systems, hydration of C_3S has a significant effect on the reaction rate of C_3A. As around 90-93% of the grain contains C_3S, C_3A hydration is dependent on C_3S reaction. In order to achieve more reaction front, C_3S needs to be dissolved and open the reactive front of C_3A. This explains the results in Fig. 6.11, and why C_3A reaction is also accelerated in the presence of Na_2SO_4 in the early ages. Na_2SO_4 in the presence of C_3S could transform into NaOH and $CaSO_4$ as described in Eq. 6.5. This explains the recrystallization of ettringite with Na_2SO_4, and a lack of hydration peak of C_3A as more C$ will be produced during the course of hydration. Hence, C_3A hydration continues to be retarded.

6.4.3. Implications of use of Na_2SO_4 in Portland cement systems

Although Na_2SO_4 is not very commonly used in OPC, it is being under investigation to activate SCMs in the blended cement systems and hybrid cements. From the current study, it could be concluded that, when Na_2SO_4 is added in neat OPC systems, there is an increase in the early age hydration and a decrease in the overall hydration by 7 days. Furthermore, the decrease in the degree of hydration is even lower in case of severely-over-sulphated systems. This could potentially lead to a loss in strength. It has been also observed that the portlandite content with the addition of Na_2SO_4 is on the lower side compared to without the use of Na_2SO_4. This should not be mistaken for lower degree of hydration in neat systems or higher reactivity of SCM in blended systems. The current results also indicate that there is there is recrystallization of ettringite which might induce a risk of expansion crack due to the presence of additional sulphates coming from Na_2SO_4 addition. Nevertheless, recrystallization of ettringite does not always lead to cracking. This is also dependent on several parameters such as the temperature of curing, porosity, elasticity, etc.[63].

6.5. Conclusions

In this chapter, a systematic study of hydration of polyphase C_3S-C_3A model cement systems with different gypsum contents, addition of Na_2SO_4, fineness and composition have been analysed. Analytical experimental techniques such as isothermal calorimetry, QXRD, TGA, ^{27}Al and ^{29}Si MAS NMR spectroscopy was used for the quantification. The major conclusions of this chapter are summarized as follows:

- The effect of C_3A-gypsum reaction on the hydration of C_3S in a polyphase C_3S-C_3A system is explained by the inhibiting effect of AFm on C-S-H nucleation and growth as proposed by Bergold et al[33] for all systems except severely-over-sulphated systems and systems with Na_2SO_4 addition.
- In super-sulphated systems and systems with Na_2SO_4, the hydration of C_3S is retarded by adsorption of ettringite thereby changing from a nucleation and growth mechanism to a dissolution controlled mechanism after 1 day of hydration.
- Hydration of C_3A is strongly associated with hydration of C_3S, as more reactive surface would be revealed with the hydration of C_3S for C_3A dissolution.
- With the addition of Na_2SO_4, a delayed ettringite formation is observed from 1 day to 7 days, which could increase the risk of cracking in concrete
- With Na_2SO_4 addition, at similar degrees of hydration of C_3S, a lower amount of portlandite content is measured, which should be attributed either to a higher C/S ratio of C-S-H with addition of Na_2SO_4 and/or reaction of Na_2SO_4 with portlandite for the formation of NaOH and calcium sulphate.
- ^{29}Si MAS NMR spectroscopy was found to be a more suitable method to measure the degree of hydration of monoclinic M1 form of C_3S compared to QXRD.

References

1. Boden T., Andres B. and Marland G. (2016) "Global CO_2 emission from fossil-fuel burning, cement manufacture, and gas flaring" Oak Ridge National Laboratory, Oak Ridge U.S.A. doi 10.3334/CDIAC/00001_V2016
2. (2015) "Activity Report", *CEMBUREAU* Brussels:
3. Scrivener K. (2012) "Issues in sustainability in cements and concrete" *Am. Ceram. Soc. Bull.* **91**:47-50.
4. Lee C. Y., Lee H. K. and Lee K. M. (2003) "Strength and microstructural characteristics of chemically activated fly ash–cement systems" *Cem. Concr. Res.* **33**:425-431.
5. Jueshi Q., Caijun S. and Zhi W. (2001) "Activation of bleneded cements containing fly ash" *Cem. Concr. Res.* **31**:1121-1127.
6. Velandia D. F., Lynsdale C. J., *et al.* (2016) "Evaluation of activated high volume fly ash systems using Na_2SO_4, lime and quicklime in mortars with high loss on ignition fly ashes" *Constr. Build. Mater.* **128**:248-255.
7. Scrivener K. L., Juilland P. and Monteriro P. J. (2015) "Advances in understanding hydration of Portland cement" *Cem. Concr. Res.* **78**:38-56.

8. Bullard J., Jennings H., *et al.* (2011) "Mechanisms of cement hydration" *Cem. Concr. Res.* **41**:1208-1223.
9. Juilland P., Gallucci E., *et al.* (2010) "Dissolution theory applied to the induction period in alite hydration" *Cem. Concr. Res.* **40**:831-844.
10. Bullard J. W., Scherer G. W. and Thomas J. J. (2015) "Time dependent driving forces and the kinetics of tricalcium silicate hydration" *Cem. Concr. Res.* **74**:26-34.
11. Juilland P. and Gallucci E. (2015) "Morpho-topological investigation of the mechanisms and kinetic regimes of alite dissolution" *Cem. Concr. Res.* **76**:180-191.
12. Kumar A., Bishnoi S. and Scrivener K. (2012) "Modelling early age hydration kinetics of alite" *Cem. Concr. Res.* **42**[7]:903-918.
13. Bellmann F., Sowoidnich T., *et al.* (2015) "Dissolution rates during the early hydration of tricalcium silicate" *Cem. Concr. Res.* **72**:106-116.
14. Stein H. N. and Stevels J. M. (1964) "Influence of silica on the hydration of 3CaO, SiO_2" *J. appl. Chem* **14**[8]:338-346.
15. Jennings H. M. and Pratt P. L. (1979) "An experimental argument for the existence of a protective membrane surrounding portland cement during the induction period" *Cem. Concr. Res.* **9**:501-506.
16. Bergold S. T., Goetz-Neunhoeffer F. and Neubauer J. (2015) "Mechanically activated alite: New insights into alite hydration" *Cem. Concr. Res.* **76**:202-211.
17. Thomas J., Biernacki J., et al. (2011) "Modelling and simulation of cement hydration kinetics and microstructural development" *Cem. Concr. Res.* **41**:1257-1278.
18. Joseph S., Bishnoi S., et al. (2017) "Modeling the effect of fineness and filler in early-age hydrationof tricalcium silicate" *J Am Ceram Soc.* **100**[3]:1178-1194.
19. Joseph S., Bishnoi S., *et al.* (2018) "Effect of the densification of C-S-H on hydration kinetics of tricalcium silicate" *J. Am. Ceram. Soc*. **101**[6]:2438-2449.
20. Nicoleau L. and Nonat A. (2016) "A new view on the kinetics of tricalcium silicate hydration" *Cem. Concr. Res.* **86**:1-11.
21. Nicoleau L. and Bertolim M. A. (2015) "Analytical Model for the Alite (C_3S) Dissolution Topography" *J. Am. Ceram. Soc.* **99**:773-786.
22. Quennoz A. and Scrivener K. (2013) "Interactions between alite and C_3A-gypsum hydrations in model cements" *Cem. Concr. Res.* **44**:46-54.
23. Mota Gasso B. (2015) "Impact of alkali salts on the kinetics and microstructural development of cementitious systems" *PhD Thesis*, EPFL Switzerland.
24. Mota B., Matschei T. and Scrivener K. (2015) "The influence of sodium salts and gypsum on alite hydration" *Cem. Concr. Res.* **75**:53-65.
25. Minard H., Garrault S., *et al.* (2007) "Mechanisms and parameters controlling the tricalcium aluminate reactivity in the presence of gypsum" *Cem. Concr. Res.* **37**:1418-1426.
26. Baquerizo L., Matschei T., et al. (2015) "Hydration states of AFm cement phases" *Cem. Concr. Res.* **73**:143-157.
27. Matschei T., Lothenbach B. and Glasser F. P. (2007) "The AFm phase in Portland cement" *Cem. Concr. Res.* **37**:118-130.
28. Taylor H. (1997) "Cement Chemistry: Second Edition" London: Thomas Telford.

29. Quennoz A. and Scrivener K. (2012) "Hydration of C_3A–gypsum systems" *Cem. Concr. Res.* **42**:1032–1041.
30. Pourchet S., Regnaud L., *et al.* (2009) "Early C_3A hydration in the presence of different kinds of calcium sulfate" *Cem. Concr. Res.* **39**:989–996.
31. Collepardi M., Baldini G. and Pauri M. (1978) "Tricalcium aluminate hydration in the presence of lime, gypsum or sodium sulfate" *Cem. Concr. Res.* **8**:571-580.
32. Sanchez-Herrero M. J., Fernandez-Jimenez A. and Palomo A. (2012) "Alkaline Hydration of Tricalcium Aluminate" *J. Am. Ceram. Soc.* **95**[10]:3317-3324.
33. Bergold S. T., Goetz-Neunhoeffer F. and Neubauer J. (2017) "Interaction of silicate and aluminate reaction in a synthetic cement system: Implications for the process of alite hydration" *Cem. Concr. Res.* **93**:32-44.
34. Hesse C., Goetz-Neunhoeffer F. and Neubauer J. (2011) "A new approach in quantitative in-situ XRD of cement pastes: Correlation of heat flow curves with early hydration reactions" *Cem. Concr. Res.* **41**:123-128.
35. Tenoutasse N. (1968) "The hydrationmechanismof C_3A and C_3S in the presence of calcium chloride and calciumsulfate" in *The 5th International Symposiumon the Chemistry of Cement*, Tokyo Japan.
36. Lothenbach B. and Nonat A. (2015) "Calcium silicate hydrates: Solid and liquid phase composition" *Cem. Concr. Res.* **78**:57-70.
37. Begarin F., Garrault S., *et al.* (2011) "Hydration of alite containing aluminium" *Adv. Appl. Ceram.* **110**[3]:127-130.
38. Pustovgar E., Mishra R., *et al.* (2017), "Influence of aluminates on the hydration kinetics of tricalcium silicate" *Cem. Concr. Res.* **100**:245-262.
39. Nicoleau L., Schreiner E. and Nonat A. (2014) "Ion-specific effects influencing the dissolution of tricalcium silicate" *Cem. Concr. Res.* **59**:118-138.
40. Donatello S., Fernandez-Jimenez A. and Palomo A. (2013) "Very High Volume Fly Ash Cements. Early Age Hydration Study Using Na_2SO_4 as an Activator" *J. Am. Ceram. Soc.* **96** [3]:900-906.
41. Zhang L. and Glasser F. P. (2000) "Critical examination of drying damage to cement pastes" *Adv. Cem. Res.* **12**[2]:79-88.
42. Zhang J. and Scherer G. W. (2011) "Comparison of methods for arresting hydration of cement" *Cem. Concr. Res.* **41**:1024-1036.
43. Snoeck D., Velasco L. F., *et al.* (2014) "The influence of different drying techniques on the water sorption properties of cement-based materials" *Cem. Concr. Res.* **64**:54-62.
44. Knapen E., Cizer O., *et al.* (2009) "Effect of free water removal from early-age hydrated cement pastes on thermal analysis" *Constr. Build. Mater.* **23**:3431-3438.
45. Lothenbach B., Durdzinski P. and De Weerdt K. (2016) "Thermogravimetric analysis" in *A practical guide to microstructural analyisis of cementitious materials*, CRC Press, 177-212.
46. Jansen D., Goetz-Neunhoeffer F., *et al.* (2011) "A remastered external standard method applied to the quantification of early OPC hydration" *Cem. Concr. Res.* **41**:602-608.
47. de Noirfontaine M., Courtial M., *et al.* (2012) "Tricalcium silicate Ca_3SiO_5 superstructure analysis: a route towards the structure of the M1 polymorph" *Zeitschrift für Kristallographie* **227**[2]:102-112.

48. Snellings R. (2016) "X-ray powder diffraction applied to cement" in *A Practical Guide to Microstructural Analysis of Cementitious Materials*, K. Scrivener, R. Snellings and B. Lothenbach, Eds., CRC press.
49. Massiot D., Fayon F., *et al.* (2002) "Modelling one- and two-dimensional Solid State NMR spectra" *Magn. Reson. Chem.* **40**:70-76.
50. Andersen M. D., Jakobsen H. J. and Skibsted J. (2004) "Characterization of White Portland Cement Hydration and the C-S-H Structure in the Presence of Sodium Aluminate by ^{27}Al and ^{29}Si MAS NMR Spectroscopy" *Cem. Concr. Res.* **34**:857-868.
51. Richardson I. G., Brough A. R., et al. (1994) "The Characterization of Hardened Alkali-Activated Blast-Blast Furnace Slag Pastes and the Nature of the Calcium Silicate Hydrate (C-S-H) Phase" *Cem. Concr. Res.* **24**:813-829.
52. Richardson I. G. and Groves G. W. (1997) "The Structure of the Calcium Silicate Hydrate Phases Present in Hardened Pastes of White Portland Cement/Blast-Furnace Slag Blends" *J. Mater. Sci.* **32**:4793-4802.
53. Dai Z., Tran T. and Skibsted J. (2014) "Aluminum Incorporation in the C–S–H Phase of White Portland Cement–Metakaolin Blends Studied by ^{27}Al and ^{29}Si MAS NMR Spectroscopy" *J. Am. Ceram. Soc.* **97**[8]:2662-2671.
54. Andersen M. D., Jakobsen H. J. and Skibsted J. (2003) "Incorporation of Aluminium in the Calcium Silicate Hydrate (C-S-H) of Hydrated Portland Cements: A High Field ^{27}Al and ^{29}Si MAS NMR Investigation" *Inorg. Chem.* **42**:2280-2287.
55. Richardson I. G., Brough A. R., et al. (1993) "Location of Aluminium in Substituted Calcium Silicate Hydrate (C-S-H) Gels as Determined by ^{29}Si and ^{27}Al NMR and EELS" *J. Am. Ceram. Soc.* **76**:2285-2288.
56. Andersen M. D., Jakobsen H. J. and Skibsted J. (2006) "A New Aluminium-Hydrate Species in Hydrated Portland Cements Characterized by ^{27}Al and ^{29}Si MAS NMR Spectroscopy" *Cem. Concr. Res.* **36**:3-17.
57. Sun G. K., Young J. F. and Kirkpatrick R. J. (2006) "The Role of Al in the C-S-H: NMR, XRD, and Compositional Results for Precipitated Samples" *Cem. Concr. Res.* **36**:18-29.
58. Skibsted J., Henderson E. and Jakobsen H. J. (1993) "Characterization of Calcium Aluminate Phases in Portland Cements by ^{27}Al MAS NMR Spectroscopy" *Inorg. Chem.* **32**:1013-1027.
59. Snellings R., Salze A. and Scrivener K. (2014) "Use of X-Ray Diffraction to Quantify Amorphous Supplementary Cementitious Materials in Anhydrous and Hydrated Blended Cements" *Cem. Concr. Res.* **64**:89-98.
60. Termkhajornkit P. and Barbarulo R. (2012) "Modeling the coupled effects of temperature and fineness of Portland cement on the hydration kinetics in cement paste" *Cem. Concr. Res.* **42**[3]:526-538.
61. Bergold S. T., Goetz-Neunhoeffer F. and Neubauer J. (2013) "Quantitative analysis of C–S–H in hydrating alite pastes by in-situ XRD" *Cem. Concr. Res.* **53**:119-126.
62. Janotka I. and Mojumdar S. C. (2007) "Degree of hydration in cement paste and C3A-sodium carbonate-water systems" *J. Therm. Anal. Calorim.* **90**:645-652.
63. Taylor H. W. F., Famy C. and Scrivener K. (2001) "Delayed ettringite formation" *Cem. Concr. Res.* **31**:683-693.

64. Bentz D., Sant G. and Weiss J. (2008) “Early-age properties of cement-based materials. I: influence of cement fineness” *J. Mater. Civ. Eng.* **20**[7]:502-508.
65. Osbaeck B. and Johansen V. (1989) “Particle size distribution and rate of strength development of Portland cement” *J. Am. Ceram. Soc.* **72**[2]:197-201.
66. Costaya M. (2008) “Kinetics and microstructural investigation on the hydration of tricalcium silicate” *PhD Thesis*, EPFL Switzerland.
67. Bishnoi S. and Scrivener K. L. (2009) “Studying nucleation and growth kinetics of alite hydration using μic” *Cem. Concr. Res.* **39**:849-860.
68. Joseph S. and Bishnoi S. (2014) "Study on the effect of particle size distribution and Blaine fineness on the hydration of cement," in *Proceedings of the RILEM International Symposium on Concrete Modeling CONMOD*, Beijing China.
69. Plank J. and C. Hirsch (2007) "Impact of zeta potential of early cement hydration phases on superplasticizer adsorption," *Cem. Concr. Res.* **37**:537-542.
70. Nachbaur L., Nkinamubanzi P., *et al.* (1998) "Electrokinetic properties which control the coagulation of silicate cement suspensions during early age hydration," *J. Colloid Interface Sci.* **202**:261-268.
71. Viallis-Terrisse H., Nonat A. and Petit J. (2001) “Zeta-potential study of calcium silicate hydrates interacting with alkaline cations” *J. Colloid Interface Sci.* **244**[1]:58-65.
72. Jönsson B., Wennerström H., *et al.* (2004) “Onset of cohesion in cement paste” *Langmuir* **20**:6702-6709.
73. Yoshioka K., Tazawa E., *et al.* (2002) "Adsorption characteristics of superplasticizers on cement component minerals" *Cem. Concr. Res.* **32**:1507-1513.
74. Bullard J., Enjolras E., et al. (2010) “A Parallel Reaction-Transport Model Applied to Cement Hydration and Microstructure Development” *Modell. Simul. Mater. Sci. Eng.* **18**:R025007.

Chapter VII

Conclusions and Perspectives

The primary objective of this thesis was to advance in scientific understanding of the reaction mechanisms that control C_3S and C_3A reactions when they are hydrated independently and in a polyphase system. A new microstructural modelling platform, CemRS (Cementitious Reaction Simulator) has been developed in C++ with the ability to model different reaction mechanisms. The model uses a statistical modelling approach to model the particle size distribution which makes it much faster than the existing models. CemRS was used to model the hydration of C_3S and C_3A-gypsum reactions in pure systems.

7.1. Hydration of C_3S in pure systems

Hydration of C_3S was studied in detail in Chapter 3 and Chapter 4. In Chapter 3 the effect of fineness and fillers on the main peak of C_3S hydration was studied and modelled. In Chapter 4, the effect of w/c and temperature profiles on the hydration till 28 days were studied. The major conclusions for the hydration of C_3S in the pure systems are summarized as:

- A new mathematical Densified Volumetric Growth (DVG) model has been developed in this thesis. It is based on a modified nucleation and growth hypothesis which assumes that the hydration kinetics of C_3S is controlled by densification of C-S-H which is linked to the internal surface area of C-S-H. When the bulk density of C-S-H increases, the internal surface area increases with the formation of additional C-S-H. The surface area diminishes with further densification, due to intra-particle impingements. This model has been carefully developed without contradicting the available evidences from the literature. A calibration and prediction approach was used to model the experimental data. The experimental data available from the literature and new original experimental data were used to validate the model. DVG model is able to capture the effect of fineness of materials including the filler effect without the need to change the parameters hereby verifying the robustness of this new model.
- Experimental results show that variation of w/c ratio studied in this work (0.4, 0.5, 0.66) do not have any effect on the hydration kinetics upto 24 hours, while there is marginal effect in the later ages until 28 days of hydration. Although w/c has only marginal effect on the hydration kinetics, it has a stronger effect on the C/S ratio of C-S-H. With increase in w/c, the C/S of C-S-H decreases. This implies that there is a higher amount

of portlandite content which is measured at higher w/c. However, this should not be mistaken as increased degree of hydration in Portland cement systems.

- When C_3S is initially cured at a lower temperature (20ºC) and then cured at higher temperature (40ºC), an increase in the degree of reaction is observed. On the other hand, when C_3S is initially cured at a higher temperature, and then cured at a lower temperature, the degree of hydration reduces. These are attributed to the effect of densification of C-S-H on the hydration kinetics of C_3S. When C_3S is initially cured at a higher temperature, the bulk density of C-S-H increases, thereby retarding the hydration in the later ages due to lower internal surface area and vice versa.
- A semi-novel technique was developed to study the instantaneous activation energy, which could be implemented to study other cementitious binder systems as well. The results reaffirmed that, the activation energy does not change at least till 3 days of hydration. This further confirms that the reaction mechanism of the initial day of hydration continues in the later ages as well.

7.2. Hydration of C_3A-gypsum systems

Hydration of C_3A was quantitatively studied with and without gypsum addition (Chapter 5). The different parameters that are investigated in this study are fineness, w/c and gypsum content. A numerical model was developed in CemRS assuming isotropic dissolution of C_3A, which uses a uniform reactive thickness concept. The major conclusions from this part of the study are:

In C_3A-gypsum systems, before depletion of gypsum (Stage 1):

- In this stage, the effect of w/c does not seem to have any effect on the kinetics or the hydration products. With increase in fineness, or decrease in gypsum content, the duration of stage 1 significantly shortens. The numerical model captures the effect of fineness and gypsum content on C_3A hydration considering an isotropic dissolution based mechanism, indicating that the reaction is controlled by surface mechanisms.
- Although the current hypothesis available in the literature for the retardation of C_3A in stage 1 (adsorption of calcium and/or sulphate ions) could explain the experimental results in this chapter, a new hypothesis is introduced. The hypothesis states that the hydration of C_3A is retarded due to the surface blocking of active sites by the formation of ettringite crystals. This could further explain the lack of retardation when Na_2SO_4 is added, as in those mixes ettringite is not formed.

C_3A-gypsum systems, main hydration peak of C_3A (Stage 2):

- Confirming previous results, a broadening and lower intensity of the main hydration peak is observed when the fineness is reduced, or gypsum content is increased.
- The peak broadening effect could be attributed to the increased time required for the desorption of calcium or sulphate ions or ettringite which covers the active sites of C_3A.

- A new model, which assumes a dissolution controlled mechanism, has been developed to capture the main hydration peak with respect to the fineness of C_3A and gypsum content.
- The instantaneous activation energy in this stage is similar to the activation energy in stage 1, which implies that the reaction mechanism does not change.

C_3A gypsum systems, beyond main hydration peak (Stage 2) & C_3A hydrated without gypsum

- It was quantitatively determined that the w/c has a significant effect on the overall degree of hydration after 7 days.
- The increased degree of hydration with an increase in w/c is attributed to the increased water activity at higher w/c ratios.
- There is an increase in the h-AFm phases with an increase in w/c.
- While instantaneous activation energy is lower at this stage, it is not conclusive enough to state a change in the mechanism. This is because, with an increase in temperature, the rate of reaction of conversion of h-AFm to C_3AH_6 is enhanced, which is an endothermic reaction

7.3. Hydration of C_3S-C_3A systems

Hydration of polyphase C_3S-C_3A systems were studied using experimental techniques (Chapter 6). The major parameters invested were the effect of fineness, composition of C_3S & C_3A, gypsum content and the addition of Na_2SO_4. The major conclusions drawn from this study are as follows:

- With the same C_3A/sulphate content, the system could be under-sulphated or properly sulphated or over-sulphated depending on the fineness of the material. Reduction in fineness leads to make a properly sulphated system, over-sulphated.
- Although there is a significant effect of the amount of gypsum content in the rate of hydration in the initial hours of hydration, the overall degree of hydration is not significantly affected unless it is a severely-over-sulphated system.
- In a severely-over-sulphated system, the degree of hydration after 7 days is significantly lower than the systems which are not severely-over-sulphated.
- The faster consumption of gypsum in a polyphase system compared to monophase systems is attributed to the increased free surface area which is available for C_3A due to the hydration of C_3S.
- When Na_2SO_4 is added to the system, although there is an increase in the degree of hydration of both C_3S and C_3A after 1 day of hydration, there is a significant reduction in the degree of hydration at 7 days for both C_3S and C_3A.
- The degree of hydration is further reduced when Na_2SO_4 is added on a severely-over-sulphated system.
- In super-sulphated systems and in other systems with the addition of Na_2SO_4, a recrystallization of ettringite, similar to delayed ettringite formation, is observed.

- The reduction in degree of hydration in severely-over-sulphated system and in systems with Na_2SO_4 is attributed to the blocking of the active sites of C_3S and C_3A due to the precipitation of ettringite.
- In the early hours of hydration (after the induction period), as C_3S is controlled by nucleation and growth mechanism, the formation of ettringite on its surface does not retard the hydration. However, at later ages, when the hydration rate is low, more ettringite precipitation in the active sites could convert the controlling mechanism of C_3S hydration from nucleation and growth to dissolution-controlled.
- With the addition of Na_2SO_4, the portlandite content is reduced. This could be due to the increased C/S ratio of C-S-H or due the reaction of Na_2SO_4 with portlandite to form calcium sulphate and sodium hydroxide.

7.4. Future Perspectives

In an attempt to answer several research questions defined at the start, this research further has generated some additional questions that should be further investigated in future research. Some of the interesting and crucial research questions could be the following:

- CemRS model different phases by treating them as monophase particles. A new approach, which could capture the synergy of hydration of the polyphase materials, needs to be developed to better mimic the hydration in Portland cement systems. A possible approach could be to model different phases in a single particle as spherical sectors depending upon the composition of polyphase system. This could possibly model the synergetic effect of C_3S-C_3A hydration. In addition, CemRS needs further improvements to address the limitations described in Chapter 2 (Section 2.5).
- The current DVG model can only capture the hydration upto 1 day. An improved model needs to be developed which can capture the hydration of C_3S for longer periods. Currently the densification of C-S-H is simulated in the model as a function of time. Alternative equations which could capture the densification as a function of instantaneous density at a time step shall be developed. This will improve the fundamental basis of the model and thus might be able to extend the model to capture the kinetics of hydration in the later ages as well.
- While the increase in w/c does not have a significant effect on the reaction rate in pure C_3S systems, it was previously found to have effect in OPC systems. The current study attributes this difference between C_3S and OPC systems to the effect of Hadley grains or to the increased heat release from C_3A hydration. However, it should be further investigated and verified. Studying the effect of w/c on polyphase and monophase model systems of C_3S-C_3A with different compositions shall shed more light in this area. It shall be studied with a combination of different analytical techniques including ^{1}H NMR relaxometry to quantify the densification of C-S-H as a function of w/c, composition and degree of hydration of the polyphase and monophase model cement systems.
- It should be further verified if the reduction in the portlandite content with the addition of Na_2SO_4 is due to the increase in C/S ratio or conversion of Na_2SO_4 to sodium

hydroxide and calcium sulphate. Quantitative studies with ^{23}Na NMR could provide further insights.

- A logical step forward will be to study the hydration of synthetic systems with synthetic supplementary cementitious materials to better understand and quantify the pozzolanic reaction. Synthetic calcium aluminosilicates shall be prepared in lab and the effect of the composition on the reactivity in the presence of synthetic C_3S and C_3A could be studied using ^{27}Al and ^{29}Si MAS NMR in combination with QXRD/PONKCS.
- The current results could be further used for the development of numerical modelling, and the results from the Chapter 6 could be further compared with the results from thermodynamic modelling.
- To better understand the effect of Na_2SO_4 on blended systems, studies on C_3S-C_3A-gypsum-fly ash-Na_2SO_4 systems could provide further insight, especially on the results in Fig. 1.1. The effect of recrystallization of ettringite and associated risk of cracking with the addition of Na_2SO_4 in hybrid cement systems should be studied on concrete. The first step forward shall be to study if there are any expansion in paste level and to quantify them. It is possible that an expansion due to ettringite formation could compensate autogenous shrinkage.

Appendix I

Pseudo code for kinetic module using DVG model

```
DVGKinetics::DVGKinetics() // Main constructor of DVG kinetics
{
   ParticleStore(); //Function to store the particles
   Coeff_initialize(); //Functions to initialize the coefficients given by user
   for(float time = TimeStep; time<TimeLimit; time+=TimeStep)
   {
      cout<<endl<<"Time:  "<<time<<endl;

/* Calculates the amount of C-S-H precipitated due to filler effect*/
      MassHydCur = MassHydCurLayers(time);

      volumeHydCur=MassHydCur/(Density_of_CSH_Calculation*Volume_reaction_Alite_CSH);

/* Calculates the dissolution depth of C3S through iterations*/
            dr_in=DepthDissolution2D(volumeHydCur, 0.05, 10);
      r_in+=dr_in;
/* Calculates the amount of C-S-H precipitated on C3S grains-without filler effect */
      temp=AliteHydLayers(time);
      MassHydCur+= temp;
      TotalMassHyd+=MassHydCur;
      TotVolHyd+=MassHydCur/(Density_of_CSH_Calculation*Volume_reaction_Alite_CSH);
/* Outputs for user - Customizable*/
  Outputs(time);
   }
}
/* Function to calculate the amount of C-S-H precipitated on C3S grains-without filler effect */
double DVGKinetics::AliteHydLayers(float time)
{
   double temp_mass_total=0;
   double temp_mass;
   double rad_2;
   double rad_1;
   double vol_chk;
   double CSHdenCur;
   t_r=0;

CSHdenCur=Den_k3_r*(1-exp(-Den_k1_r*pow(time,Den_k2_r)))+Den_k4_r*time;

   for(int i=0; i<NoParticlesAlite;i++)
   {
      if(Alite[i].NoParticles>0){
       if(Alite[i].radius<1)
            Gwt_rad1pow=Gwt_rad1pow_1m;
         else
            Gwt_rad1pow=Gwt_rad1pow_1p;
      temp_mass=0;
```

```
    if(Alite[i].radius-Alite[i].radius_in>0.01)
    {
      dr_itr= (Alite[i].dr_D+Alite[i].radius_in)/NoLayers;
      for(rad_itr=Alite[i].radius-Alite[i].radius_in; rad_itr<Alite[i].dr_D+Alite[i].radius;rad_itr+=dr_itr)
      {
        if(rad_itr<=Alite[i].radius)
          t_r=time;
        else
        {
            Gwt_t=max(Alite[i].radius,0.);
          for(double t_temp =0; t_temp<=time && Gwt_t<rad_itr; t_temp+=2*TimeStep)
          {
            dDenRad_itr = Gwt_k1_r/(Gwt_k2_r+pow(t_temp,Gwt_k3_r))+Gwt_k4_r;
            if(time>TimeLimit1)
              dDenRad_itr =
Gwt_k1_r/(Gwt_k2_r+pow(t_temp,Gwt_k3_r))+Gwt_k4_r/(1+gwtRed*pow(time-TimeLimit1,gwtRed2));

            Gwt_t+=
2*TimeStep*dDenRad_itr*(1+Gwt_f)*(Gwt_radConst*pow(Alite[i].radius,Gwt_rad1pow));
            t_r=time-t_temp;
          }
        }
        trt=t_r-TimeStep;
        if(trt>0)
          temp_mass+= 4*pi*pow(rad_itr,2)*((exp(-Den_k2_r*pow(t_r-TimeStep,Den_k3_r))-exp(-
Den_k2_r*pow(t_r,Den_k3_r)))*Den_k1_r)*dr_itr;
        else
          temp_mass+= 4*pi*pow(rad_itr,2)*((exp(-Den_k2_r*pow(0,Den_k3_r))-exp(-
Den_k2_r*pow(t_r,Den_k3_r)))*Den_k1_r)*dr_itr;
      }
    Alite[i].rad2=t_r;
    temp_mass+=4*pi*(pow(Alite[i].radius-Alite[i].radius_in_m1,3.0)-pow(Alite[i].radius-
Alite[i].radius_in,3.0))*CSHdenCur*(1+Den_f)/3.0;
    rad_1 = Alite[i].radius-Alite[i].radius_in;
    vol_chk = 4*pi*pow(rad_1,3)/3.0 -
temp_mass/(Density_of_CSH_Calculation*Volume_reaction_Alite_CSH);
    if(vol_chk<0)
    {
      rad_2=rad_1;
      temp_mass = (4*pi*pow(Alite[i].radius-
Alite[i].radius_in,3)/3.0)*Density_of_CSH_Calculation*Volume_reaction_Alite_CSH;
    }
    else
      rad_2 = rad_1 - pow(3*vol_chk/(4.0*pi), 1/3.0);

    Alite[i].radius_in_m1=Alite[i].radius_in;
    Alite[i].radius_in += rad_2;
    Alite[i].dr_D+=dDenRad_r*TimeStep*Gwt_radConst*pow(Alite[i].radius,Gwt_rad1pow);
    if(Alite[i].radius_in>Alite[i].radius)
      Alite[i].radius_in=Alite[i].radius;
    }
    temp_mass_total+=(temp_mass)*Alite[i].NoParticles;
    Alite[i].D_den = CSHdenCur*(1+Den_f);
  }
  }
  for(int i=0; i<NoParticlesFiller; i++)
    Filler[i].D_den = CSHdenCur*(Den_f);
```

```
   return temp_mass_total;
}

/* Function to calculate the amount of C-S-H precipitated due to filler effect*/
double DVGKinetics::MassHydCurLayers(float time)
{
   double temp_mass=0;
   double Gwt_tm1;
   for(int i=0; i<NoParticlesAlite;i++)
   {
      if(Alite[i].NoParticles>0){
      if(Alite[i].radius<1)
            Gwt_rad1pow=Gwt_rad1pow_1m;
         else
            Gwt_rad1pow=Gwt_rad1pow_1p;
      if(Alite[i].radius-Alite[i].radius_in>0.01)
      {
         Gwt_tm1=0;
         dr_itr= (Alite[i].dr_D+Alite[i].radius_in)/NoLayers;
         for(rad_itr=Alite[i].radius-Alite[i].radius_in; rad_itr<Alite[i].dr_D+Alite[i].radius;rad_itr+=dr_itr)
         {
            if(rad_itr<=Alite[i].radius)
               t_r=time;
            else
            {
               Gwt_t=max(Alite[i].radius,0.);
               for(double t_temp =0;t_temp<=time&& Gwt_t<rad_itr; t_temp+=2*TimeStep)
               {

                  dDenRad_itr = Gwt_k1_r/(Gwt_k2_r+pow(t_temp,Gwt_k3_r))+Gwt_k4_r;
                  if(time>TimeLimit1)
                     dDenRad_itr =
Gwt_k1_r/(Gwt_k2_r+pow(t_temp,Gwt_k3_r))+Gwt_k4_r/(1+gwtRed*pow(time-TimeLimit1,gwtRed2));
                  Gwt_t+=
2*TimeStep*dDenRad_itr*(1+Gwt_f)*(Gwt_radConst*pow(Alite[i].radius,Gwt_rad1pow));
                  t_r=time-t_temp;
               }
            }
            trt=t_r-TimeStep;
            if(trt>0)
               temp_mass+= 4*pi*pow(rad_itr,2)*Den_f*((exp(-Den_k2_r*pow(t_r-TimeStep,Den_k3_r))-exp(-
Den_k2_r*pow(t_r,Den_k3_r)))*Den_k1_r)*dr_itr*Alite[i].NoParticles;
            else
               temp_mass+= 4*pi*pow(rad_itr,2)*Den_f*((exp(-Den_k2_r*pow(0,Den_k3_r))-exp(-
Den_k2_r*pow(t_r,Den_k3_r)))*Den_k1_r)*dr_itr*Alite[i].NoParticles;

         }
      Alite[i].dr_D+=dDenRad_f*TimeStep*Gwt_radConst*pow(Alite[i].radius,Gwt_rad1pow);
      Alite[i].radius_in+=dr_in;
      }
      else
      {
        Gwt_tm1=0;
         if(Alite[i].time_full==0)
            Alite[i].time_full=time;
         dr_itr= (Alite[i].dr_D+Alite[i].radius_in)/NoLayers;
         for(rad_itr=Alite[i].radius-Alite[i].radius_in; rad_itr<Alite[i].dr_D+Alite[i].radius;rad_itr+=dr_itr)
```

```
        {
          if(rad_itr<=Alite[i].radius)
            t_r=time;
          else
          {
            Gwt_t=max(Alite[i].radius,0.);
            for(double t_temp =0; t_temp<=time && Gwt_t<rad_itr; t_temp+=2*TimeStep)
            {
              if(t_temp<Alite[i].time_full)
              {
                dDenRad_itr = Gwt_k1_r/(Gwt_k2_r+pow(t_temp,Gwt_k3_r))+Gwt_k4_r;
                if(time>TimeLimit1)
                  dDenRad_itr =
Gwt_k1_r/(Gwt_k2_r+pow(t_temp,Gwt_k3_r))+Gwt_k4_r/(1+gwtRed*pow(time-TimeLimit1,gwtRed2));
                Gwt_t+=
2*TimeStep*dDenRad_itr*(1+Gwt_f)*(Gwt_radConst*pow(Alite[i].radius,Gwt_rad1pow));
                t_r=time-t_temp;
              }
              else
              {
                dDenRad_itr = Gwt_k1_r/(Gwt_k2_r+pow(t_temp,Gwt_k3_r))+Gwt_k4_r;
                if(time>TimeLimit1)
                  dDenRad_itr =
Gwt_k1_r/(Gwt_k2_r+pow(t_temp,Gwt_k3_r))+Gwt_k4_r/(1+gwtRed*pow(time-TimeLimit1,gwtRed2));
                Gwt_t+=
2*TimeStep*dDenRad_itr*(Gwt_f)*(Gwt_radConst*pow(Alite[i].radius,Gwt_rad1pow));
                t_r=time-t_temp;
              }
            }
          }
          trt=t_r-TimeStep;
          if(trt>0)
            temp_mass+= 4*pi*pow(rad_itr,2)*Den_f*((exp(-Den_k2_r*pow(t_r-TimeStep,Den_k3_r))-exp(-
Den_k2_r*pow(t_r,Den_k3_r)))*Den_k1_r)*dr_itr*Alite[i].NoParticles;
          else
            temp_mass+= 4*pi*pow(rad_itr,2)*Den_f*((exp(-Den_k2_r*pow(0,Den_k3_r))-exp(-
Den_k2_r*pow(t_r,Den_k3_r)))*Den_k1_r)*dr_itr*Alite[i].NoParticles;
        }
      Alite[i].dr_D+=dDenRad_f*TimeStep*Gwt_radConst*pow(Alite[i].radius,Gwt_rad1pow);
      }
    }
    }
    for(int i=0; i<NoParticlesFiller; i++)
    {
      if(Filler[i].NoParticles>0){
      if(Filler[i].radius<1)
          Gwt_rad1pow=Gwt_rad1pow_1mf;
        else
          Gwt_rad1pow=Gwt_rad1pow_1pf;
        dr_itr= (Filler[i].dr_D)/NoLayers;
        for(rad_itr=Filler[i].radius; rad_itr<Filler[i].dr_D+Filler[i].radius;rad_itr+=dr_itr)
        {
           Gwt_t=Filler[i].radius;
            for(double t_temp =0; Gwt_t<rad_itr; t_temp+=TimeStep)
            {
              dDenRad_itr = Gwt_k1_r/(Gwt_k2_r+pow(t_temp,Gwt_k3_r))+Gwt_k4_r;
              if(time>TimeLimit1)
```

```
                dDenRad_itr =
Gwt_k1_r/(Gwt_k2_r+pow(t_temp,Gwt_k3_r))+Gwt_k4_r/(1+gwtRed*pow(time-TimeLimit1,gwtRed2));
                Gwt_t+= TimeStep*dDenRad_itr*(Gwt_f)*(Gwt_radConst*pow(Alite[i].radius,Gwt_rad1pow));
                t_r=time-t_temp;
              }
          trt=t_r-TimeStep;

          if(trt>0)
            temp_mass+= 4*pi*pow(rad_itr,2)*Den_f*((exp(-Den_k2_r*pow(t_r-TimeStep,Den_k3_r))-exp(-
Den_k1_r*pow(t_r,Den_k2_r)))*Den_k1_r)*dr_itr*Filler[i].NoParticles;
          else
            temp_mass+= 4*pi*pow(rad_itr,2)*Den_f*((exp(-Den_k2_r*pow(0,Den_k3_r))-exp(-
Den_k1_r*pow(t_r,Den_k2_r)))*Den_k1_r)*dr_itr*Filler[i].NoParticles;
        }

       Filler[i].dr_D+=dDenRad_f*TimeStep*Gwt_radConst*pow(Filler[i].radius,Gwt_rad1pow);
  }
  }
  return temp_mass;
}
/* Function to calculate the dissolution depth of C3S through iterations*/

double DVGKinetics::DepthDissolution2D(double volume, double PerTolerenceMass, int itrLim)
{
  double temp_vol=0;
  double itr_Pos=0;
  double itr_neg=0;
  int ijkDOD =0;
  while(temp_vol/volume>1+PerTolerenceMass || temp_vol/volume<1-PerTolerenceMass)
  {
    ijkDOD++;

      if(ijkDOD>100000)
        exit(EXIT_FAILURE);
    if(temp_vol/volume>1+PerTolerenceMass)
    {
      dr_in_filler-=dr_tolerence;
      itr_neg++;
    }
    else
    {
      dr_in_filler+=dr_tolerence;
      itr_Pos++;
    }
    temp_vol=0;
  for(int i=0; i<NoParticlesAlite; i++)
  {
    if(Alite[i].radius-Alite[i].radius_in-dr_in_filler>0)
      temp_vol+= (4*pi*pow(Alite[i].radius-Alite[i].radius_in,3)/3.0-4*pi*pow(Alite[i].radius-Alite[i].radius_in-
dr_in_filler,3)/3.0)*Alite[i].NoParticles;
    else if(Alite[i].radius-Alite[i].radius_in>0)
      temp_vol+= (4*pi*pow(Alite[i].radius-Alite[i].radius_in,3)/3.0)*Alite[i].NoParticles;
    else
      temp_vol+=0.0*Alite[i].NoParticles;
  }
  if(itr_Pos>itrLim)
  {
```

```
    if( itr_neg>itrLim)
    {
      if(itr_Pos<5*itrLim && itr_neg<5*itrLim)
        {
          itr_Pos=0;
          itr_neg=0;
          dr_tolerence=dr_tolerence/2.0;
        }
    }
    else
    {
      itr_Pos=0;
      itr_neg=0;
      dr_tolerence=dr_tolerence*2.0;
    }
  }
  }
  return dr_in_filler;
}
```

Input parameters for simulation of DVG model

Calibration parameters

	Purpose	Typical Range
G_1	Defines outer growth rate of C-S-H	3-20
G_2	Defines outer growth rate of C-S-H	100-1000
G_3	Defines outer growth rate of C-S-H	2-5
G_4	Defines outer growth rate of C-S-H	0.001-0.01
D_1	Defines bulk density of C-S-H	0.5-1.5
D_2	Defines bulk density of C-S-H	0.001-0.5
D_3	Defines bulk density of C-S-H	2-3
G_f	Defines outer growth rate of C-S-H due to filler effect	0.5-1.2
D_f	Defines the densification of C-S-H due to filler effect	0.5-1.2
a_{11}	Defines the effect of particle size on outer growth of C-S-H	1-2.5
a_{12}	Defines the effect of particle size on outer growth of C-S-H	0.2-0.8
a_{11f}	Defines the effect of particle size on outer growth of C-S-H for filler	0.1-0.5
a_{12f}	Defines the effect of particle size on outer growth of C-S-H for filler	0.1-0.5

Material properties

Particle size distribution	Cumulative particle size distribution from laser diffraction experiment or from Rosin Rammler equations
Specific gravity	obtained from Pycnometry for alite and inert fillers

Mix Design
Percentage of alite, fillers and water to cement ratio
Reaction parameters

Dry density of C-S-H	2.6 g/cm^3
Density of CH	2.24 g/cm^3
Density of Water	1 g/cm^3
Density of C_3S[1]	3.15 g/cm^3
Volumetric ratio of C_3S	1
Volumetric ratio of water	1.318
Volumetric ratio of C-S-H	1.2073
Volumetric ratio of CH	0.593

Other user defined variables

Image size	Defines the size of the side of image (100-250 µm)
Resolution	No of pixels per µm (10-100)
Maximum Diameter	Maximum diameter of particles, truncated for microstructure (30-100 µm)
Minimum Diameter	Minimum diameter of particles, truncated for microstructure (0.1-1µm)
Nuclei CH	Defines no of nuclei for simulation of portlandite in microstructure (10^5-10^7)
No of Layers	Number of layers for modelling growth of C-S-H (50-100)
dr_tolerence	Allowed tolerance for mass balance (10^{-4} – 10^{-7})
Computational volume	Computational volume for simulation of kinetics (1mm^3)
Particle Steps	Particle range to be defined in statistical particle size distribution <1µm (0.01 µm) >1 µm & <10 µm (0.1 µm) >10 µm & <100 µm (0.2 µm) >10 µm (1µm)
Time Limit	Maximum time to be simulated (24 hours)
Time Step	Time step for simulation (0.01 – 0.1 hours)

[1] While a measured density was used for simulating the particles, an assumed density of 3.15 is used for the calculations of volumetric amount of the reactants and products following the stoichiometric equation of C_3S hydration (Refer Eq. 3.9 and 3.10)

Appendix II

Fig. A2.1 shows the comparison of heat release from the model developed for C_3A hydration and the experimental results from the published article[1]. Table A2.1 shows the parameters used for simulation. As the w/c ratio used in these mixes was very high (w/c 25), it is assumed that the model follows pure isotropic dissolution after the τ_2.

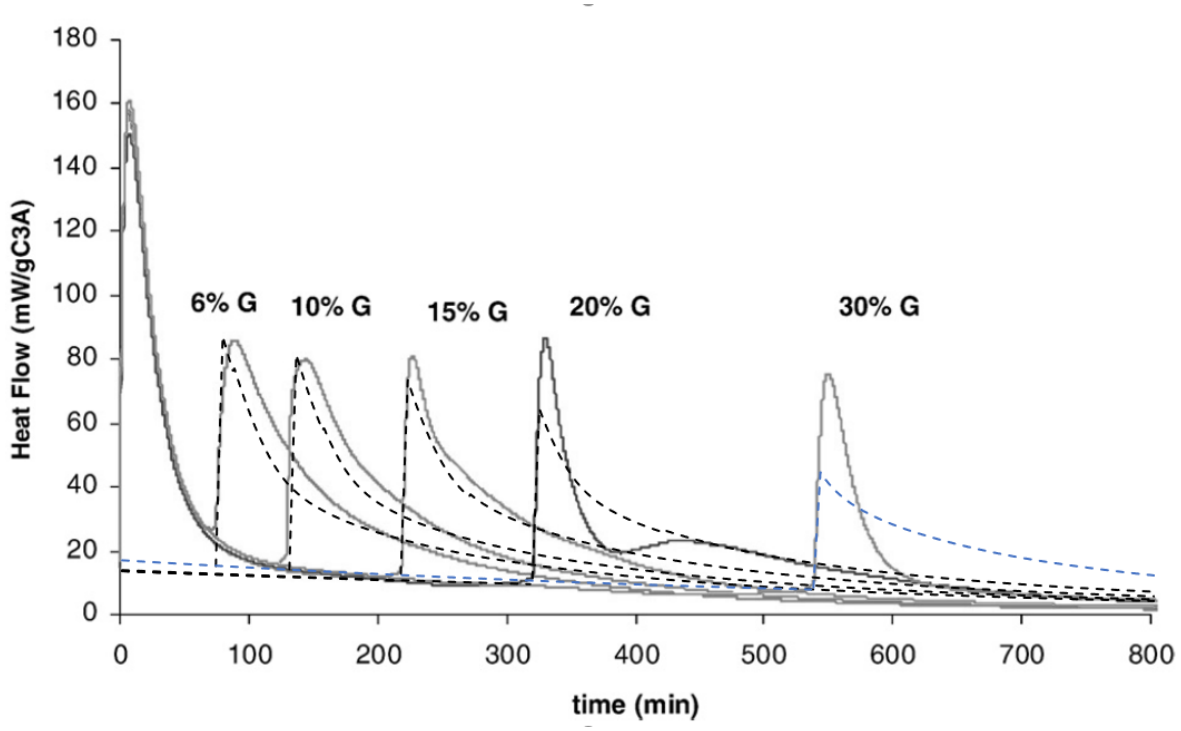

Figure A2.1: Comparison of the heat release from [1] and from numerical model

Table A2.1: Coefficients used for simulation

Mix	c_1 (µm/h)	c_2 (µm/h^2)	c_3 (µm/h)	τ_{23} (h)	k_1
6% G	0.023	3	0.3	-	-
10% G	0.023	3	0.3	-	-
15% G	0.023	3	0.3	-	-
20% G	0.023	3	0.3	-	-
30% G	0.029	3	0.3	-	-

References

1. Pourchet S., Regnaud L. et al. (2009) “Early C_3A hydration in the presence of different kinds of calcium sulfate” *Cem. Concr. Res.* **39**:989–996.

Appendix III

Deconvolutions from ^{27}Al and ^{29}Si MAS NMR for C_3S-C_3A polyphase model cements (Chapter 6)

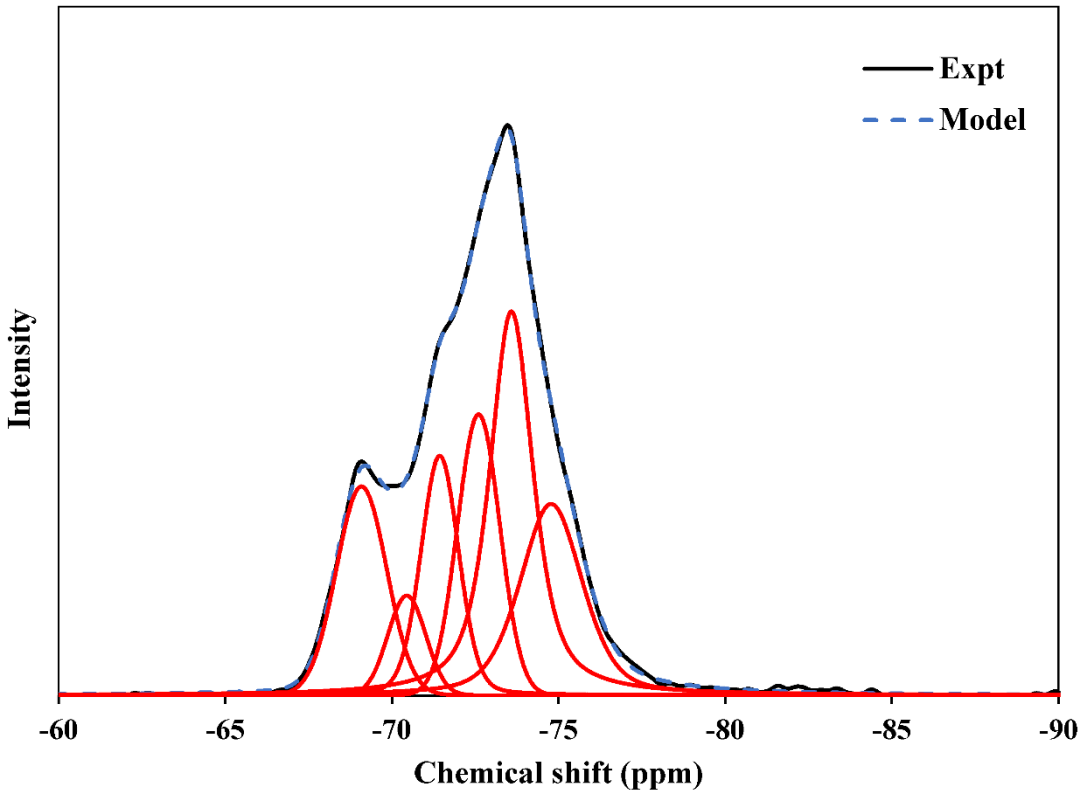

Figure A3.1: Deconvolution of anhydrous p90. Black line represents the actual measurement, red lines are the deconvolution lines and blue dashed line is the model from the deconvolution.

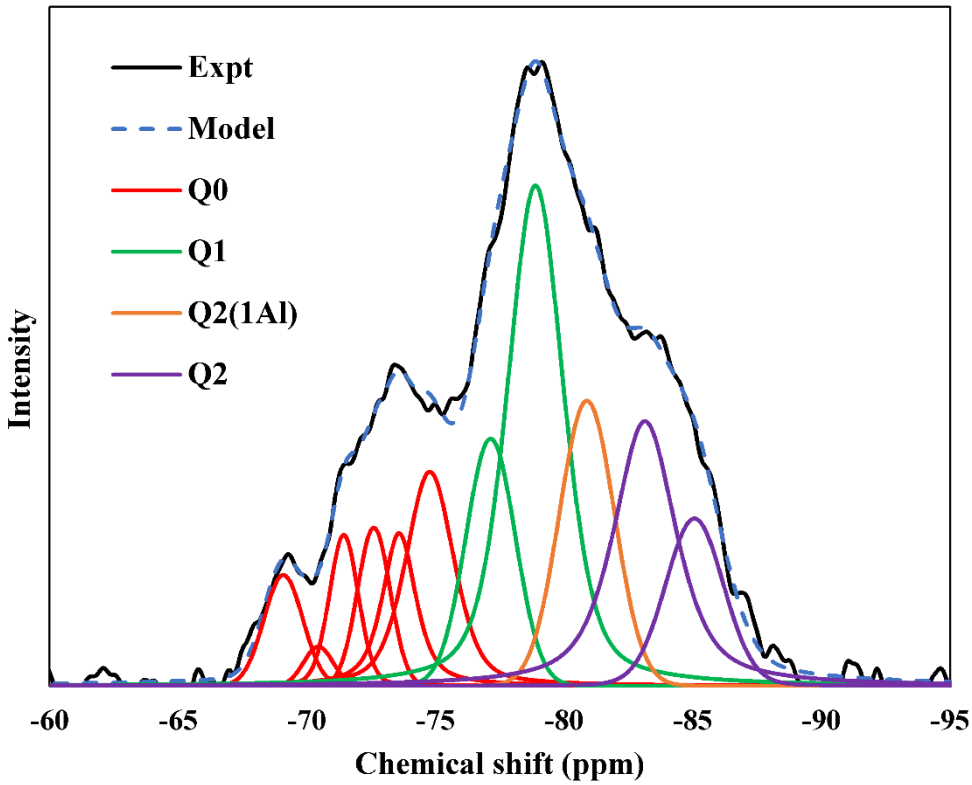

Figure A3.2: Example of a deconvolution for hydrated paste: ^{29}Si MAS NMR deconvolution of p90_4g_7d. Black line represents the actual measurement, red lines are Q^0 sites, green are Q^1 sites, orange is Q^2(1Al) site, violet are Q^2 and blue dashed line is the model from the deconvolution.

Table A3.1: Deconvolution of ^{29}Si NMR in the hydrated systems for all mixes of Table 6.2 in Chapter 6

Abbr.	**Q^0**	**Q^0**	**Q^0**	**Q^0**	**Q^0**	**Q^0**	**Q^1**	**Q^1**	**Q^2(1AL)**	**Q^2**	**Q^2**
p90	14.65	5.3	13.62	16.61	30.18	19.65	0	0	0	0	0
p90_4g_1d	8.04	3.75	8.82	9.85	17.11	12.64	5.97	15.72	7.92	7.82	2.36
p90_4g_7d	3.42	0.91	3.73	4.07	5.22	9.55	9.61	26.39	12.38	16.82	7.93
p90_4g_NS_1d	6.8	2.75	7.8	8.53	12.28	12.35	6.33	22.2	9.92	8.91	2.15
p90_4g_NS_7d	5.75	2.1	6.12	6.74	10.73	9.59	8.29	26.32	11.57	9.57	3.21
p90_6g_1d	7.21	3.08	7.72	8.45	12.9	13.23	7.51	16.27	13.58	5.82	4.23
p90_6g_7d	3.45	1.63	3.7	5.12	4.83	10.41	8.5	27.69	17.04	11.01	6.63
p90_C_6g_1d	10.42	3.78	10.25	11.69	18.56	15.66	3.08	11.75	7.27	3.63	3.91
p90_C_6g_7d	4.72	2.07	5.64	6.12	10.25	10.45	7.15	24.06	13.74	8.56	7.24
p90_C_6g_NS_1d	9.56	2.85	10.05	10.79	18.28	11.97	5.58	15.37	6.92	5	3.63
p90_C_6g_NS_7d	6.97	2.97	6.59	8.55	11.39	11.12	7.22	22.9	8.14	9.48	4.68
p90_8g_1d	7.59	2.71	7.9	9.38	12.89	14.06	6.81	15.13	12.97	4.92	5.63
p90_8g_7d	2.34	1.4	3.75	4.34	4.99	10.42	8.69	25.95	17.58	12.15	8.39
p90_8g_NS_1d	7.94	2.91	7.39	8.96	14.89	10.94	7.8	19.08	10.52	5.81	3.76
p90_8g_NS_7d	4.17	2.07	4.61	6.02	9.22	8.87	7.15	29.2	12.91	9.49	6.3
p93	17.64	5.59	15.49	16.04	32.72	12.53	0	0	0	0	0
p93_4g_1d	10.57	4.44	10	11.67	20.54	15.79	3.72	11.47	6.33	4.14	1.33
p93_4g_7d	5.64	2.36	6.63	6.75	9.56	11.39	7.99	23.96	12.8	6.93	5.97
p93_4g_NS_1d	8.91	3.43	9.49	9.65	18.28	13.57	5.04	16.6	8.8	3.38	2.85
p93_4g_NS_7d	6.23	3.05	6.24	7.07	11.84	10.5	5.83	26.78	9.5	8.6	4.34
p93_8g_1d	11.03	4.7	11	11.81	21.01	16.78	2.81	9.97	6.28	1.96	2.66
p93_8g_7d	7.79	3.67	8.19	8.75	15.15	12.76	5.76	18.07	9.38	4.62	5.88
p93_8g_NS_1d	9.05	4.11	9.5	10.8	18.3	15.57	3.9	13.14	8.88	3.53	3.24
p93_8g_NS_7d	7.3	3.34	7.87	8.45	14.01	12.32	6.46	18.96	10.8	5.31	5.18

p93_C_4g_1d	12.41	5.1	11.85	13.95	22.22	15.78	1.81	8.84	4.33	2.3	1.41
p93_C_4g_7d	8.3	3.36	8.92	9.92	15.4	13.38	5.25	15.61	9.7	6.34	3.82
p93_C_4g_NS_1d	11.01	4.35	11.05	11.84	20.83	14.28	3.09	11.85	5.82	5.04	0.85
p93_C_4g_NS_7d	7.89	3.18	8.58	9.03	15.91	11.78	4.47	19.99	7.53	7.41	4.23
p93_C_8g_1d	13.85	5.69	12.96	14.86	23.7	14.5	1.5	6.94	3.3	1.71	0.99
p93_C_8g_7d	10.53	4.53	10.61	11.69	19.38	14.1	3.47	12	6.67	3.16	3.86
p93_C_8g_NS_1d	12.34	5.32	11.5	13.46	21.32	13.91	2.33	10.16	5.11	3.06	1.5
p93_C_8g_NS_7d	10.09	4.34	9.92	11.1	17.01	12.82	4.7	14.62	6.59	5.75	3.05

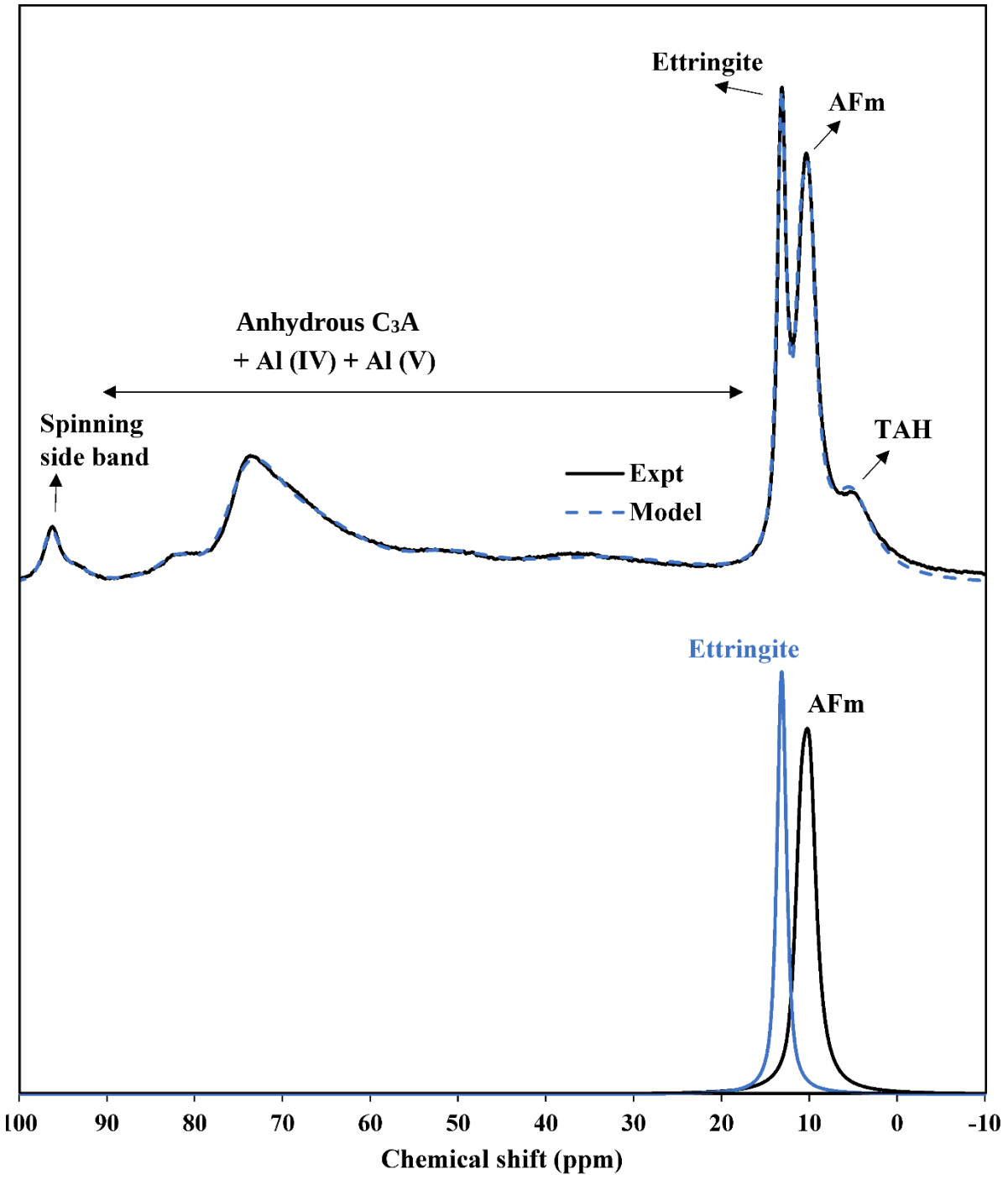

Figure A3.3: Example of a deconvolution for hydrated paste: ^{27}Al MAS NMR deconvolution of p90_4g_N$_1d; (Top) Black line represents the actual measurement, blue dashed line is the model from the deconvolution; (Bottom) Blue line represent the deconvolution peak for ettringite and black represent the deconvolution peak for AFm.

Shiju Joseph

Personal Information

Address	Vital Decosterstraat 51, Leuven 3000, Belgium
Email	shiju.joseph@live.com
Date of birth	15th April 1989
Place of birth	Palai, India
Nationality	Indian

Education

April 2015 – Present — **PhD Researcher**
KU Leuven

Thesis: *Experimental and numerical analysis on the hydration of C_3S/C_3A systems*

May 2014 – April 2015 — **Predoctoral Fellow**

July 2011- May 2013 — **M.Tech in Construction Engineering and Management**
Indian Institute of Technology, Delhi

Thesis: *Modelling Early Age Hydration and Risk of Thermal Cracking in Mass concrete*

Sep. 2007 – May 2011 — **Bachelors in Technology in Civil Enginnering**
College of Engineering, Trivandrum

Thesis: *Engineered Cementitious Composites using Quarry Dust and Recron 3S fibre*

Experience

May 2014 - Present — **Research Assistant**
KU Leuven

Tasks:
- Supervised 5 Master thesis
- Ongoing supervision: 1 Master thesis and 1 Bachelor Thesis
- Organized cement and concrete lab courses for Bachelor's and Master's students

June 2013 – April 2014 — **Senior Project Assistant**

Projects:
- *Piolet production of low carbon cement in India*
- *Study on the effects of chemistry of fly-ashes and cements on development of properties*

July 2011 - May 2013 — **Teaching Assistant**

Tasks: Guiding students in Materials Lab

Curriculum Vitae

Journal Publications

Joseph S., Bishnoi S., Van Balen K., Cizer, Cizer Ö. (2018). Effect of the densification of C-S-H on hydration kinetics of tricalcium silicate. ***Journal of the American Ceramic Society***, 101 (6), 2438-2449.

Bishnoi S., **Joseph S**., Kaur A. (2018). Microstructural modelling of the strength of mortars containing fly ash using µic. ***Construction and Building Materials***, 163, 912-920.

Carette J., **Joseph S**., Cizer Ö., Staquet S. (2018). Decoupling the autogenous swelling from the self-desiccation deformation in early age concrete with mineral additions: Micro-macro observations and unified modelling. ***Cement & Concrete Composites***, 85, 122-132.

Joseph S., Bishnoi S., Van Balen K., Cizer Ö. (2017). Modeling the effect of fineness and filler in early age hydration of tricalcium silicate. ***Journal of the American Ceramic Society***, 100 (3), 1178-1194.

Joseph S., Bishnoi S., Maity S. (2016). An economic analysis of the production of Limestone Calcined Clay cement in India. ***Indian Concrete Journal***, 90 (11), 22-27.

Bishnoi S., Maity S., Mallik A., **Joseph S.**, Krishnan S. (2014). Pilot Scale Manufacture of limestone calcined clay cement: The Indian experience. ***Indian Concrete Journal***, 88 (6), 22-28.

Conference Proceedings

Joseph S., Bishnoi S., Van Balen K., Cizer Ö. (2017). Modelling early age hydration kinetics of C_3S blended with different particle size distributions. . *International conference on advances in construction materials and systems, ICACMS 2017*. Chennai, India (art.nr. 189).

Uppalapati S., **Joseph S.**, Cizer Ö. (2017). Autogenosu shrinkage and strength development of alkali-activated slag_fly ash mortar blends. *5th Internation Slag Valorisation symposium From fundamentals to applications. 5th International Slag Valorisation Sysposium*. Leuven, 03-05 April 2017 (pp. 393-396).

Joseph S., Van Balen K., Bishnoi S., Cizer Ö. (2016). CemRS: fast and efficient modelling platform for the simulation of cementitious systems. International RILEM Conference Materials Systems and Structures in Civil Engineering 2016 (MSSCE 2016) on Service Life of Cement-Based Materials and Structures: Vol. 2. International RILEM Conference on Materials, Systems and Structures in Civil Engineering, Conference segment on Service Life. Lyngby Denmark, August 2016 (pp. 573-579).

Joseph S., Joseph A., Bishnoi S. (2015). Economic implications of limestone clinker calcined clay cement (LC3) in India. Calcined Clays for Sustainable Concrete: Vol. 1. Calcined Clays for Sustainable Concrete. Lausanne, June 23-25, 2015 (pp. 501-508).

Joseph S., Bishnoi S. (2014). Study on the effect of particle size distribution and Blaine fineness on the hydration of cement. . *CONMOD*. Beging, China, Sep, 2014 RILEM.

Curriculum Vitae

Kaur A., **Joseph S.**, Bishnoi S. (2014). Prediction of strenght of mortars containing fly ash. . *CONMOD*. Bejing, China, September 2014.

Kaur A., **Joseph S.**, Bishnoi S. (2014). Modelling strength of mortars containing fly ash. *Recent Developments in Structural Engineering Extended Abstracts and Programme Schedule of Structural Engineering Convention 2014. Structural Engineering Convention*, IIT Delhi. New Delhi, India, December 2014 (art.nr. SEC14AXB).

Joseph S., Bishnoi S. (2013). Numerical Simulations to choose Concrete Strategies to Prevent Thermal Cracks. Proceedings of the 13th NCB International Seminar on Cement and Building Materials. *NCB International Seminar on Cement and Building Materials*. New Delhi, India, 19-22 November 2013 (art.nr. A-55).